Advanced supramolecular assemblies based on terpyridine metal complexes : understanding reaction parameters and designing new materials

Please check the document version of this publication:

ADVANCED SUPRAMOLECULAR ASSEMBLIES BASED ON TERPYRIDINE METAL COMPLEXES:

UNDERSTANDING REACTION PARAMETERS AND DESIGNING NEW MATERIALS

PROEFSCHRIFT

ter verkrijging van de graad van doctor aan de
Technische Universiteit Eindhoven, op gezag van de
Rector Magnificus, prof.dr.ir. C.J. van Duijn, voor een
commissie aangewezen door het College voor
Promoties in het openbaar te verdedigen
op maandag 1 december 2008 om 14.00 uur

door

Carmen Manuela Chiper

geboren te Panciu, Roemenië

Dit proefschrift is goedgekeurd door de promotoren:

prof.dr. U. S. Schubert
en
prof.dr. J.-F. Gohy

Copromotor:
dr.ir. R. Hoogenboom

ADVANCED SUPRAMOLECULAR ASSEMBLIES BASED ON TERPYRIDINE METAL COMPLEXES:

UNDERSTANDING REACTION PARAMETERS AND DESIGNING NEW MATERIALS

Committee: Prof. Dr. U. S. Schubert (Eindhoven University of Technology)

Prof. Dr. J.-F. Gohy (Université Catholique de Louvain, Belgium)

Dr. R. Hoogenboom (Eindhoven University of Technology)

Prof. Dr. J. S. Siegel (Zurich University, Switzerland)

Prof. Dr. W. Binder (Martin Luther University Halle, Germany)

Prof. Dr. R. Sijbesma (Eindhoven University of Technology)

Părinților mei

Table of contents

Chapter I

Towards main chain metallo-terpyridyl supramolecular polymers - "The metal does the trick"

Abstract

Metallo-supramolecular chemistry offers a lot of potential for stimuli-responsive polymeric materials where the environment can have a large impact on the reversibility and strength of interactions between the individual components. The possibility of manipulating the strength of the intermolecular non-covalent bonds can result in impressive modifications of the metallo-supramolecular structure and, subsequently, produces changes in the properties of the designed material. The present chapter provides an overview on recent developments in the field of metallo-polymerization of chelating polypyridyl ligands, as introduction to the main research topic of this thesis. Synthetic strategies are described followed by discussion regarding the characterization and the application of the reviewed metallo-supramolecular structures, mainly based on terpyridines.

1.1 Introduction

Based on its versatility and nearly unlimited potential, supramolecular chemistry became a burgeoning field since the Nobel Prize has been awarded to the work of Lehn, Pedersen, and Cram in 1987 on crown ethers and host-guest interactions.[1] The availability of a large variety of supramolecular interactions having different specificities and stabilities offers unlimited possibilities to create diverse non-covalent "supra-structures", carriers of tunable and unique properties that can be used for applications in various fields.[2] Nature provides us with many inspiring examples of perfect combinations between covalent, organic and macromolecular as well as supramolecular chemistry (DNA structures, metallo-proteins, *etc.*) demonstrating that the reversibility of such structures is fundamental for the self-assembly process which allows the supramolecular systems to adapt to the local changes (enthalpically and entropically favored). The intermolecular bonds are the result of different types of interactions and, generally, they are weaker than the covalent bonds. The first example of a supramolecular main-chain polymer was based on hydrogen bonding and was reported by Lehn and his co-workers who successfully self-assembled an equimolar mixture of *bis*-uracil and 2,6-diaminopyridine.[3] It was established that the strength of a single hydrogen bond is usually too weak and highly dependent on the electronic nature of the donor as well as acceptor and, most importantly, can be tremendously manipulated by varying the solvent polarity.[4]

While the supramolecular field is continuously expanding based on the work of many research groups worldwide, we will focus in the following only on the "supra-interactions" based on metal-ligand coordination, namely terpyridine-like ligands that were reported in recent years. Many previously published comprehensive reviews clearly emphasized the importance of metallo-polymers in current research fields.[5-9] Metallo-supramolecular polymers are based on metal ions belonging to the main group (p-block), d-block (transition metal ions) as well as f-block (lanthanides and actinides). The architecture of the synthesized structures depends on the localization of the metal ion: main chain or side-chain metallo-polymers. If a polymer is only based on covalent bonds then the resulting structures are stable (that means also irreversible). For the case of non-covalent interactions, the switchability of the formed metal bond is achievable and these structures are more dynamic being able to mimic the behavior of natural supra-structures. In addition, such switchable systems offer a platform for the development of smart materials.

The aim of the present discussion is to provide an overview of recent literature on metallo-polymerization of various terpyridine-like chelating units yielding main-chain linear metallo-

homopolymers or block copolymers. For other types of metallo-supramolecular polymers, the reader is referred to previous comprehensive reviews of the metallo-polypyridyl assemblies.[10-12] Special attention will be paid to 2,2':6,2''-terpyridine ligands and related ligands as basis for various main chain metallo-supramolecular structures.

1.2 Metallo-supramolecular homopolymers

1.2.1 General aspects

Generally, metallo-supramolecular homopolymers result from the complexation of metal ions and ditopic chelating ligands (Figure 1.1). The advantage of metal-ligand coordination in comparison to other supra-interactions is its high specificity and directionality, while the toxicity of some metal ions could be seen as a drawback of the discussed concept. In comparison to hydrogen bonding, which is also specific and directional, the strength of the metal-coordination bond can be easily tuned by changing the metal ion. As shown in Figure 1.1, the chelating macro-monomer is connected by a (transition) metal ion *via* coordinative bonds resulting in a metallo-supramolecular polymer. This concept requires that the chelating monomer is a telechelic system capable of a continuous chain extension in the presence of a metal ion by following the well-known polycondensation-like mechanism.
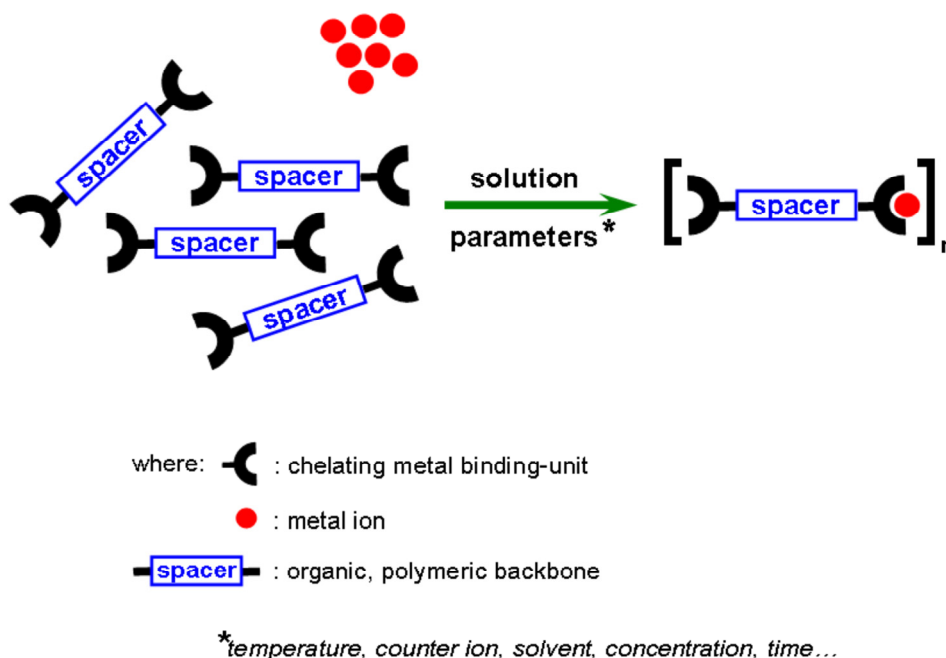
Figure 1.1: *Schematic representation of the metallo-supramolecular polymerization process.*

In an excellent review by Dobrowa and Würthner, the authors point out the major difference between classical polymers and coordination polymers (Equation 1.1): the dependence of the

degree of polymerization (DP) on the solvent and temperature dependent binding constant (K) and, related therewith, the concentration in case of coordination polymers.[13,14]

$$DP \sim (K[M])^{1/2}$$ **Equation 1.1**

The above equation (1.1) defines the advantage of the metallo-supramolecular polymerization concept: the possibility of chosing the metal-chelating ligand combination in such a way to control the binding strength (thermodynamic feature) and exchange rate (kinetic feature).

The metallo-polymerization process is mainly driven by the strength of the coordination bond between the metal ion and the chelating unit from the supramolecular ligand. The nature of this interaction is predominantly donation of a lone electron pair of the ligand (Lewis base) to the metal ion (Lewis acid) combined with electrostatic attractions between the formed positively charged metal ion and the negatively polarized/charged donor atom of the ligand.[15]

To generate high molar mass metallo-supramolecular polymers special attention has to be paid to several important factors that can be used to influence the polymer ***during*** but also ***after*** the construction of the metallo-supramolecular assemblies. The possibility of altering the polymeric structure of the polymer after its preparation represents a significant advantage compared to covalent polymers. These factors are briefly discussed in the following:

• *Chelating ligand*

The design of the telechelic chelating ligand contributes strongly to the final strength and architecture of the metallo-supramolecular structure. Moreover, the design of the spacer dictates the properties and structure of the newly designed metallo-supramolecule: linear or cyclic, high or low molar mass, soluble or insoluble, symmetric or asymmetric.

• *Metal ion (transition and lanthanide)*

Each metal ion is characterized by an individual binding strength and an exchange rate; by a simple variation of the metal ion, different stabilities of the targeted metallo-supramolecular assemblies can be achieved. Moreover, different geometries are available since the coordination of the transitional metal ions varies from, *e.g.*, linear, trigonal-planar, T-shaped, tetrahedral, square-planar, square-pyramidal, octahedral, trigonal-prismatic, pentagonal-bipyramidal to trigonal-bipyramidal. For the case of the lanthanide ions that are characterized by a larger atomic radius, the possibility of higher coordination numbers from 7 to 10 offers further opportunities for designing new architectures.

• *Counter ion*

Due to the fact that counter ions are involved in the vicinity of the positive metal ions, their presence affects the morphology of the metallo-supramolecular assembly, in particular in the solid state. Moreover, the size of the counter ions can determine the spatial arrangement of the synthesized metallo-supramolecular structure. On the other hand, in solution, the characteristics of the counter ion (*e.g.* hydrophobicity, hydrophilicity) can dramatically influence the solubility of the final metallo-supramolecular assembly. In this respect, it is known that a simple ion exchange can result in a significant change in solubility. Moreover, the ionic interactions between the charged species can furthermore contribute to the assembly processes.

• *Solvent*

The solvent plays an important role in the preparation of high molar mass metallo-assemblies taking into account that the solvent can compete during the synthesis with the chelating ligand in "catching" the available metal ions or can dramatically influence the rearrangement of the intermediary reaction product leading to the formation of the most stable reaction product. Moreover, the solvent can influence the stability of the resulting metallo-supramolecular structures, in particular in the case of weak metallo-complexes.

• *Temperature*

Depending of the considered ligand-metal ion system, variation of the temperature during the preparation could bring important modifications into the structure of the aimed metallo-supramolecular polymers (in particular on the modification of the intermediate defect structures). Furthermore, the temperature has an important role on influencing the balance between thermodynamic stability and kinetic lability of the synthesized metallo-supramolecular assemblies.

• *Concentration*

Since the metallo-polymerization approach follows a polycondensation mechanism, high degrees of polymerization are only achievable at high concentrations of the monomers. Moreover, a high concentration can influence the architecture of the final supramolecule which can be linear or cyclic. Special attention has to be paid to the stoichiometry of the reaction components which has to be precisely 1:1, when aiming for high molar mass materials.

The aim of synthesizing metallo-supramolecular structures is to create novel materials that can reveal specific and multifunctional properties (Figure 1.2). The building blocks should therefore be carefully selected in order to create new materials with tunable and tailored

properties. Beside the use of low molar mass ditopic "organic" ligands, telechelic polymers bearing suitable ligands at their extremity are extremely valuable candidates for the formation of metallo-supramolecular polymers. In this way, the properties of the designed materials can be manipulated not only by the careful choice of the metal ions, but also by the polymer backbone (Figure 1.2). This allows the formation of materials synergistically combining the characteristic features of the metal ligand complexes (special electrochemical, optical, magnetic properties) to the ones of polymers (processability, mechanical properties, solubility, *etc.*).
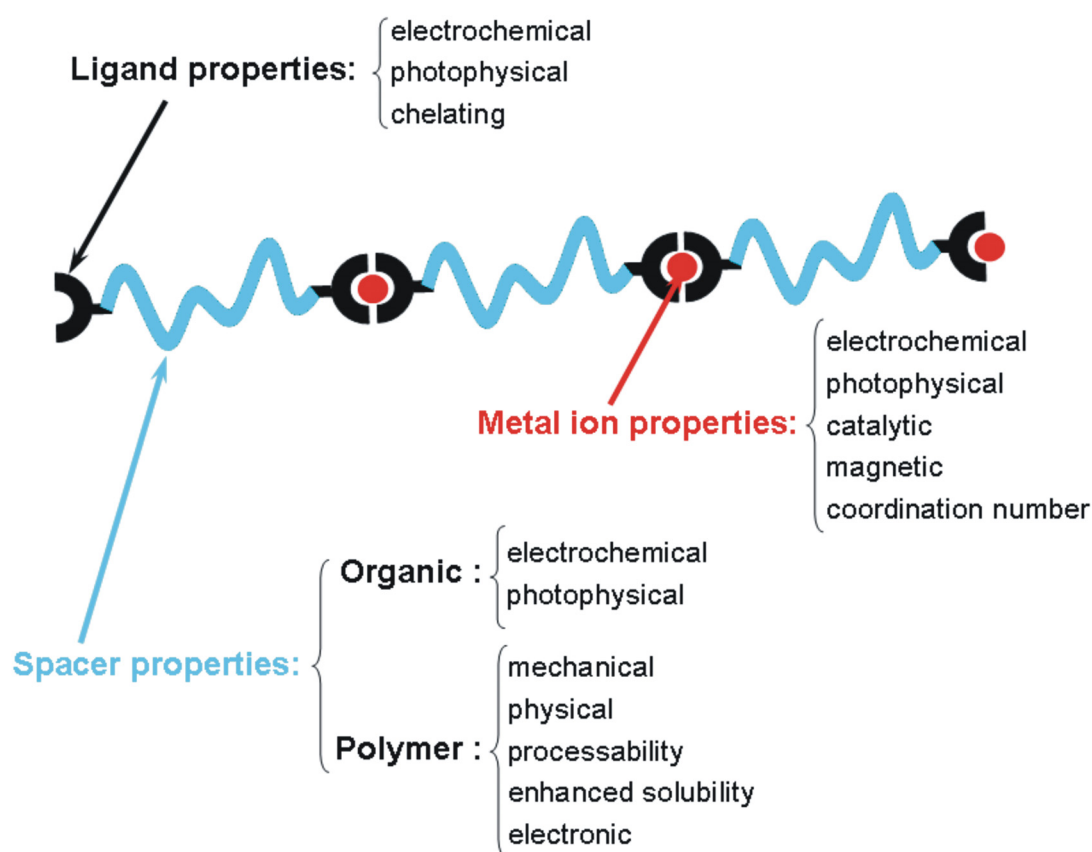
Figure 1.2: *Schematic overview of the properties of metallo-supramolecular polymers.*

1.2.2 Inert metallo-supramolecular homopolymers based on terpyridine units

The experimental efforts performed for the incorporation of inert transition metal ions in low oxidation state such as ruthenium(II), osmium (II), nickel(II) and iridium(III) can be explained by the fact that the resulting structures generally combine high thermal, chemical and photochemical stability with interesting (electro)-optical and magnetic properties. Moreover, their high stability due to formation of kinetic inert coordinative bonds provides the possibility to characterize this type of structures by means of various techniques, such as *e.g.* size exclusion chromatography (SEC).

Rehahn *et al.*[16] pioneered the field of metallo-supramolecular polymers based on terpyridine chelating ligands almost 10 years ago (for earlier examples based on bipyridines, see *e.g.* ref. 17). The most well-known example of metallo-chain extended polymerization was presented by his research group. A soluble metallo-supramolecular polymer based on Ru(II)tpy$_2$ connectivity that was prepared following two different synthetic routes: 1) the coordination of the telechelic terpyridine ligand with an activated Ru(III) species and 2) Pd-catalized polycondensation of the Ru(II) *bis*-terpyridine complex bearing halogen functionality with a diboronic acid (Scheme 1.1). The comparison of the final reaction products by means of viscosimetry and ^{1}H-NMR spectroscopy showed that method 1 led to high molar masses species in comparison to method 2, which produced only oligomeric structures.
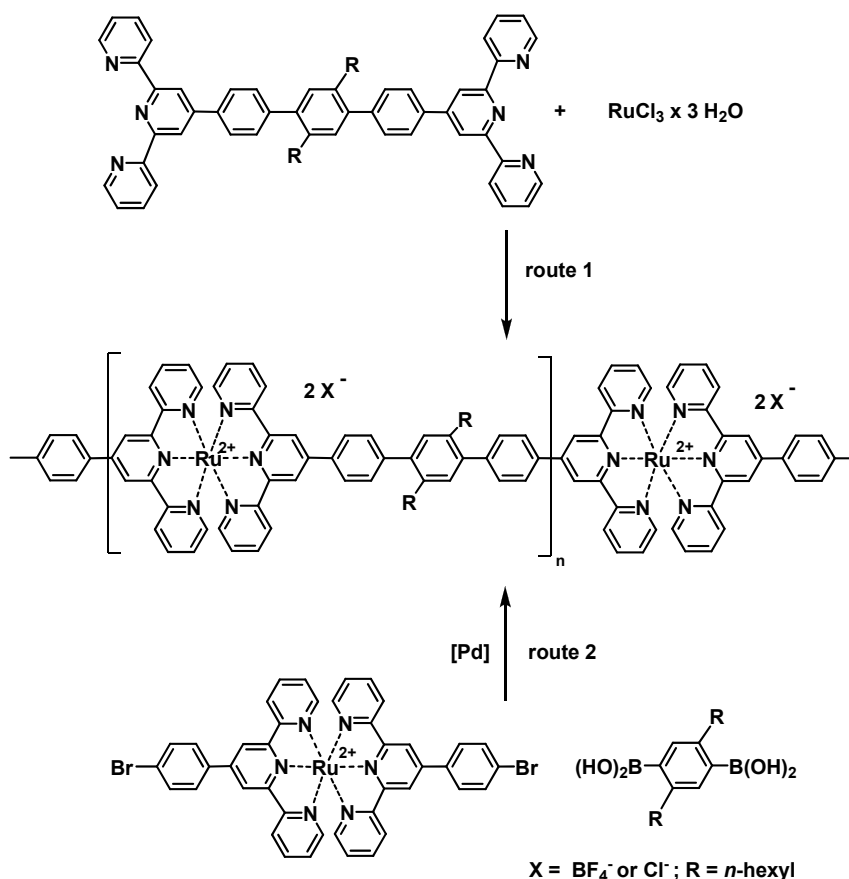
Scheme 1.1: *Schematic representation of the synthesis of Ru(II) chain extended polymers via two different routes.[16]*

Due to their inert characteristic, these assemblies were used as model systems to study the polyelectrolyte behavior since their rigid conformation is limiting the conformational degrees of freedom in solution. By using a combination of spectroscopic techniques, it was demonstrated that in the case of rod like metallo-supramolecular polymers, the counter ions

interact preferentially with the polyion and their spatial distribution reflects the spatial distribution of the charges on the polyion (Figure 1.3).[18]
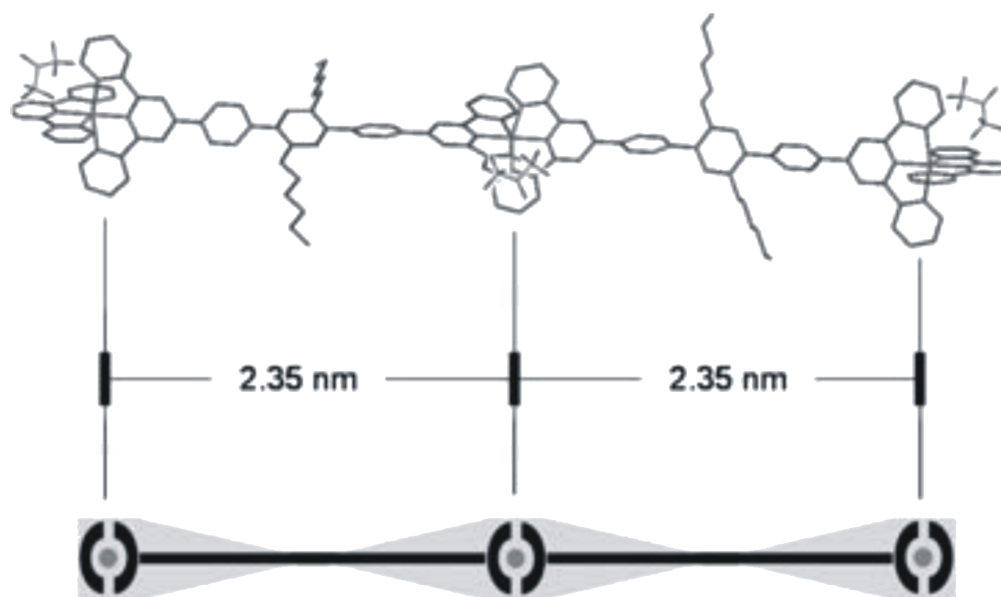
Figure 1.3: *Reprinted image showing the schematic representation of possible localized binding FS (Fremy's salt) to Ru(II) centers in a Ru(II)tpy$_2$-coordination polymer.[18]*

The formation of a metallo-*bis*-terpyridine complex is influenced by two key complexation factors. The first factor is the formation of the *mono*-terpyridine *mono*-complex by combining one terpyridine ligand with one metal ion. In the second step the metallo-*bis*-terpyridine complex is formed by adding another terpyridine ligand into the system. The possible exchange in solution between the ligand, metal ion, *mono*-complex and *bis*-complex is comprehensively described by Kurth *et al.* for terpyridine metallo-supramolecular structures.[19,20] By using rigid, π-conjugated, *mono*-(or *poly*)phenylenes *bis*-terpyridines and transition metal ions such as Ru(II) a large number of metallo-supramolecular polyelectrolytes (MEPEs) were prepared (Figure 1.4).[21,22] The attractive optical, electrochemical and electrochromic properties of the synthesized metallo-suprastructures could be easily investigated due to their good solubility in different solvents including water. Furthermore, conclusions on the structure-property relationship of the designed structures could be drawn. The study revealed important insights concerning the design of electrochromic materials: the switching rates and stability of metallo-supramolecular polyelectrolytes (MEPEs) are influenced by the electronic character of the substituents located on the external pyridine ring of the ligands. Electron-donating groups generate faster switching rates, while electron-withdrawing groups lower the rates and decrease the stability. The optical properties are affected mainly by steric factors near the metal center. Bulky groups enhance the optical

memory by protecting the metal center from being reduced and larger conjugated spacers linking the terpyridine moieties result in an increased molar absorbance of the MLCT.
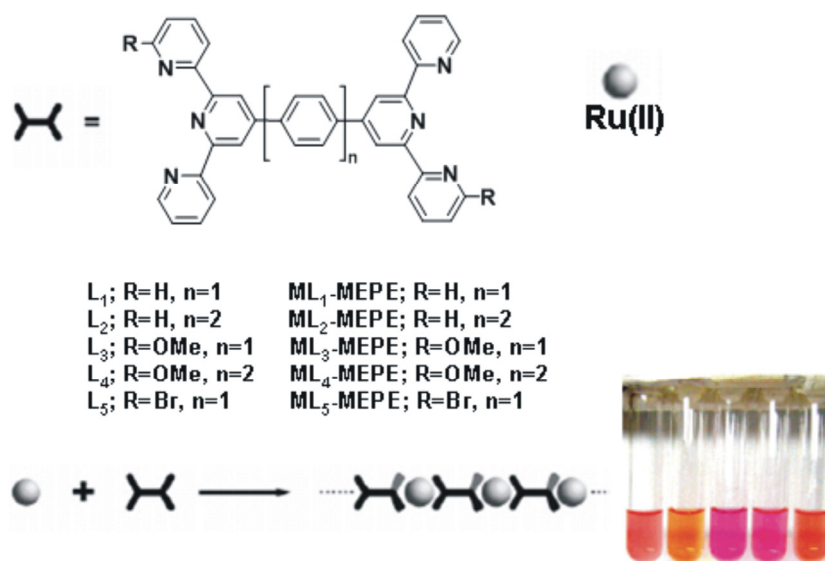
Figure 1.4: *Schematic representation of the synthesis of metallo-supramolecular polyelectrolytes based on Ru(II)tpy₂ connectivity.[21,22]*

Schubert *et al.*[23-25] focused on the synthesis and characterization of chain extended polymers based on Ru(II)tpy₂ connectivity by varying the spacer from oligomers to polymers ones (Scheme 1.2). The utilization of different chemical approaches was also part of the investigations.[23]
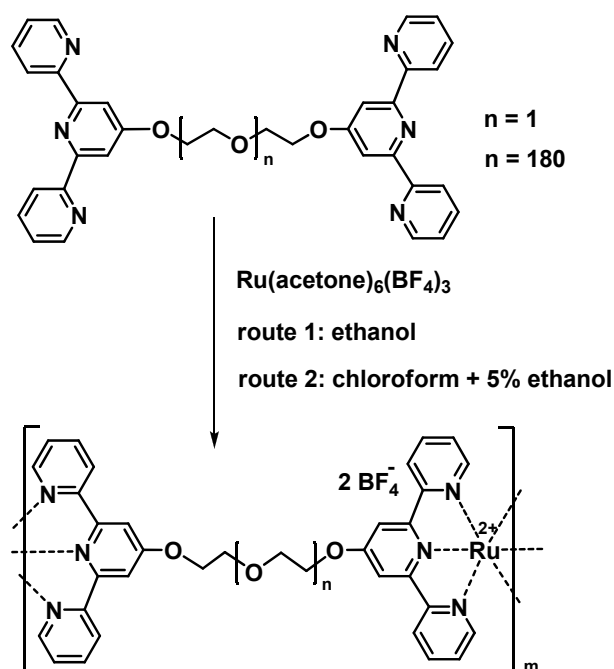
Scheme 1.2: *Schematic representation of the synthesis of metallo-supramolecular polyelectrolytes based on Ru(II)tpy₂ connectivity.[23]*

It was found that the length of the spacer is important for the formation of linear or cyclic species and, thus, the degree of polymerization could be varied. The polymeric nature was proven by the film-forming properties of the resulting Ru(II) coordination polymers and confirmed by viscosity measurements. To suppress the polyelectrolyte effect of the poly-charged Ru(II) coordination polymer, the addition of different concentrations of salt was required for the viscosity experiments. Atomic force microscopy (AFM) imaging revealed a lamella organization of the polymer chains. Further studies to determine the molar mass were performed by analytic ultracentrifugation and SEC.[24,25]

Generally, for this type of structures, classical characterization techniques are challenging. To determine the molar mass of these metallo-suprapolymers, apart from ^{1}H-NMR spectroscopy, SEC is one of the most used characterization tools for polymers. In the case of strong metal-ligand interactions (as here the discussed Ru(II)tpy$_2$ complexes), the main difficulty met in the application of SEC is the fragmentation of the complex during the measurement. However, after the optimization of the SEC conditions, the method proved to be suitable for the evaluation of metal-containing supramolecular homo and block copolymers based on metal ions with high-binding strength (*e.g.* Ru(II)).[24,26]

Recently, the group of Schubert further extended the possibility of SEC characterization for other metallo-*bis*(terpyridine) homopolymers.[27] The results revealed that the Ni(II)tpy$_2$ connectivity behaves as an inert system and, therefore, SEC proved to be a suitable characterization technique. Moreover, chain extended polymerization was performed on low molar mass telechelic terpyridine PEG leading to the formation of high molar mass Ni(II) suprapolymers. Due to the paramagnetic nature of Ni(II) ions, ^{1}H-NMR spectroscopy could not be used as alternative characterization method. Thus, for the moment Ni(II)tpy$_2$ homopolymers remain challenging from the analysis point of view.

1.2.3 Labile metallo-supramolecular homopolymers based on terpyridine units

In the case of weaker metal-ligand interactions, such as *e.g.* iron(II), zinc(II), cobalt(II) or lanthanides, in combination with terpyridine ligands, the lability of the synthesized metallo-structures is increased in comparison to the inert complexes described in section 1.2.2. Thus, the main difficulty for these systems is their characterization which has to be adapted to the specific features of the created metallo-ligand connectivity.

Schubert *et al.* reported a large variety of labile metallo-terpyridine supramolecular polymers for characterization studies.[28-30] It was concluded that for more dynamic systems, such as *e.g.* Fe(II) and Co(II) terpyridine complexes, their characterization can not be performed by

SEC.[27] The formation of high molar mass coordination polymers based on *bis*-terpyridine PEG (M_n = 8,000 g/mol) was studied with various transition metal ions (Scheme 1.3). The experimental results of the study proved the influence of different metal ions, such as *e.g.* cadmium(II), copper(II), cobalt(II), nickel(II), iron(II) on the degree of polymerization, and the resulting molar masses were analyzed. The polymers were characterized in detail utilizing ^{1}H-NMR, UV-Vis spectroscopy, matrix-assisted laser desorption/ionisation-time of flight mass spectrometry (MALDI-TOF-MS) and viscosity measurements. The molar mass was estimated on the basis of concentration-dependent viscosity measurements. The relative viscosity results can be qualitatively correlated to the thermodynamic stability of the metallo-*bis*-terpyridine complexes. Thus, the relative viscosity drops in the cases of cadmium(II), copper(II), and cobalt(II) ions, decreases much less for iron(II) and for the case of nickel(II) ions a plateau is reached that is almost independent of the amount of added metal salt. These observations also correspond qualitatively to the thermodynamic stability of the metallo-*bis*-terpyridine complexes.[31,32]
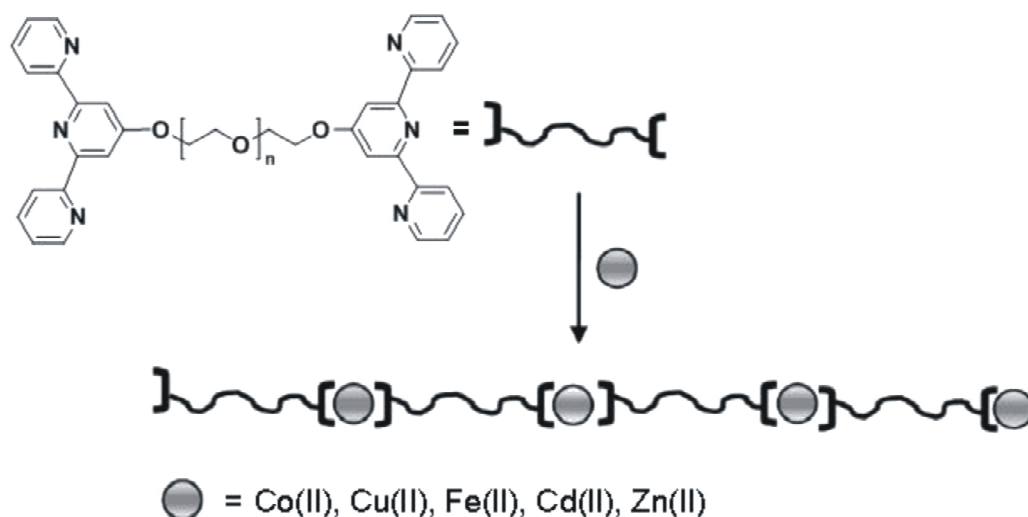
Scheme 1.3: *Schematic representation of the synthesis of metallo-chain extended polymers described by Schubert et al.[28]*

The same group also reported the combination of hydrogen bonds and metal-ligand coordination (Scheme 1.4).[33] Thus, by using a hydroxy-functionalized terpyridine as initiator, a *mono*-terpyridine poly(ε-caprolactone) ligand was synthesized by tin octanoate-catalyzed ring-opening polymerization of ε-caprolactone. The ω-hydroxy group of the resulting ligand was subsequently reacted with an isocyanato-ureidopyrimidinone, yielding polymers bearing a metal-coordinating unit at one end and a hydrogen-bonding moiety on the other side. The addition of metal ions such as Fe(II) or Zn(II) resulted in the formation of high molar mass supramolecular chains extended polymers with new properties as a result of the combined

types of non-covalent interactions in the main chain. The existence of the resulting supramolecular materials could be proven by means of detailed studies of capillary viscosimetry and rheometry. Two factors were important for the degree of polymerization: the hydrogen bonding moiety and the terpyridine complex. In comparison to the linear coordination polymers based on Fe(II)tpy$_2$ or Ru(II)tpy$_2$ connectivity (with an almost linear dependency of the relative viscosity on the concentration), an exponential behavior was found for the Fe(II) chain-extended polymer, revealing a strong dependence of the chain length with the concentration which is a typical behavior for hydrogen-bonded polymers.[33] For the case of the Zn(II) chain-extended polymer the viscosity measurements revealed lower values compared to the corresponding polymer based on Fe(II) ions. This result can be attributed to the more labile character and lower binding strength of Zn(II) ions compared to Fe(II) ions. Detailed rheometry studies revealed improved material properties of the Fe(II) and Zn(II) supramolecular polymers compared to the precursors and a strong influence of the metal ions as well as the counter ions to the properties in bulk.
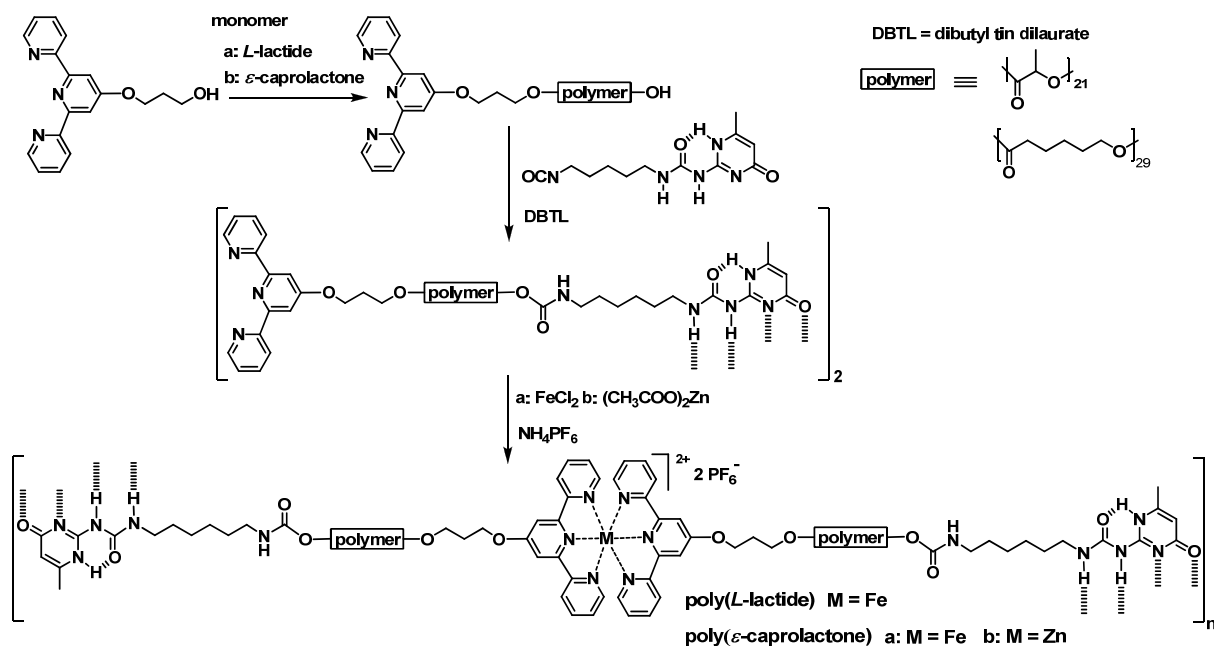
Scheme 1.4: *Schematic representation of the synthesis of metallo-chain extended polymers described by Schubert et al.[33]*

Kurth *et al.*[34,35] studied the metallo-polymerization with labile transition metal ions such as *e.g.* Fe(II), Co(II), Zn(II) of telechelic terpyridine ligands bearing short (aromatic) spacers. The synthesized structures revealed strong polyelectrolyte properties and displayed further self-assembly into a layered architectures with anionic polymers (Figure 1.5). Moreover, by

simple exchange of the counter ions, metallo-amphiphilic polyelectrolyte complexes were achievable.
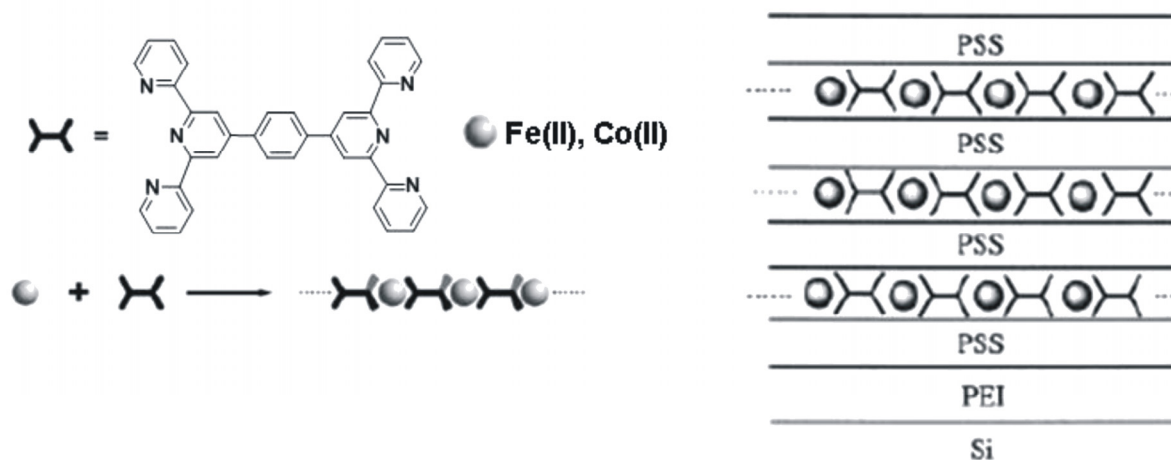
Figure 1.5: *Reprinted image of the assembly of multilayers by sequential deposition of oppositely charged polyelectrolytes. PEI = polyethyleneimine, PSS = poly(styrene sulfonate).[35]*

The same group polymerized π-conjugated, *mono*-(or *poly*)phenylene ring functionalized *bis*-terpyridines (discussed in 1.2.2; Figure 1.4) with transition metal ions such as Fe(II) or Co(II), which allowed a tuning of the optical, electrochemical and electrochromic properties of the obtained metallo-supramolecular polyelectrolytes (MEPEs).[21,22] An important feature of these synthesized materials is the color that can be easily modified covering the whole visible region through the design of the ligands or the choice of the metal ions. This interesting property can be used for electrochromic applications. Moreover, the experimental results showed that the stability of the MEPEs is mainly driven by the ligand, which can be explained by the electronic nature of the substituents of the external pyridine ring from the terpyridine ligand. The optical response due to the combination ligand (with variation of the substituents) and metal ion can be easily observed by the different colors displayed by MEPEs. For the case of Fe(II)-MEPEs the color varied from dark-blue to purple, blue, sky-blue, and grass-green. In the case of Co(II)-MEPEs the colors were orange, red, yellow, and pale-yellow, respectively. Intermediate colors could be obtained by mixing different MEPEs in appropriate ratios. Apparently, the interactions between the ligands and the metal ions were strengthened by electron-rich OMe groups. In contrast, an electron-deficient substituent weakened the coordination between the ligands and metal ions inducing deterioration during the redox processes.

Recently, Kurth *et al.*[36] also reported the synthesis of cross-linked metallo-supramolecular polyelectrolytes (MEPEs) based on Fe(II)tpy$_2$ connectivity, as shown in Scheme 1.5. Detailed studies performed on those structures showed that the molar mass of the networks is large and depends on the cross-linking degree. The coordination networks were synthesized with various degrees of cross-linking. It was found that between 1.5% and 9% cross-linking degree, the networks were soluble in water and acetic acid solutions. For higher cross-linking degrees (larger than 9%) the solutions were heterogeneous with a colored solid precipitating from solution.[36] Due to the presence of charges in the MEPE, the soluble networks are suitable systems for film formation on the basis of layer-by-layer self-assembly and, therefore, it is possible to study the details of the film growth. UV-Vis spectroscopy, X-ray reflectivity, AFM, and ellipsometry indicate that the film growth was linear and continuous.
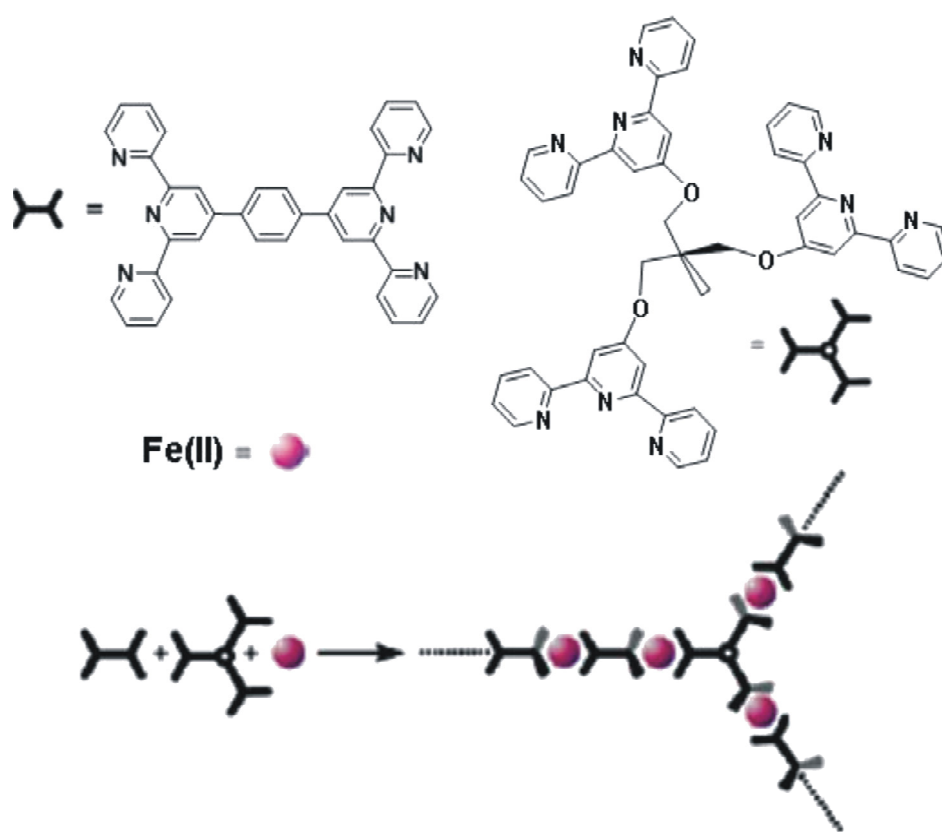
Scheme 1.5: *Schematic representation of the synthesis of metallo-supramolecular coordination polyelectrolytes (MEPEs) based on Fe(II)tpy$_2$ connectivity.*[36]

Würthner *et al.*[37] studied in detail the thermodynamics of the complexation between terpyridine ligands and Zn(II) ions. The research results concluded that Zn(II) ions offer an interesting balance between the reversibility of the complexation process and the stability of the designed structures due to high binding constants. Moreover, Würthner and his co-

workers prepared telechelic terpyridine ligands bearing an organic fluorophore spacer (Figure 1.6).
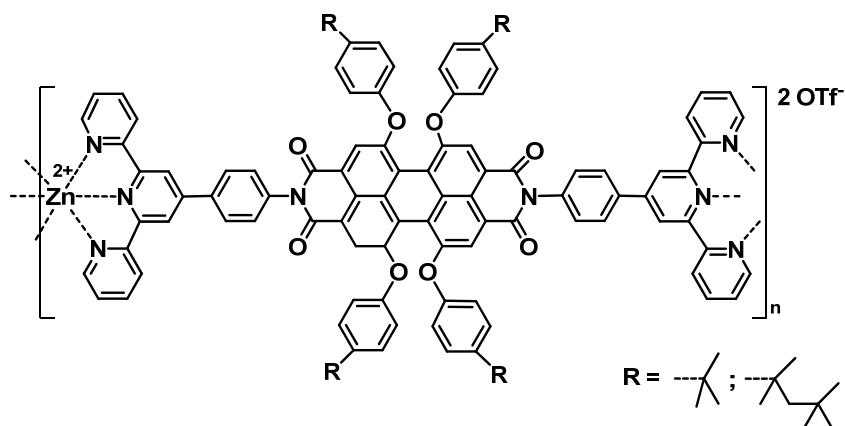
Figure 1.6: *Schematic representation of the Zn(II) terpyridine supramolecular polymers containing a bisimide fluorophore synthesized by Würthner et al.[40]*

These type of macro-monomers were subsequently polymerized with Zn(II) ions. The obtained metallo-supramolecular Zn(II) polymers revealed the influence of the metal ion on the electroluminescent properties of the synthesized metallo-assemblies.[38,39] The structures were assigned by NMR (^{1}H and DOSY) spectroscopy, AFM as well as fluorescence spectroscopy.[40] These synthesized Zn(II) coordination polymers revealed very good fluorescent properties (very strong red-light emitting) with the potential to be incorporated into layered polyelectrolyte devices.

Che *et al.*[41] also studied the incorporation of Zn(II) ions through polycondensation of *bis*-terpyridine ligands bearing various π-conjugated architectures of the spacer (Figure 1.7). The resulting Zn(II) coordination polymers were characterized by means of ^{1}H-NMR spectroscopy, viscosity, photophysical and electrochemical methods. The synthesized Zn(II) chain extended polymers exhibited violet to yellow light emission. Moreover, these materials showed high luminescence and good thermal stabilities. The electroluminescence in the blue region was encouraging enough to conclude that these types of materials have the potential to become high-performance emissive or host materials for electroluminescent devices.
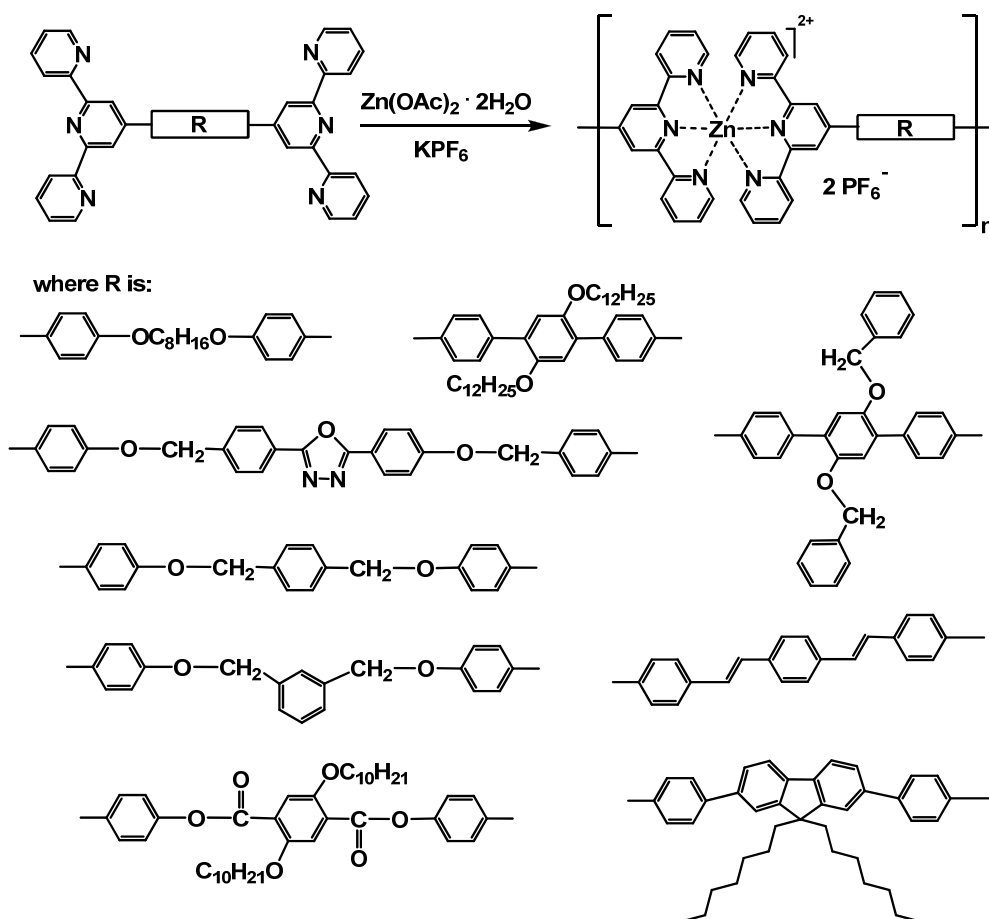
Figure 1.7: *Schematic representation of the Zn(II) coordination polymers prepared by Che et al.*[41]

Chen *et al.*[42,43] followed the same strategy of incorporating *bis*-terpyridine ligands bearing chromophores or π-conjugated spacers into polymeric structures *via* Zn(II) polymerization (Scheme 1.6). The photophysical properties revealed once again the efficiency of the utilized Zn(II)tpy$_2$ connectivity. These polymers exhibited blue photoluminescence (PL) emissions (around 420 nm) with quantum yields of 11 to 23% (in DMF) and the PL results revealed that the formation of excimers were suppressed by the incorporation of carbazole pendant groups. In addition, the electroluminescence emission (EL) results showed green EL emissions (around 550 nm).
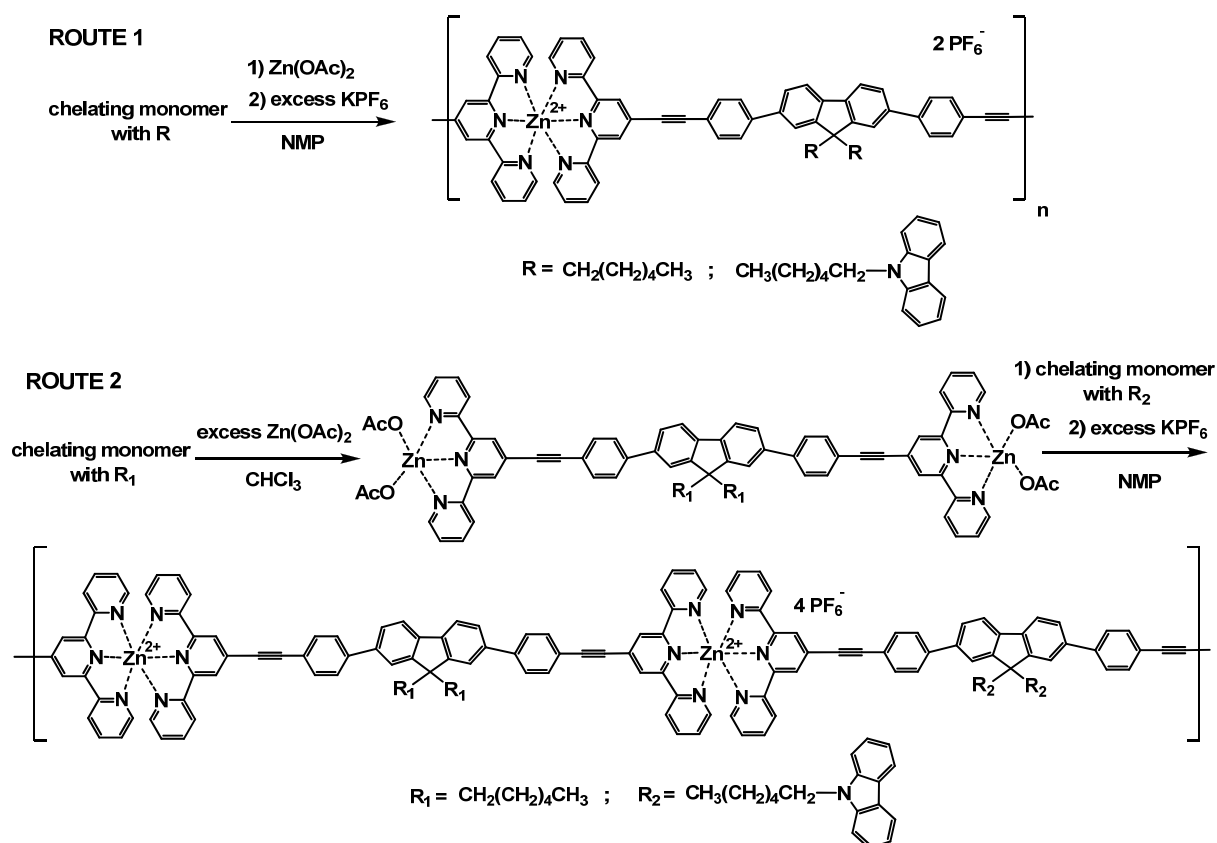
Scheme 1.6: *Schematic representation of the synthesis of Zn(II) homopolymers (route 1) and Zn(II)-alt-copolymers (route 2) by Chen et al.*[42,43]

1.3 Advanced metallo-supramolecular structures

1.3.1 AB$_n$A metallo block copolymers based on terpyridine ligands

As already mentioned, the formation of metallo-supramolecular polymers and block copolymers is greatly affected by the reaction conditions such as the stoichiometry of the reactants, the type of solvent and salt, the temperature and concentration.

A straightforward approach for the synthesis of AB$_n$A block copolymers *via* Ru(II) terpyridine complexation has been described by Schubert *et al.*[44] (Scheme 1.7). The applied combinatorial optimization approach allowed a systematic screening to identify the best reaction condition for the one-pot polymerization of *bis*-terpyridine-hexadecane with RuCl$_3$ under reductive conditions.

In addition, the gained knowledge was further applied to the designed synthesis of a Ru(II)AB$_n$A supramolecular triblock copolymer utilizing a *mono*-terpyridine-poly(ethylene glycol) as a chain stopper during the metallo-polycondensation-reaction of *bis*-terpyridine-hexadecane. The resulting Ru(II)AB$_n$A triblock copolymer could be characterized by means of ^{1}H-NMR and UV-Vis spectroscopy as well as SEC. The amphiphilicity of the synthesized

structures was proven by the formation of micelles in water which were investigated by dynamic light scattering, atomic force microscopy, as well as transmission electron microscopy.
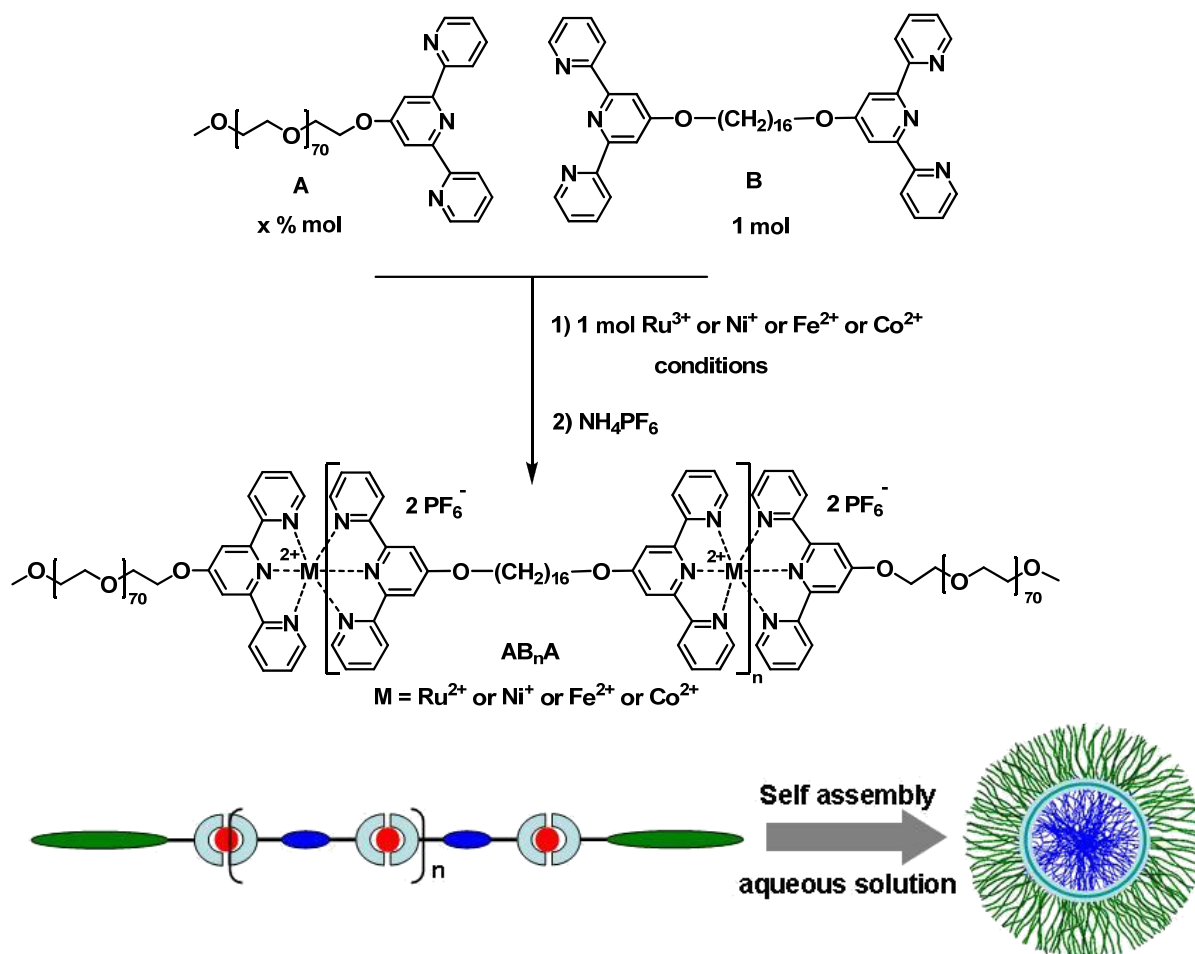
Scheme 1.7: *Schematic representation of the synthesis of the M(II)AA, B_n and AB_nA (block co)polymers.*[44,45]

The concept was later expanded to other transition metal ions, namely to Ni(II), Fe(II), and Co(II). The formation of AB_nA supramolecular triblock copolymers based on Ni(II)tpy$_2$, Fe(II)tpy$_2$ and Co(II)tpy$_2$ connectivities was studied by using individually optimized synthetic approaches and characterization methods, according to the metal ion used. In addition, for the case of Ni(II)AB_nA supramolecular triblock copolymers variation of the end capper was performed in order to vary the length of the middle block B, that could be proven by SEC. Further micellization studies showed that the new synthesized materials self-assemble in aqueous solution due to their amphiphilicity.[45]

1.3.2 Metallo polymers based on terpyridine related ligands

Rowan, Weder *et al.*[46-53] developed the concept of photoactive mechano-responsive gels based on the use of a *bis*-terpyridine related ligand, namely 4-functionalized-pyridine *bis*(2,6-*bis*(1'-methylbenzimidazolyl) (HO-BIP) (Figure 1.8). The interesting aspect of this concept is that the studied ligands can form 2:1 metal complexes with transition-metal ions and 3:1 complexes with lanthanide ions; therefore it is possible to create gels by mixing the telechelic chelating ligand with a combination of lanthanoid (cross-linker) and transition metal (chain extender) ions, respectively.
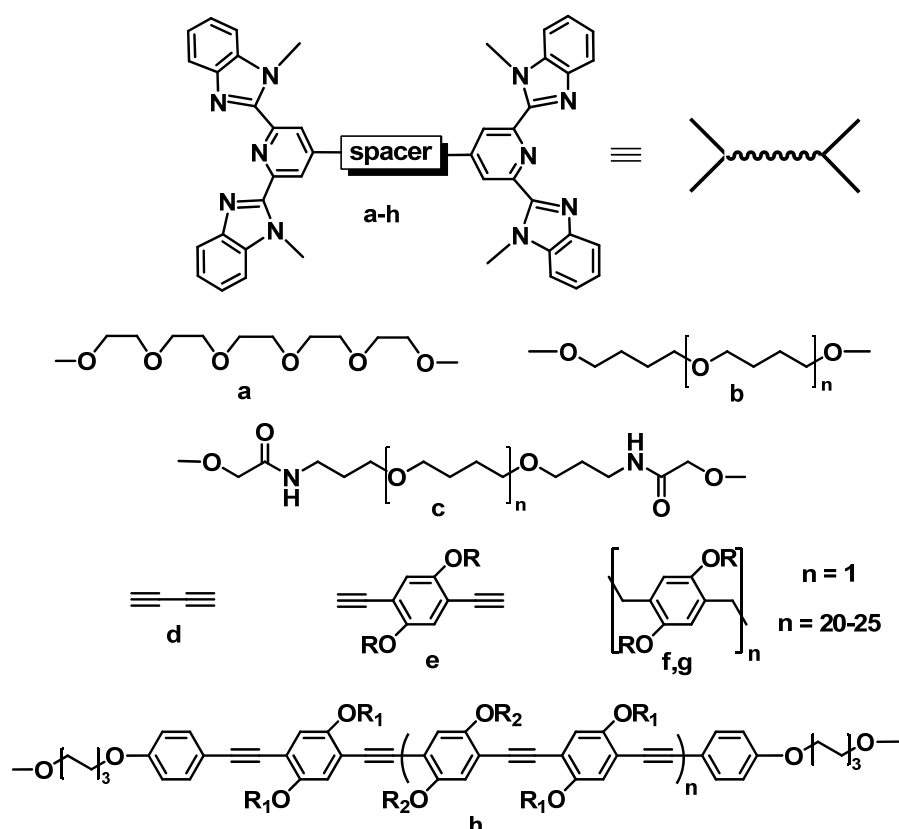
Figure 1.8: *Schematic representation of the ditopic ligands published by Rowan et al.[46]*

Taking into account that lanthanides are weaker binding metal ions compared to the transition metal ions, the metal complexes based on lanthanides could be successfully treated as switchable branching points, which were able to give a response upon changing the temperature or mechanic stress. Addition of lanthanoid metal ions (<5 mol% per ligand) followed by the addition of transition metal ions (>95 mol% per ligand) to a solution of the telechelic chelating monomer yielded the formation of metallo-supramolecular gels (Figure 1.9). These gels exhibited responses to thermo, chemo (with formic acid) and mechanical stimuli. The mechano-responsive nature of the metallo-polymer based on Zn/La gel exhibited

a thixotropic (shear-thinning) behavior. Shaking the gel resulted in the formation of a free-flowing liquid, which upon standing for a approximately 20 seconds yielded in the reformation of the gel-like material. Moreover, it was found that the lanthanide gels exhibited very strong luminescence properties based on the energy transfer from the ligand to the metal ion (*e.g.* Eu(III)). This phothophysical property could be interrupted by heating or mechanical stress and, subsequently, the luminescence color changed from red to blue, the emission being then attributed to the ligand center.
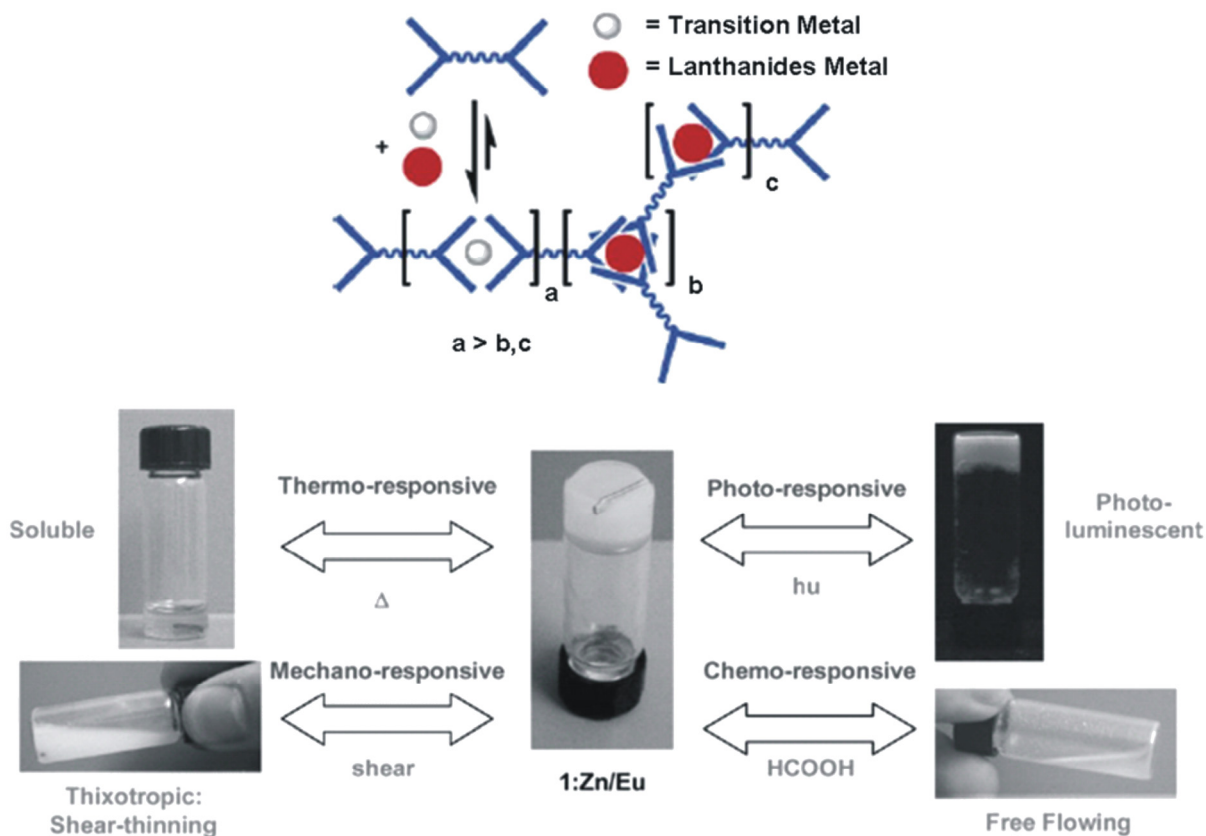
Figure 1.9: *Image reprinted from ref. 43 showing the concept developed by Rowan et al.*

Another terpyridyl analogous back-to-back ligand was developed and studied by Ruben *et al.*[54] The linear building block ligand 1,4-*bis*(1,2':6',1"-*bis*-pyrazolylpyridin-4'-yl)benzene was prepared by Suzuky cross-coupling, which was subsequently converted into a linear Fe(II) coordination oligomer/polymer (Scheme 1.8). The synthesized and characterized metallo-supramolecular polymer exhibited a reversible spin transition (ST) above room temperature with a wide hysteresis loop (aprox. 10 K), as proven by magnetic and Mössbauer studies.
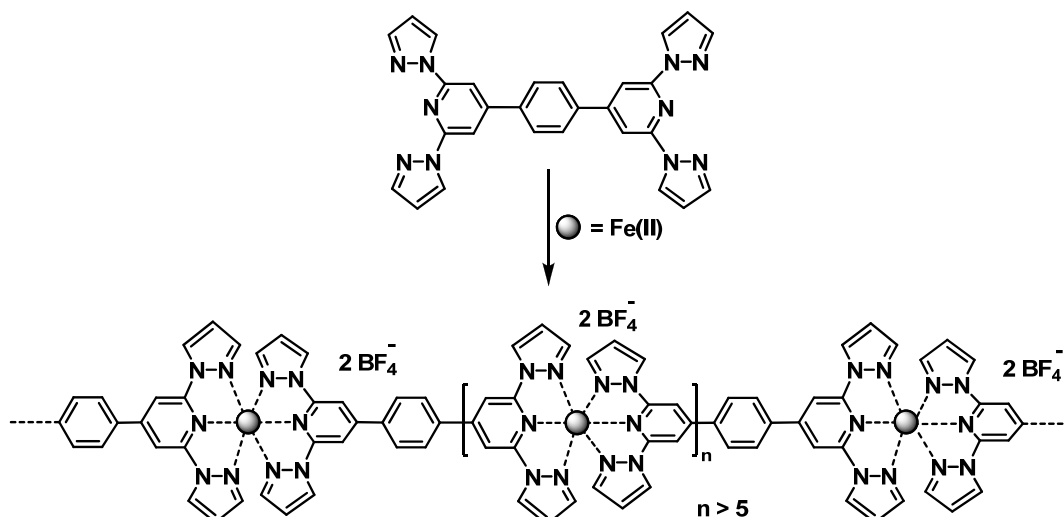
Scheme 1.8: *Schematic representation of an Fe(II) coordination polymer synthesized by Ruben et al.[54]*

Hecht *et al*[55,56] synthesized poly[(1,2,3-triazol-4-yl-1,3-pyridine)-*alt*-(1,2,3-triazol-1-yl-1,3-phenylene)]s *via* a step-growth polymerization using Cu-catalyzed 1,3-dipolar cycloaddition reactions ("click chemistry", Figure 1.10).

anti-anti
helically folded polymer

syn-syn
metallo-supramolecular crosslinked gel
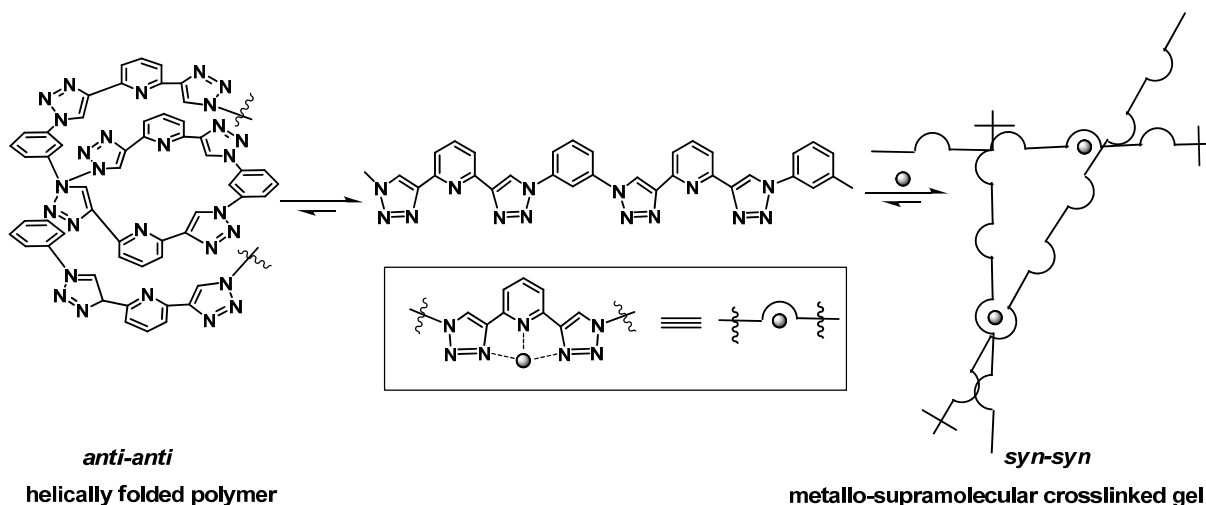
Figure 1.10: *Schematic representation of the metallo-chain extended polymers based on 2,6-bis(1,2,3-triazol-4-yl)pyridine (BPT) chelating units.[55,56]*

It was found that the repeating unit 2,6-*bis*(1,2,3-triazol-4-yl)pyridine named BTP had a strong preference to adopt an *anti-anti* conformation and, therefore, the extended heteroaromatic polymer strands adopted a helical conformation which was proven by circular dichroism (CD) spectroscopy. The addition of Fe(II), Zn(II) and Eu(III) metal ions led to instantaneously gel formation as a result of the coordinative cross-linking of the polymer chains.

1.4 Aim and outline of the thesis

Nowadays, polymers containing supramolecular binding units are synthetically accessible. The combination of macromolecular and supramolecular chemistry opens unexplored avenues to obtain new functional materials that can be designed for a specific application.

Supramolecular materials can be constructed *via* a large number of weak and reversible non-covalent interactions (*e.g.* hydrogen bonding, metal coordination, π-π or host-guest interactions, electrostatic effects, solvophobic or van der Waals forces). All of these non-covalent interactions have certain advantages and disadvantages. Concerning metal-ligand interactions, the adjustability of their binding strength in a rather broad range as well as their directionality can be considered as major advantages, whereas the toxicity of some transition metal ions represents obviously a disadvantage. One of the often used chelating ligands in the current research of metallo-supramolecular chemistry is 2,2':6,2"-terpyridine (tpy) and its derivatives. The main interest for metallo-terpyridine "supra-structures" is the large possibility of combinations between various polymers bearing the terpyridine moiety and a wide range of transition metal ions. In this way, novel materials with tunable properties which combine at the same time the polymer properties with the characteristics offered by the metal-ligand coordination can be synthesized.

The aim of this thesis is the functionalization of 2,2':6,2"-terpyridine (tpy) units with various polymers (or organic molecules) in the 4'-position, followed by the metal complexation of the terpyridine moiety in order to design various metallo-supramolecular polymer architectures. Special attention is offered to the transition metal ions since their different binding strengths and stabilities towards terpyridine ligands offer possibilities for constructing materials having tunable properties. Thus, by varying the metal ion and the available terpyridine functionalized polymers, homo- and heteroleptic *bis*-terpyridine supramolecular assemblies can be synthesized. The resulting "supra-structures" containing M(II) *bis*-terpyridine connectivity are studied in detail with respect to their stabilities, photochemical, photophysical and self-assembly properties in solution.

The present dissertation thesis is divided in six sections:

Chapter I reviews the metallo-supramolecular polymerization of terpyridines and its derivatives resulting in main-chain metallo-supramolecular polymers. An overview is provided for the synthesis and the properties of metallo-polymers incorporating tridentate terpyridine-type ligands and analogous chelating units, by using various transition metal ions.

Special attention is paid to the incorporation of the metal-complexes into the polymer backbone and the properties of the designed materials.

Chapter II deals with the terpyridine post-functionalization of polymers/or small molecules in order to create chelating building blocks for metallo-complexation. The large possibilities for the functionalization of terpyridine ligands in the 4'-position allows a straightforward access to the various supramolecular monomers and polymers.

Chapter III focuses on the diversity of metal-ligand interactions, which vary from very strong to very weak according to the combination of metal ions and ligands used. Therefore, the synthesized metallo-*bis*-terpyridine complexes exhibit different stabilities and their characterization has to be adjusted. For this reason SEC stability studies are performed on Ni(II), Fe(II) and Co(II) *bis*-terpyridine poly(ethylene glycol) model systems. With the gained insights regarding the stability of the mentioned structures, metallo-polymerization is performed on the most stable system besides Ru(II), namely Ni(II)tpy$_2$. Furthermore, the synthesis of A-*b*-B-*b*-A triblock copolymers based on a M(II)tpy$_2$ connectivity with the Ni(II), Fe(II) and Co(II) metal ions is conducted. The use of different metal ions offers the possibility of designing new materials with different stabilities and properties, which might be used for the preparation of switchable systems. The micellization of the synthesized amphiphilic A-*b*-B-*b*-A triblock copolymers is studied by dynamic light scattering (DLS), cryo-transmission electron microscopy (cryo-TEM) and atomic force microscopy (AFM).

Chapter IV describes the synthesis of different metallo-supramolecular assemblies synthesized *via* Ru(II) terpyridine complexation. By using *mono*-terpyridine end functionalized poly(ethylene glycol) as hydrophilic block **A** and different rigid-rod conjugated ditopic terpyridyl ligands as hydrophobic block **B** various **AB** or **ABA** Ru(II) block-copolymers are prepared. The detailed characterization and analysis of their properties is discussed. The aqueous self-assembly of these synthesized materials is studied by cryo-TEM, AFM and DLS. In order to prepare water soluble chain extended metallo-homopolymers, Ru(II) polycondensation is performed in an one step synthesis procedure by using as chelating monomer *bis*-terpyridine-poly(ethylene glycol). The optimized reaction conditions and the characterization of the synthesized Ru(II) chain extended polymer are discussed.

Chapter V discusses the synthesis of supramolecular assemblies by Zn(II) complexation of various *bis*-terpyridine containing conjugated spacers. The synthesized chain extended polymers based on Zn(II)tpy$_2$ are analyzed by different techniques including UV-Vis absorption spectroscopy, emission spectroscopy, photoluminescence quantum yield, cyclic

voltammetry, DFT (Density Functional Theory) and Raman spectroscopy. Moreover, the properties of these polymers are presented and discussed.

Chapter VI deals with metallo-supramolecular polymers with thermo-responsible behavior. The combination of metallo-coordination interactions and thermo-responsible polymers offers new possibilities for designing materials with switchable behavior. The influence of the metal ion and also of the counter ion is analyzed. Furthermore, the switchability of one of the designed metallo-homopolymer is tested by performing a competitive reaction with hydroxyethyl-ethylenediaminetriacetic acid (HEEDTA). The possibility of opening and re-closing the designed metallo-systems is presented and discussed.

1.5 References

1   J.-M. Lehn, *Chem. Soc. Rev.* **2007**, *36*, 151.

2   J.-M. Lehn, Supramolecular Chemistry - Concepts and Chemistry; VCH: Weinheim, Germany, **1995**.

3   C. Foquey, J. M. Lehn, A. M. Levelut, *Adv. Mater.* **1990**, *5*, 254.

4   L. Brunsveld, B. J. B. Folmer, E. W. Meijer, R. P. Sijbesma, *Chem. Rev.* **2001**, *101*, 4071.

5   R. D. Archer, Inorganic and Organometallic Polymers, Wiley-VCH, Weinheim **2001**.

6   I. Manners, Synthetic Metal-containing Polymers, Wiley-VCH, Weinheim **2004**.

7   U. S. Schubert, G. R. Newkome, I. Manners, Metal-containing and Metallo-supramolecular Polymers and Materials, Vol. 928, ACS, Washington, DC **2006**.

8   A. S. Abd-El-Aziz, I. Manners, Frontiers in Metal-containing Polymers, Wiley, Hoboken, NJ **2007**.

9   V. Chandrasekhar, Inorganic and Organometallic Polymers, Springer, New York **2005**.

10   U. S. Schubert, C. Eschbaumer, *Angew. Chem. Int. Ed.* **2002**, *41*, 2892.

11   P. Andres, U. S. Schubert, *Adv. Mater.* **2006**, *16*, 1043.

12   H. Hofmeier, U. S. Schubert, *Chem. Soc. Rev.* **2004**, *33* , 373.

13   R. Dobrowa, F. Würthner, *J. Polym. Sci., Part A: Polym. Chem.* **2005**, *43*, 4981.

14   A. Ciferri, *Macromol. Rapid Commun.* **2002**, *23*, 511.

15   A. N. Khlobystov, A. J. Blake, N. R. Champness, D. A. Lemenovskii, A. G. Majouga, N. V. Zyk, M. Schroder, *Coord. Chem. Rev.* **2001**, *222*, 155.

16   S. Kelch, M. Rehahn, *Macromolecules* **1999**, *32*, 5818.

17   C. D. Eisenbach, U. S. Schubert, *Macromolecules* **1993**, *26*, 7372.

18   D. Hinderberger, O. Schmelz, M. Rehahn, G. Jeschke, *Angew. Chem. Int. Ed.* **2004**, *43*, 4616.

19   D. G. Kurth, M. Higuchi, *Soft Matter* **2006**, *2*, 915.

20   V. A. Friese, D. G. Kurth, *Coord. Chem. Rev.* **2008**, *252*, 199.

21   F. S. Han, M. Higuchi, D. G. Kurth, *Adv. Mater.* **2007**, *19*, 3928.

22   F. S. Han, M. Higuchi, D. G. Kurth, *J. Am. Chem. Soc.* **2008**, *130*, 2073.

23   H. Hofmeier, S. Schmatloch, D. Wouters, U. S. Schubert, *Macromol. Chem. Phys.* **2003**, *204*, 2197.

24   M. A. R. Meier, H. Hofmeier, C. H. Abeln, C. Tziatzios, M. Rasa, D. Schubert, U. S. Schubert, *e-polymers* **2006**, *16*, 1.

25   M. Rasa, B. G. G. Lohmeijer, H. Hofmeier, H. M. L. Thijs, D. Schubert, U. S. Schubert, C. Tziatzios, *Macromol. Chem. Phys.* **2006**, *207*, 2029.

26   M. A. R. Meier, B. G. G. Lohmeijer, U. S. Schubert, *Macromol. Rapid Commun.* **2003**, *24*, 852.

27   M. Chiper, M. A. R. Meier, J. M. Kranenburg, U. S. Schubert, *Macromol. Chem. Phys.* **2007**, *208*, 679.

28   S. Schmatloch, A. M. J. van den Berg, A. S. Alexeev, H. Hofmeier, U. S. Schubert, *Macromolecules* **2003**, *36*, 9943.

29   S. Schmatloch, M. Fernàndez González, U. S. Schubert, *Macromol. Rapid Commun.* **2002**, *23*, 957.

30   S. Schmatloch, A. M. J. van den Berg, M. W. M. Fijten, U. S. Schubert, *Macromol. Rapid Commun.* **2004**, *25*, 321.

31   R. H. Hoyler, C. D. Hubbard, S. F. A. Kettle, R. G. Wilkins, *Inorg. Chem.* **1966**, *5*, 622.

32   M. Satterfield, J. S. Brodbelt, *Inorg. Chem.* **2001**, *40*, 5393.

33   H. Hofmeier, R. Hoogenboom, M. E. L. Wouters, U. S. Schubert, *J. Am. Chem. Soc.* **2005**, *127*, 2913.

34   H. Krass, E. A. Plummer, J. M. Haider, P. R. Barker, N. W. Alcock, Z. Pikramenou, M. J. Hannon, D. G. Kurth, *Angew. Chem. Int. Ed.* **2001**, *113*, 3980.

35   M. Schütte, D. G. Kurth, M. R. Linford, H. Cölfen, H. Möhwald, *Angew. Chem. Int. Ed.* **1998**, *37*, 2981

36   T. K. Sievers, A. Vergin, H. Möhwald, D. G. Kurth, *Langmuir* **2007**, *23*, 12179.

37   R. Dobrawa, P. Ballester, F. Würthner, Metal-containing and Metallosupramolecular Polymers and Materials; *ACS Symposium Series* 928; Washington, DC; **2006**.

38   R. Dobrawa, F. Würthner, *Chem. Commun.* **2002**, 319.

39   F. Würthner, *Chem. Commun.* **2004**, 1564.

40   R. Dobrawa, M. Lysetska, P. Ballester, M. Grüne, F. Würthner, *Macromolecules* **2005**, *38*, 1315.

41   S. C. Yu, C. C. Kwok, W. K. Chan, C. M. Che, *Adv. Mater.* **2003**, *15*, 1634.

42   Y.-Y. Chen, Y.-T. Tao, H. C. Lin, *Macromolecules* **2006**, *39*, 8559.

43   Y.-Y. Chen, H.-C. Lin, *J. Polym. Sci., Part A: Polym. Chem.* **2007**, *45*, 3243.

44   M. A. R. Meier, D. Wouters, C. Ott, P. Guillet, C.-A. Fustin, J.-F. Gohy, U. S. Schubert, *Macromolecules* **2006**, *39*, 1569.

45   M. Chiper, M. A. R. Meier, D. Wouters, S. Hoeppener, C.-A. Fustin, J.-F. Gohy, U. S. Schubert, *Macromolecules* **2008**, *41*, 2771.

46   S. J. Rowan, J. B. Beck, *Faraday Discuss.* **2005**, *128*, 43.

47   D. Knapton, P. K. Iyer, S. J. Rowan, C. Weder, *Macromolecules* **2006**, *39*, 4069.

48   Y. Zhao, J. B. Beck, S. J. Rowan, A. M. Jamieson, *Macromolecules* **2004**, *37*, 3529.

49   J. B. Beck, J. M. Ineman, S. J. Rowan, *Macromolecules* **2005**, *38*, 5060.

50   D. Knapton, M. Burnworth, S. J. Rowan, C. Weder, *Angew. Chem. Int. Ed.* **2006**, *45*, 5825.

51   P. K. Iyer, J. B. Beck, C. Weder, S. J. Rowan, *Chem. Commun.* **2005**, 319.

52   M. Burnworth, J. D. Mendez, M. Schroeter, S. J. Rowan, C. Weder, *Macromolecules* **2008**, *41*, 2157.

53   D. Knapton, S. J. Rowan, C. Weder, *Macromolecules* **2006**, *39*, 651.

54   C. Rajadurai, O. Fuhr, R. Kruk, M. Ghafari, H. Hahn, M. Ruben, *Chem. Commun.* **2007**, 2636.

55   R. M. Meudtner, S. Hecht, *Macromol. Rapid Commun.* **2008**, *29*, 347.

56   R. M. Meudtner, M. Ostermeier, R. Goddard, C. Limberg, S. Hecht, *Chem. Eur. J.* **2007**, *13*, 9834.

Chapter II

Supramolecular ligands:
postfunctionalization of terpyridines in the 4'-position

Abstract

Metal-binding domains based on 2,2':6,2''-terpyridines have drawn the attention of organic, inorganic, nano- and, in particular, supramolecular chemists. The synthesis of 4'-chloro 2,2':6,2''-terpyridine is described in the beginning of this chapter. Further functionalization of the terpyridine ligand in the 4'-position was performed by direct or sequential postfunctionalization of different substrates yielding a variety of chelating terpyridine building blocks. For all synthesized compounds detailed characterization was performed. The synthetic pathways described here offer a straightforward access to supramolecular (macromolecular) building blocks required for the construction of metallo-supramolecular polymers.

2.1 Introduction

In comparison to analogous systems, such as *e.g.* 2,2'-bipyridine (bpy) and 1,10-phenanthroline (phen), which captured early on the attention in coordination chemistry, 2,2':6,2"-terpyridine (tpy) chemistry only gained significant interest in coordination and supramolecular chemistry in the last decades. The tpy binding unit itself was synthesized and characterized almost one century ago by Morgan and Burstall.[1,2] In most cases, 2,2':6,2"-terpyridine acts as a tridentate nitrogen donor ligand and seldomly as bidentate nitrogen or monodentate nitrogen donor.[3] Due to the presence of the nearly coplanar three nitrogen donor atoms in the molecule, the metal binding capacity is dramatically increased in comparison with *bi-* and *mono*-nitrogen aromatic ligands. Moreover, upon 4'-functionalization, the terpyridine molecule remains C_{2v} symmetrical with a rotation axis through the changed 4'-position and, therefore, the possibility of forming *fac* and *mer* metallo *bis*-terpyridine complexes *via* complexation is excluded.

The functionalization of the terpyridine moiety with polymer chains could be performed by following one of the routes:[4,5] (1) postfunctionalization with a defined polymer (or organic molecule) bearing an end-functional group; (2) synthesizing a terpyridine initiator which subsequently can initiate a polymerization; (3) using a terpyridine bearing a polymerizable group as a monomer/co-monomer. Each of the mentioned approaches has advantages and disadvantages which are mainly related to: (1) the degree of functionalization of the starting material and (2) narrow molar mass distribution of the synthesized polymer/block copolymer. This chapter is focused on the synthesis of 4'-chloro terpyridine and its subsequent use for the direct 4'-postfunctionalization of various polymers (bearing mono and telechelic functionalities) or organic molecules (Figure 2.1).
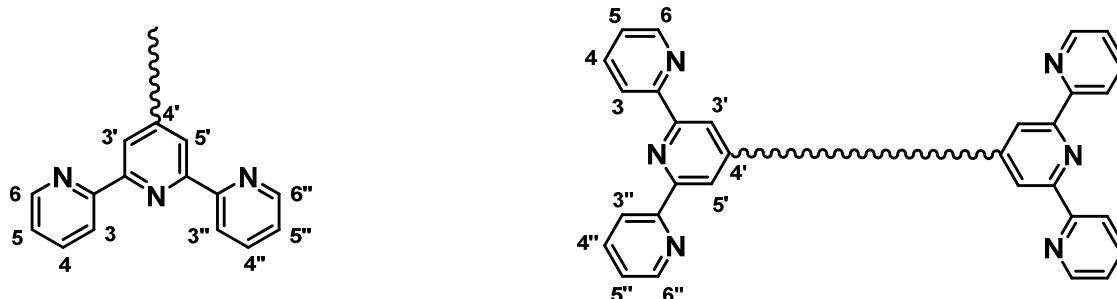
Figure 2.1: *Schematic representation of the 4'-functionalized terpyridine ligands (mono-fuctionalized and telechelic structures).*

2.2 Direct postfunctionalization of 4′-chloro-2,2′:6,2″-terpyridine

2.2.1. Synthesis and characterization of 4'-chloro-2,2':6,2''-terpyridine

4'-Chloro-2,2':6,2''-terpyridine represents a versatile ligand that is of particular interest in the design of extended supramolecular assemblies with controlled stereochemistry. The functionalized terpyridine ring system is accessible *via* a multitude of synthetic methods[6] such as *e.g.* initially Kröhnke[7] or Potts[8], and more recently Stille[9] and Suzuki[10] advanced coupling methods.

Since the main objective of this chapter is the synthesis of 4'-functionalized terpyridine building blocks *via* postfunctionalization of various substrates, mainly using 4'-chloro-2,2':6,2''-terpyridine **3**, our initial efforts focused on synthesizing the desired chelating ligand **3** by following the approach described in Scheme 2.1.[11-13]
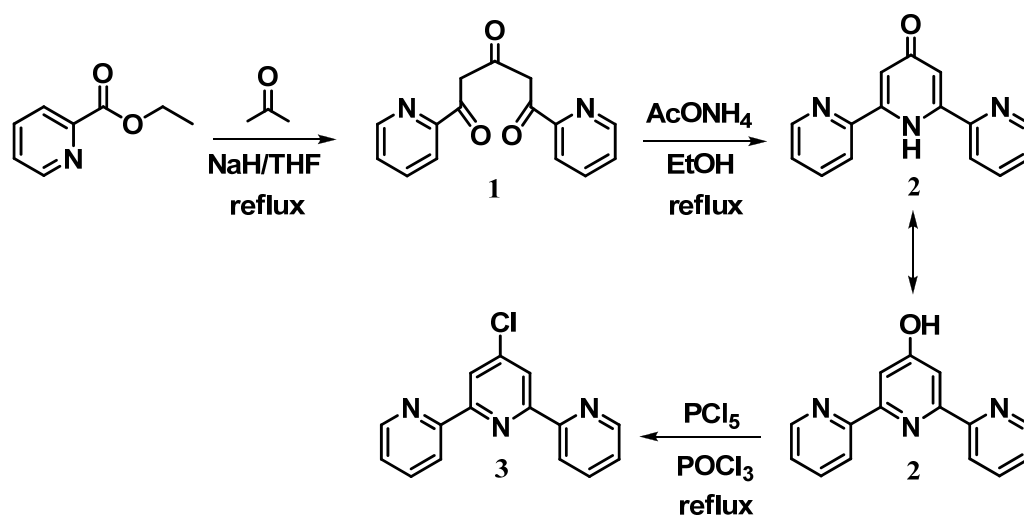
Scheme 2.1: *Schematic representation of the synthesis of 2,6-bis(pyrid-2-yl)-4-pyridone **2** and 4'-chloro-terpyridine **3**.*

The adopted synthetic route consists in a three step reaction that has the main advantage of being accessible on small and large scale.[12] Thus, in the first step a Claisen condensation was performed between acetone and ethyl picolinate. Subsequently, the resulting 1,3,5-trione **1** was subjected to a Kröhnke synthesis yielding to the formation of 2,6-*bis*(pyrid-2-yl)-4-pyridone **2** which was further reacted with PCl$_5$ in POCl$_3$ in order to form the desired 4'-chloro terpyridine **3**. Characterization by means of ^{1}H and ^{13}C-NMR spectroscopy, GC-MS, and elemental analysis proved the purity of compounds **2** and **3**, respectively (see Experimental Part).

Both of the synthesized ligands **2** and **3** are very helpful moieties for further functionalization steps by performing a Williamson type ether condensation reaction with compounds bearing

halide, hydroxyl or thiol functionalities.[14,34] In the following sections we will focus only on the attachment of 4'-chloro terpyridine to various organic molecules and polymers by performing etherification reactions with hydroxy-end groups.

2.2.2 Alkyl, alkoxy and carboxy 4'-terpyridine functionalization

Small organic molecules could be relatively easily transformed into terpyridine chelating monomers that can be further used in metallo-complexation reactions. The synthesis follows the 4'-terpyridine postfunctionalization procedure *via* a nucleophilic substitution reaction with special attention regarding the molar ratio between the utilized substrate and the 4'-chloro terpyridine **3**, as described in the literature.[15,34,37] Previous studies performed in our group offered a special attention to the conversion of the reactant by varying the reaction temperature.[16] Here, the 4'-postfunctionalization was performed in a suspension of KOH in DMSO at 80 °C (Scheme 2.2). The presence of the strong base in the system initiates the nucheophilic attack by abstracting the proton from the hydroxy-end group. Subsequently, the generated anion is attacking the 4'-chloro terpyridine in 4'-position perturbing the electronic system of the middle ring. This intermediate could be easily noticed during the addition of 4'-chloro terpyridine to the reaction mixture by the formation of a red-brownish color which disappeared as soon as all the intermediate was consumed. By the elimination of the chloride anion the aromaticity of the ring was re-established and the desired terpyridine moiety was attached to the substrate.
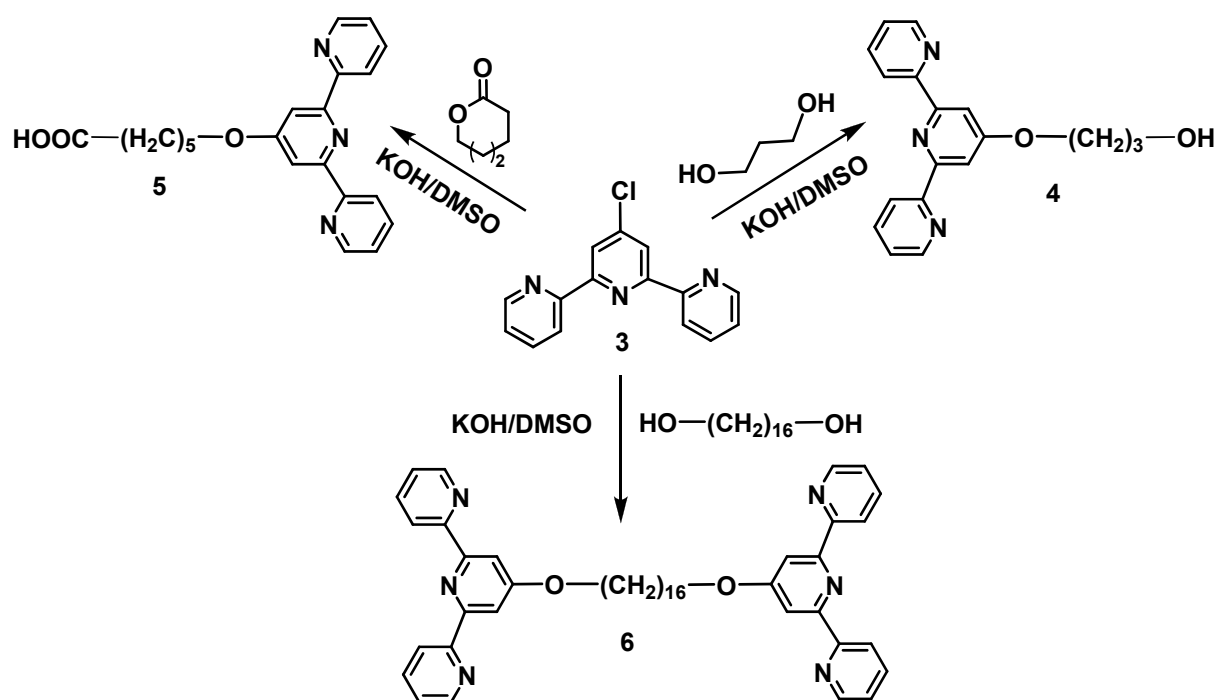
Scheme 2.2: *Schematic representation of the synthesis of 4, 5, 6 by DMSO route.*

By following the reaction approach presented in Scheme 2.2, three different terpyridine macro-monomers **4**, **5** and **6** respectively, were made available for further chemical transformations. The synthesized chelating synthons were characterized by means of ^{1}H-NMR spectroscopy and mass spectrometry as described in the Experimental Part. Further reference to their chemical structures will be done in the following chapters since these ligands were used for subsequent metallo-polymerization reactions.

2.2.3 Poly(ethylene glycol) functionalized terpyridines

Poly(ethylene glycol) (PEG) is one of the most commonly known and used water soluble polymers.[17] By the addition of a binding motif such as *e.g.* terpyridines at the end of the PEG, chelating supramolecular monomers are available for further metallo-polymerization. *Mono-* and *bis*-hydroxy PEG offer great opportunities to introduce terpyridine moieties at the terminal hydroxyl groups of the polymer backbone by performing a nucleophilic substitution reaction. In general, for this type of functionalization two similar approaches were followed: the first one using a suspension of KOH in DMSO at 60-80 $^{\circ}$C and the second one using ^{t}BuOK in dry THF at 60-70 $^{\circ}$C (Scheme 2.3).
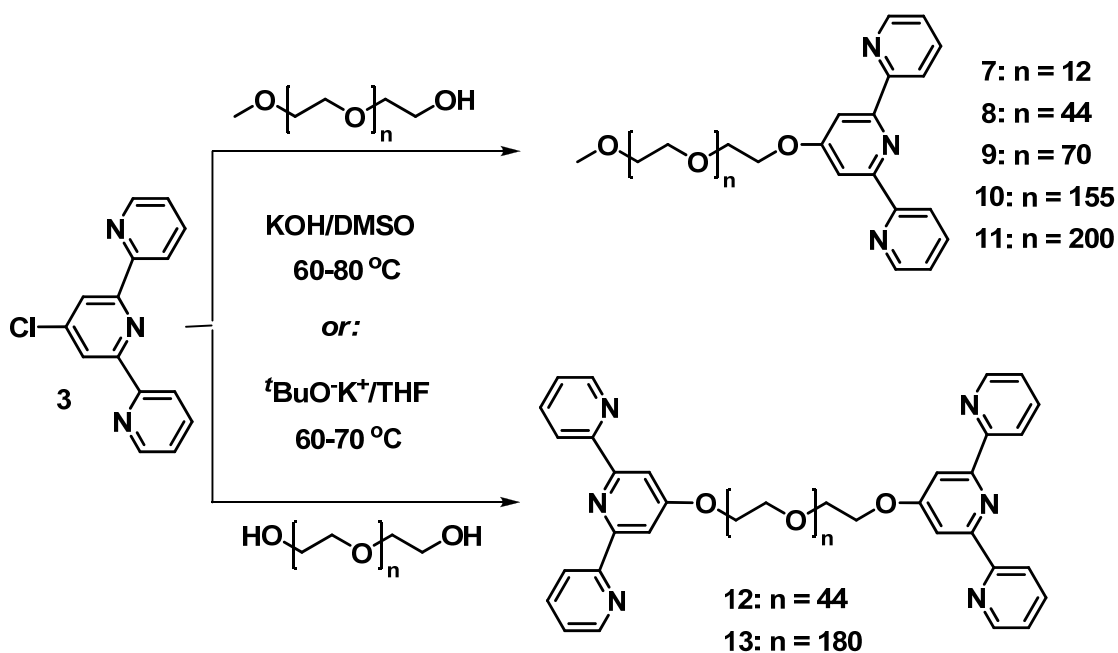
Scheme 2.3: *Schematic representation of the synthesis of mono-terpyridine PEG and bis-terpyridine PEG.*

Both mentioned approaches (DMSO and THF) could be applied to several *mono*-hydroxy-PEGs with different molar masses (M$_n$ = 550; 2,000; 3,000; 7,200; 9,000 g/mol, respectively) and also to the telechelic PEG with M$_n$ = 2,000 and 8,000 g/mol, respectively. The molar ratio

between 4'-chloro terpyridine and the utilized polymer was 2:1 for the case of *mono*-hydroxy-PEG and 4:2 when a telechelic PEG was used. The reaction was performed at 70 °C by following the DMSO or THF route for 24 to 48 hours (see Experimental Part). The purification of the crude functionalized product was achieved by performing size exclusion chromatography (BioBeads in THF or CH_2Cl_2; see Experimental Part) where the excess of 4'-chloro terpyridine could be easily removed. Further precipitation in cold diethyl ether yielded to the desired *mono* or *bis*-terpyridine PEG. All reaction products were characterized by different techniques including ^{1}H-NMR and UV-Vis spectroscopy, SEC and MALDI-TOF-MS.

Examination of the ^{1}H-NMR spectra of all purified terpyridine functionalized PEG compounds revealed two important chemical shifts. One shift was observed in the terpyridine region: the 3',5' singlet from 4'-chloro terpyridine at 8.50 ppm moved to 8.01 ppm in the final product due to the replacement of the chloro to an oxygen atom, proving the formation of the ether bond between terpyridine and hydroxy-PEG. The second significant shift was noticed for the methylene groups of the PEG backbone situated next to the hydroxyl end-group that shifted out of the broad overall PEG signals at 3.6 ppm upon formation of the ether bond with the terpyridine moiety (Figure 2.2).
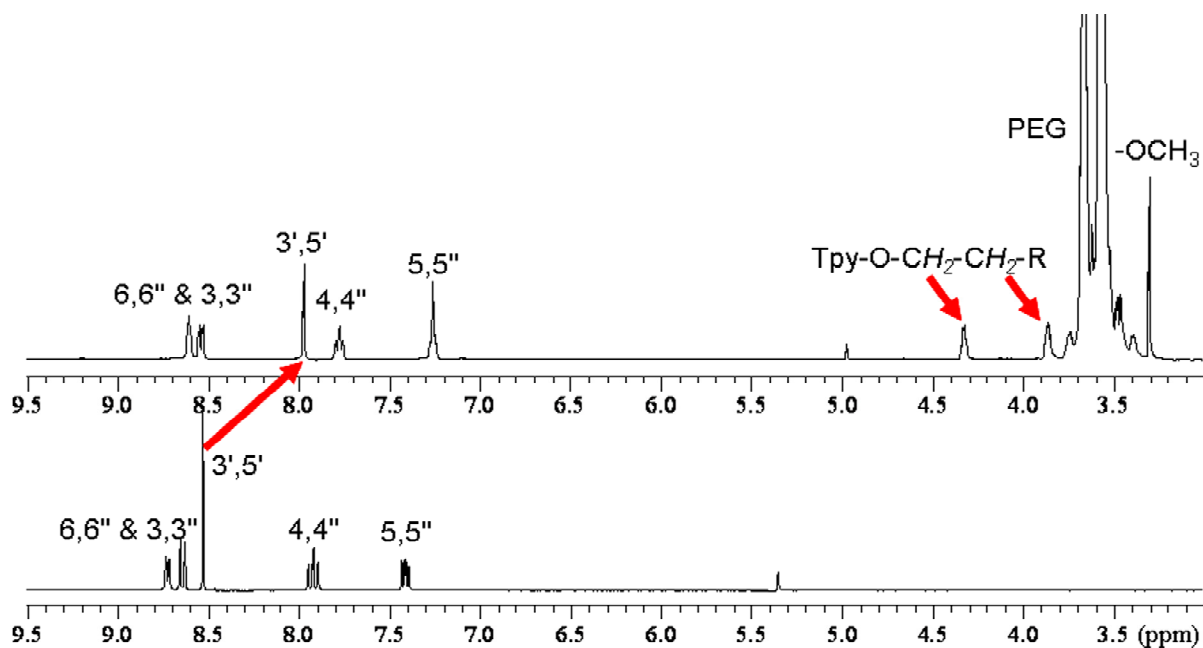
Figure 2.2: *^{1}H-NMR spectra (in CD_2Cl_2) for the 4'-chloro terpyridine 3 (bottom) and mono-terpyridine PEG 8 (top).*

The size exclusion chromatography (SEC) traces of the synthesized chelating PEGs **8-13** showed monomodal distributions (Figure 2.3 and 2.4). In comparison to the unfunctionalized PEG, the synthesized chelating ligands revealed slightly increased molar mass (Figure 2.4).

The SEC characterization could not be applied to *mono*-terpyridine PEG **7** with $M_n = 600$ g/mol since the molar mass of the mentioned ligand was too low and SEC with RI signal revealed a peak at the same position as the peak of the utilized SEC eluent.
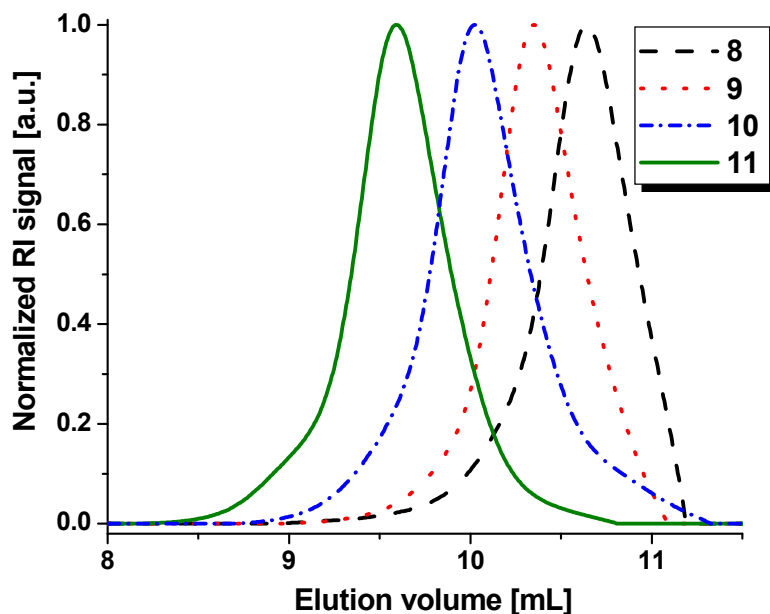
Figure 2.3: *Comparison of the SEC traces (RI detector) for the mono-terpyridine PEG **8** with M_n = 2,200 g/mol (dashed line), **9** with M_n = 3,200 g/mol (dot line), **10** with M_n = 7,200 g/mol (short dash dot line) and **11** with M_n = 9,000 g/mol (solid line). Eluent containing DMF with 5 mM NH$_4$PF$_6$.*
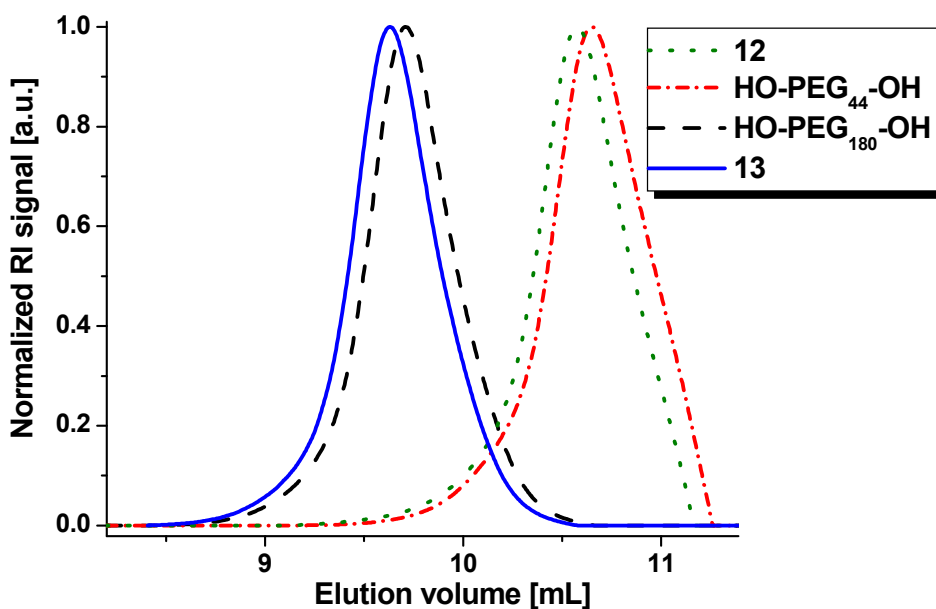
Figure 2.4: *SEC elution distribution (RI detector) for the bis-terpyridine PEG **12** in comparison to the telechelic PEG (M_n = 2,000 g/mol) as well as the bis-terpyridine PEG **13** in comparison to the telechelic PEG (M_n = 8,000 g/mol). Eluent containing DMF with 5 mM NH$_4$PF$_6$.*

Moreover, SEC with an in-line diode array detector demonstrated the purity and the presence of the attached terpyridine supramolecular moiety over the complete molar mass distribution as indicated by the typical UV-Vis absorption band at 290 nm which is characteristic for the terpyridine unit (Figure 2.5).
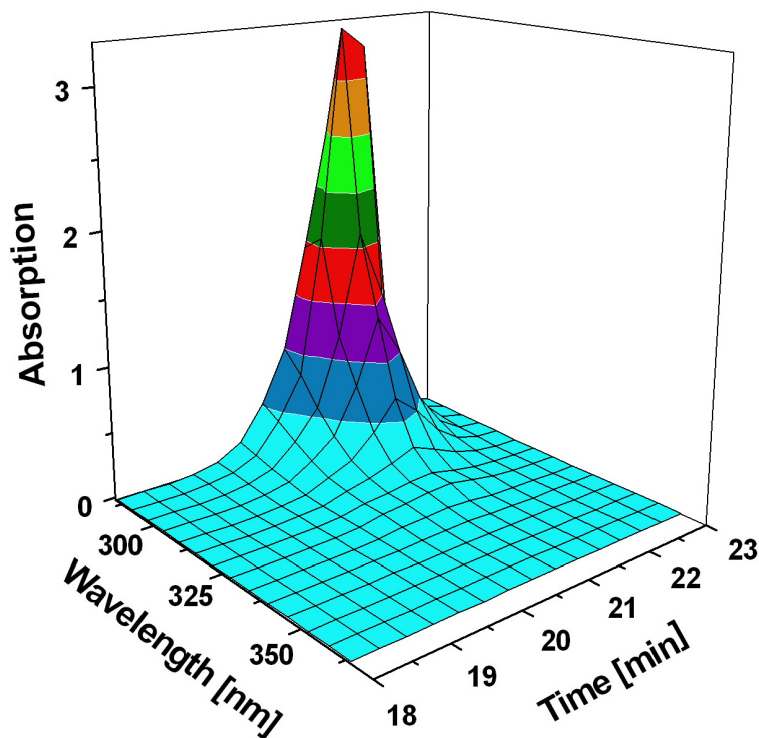
Figure 2.5: *Characteristic SEC elution distribution (PDA detector) for the mono-terpyridine PEG **8** (M_n = 2,200 g/mol). Eluent containing DMF with 5 mM NH_4PF_6.*

MALDI-TOF-MS indicated the derivatization of the hydroxyl groups with terpyridine moieties for all the synthesized chelating monomers **7-13**. Figure 2.6 (top) shows as an example that the molar mass of the *mono*-terpyridine PEG **9** is shifted towards higher molar mass due to the attachment of the terpyridine unit at the end of the parent methoxy-PEG. A similar result was observed for the case of telechelic structures based on PEG (see Figure 2.6 bottom).
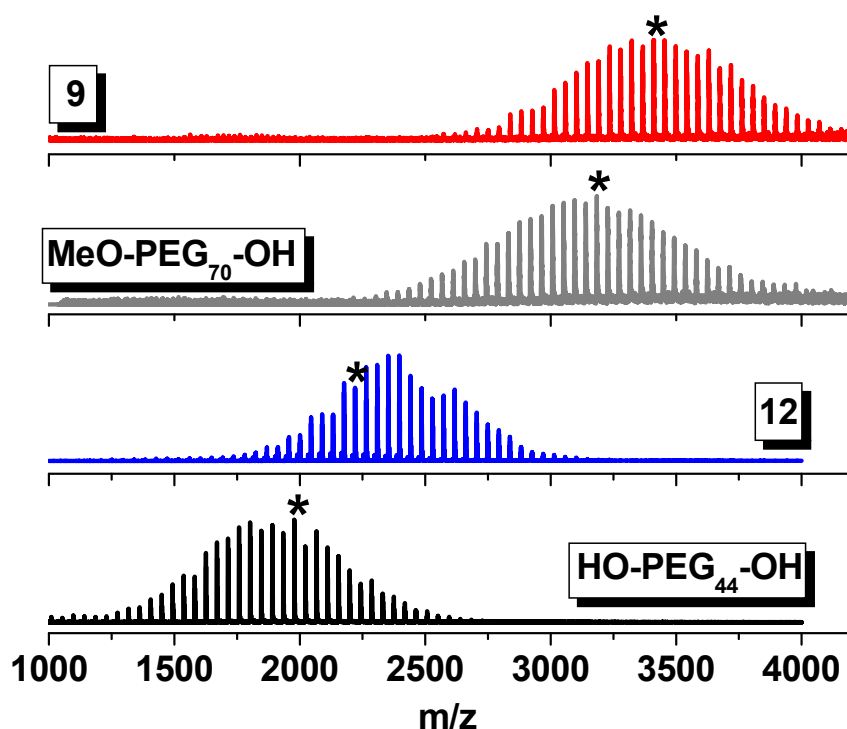
Figure 2.6: *Characteristic MALDI-TOF-MS spectra. Bottom: comparison between the parent HO-PEG$_{44}$-OH and bis-terpyridine PEG **12** (the marked peak corresponds to n = 44). Top: comparison between MeO-PEG$_{70}$-OH and mono-terpyridine PEG **9** (the marked peak corresponds to n = 70).*

2.2.4 Polytetrahydrofuran functionalized terpyridines

Polytetrahydrofuran (PTHF) is a frequently used soft segment for thermoplastic and crosslinked elastomers.[18] PTHF was selected because of its very low glass transition temperature (T$_g$) and melting temperature (T$_m$). By attaching terpyridine moieties to the synthesized methoxy-PTHF or telechelic-PTHF new chelating macro-monomers with high flexibility in the self-assembly process could be made available for further metallo-complexation.

It is known that THF reacts with electrophilic initiators in order to form PTHF. Such types of polymerizations have been intensively studied by Goethals *et al.*[19,20] Polymerization of THF proceeds *via* a cationic mechanism, in which the propagating species is an oxonium ion that is ring-opened by the attack of the additional THF monomer. A counter anion of relatively low nucleophilicity, such as *e.g.* -BF$_4$, -PF$_6$, -CF$_3$SO$_3$ or -FSO$_3$, is required to achieve a living polymerization. In the following section, the formation of methoxy-PTHF and telechelic PTHF followed by the postfunctionalization with 4'-chloro terpyridine **3** is discussed.

2.2.4.1 Methoxy-polytetrahydrofuran functionalized terpyridine

In order to synthesize methoxy-PTHF, a bulk polymerization of THF **14** using trifluoromethanesulphonate (methyl triflate) as initiator was performed at room temperature. The general living cationic polymerization mechanism is presented in Scheme 2.4.[21]
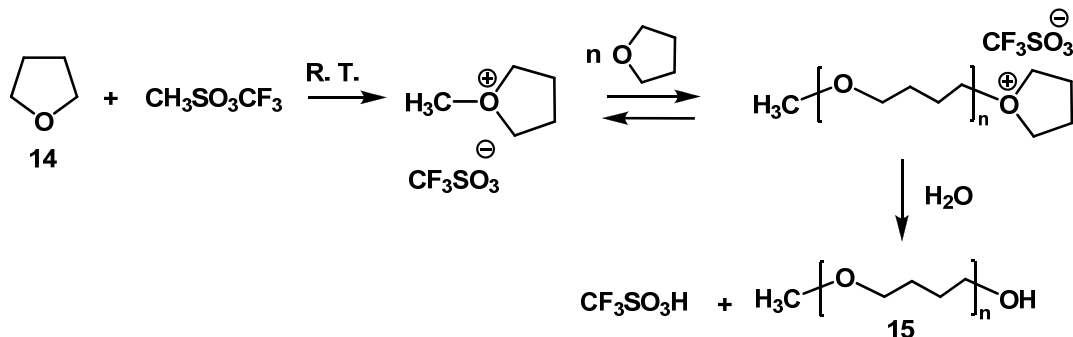
Scheme 2.4: *Schematic representation of the polymerization of THF with methyl triflate.*

Thus, the polymerization is initiated by methyl triflate (electrophilic initiator) that leads to the formation of the cationic oxonium ring. Subsequently, the newly formed species undergoes a nucleophilic attack from the monomer (THF) and propagation occurs. By addition of a nucleophilic terminating agent such as water to the system, the polymerization is stopped by end capping the polymer chain with a new functionality, in this case -OH.

Following the mechanism depicted in Scheme 2.4, the living polymerization of THF **14** was performed in bulk for 15 minutes at r.t. followed by the end capping with water yielding methoxy-PTHF **15**. The purification was performed by extracting the polymer with chloroform and the organic phase was dried with Na_2SO_4. The resulting polymer was dried for a longer time *in vacuo* yielding in a white wax. Characterization of **15** was performed by means of ^{1}H-NMR spectroscopy and SEC. The ^{1}H-NMR spectrum of **15** revealed the presence of the polymer backbone at 3.5 to 3.3 ppm and 1.7 to 1.5 ppm as it can be seen in Figure 2.7. SEC investigations (RI detector) showed a monomodal molar mass distribution of the synthesized methoxy-PTHF **15** with a $M_n = 4,400$ g/mol when a PEG calibration was used (Figure 2.8).

The postfunctionalization of the synthesized methoxy-PTHF **15** was performed by following one of the routes already described in Section 2.2.3. Hence, by using ^{t}BuOK in dry THF the deprotonation of the hydroxy group of the polymer took place; subsequent addition of an excess of 4'-chloro terpyridine led to the formation of the desired *mono*-terpyridine methoxy-PTHF **16** (Scheme 2.5). The nucleophilic substitution reaction was performed for 24 hours at

65 °C. The purification of the reaction product was finalized by performing size exclusion chromatography (BioBeads S-X1 in THF).
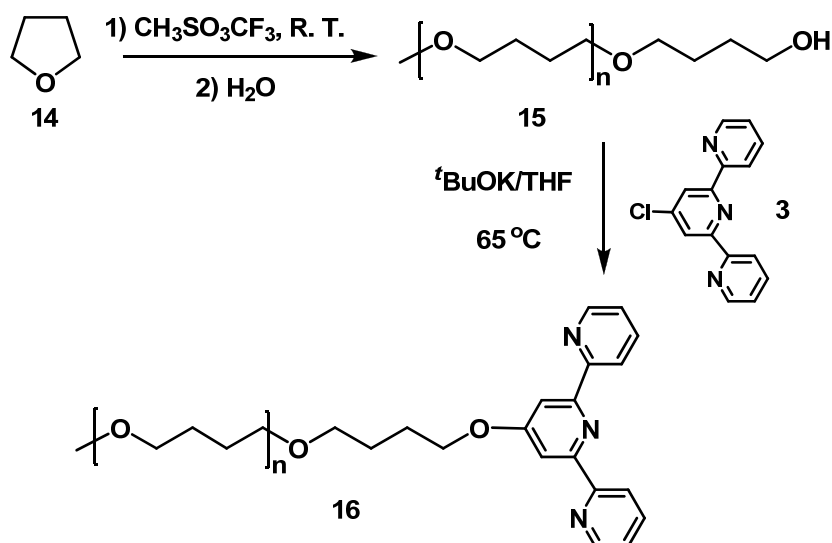
Scheme 2.5: *Schematic representation of the synthesis of methoxy-PTHF **15** and mono-terpyridine methoxy-PTHF **16** by the THF route.*

^{1}H-NMR and UV-Vis spectroscopy as well as SEC techniques were used to prove the purity of *mono*-terpyridine-PTHF **16**. The change of functionality in **16** was observed by ^{1}H-NMR spectroscopy (Figure 2.7) where a shift for the methylene protons next to the PTHF backbone towards low magnetic field was noticed compared to the methylene protons in the unfunctionalized methoxy-PTHF **15**.
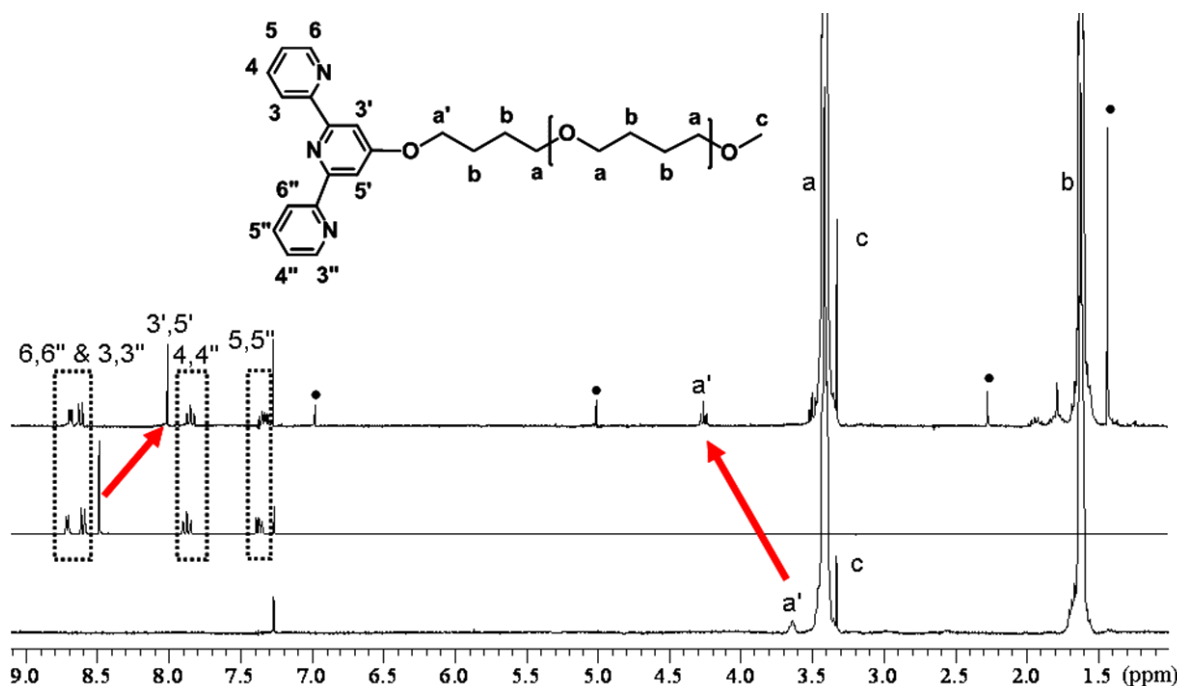
Figure 2.7: *^{1}H-NMR spectra (in CDCl₃) for methoxy-PTHF **15** (bottom), 4'-chloro terpyridine **3** (middle) and mono-terpyridine PTHF **16** (top). The dots represent BHT (butylated hydroxytoluene: stabilizer in diethyl ether and THF).*

Another typical upfield shift of the 3',5' singlet protons from the terpyridine moiety was observed when the 4'-chloro terpyridine **3** was converted into its corresponding *mono*-terpyridine PTHF **16** (Figure 2.7).

SEC (RI detector with CHCl$_3$ eluent) of *mono*-terpyridine-PTHF **16** demonstrated an increased molar mass in comparison to the starting material **15**. Moreover SEC with an UV detector revealed that compound **16** is UV-Vis active due to the attachment of the terpyridine moiety at the end of the polymer in contrast to the non-absorbing unfunctionalized methoxy-PTHF **15** (Figure 2.8). On the other hand the SEC (RI and UV) curves of *mono*-terpyridine-PTHF **16** revealed a tailing at higher elution volumes that might be caused by smaller molar mass species which can be the result of a depolymerisation process as a side (or competitive) reaction.
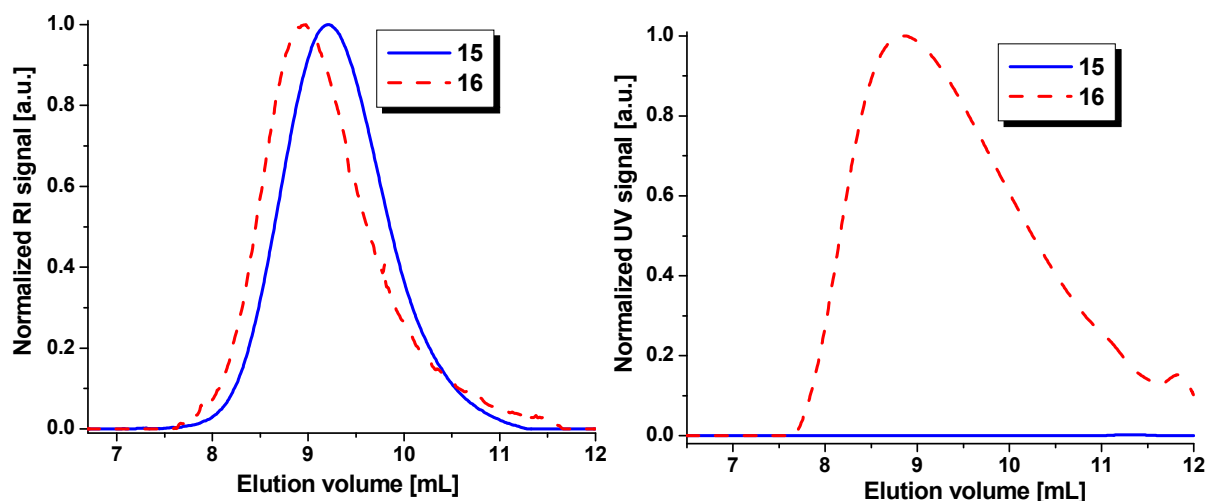
Figure 2.8: *SEC elution distribution (RI detector: left) for the mono-terpyridine PTHF **16** (dashed line) and methoxy-PTHF **15** (solid line). SEC elution distribution (UV detector: right) for the mono-terpyridine PTHF **16** (dashed line) and methoxy-PTHF **15** (solid line). Eluent containing CHCl$_3$:NEt$_3$:2-PrOH (94:4:2).*

2.2.4.2 Telechelic-polytetrahydrofuran functionalized terpyridine

To obtain telechelic PTHF, a bulk polymerization of THF **14** using triflic anhydride as initiator was performed at room temperature. The reaction followed a living cationic polymerization mechanism as depicted in Scheme 2.6.[21] In this case, the polymerization is initiated at room temperature by triflic anhydride (electrophilic initiator) that leads to the formation of the cationic tetrahydrofuranic ring. Subsequently, the newly formed species undergoes nucleophilic attack from the monomer (THF) and propagation occurs. By the addition of water as nucleophile (terminating agent) to the system, the polymerization was stopped by end capping the polymer chain with an -OH functionality.
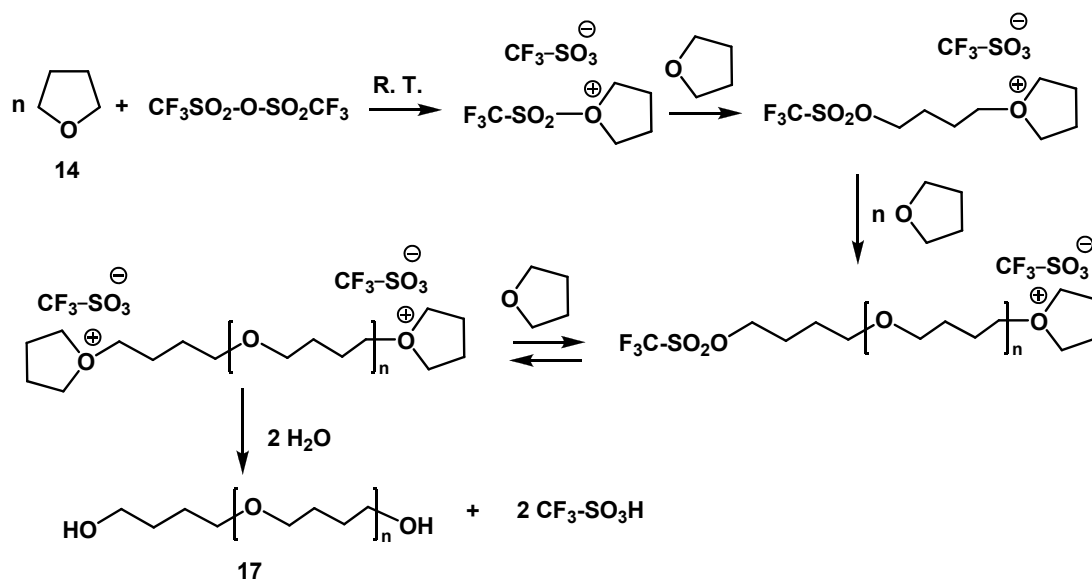
Scheme 2.6: *Schematic representation of the mechanism for the polymerization of THF with triflic anhydride.*

The bulk polymerization of **14** was performed for 15 minutes at r.t. followed by the addition of the nucleophile agent (water) yielding telechelic hydroxy-PTHF **17**. The polymer was purified similar to the methoxy PTHF **12**, yielding at the end a white wax too. Characterization of **17** was performed by means of ^{1}H-NMR spectroscopy and SEC. The ^{1}H-NMR spectrum of **17** revealed the presence of the characteristic polymer backbone at 3.53 to 3.35 ppm and 1.73 to 1.48 ppm. Moreover, SEC investigations showed a monomodal molar mass distribution of the synthesized telechelic PTHF **17** with a M_n = 5,800 g/mol when a PEG calibration was used (Figure 2.9).
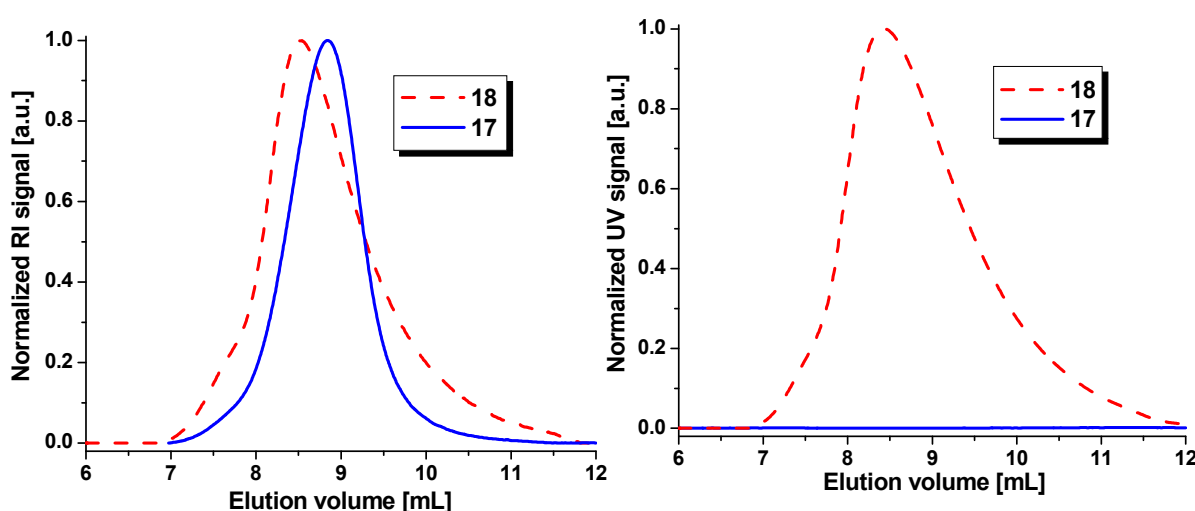
Figure 2.9: *SEC elution distribution (RI detector: left) for the bis-terpyridine PTHF **18** (dashed line) and the telechelic-PTHF **17** (solid line). SEC elution distribution (UV detector: right) for the bis-terpyridine PTHF **18** (dashed line) and the telechelic-PTHF **17** (solid line). Eluent containing CHCl$_3$:NEt$_3$:2-PrOH (94:4:2).*

The postfunctionalization of the synthesized telechelic PTHF **17** (Scheme 2.7) was achieved by following the same approach utilized for the derivatization of methoxy-PTHF **15** (^{t}BuOK in dry THF at 65 °C) described in section 2.2.4.1.
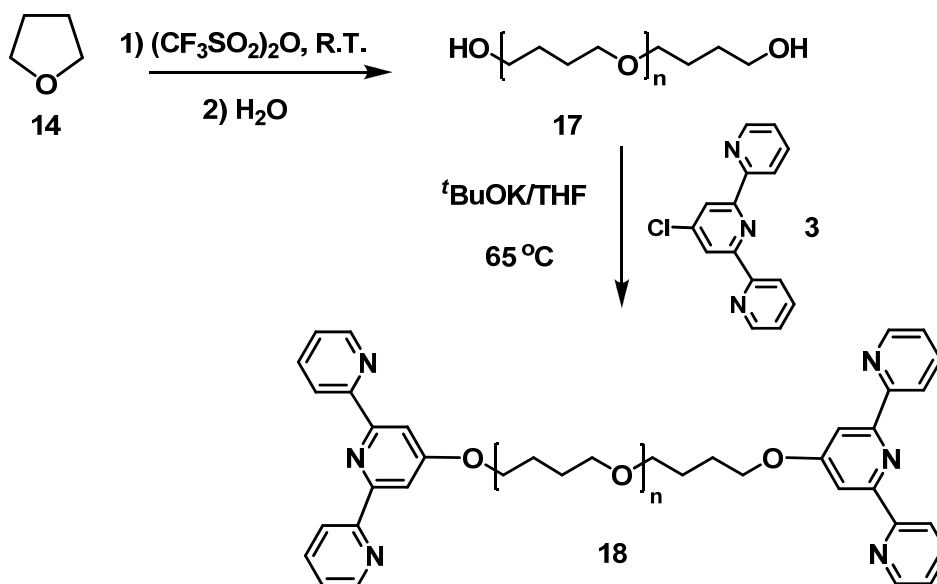
Scheme 2.7: *Schematic representation of the synthesis of telechelic PTHF **17** and bis-terpyridine PTHF **18** by the THF route.*

The purity of **18** was proven by ^{1}H-NMR and UV-Vis spectroscopy as well as SEC. The change of functionality for the telechelic PTHF **17** could be followed by ^{1}H-NMR spectroscopy. A clear shift was observed for the methylene protons next to the PTHF backbone towards low magnetic field as compared to the methylene protons in the unfunctionalized PTHF **17**. A characteristic moderate upfield shift of the 3',5' singlet protons ($\Delta\delta \approx 0.5$ ppm) from the terpyridine moiety was observed when the 4'-chloro terpyridine **3** was converted into its corresponding *bis*-terpyridine PTHF **18**.

SEC (RI detector) of *bis*-terpyridine-PTHF **18** demonstrated a slightly increased molar mass in comparison to the unfunctionalized PTHF **17**. In addition SEC coupled with an UV detector revealed that compound **18** is UV-Vis active due to the attachment of the terpyridine moiety at the end of the polymer backbone in comparison to **17** that does not give an UV-Vis signal since no conjugated units are present in the polymer chain (Figure 2.9). As it can be observed in Figure 2.9, SEC (RI and UV) curves of *bis*-terpyridine PTHF **18** revealed a tailoring at higher elution volume similar to the *mono*-terpyridine-PTHF **17**. The presence of some fractions with lower molar mass species in the final compound **18** could be explained by possible depolymerisation reaction called retro-scission (as side process) since the ceiling temperature for PTHF is $T_c = 83$ °C.[22]

2.2.5 Poly(2-ethyl-2-oxazoline) terpyridine functionalization

The living cationic ring-opening polymerization of 2-oxazolines is a well-kown polymerization technique for the synthesis of various architectures of polymers.[23] The living cationic polymerization of 2-ethyl-2-oxazolines (EtOx) initiated by methyl tosylate and terminated with water is outlined in Scheme 2.8.
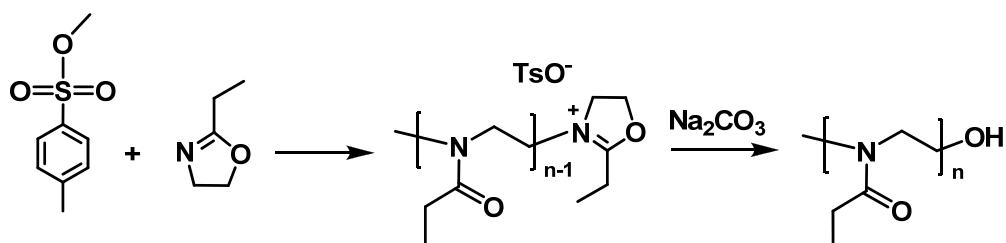
Scheme 2.8: *Schematic representation of the general mechanism of the polymerization of EtOx with methyl tosylate.*

Following the mechanism shown in Scheme 2.8, a PEtOx **19** with M_n = 5,000 g/mol was synthesized and characterized. In the next step, the synthesized PEtOx was postfuctionalized with 4'-chloro terpyridine **3** *via* the ^{t}BuOK/THF route at 60 °C (Scheme 2.9). Further purification of the reaction product **20** was performed by BioBeads S-X1 in THF where the excess of the 4'-chloro terpyridine **3** could be removed.
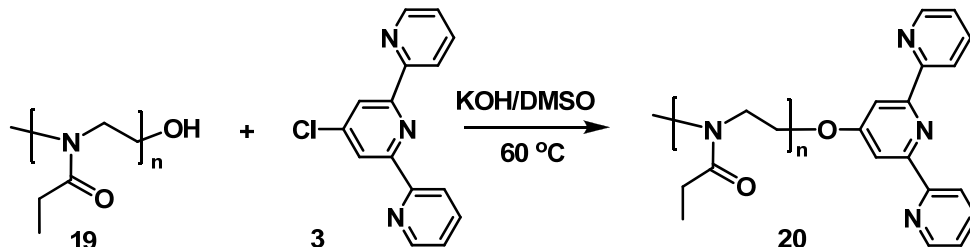
Scheme 2.9: *Schematic representation of the synthesis of mono-terpyridine PEtOx **20** by the ^{t}BuOK/THF route.*

The resulting *mono*-terpyridine PEtOx **20** was characterized by means of ^{1}H-NMR and UV-Vis spectroscopy as well as SEC. The ^{1}H-NMR spectrum is dominated by the characteristic peaks of the terpyridine moiety in the aromatic region (specific shift for 3',5' singlet from 8.5 ppm to 8.01 ppm in **20**) and by the polymeric chain of PEtOx in the aliphatic region. Molar mass characterization was performed using SEC with a refractive index (RI) as well as an in-line diode array detector (PDA). The overlay of the SEC traces (RI detector) displayed a typical slightly increased molar mass of the *mono*-terpyridine PEtOx **20** in comparison to the unfunctionalized PEtOx **19**. In addition to that, SEC (PDA detector) revealed the existence of

the terpyridine moiety on the polymer backbone by the presence of a strong absorption at 290 nm (Figure 2.10).
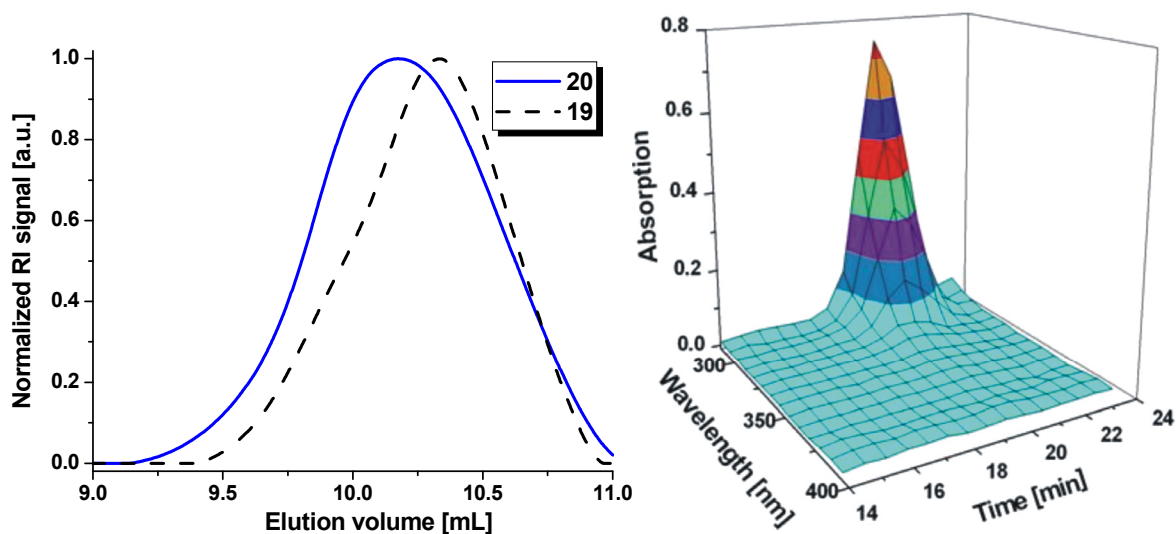
Figure 2.10: *Left: SEC elution distribution (RI detector) for mono-terpyridine PEtOx$_{50}$ **20** in comparison to the PEtOx$_{50}$ **19**. Right: SEC elution distribution (PDA detector) for the mono-terpyridine PEtOx$_{50}$ **20**. Eluent containing DMF with 5 mM NH$_4$PF$_6$.*

The IR spectra also showed that indeed the functionalization of **19** with the terpyridine moiety was successful as indicated by the presence of the typical IR bands such as *e.g.* 1650 cm^{-1} (C=O), 2971 cm^{-1} (CH aliphatic) and 1430 (C-N) of the polymer backbone as well as the tpy moiety in the final product **20**.

2.2.6 Polysiloxane terpyridine functionalization

Polydimethylsiloxanes (PDMS) is another important class of polymers with widespread applications in many fields such as, *e.g.*, biomedical, coatings, membranes, microfluids, and stamps for soft nanolithography.[24] The outstanding properties of PDMS, such as its low glass transition temperatures, high thermal and oxidative stability, UV-Vis resistance, good electrical properties and high permeability to many gases, as well as low surface energy and hydrophobicity, attracted our attention. With all these characteristics, PDMS could be considered a very appealing building block for supramolecular chemistry. For this purpose a terpyridine ligand bearing PDMS was targeted (Scheme 2.10).
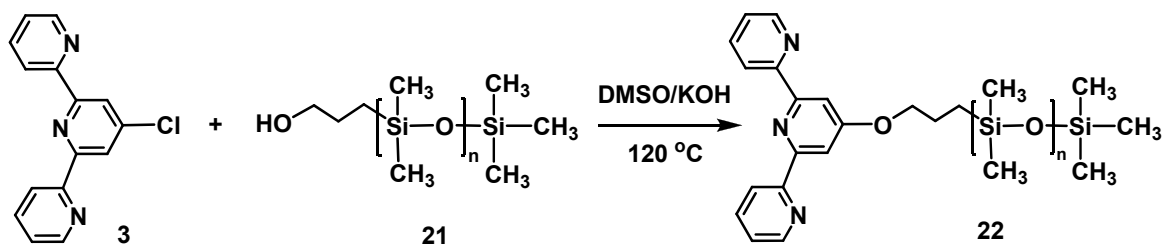
Scheme 2.10: *Schematic representation of the synthesis of mono-terpyridine PDMS 22 by DMSO route.*

The synthesis of the *mono*-terpyridine PDMS ligand has been accomplished by reacting the *mono*-hydroxy functionalized PDMS **21** with 4'-chloro terpyridine **3** in DMSO under basic conditions (KOH/DMSO route). The product was purified by repetitive column chromatography (BioBeads S-X1 in THF). The rather low yield of the product (25%) could be explained by the limited solubility of the hydrophobic polymer in DMSO even if the reaction was performed at 120 °C. However, no conversion was achieved by changing to better solubilizing solvents, such as *e.g.* THF, or by adopting a different substitution approach (*e.g.* activation of the hydroxyl group followed by the reaction with amino-terpyridine). The formation of the *mono*-terpyridine PDMS ligand **22** was proven by ^{1}H-NMR, UV-Vis and IR spectroscopy as well as SEC.

The ^{1}H-NMR spectrum of **22** revealed the characteristic shifts registered for the substituted terpyridine ligands. Thus, an upfield shift in the aromatic region of approx. 0.44 ppm for the 3',5' terpyridine singlet indicated that indeed the ether bond has been created between 4'-chloro terpyridine and the utilized hydroxy-PDMS **21**. Moreover, a downfield shift of approx. 0.70 ppm has been noticed upon terpyridine functionalization with PDMS **21** for the methylene protons next to hydroxy moiety situated at 3.71 ppm in the unfunctionalized **21** and shifted to 4.42 ppm in the final product **22**.

The IR spectrum also confirmed the functionalization of PDMS with the terpyridine moiety. The coupling between the terpyridine ligand **3** and PDMS **21** to yield the *mono*-terpyridine PDMS **22** was proven by the presence of the typical bands for PDMS at 1240 cm^{-1}, 1010 cm^{-1} and 780 cm^{-1} (Si-O-Si) together with characteristics bands for the terpyridine at 1540 cm^{-1} and 1380 cm^{-1} (C=C and C=N), respectively.

SEC measurements with a RI detector (DMA eluent) revealed a shift of the molar mass of **22** to lower elution volumes in comparison to the starting material **21**. Moreover, SEC with an UV-Vis detector (performed with the same eluent) exhibited a strong UV-VIS absorption at 290 nm which belongs to the terpyridine moiety present at the end of the functionalized PDMS backbone **22** (Figure 2.11). Apart from a clear SEC shift of the molar masses of the

synthesized *mono*-terpyridine PDMS ligand **22**, SEC also revealed the presence of some higher molar mass species at lower elution volume (possible coupled polymer chains due to not very suitable reaction conditions). Further purifications (fractionation by BioBeads) could not yield in a monomodal distribution of the molar mass of **22**.
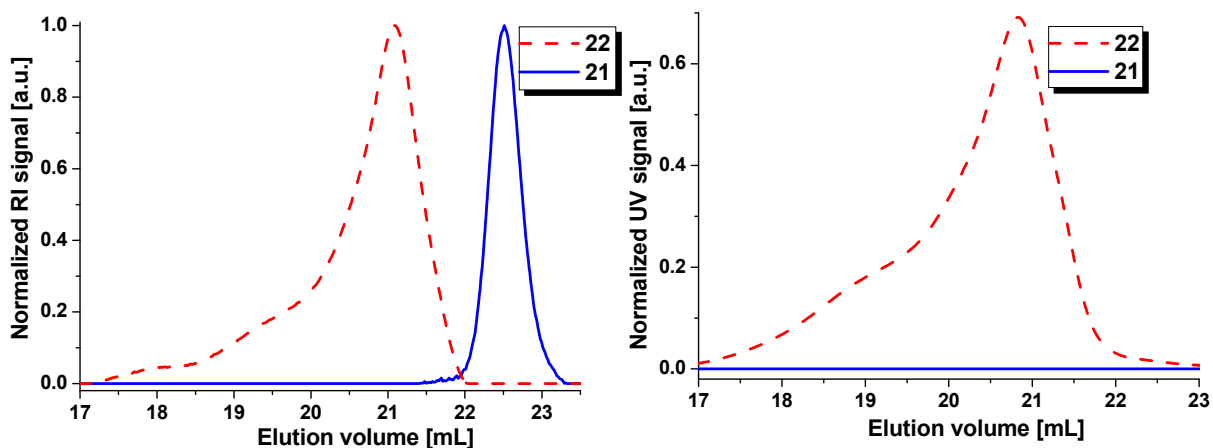
Figure 2.11: *Left: SEC elution distribution (RI detector) for the mono-terpyridine PDMS **22** (dashed line) and PDMS **21** (solid line). Right: SEC elution distribution (UV detector) for the mono-terpyridine PDMS **22** (dashed line) and PDMS **21** (solid line). Eluent containing DMA with 49.5 mmol/L LiCl.*

These results convinced us that the direct postfuctionalization of PDMS **21** was achieved, although very low yields and an increased polydispersity index of the final product **22** were observed.

2.2.7 Pluronic terpyridine functionalization

Block copolymers are another important targeted class for 4'-terpyridine postfunctionalization. From the multitude of available triblock copolymers our attention was attracted by the polymers/copolymers able to exhibit reversible phase transitions upon increasing the temperature, such as *e.g.* poly(ethylene oxide) (PEG)-poly(propylene oxide) (PPG) copolymers and poly(*N*-isopropylacrylamide) (PNIPAM) (see also 2.3.1).

Triblock copolymers of poly(ethylene oxide) (PEG) and poly(propylene oxide) (PPG) with the block sequence $(PEG)_m$-$(PPG)_n$-$(PEG)_m$ consisting of hydrophilic (PEG) segments and hydrophobic (PPG) segments are an important class of temperature-responsive copolymers known as Pluronics[®].[25] They are non-ionic amphiphilic molecules which are both surface active and are capable of forming micelles or vesicles in aqueous solutions induced by a temperature change; the block copolymers self-assemble upon rising the temperature. They are commercially available in a large variety of molar masses and PEG/PPG ratios with trade name Pluronics[®] (or Poloxamer[®]) from the BASF. The mentioned triblock copolymers

represent an industrially important class of surfactants and are intensively used in various fields with a special interest in pharmaceutics and personal care.[26]

For the preparation of the *bis*-terpyridine functionalized Pluronics®, the straightforward synthetic pathway (postfunctionalization with 4'-chloro terpyridine **3** *via* nucleophilic substitution in KOH/DMSO at 60 °C) was followed. The mentioned approach has been extensively discussed in the previous sections of this chapter (see, *e.g.*, section 2.2.2 and 2.2.3). Thus, $(PEG)_{10}$-$(PPG)_{30}$-$(PEG)_{10}$ with M_n = 2,800 g/mol was subjected to functionalization reactions with 4'-chloro terpyridine. Moreover, the inverse triblock copolymer $(PPG)_{14}$-$(PEG)_{24}$-$(PPG)_{14}$ with M_n = 2,700 g/mol was functionalized in the same fashion. The resulting chelating triblock copolymers **23** and **24** (Figure 2.12) were characterized by means of ^{1}H-NMR and UV-Vis spectroscopy as well as SEC.
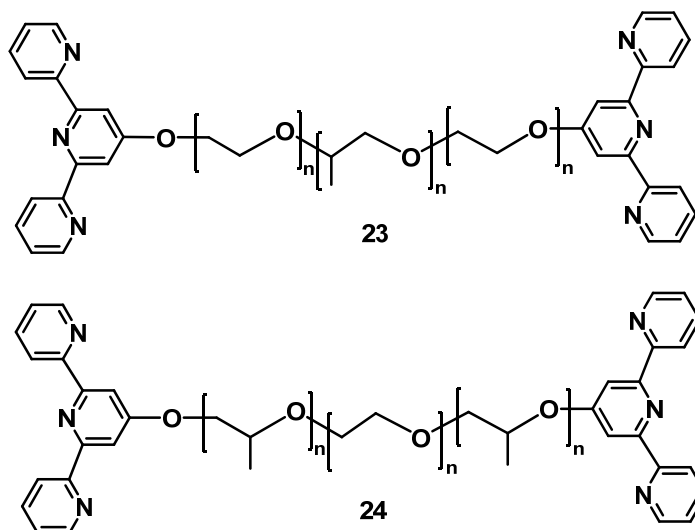
Figure 2.12: *Schematic representation of the synthesized bis-terpyridine Pluronics® 23, 24 by the DMSO route.*

The attachment of the terpyridine unit to the end of the block copolymers could be proven by ^{1}H-NMR spectroscopy. In the purified products **23** and **24** the characteristic moderate upfield shift of the 3',5' singlet protons ($\Delta\delta \approx 0.5$ ppm) from the middle ring of the terpyridine unit was observed that proved the ether bond formation between the 4'-chloro terpyridine **3** and hydroxyl functionality of the Pluronics®.

The SEC measurements with RI detector (DMA eluent) showed a slightly increased molar mass in comparison to the starting materials. In addition to that, SEC measurements with UV-Vis detector (performed with the same eluent) revealed a strong UV-VIS absorption at 290 nm demonstrating the presence of the terpyridine moiety on the functionalized Pluronics® (Figure 2.13 and 2.14).
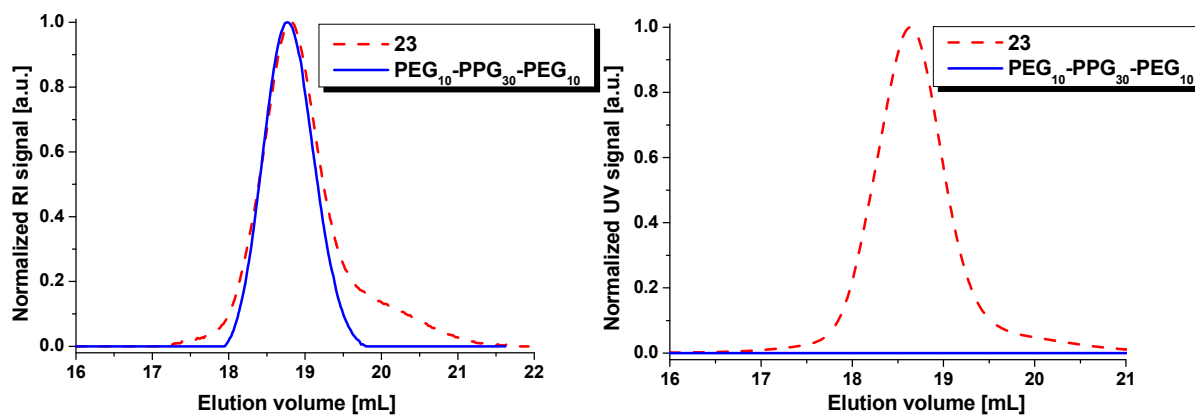
Figure 2.13: *Left: SEC elution distribution (RI detector) for the bis-terpyridine Pluronic® 23 in comparison to the unfunctionalized telechelic Pluronic®. Right: SEC elution distribution (UV detector) for the bis-terpyridine Pluronic® 23 in comparison to the unfunctionalized telechelic Pluronic®. Eluent containing DMA with 49.5 mmol/L LiCl.*
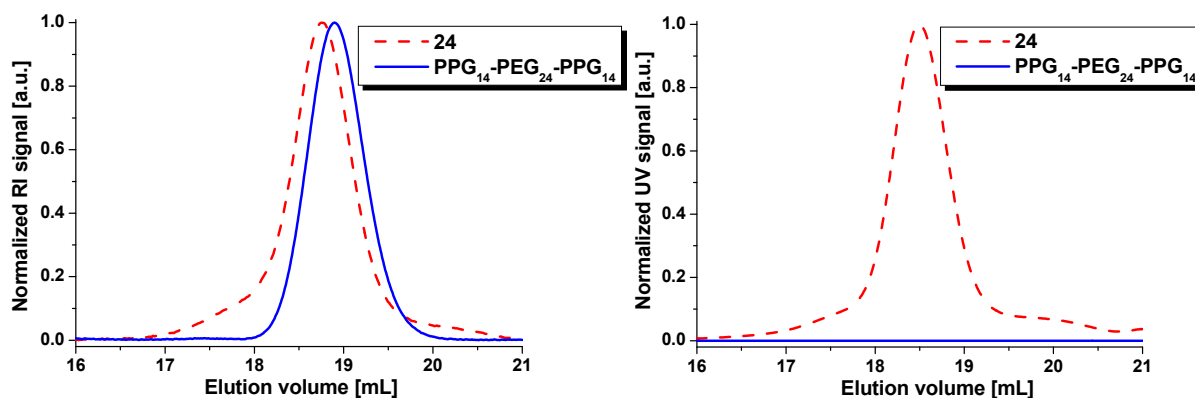
Figure 2.14: *Left: SEC elution distribution (RI detector) for the bis-terpyridine Pluronic® 24 in comparison to the telechelic Pluronic®. Right: SEC elution distribution (UV detector) for the bis-terpyridine Pluronic® 24 in comparison to the telechelic Pluronic®. Eluent containing DMA with 49.5 mmol/L LiCl.*

2.3 Sequential terpyridine-functionalization

2.3.1 PNIPAM terpyridine-functionalization

Another appealing feature for "smart materials" is the combination of LCST (lower critical solution temperature) polymers and chelating units such as terpyridines that could be used for further metallo-supramolecular self-assembly procedures. Harruna *et al.* described the combination of chelating ligands (bipyridines or terpyridines) and thermosensitive polymers by performing reversible addition-fragmentation chain transfer (RAFT) polymerization using a bipyridine-functionalized dithioester as a RAFT agent and also *via* a terpyridine-functionalized chain transfer agent (CTA) that produces well-controlled macromolecular architectures with terpyridine functionalities at one chain end *via* RAFT polymerization.[27,28] However, detailed LCST studies were not reported for the synthesized metallo-terpyridine

compounds. Thus, a new strategy to introduce the terpyridine moiety at the end of a thermosensitive polymer backbone was targeted.

From the multitude of available temperature-responsive polymers we focused our research on the combination of Pluronics® (as described in the previous section) and PNIPAM with a terpyridine moiety which can be subjected to metal complexation and LCST studies (see Chapter 6). In order to end-functionalize PNIPAM with a terpyridine moiety, an activation approach has been followed.

First, well-defined poly(*N-iso*propylacrylamide) PNIPAM **27** was synthesized *via* controlled radical polymerization RAFT[29] of *N-iso*propylacrylamide **25** in toluene/anisole for 7 hours at 80 °C (Scheme 2.11).[30,31] The SEC analysis (RI detector) of the obtained pink PNIPAM-RAFT showed a monomodal molar mass distribution. Moreover, SEC revealed a strong UV absorption due to the RAFT agent connected to the synthesized polymer. In addition, ^{1}H-NMR spectroscopy proved the formation of the desired polymer bearing the aromatic protons from the RAFT agent (5H, 7.4-7.9 ppm). By considering the same peaks from the repetitive units and aromatic protons from the RAFT agent, the M_n value of the synthesized polymer was calculated to be 4,000 g/mol. The cleavage of the RAFT agent[32] from the obtained PNIPAM-RAFT **26** was performed by aminolysis at room temperature with hexylamine in dichloromethane. After approximate 30 minutes the pink color of the reaction mixture disappeared as a proof that the RAFT agent (responsible of the mentioned color) was removed from the polymer backbone.
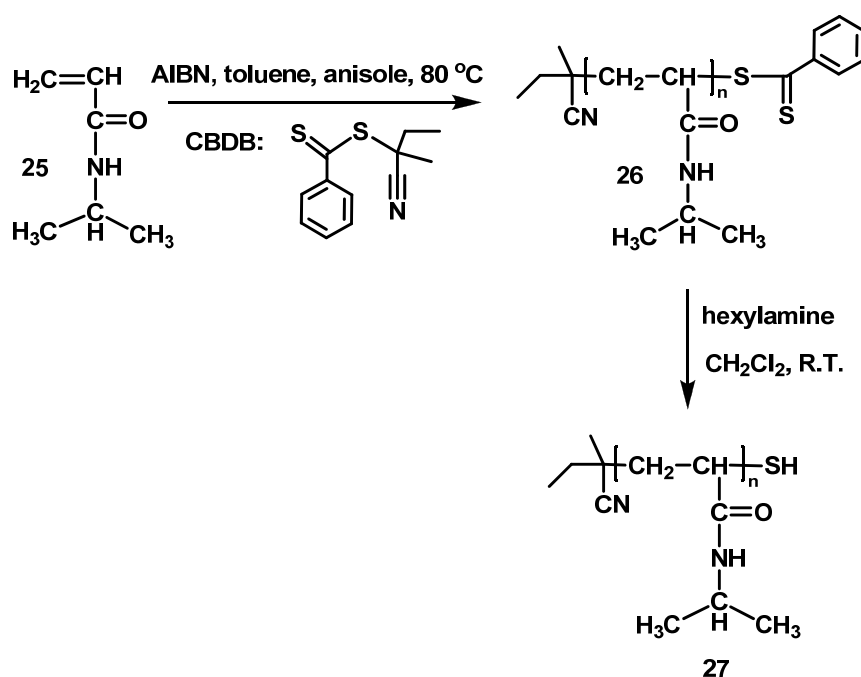
Scheme 2.11: *Schematic representation of the synthesis of the PNIPAM-RAFT **26** and PNIPAM-SH **27**.*

The successful removal of the RAFT agent was confirmed by ^{1}H-NMR spectroscopy that revealed the complete disappearance of the aromatic protons from the RAFT agent. Moreover, size exclusion chromatography SEC (RI and UV-Vis detector) showed that after aminolysis, the prepared PNIPAM-SH **27** without RAFT agent did not absorb anymore in the UV-Vis range (due to the lack of conjugation) while it was still detected by the RI detector proving that the RAFT agent had been removed.

For the subsequent end-group functionalization of PNIPAM-SH **27** with a terpyridine moiety, an activation approach was chosen so that the coupling reaction could be performed under mild conditions. Thus PNIPAM **27** was activated with *N,N'*-carbonyldiimidazole (CDI) in dry dichloromethane at room temperature, as depicted in Scheme 2.12. Imidazolides are known to be very reactive species towards primary amines; the coupling with the amino-terpyridine **29** (performed in dry THF under reflux for 72 h) resulted in the formation of PNIPAM end functionalized *mono*-terpyridine **30**. The amino-terpyridine **29** was prepared from chloro-terpyridine and amino-pentanol according to a literature procedure.[33,34]
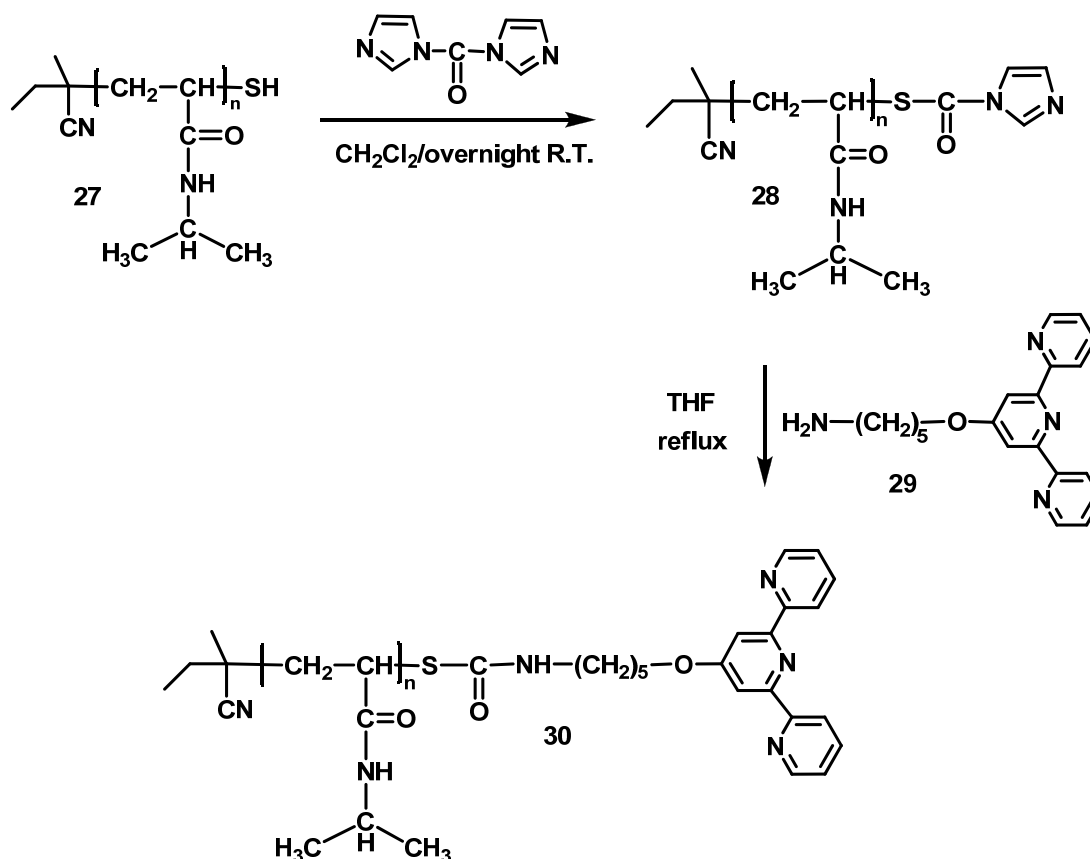
Scheme 2.12: *Schematic representation of the synthesis of the mono-terpyridine PNIPAM 30.*

The crude product **30** was purified by preparative size exclusion chromatography (BioBeads S-X1 in dichloromethane). The ^{1}H-NMR spectrum of the pure product **30** proved the coupling

of the thiol end group to the amino functionality by the shift of the methylene protons next to the amino functionality from 2.75 to 3.0 ppm. SEC analysis (RI detector) of PNIPAM end functionalized *mono*-terpyridine **30** displayed a slight increase of the molar mass in comparison to the starting material PNIPAM-RAFT **26** (Figure 2.15 left). Moreover, SEC with an in-line diode array detector demonstrated the presence of the terpyridine moiety over the complete molar mass distribution, as indicated by the typical UV-Vis absorption band around 290 nm which is characteristic for the terpyridine unit attached to the end of the polymer chain (Figure 2.15 right).
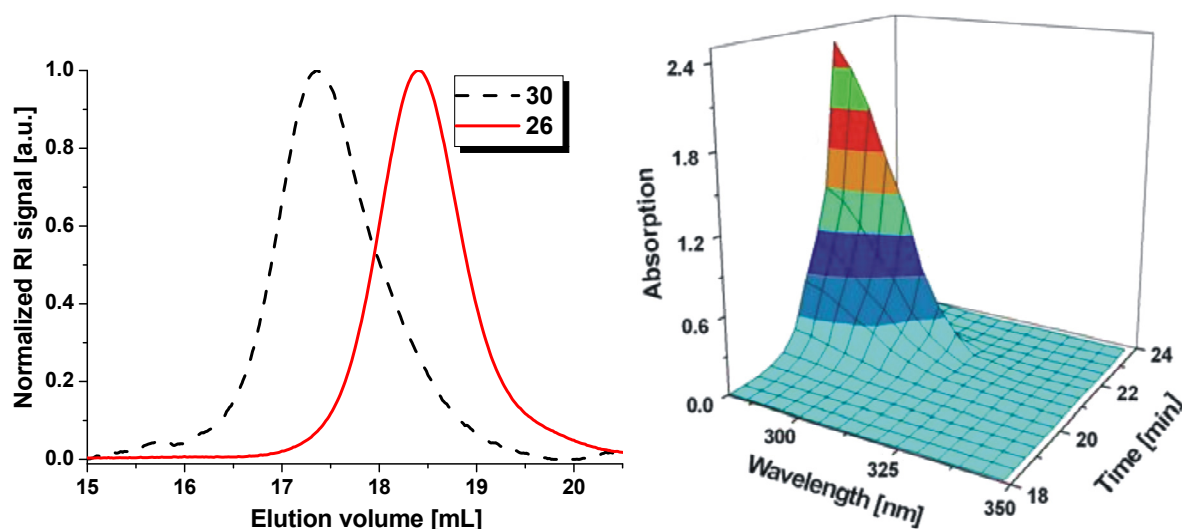
Figure 2.15: *Left: SEC elution curves (RI detector; eluent containing DMA with 49.5 mmol/L LiCl) for the mono-terpyridine PNIPAM 30 (dashed line) and PNIPAM-RAFT 26 (solid line). Right: SEC elution curve (PDA detector; eluent containing DMF with 5 mM NH₄PF₆) for the mono-terpyridine PNIPAM 30.*

2.4 Conclusions

This chapter describes the synthesis of the supramolecular chelating ligand 4'-chloro-2,2':6,2"-terpyridine **3** *via* a three step reaction approach. Subsequently, the prepared and characterized ligand **3** was successfully used for the postfunctionalization of various polymers. The end functionalization was achieved mainly by performing nucleophilic substititution reactions between various polymeric substrates bearing a hydroxy moiety and 4'-chloro-2,2':6,2"-terpyridine **3** in basic media. Following this approach a series of *mono* and *bis*-terpyridine functionalized polymers were prepared and characterized. Furthermore, a sequential approach was used for the functionalization of PNIPAM with the terpyridine ligand. As a result, tailor-made terpyridine containing building blocks were accessible for further metallo-polymerization studies.

2.5 Experimental

Materials and instrumentation
Solvents were purchased from Biosolve and all other compounds were obtained from Aldrich, Acros or Fluka. All chemicals were of reagent grade and used as received unless otherwise specified. Compound **29** was synthesized and characterized according to a literature procedure.[33,34] Azobis(*iso*butyronitrile) (AIBN) was recrystallized from methanol and NIPAM was recrystallized from hexane. 2-Cyano-2-butyl dithiobenzoate (CBDB) was prepared according to a literature procedure for a related compound.[35] Purified solvents were used where required. Tetrahydrofuran was distilled from molecular sieves, dichloromethane from calcium hydride; chloroform and DMSO were dried over molecular sieves. Reactions were performed under an atmosphere of argon where required. Preparative size exclusion chromatography was carried out on BioBeads S-X1 or S-X3 columns (dichloromethane or tetrahydrofuran). Visualization of the collected fractions was done by spotting on TLC plates followed by evaluation under UV irradiation or by subjecting the TLC plates to an aqueous solution of $FeCl_2 \times 4 H_2O$ to visualise the terpyridine moiety.

Instrumentation. Size exclusion chromatography (SEC) was performed on a Shimadzu system with a RID-6A refractive index detector and a PL gel 5 mm Mixed-D column. A solution of 49.5 mmol/L of lithium chloride in *N,N*-dimethylacetamide (DMA) was used as the eluent at a flow rate of 1 mL/min and a column temperature of 60 °C; a polystyrene calibration was utilized. The column temperature was 50 °C. Size exclusion chromatograms were also measured on a Waters SEC system consisting of an isocratic pump, a solvent degasser, a column oven, a 2996 photodiode array (PDA) detector, a 2414 refractive index detector, a 717 plus autosampler and a Styragel HT 4 GPC column with a precolumn installed. The eluent was *N,N*-dimethyl-formamide (DMF) with 5 mM NH_4PF_6 at a flow speed of 0.5 mL/min; a linear PEG calibration was used. The column temperature was 50 °C. Moreover, size exclusion chromatograms were measured on a Shimadzu system equipped with a SCL-A10 system controller, a LC-10AD pump, a RID-10A refractive index detector, a SPD-10A UV-detector at 254 nm and a PLgel 5 mm Mixed-D column at 50 8C utilizing chloroform: triethylamine: 2-propanol (94:4:2) mixture as eluent at a flow rate of 1 mL/min. The molecular weights were calculated against PEG standards. IR spectra were recorded on a Perkin Elmer 1600 FT-IR spectrometer. Nuclear magnetic resonance (NMR) spectra were recorded on a Varian Gemini 400 MHz spectrometer at 298 K. Chemical shifts are reported in parts per million (δ) downfield from an internal standard, tetramethylsilane (TMS) in THF-d_8, $CDCl_3$, CD_2Cl_2 or CD_3COCD_3. Coupling constants (*J* values) are reported in Hertz (Hz). UV spectra were recorded on a Perkin Elmer Lamda-45 (1 cm cuvettes). MALDI-TOF-MS was performed on a Voyager-DE[(tm)] PRO Biospectrometry[(tm)] Workstation (Applied Biosystems) time-of-flight mass spectrometer reflector, using dithranol as matrix. GC-MS analysis was performed on a Shimadzu GC-MS-QP5000, the mass values are reported as mass/charge ratio (*m/z*). Elemental analyses were carried out on a Carlo Erba Instruments EA1108 CHNS/O Elemental Analyzer and an EuroEA3000 Series EuroVector Elemental Analyzer for CHNS-O.

1,5-Bis(2-pyridyl)-1,3,5-tricarbonyl pentane (1)
A solution of acetone (6.42 mL, 75 mmol) and 2-ethyl pycolinate (37.4 mL, 165 mmol) in dry THF (90 mL) was added *very slowly*, dropwise, to a refluxing suspension of sodium hydride (95%, 5.7 g, 225 mmol) in dry THF (300 mL) under argon atmosphere. The reaction mixture was additionally refluxed (3 h) followed by the THF removal in vacuo. The resulting orange paste was *carefully* treated with water and the obtained orange solution was filtered through Celite. The pH of the filtrate was adjusted to pH = 7 by the dropwise of CH_3COOH, resulting in the precipitation of the crude product. Further work-up was performed by washing the yellow solid with water and dried. The pure product was obtained as yellow needles by recristalization from ethanol overnight. Yield of **1**: 22.68 g (68%). ^{1}H-NMR (400 MHz, CD_2Cl_2, 25 °C): δ (ppm) = 8.7 (m), 8.03-8.12 (m), 7.81-7.87 (m), 7.37-7.50 (m), 6.98 (s), 6.81 (s), 4.45 (s). GC-MS (CH_2Cl_2): *m/z* = 268 (M^+).

2,6-Bis(pyrid-2-yl)-4-pyridone (2)
A mixture of 17.16 g (64 mmol) of 1,5-*bis*-(2'-pyridyl)-1,3,5-tricarbonyl pentane **1** and 34.66 g NH_4OH (450 mmol) in 500 mL ethanol was refluxed under argon for 50 h. The flask was attached to a Soxhlet filled with molecular sieves that where changed 3 times during the refluxing hours in order to

remove the resulting water from the system. After the completion of the reaction, the ethanol was partially removed (approximately 80%). The remaining solution was kept overnight at room temperature yielding in a white precipitate which was further washed with diethyl ether. The pure product was obtained as white powder. Yield of **2**: 10.92 g (68%). ^{1}H-NMR (400 MHz, CD$_2$Cl$_2$, 25 °C): δ (ppm) = 12.07 (s, N*H*), 8.79 (m), 7.94 (m), 7.45 (m), 7.45 (m), 7.26 (m). GC-MS (CH$_2$Cl$_2$): *m/z* = 249 (M$^+$).

4'-Chloro terpyridine (3)

A mixture of 6.00 g (24.08 mmol) 2,6-*bis*(pyrid-2-yl)-4-pyridone **2** and 12.54 g (60.173 mmol) PCl$_5$ in 207 mL POCl$_3$ was heated under refluxed in the presence of argon for 24 h. After the completion of the reaction the solvent was removed under vacuum. To the resulting crude product was added slowly under *caution* water followed by the extraction in CH$_2$Cl$_2$. To the remaining water phase was added Na$_2$CO$_3$ and the neutralized compound was extracted with CH$_2$Cl$_2$. All the organic phases were collected and dried over MgSO$_4$ followed by the removal of the solvent (approximately 80%) *in vacuo*. From the remaining solution crystals were growing overnight in the freezer. Yield of **3**: 4.00 g (62%). ^{1}H-NMR (400 MHz, CD$_2$Cl$_2$, 25 °C): δ (ppm) = 8.72 (d, 2H, J = 5.1 Hz; H^6, H$^{6''}$), 8.63 (d, 2H, J = 8.4 Hz; H^3, H$^{3''}$), 8.53 (s, 2H, H$^{3'}$, H$^{5'}$), 7.91 (td, 2H, J = 8.0, 1.8 Hz; H^4, H$^{4''}$), 7.41 (td, 2H, J = 8.1, 2.0 Hz; H^5, H$^{5''}$). GC-MS (CH$_2$Cl$_2$): *m/z* = 267 (M$^+$).

3-(2,2':6',2''-Terpyridine-4'-yloxy)-propan-1-ol (4)

Compound **4** was synthesized according to a modified literature procedure[36,34] as following: 4'-chloro terpyridine **3** (2.08 g, 7.686 mmol) was added to a mixture of powdered KOH (880 mg, 0.015 mmol), 1,3-propandiol (6.2 g, 81.57 mmol) and water free DMSO (30 ml) preliminarily stirred at 50 °C for 30 minutes. The resulting reaction mixture was stirred at 50 °C overnight and then poured into deionized water. The final product **4** was purified by repetitive recrystalization from THF. Yield of **4**: 0.9 g (36%). ^{1}H-NMR (300 MHz, CDCl$_3$, 25 °C) δ (ppm) = 8.70 (m, 2H, H^6, H$^{6''}$), 8.64 (m, 2H, H^3, H$^{3''}$), 8.07 (s, 2H, H$^{3'}$, H$^{5'}$), 7.89 (m, 2H, 1.8 Hz; H^4, H$^{4''}$), 7.31 (m, 2H, H^5, H$^{5''}$), 4.44 (t, J = 6.0 Hz; 2H, H$^\gamma$), 3.9 (t, J = 6.0 Hz; 2H, H$^\alpha$), 2.13 (m, 2H, H$^\beta$). MALDI-TOF-MS *m/z* = 308 (MH$^+$). C$_{18}$H$_{17}$N$_3$O$_2$ (307.35): calcd. C 70.34, H 5.58, N 13.67; found C 70.01, H 5.35, N 13.40.

6-(2,2':6',2''-Terpyridine-4'-yloxy)-hexanoic acid (5)

Compound **5** has been synthesized according to a modified literature procedure.[34] To a homogeneous suspension of powdered KOH (3.7 g, 66 mmol) and water free DMSO (30 mL) preliminarily stirred at 60 °C for 30 minutes, ε-caprolactone (2.98 g, 26.15 mmol) was added slowly. After 30 minutes of additional stirring 4'-chloro terpyridine **3** (3.48 g, 13 mmol) was added *via* a dropping funnel. The reaction was stirred over the weekend and then poured into deionised water. Further adjustment of the pH value was done by the addition of few drops of hydrochloric acid into the solution until a precipitate was formed. The final product was purified by repetitive recrystalization from THF. Yield of **5**: 4.00 g (93%). ^{1}H NMR (300 MHz, THF-d$_8$, 25 °C) δ (ppm) =10.59 -COO*H*, 8.60 (m, 4H, H$^{6,6''}$), 8.06 (s, 2H, H$^{3',5'}$), 7.81 (ddd, J = 1.6, 4.9, 7.3 Hz, 2H, H$^{4,4''}$), 7.28 (ddd, J = 1.1, 3.9, 4.9 Hz, 2H, H$^{5,5''}$), 4.21 (t, J = 6.1 Hz, 2H, H$^\gamma$), 2. 25 (t, J = 6.7 Hz, 2H, H$^\beta$), 1.85 (m, 2H, H$^\varepsilon$), 1.73-1.64 (m, 4H, H$^\gamma$, H$^\delta$). C$_{21}$H$_{21}$N$_3$O$_3$ (363.41) calcd. C 69.41, H 5.82, N 11.56; found C 69.11, H 5.75, N 11.40.

Synthesis of 1,16-bis(2,2':6',2''-terpyridin-4'-yloxy)hexadecane (6)

Compound **6** was synthesized according to a modified literature procedure as following.[37] 4'-Chloro terpyridine **3** (4.23 g, 15. 81 mmol) dissolved in approximate 35 mL water free DMSO was added *via* a dropping funnel to a mixture of powdered KOH (1.77 g, 31.60 mmol), 1,16-hexadecanol (1.02 g, 3.95 mmol) and water free DMSO (40 mL) preliminarily stirred at 70 °C for 30 minutes. The resulting reaction mixture was stirred at 70 °C over the weekend, then poured into deionized water. The crude precipitate was further washed with deionized water and acetone. Yield of **6**: 2.5 g (88%). ^{1}H-NMR (400 MHz, CD$_3$COCD$_3$, 25 °C): δ (ppm) = 8.67 (m, 8H, H^6, H$^{6''}$, H^3, H$^{3''}$), 8.08 (s, 4H, H$^{3'}$, H$^{5'}$), 7.95 (td, 4H, J = 7.6, 2.0 Hz; H^4, H$^{4''}$), 7.44 (td, 4H, J = 5.9, 1.8 Hz; H^5, H$^{5''}$), 4.28 (t, 4H, J = 6.2 Hz, tpyOC*H$_2$*), 1.89 (m, 4H, OCH$_2$C*H$_2$*), 1.55 (m, 4H, OCH$_2$CH$_2$C*H$_2$*), 1.3-1.42 (m, 20H, OCH$_2$CH$_2$CH$_2$*(CH$_2$)$_{10}$*-CH$_2$CH$_2$CH$_2$O). MALDI-TOF-MS *m/z* = 721.9 (MH$^+$, 35%), 743.9 (MNa$^+$, 100%).

General synthesis and purification of mono-terpyridine PEG (KOH/DMSO route)
Powdered KOH (700 mg, 12.5 mmol, 5 eq.) and α-methoxy-ω-hydroxy-PEG with M_n = 2,000; 3,000; 7,000 and 9,000 g/mol (5.00 g, 1 eq.) were stirred under argon in dry DMSO at 70 °C. After 30 minutes a 2.2 fold excess of 4'-chloro-2,2':6',2''-terpyridine **3** was added to the solution *via* a dropping funnel. The mixture was heated under reflux for 24 h, then poured into cold water and extracted with CH_2Cl_2. The combined organic layers were dried with Na_2SO_4 and removed *in vacuo*. The crude compound was further purified by preparative size exclusion chromatography (BioBeads SX-1, THF), followed by double precipitation from tetrahydrofuran (THF) into diethyl ether.

General synthesis and purification of mono-terpyridine PEG (^{t}BuOK/THF route)
Powdered ^{t}BuOK (3 eq.) and α-methoxy-ω-hydroxy-PEG (5.00 g, 1 eq.) were stirred under argon in dry THF at 70 °C. After 30 minutes a 2-fold excess of 4'-chloro-2,2':6',2''-terpyridine **3** was added *via* a dropping funnel to the solution. The mixture was refluxed for 24 h, then poured into cold water and extracted with CH_2Cl_2. The reaction product was purified by preparative size exclusion chromatography (BioBeads SX-1, THF), followed by precipitation from THF into diethyl ether and washed with cold hexane.

Mono-terpyridine PEG$_{12}$ (7)
Purification by BioBeads SX-3, CH_2Cl_2. Yield: 3.9 g (90%) ^{1}H-NMR (400 MHz, CD_2Cl_2, 25 ˚C): δ (ppm) = 8.68 (d, 2H, J = 5.1 Hz; H^6, $H^{6''}$), 8.63 (d, 2H, J = 8.4 Hz; H^3, $H^{3''}$), 8.00 (s, 2H, $H^{3'}$, $H^{5'}$), 7.84 (td, 2H, J = 8.0, 1.8 Hz; H^4, $H^{4''}$), 7.33 (td, 2H, J = 8.1, 2.0 Hz; H^5, $H^{5''}$), 4.39 (m, 2H, tpyOCH_2), 3.93 (m, 2H, tpyOCH$_2$CH_2), 3.49-3.34 (m, 48H, PEG backbone), 3.35 (s, 3H, OCH_3). UV-Vis (H_2O): λ_{max} (ε) = (L mol^{-1} cm^{-1}): 278 (13 200), 234 (17 000). IR (ATR): 2 884, 2 741 (CH_2), 1 601, 1 583, 1 565 (tpy). MALDI-TOFMS: M_n = 500 g/mol, M_w = 550 g/mol, PDI = 1.1.

Mono-terpyridine PEG$_{44}$ (8)
Yield: 5.1 g (91%). ^{1}H-NMR (400 MHz, CD_2Cl_2, 25 ˚C): δ (ppm) = 8.68 (d, 2H, J = 5.1 Hz; H^6, $H^{6''}$), 8.63 (d, 2H, J = 8.4 Hz; H^3, $H^{3''}$), 8.00 (s, 2H, $H^{3'}$, $H^{5'}$), 7.84 (td, 2H, J = 8.0, 1.8 Hz; H^4, $H^{4''}$), 7.33 (td, 2H, J = 8.1, 2.0 Hz; H^5, $H^{5''}$), 4.39 (m, 2H, tpyOCH_2), 3.93 (m, 2H, tpyOCH$_2$CH_2), 3.49-3.34 (m, 176H, PEG backbone), 3.35 (s, 3H, OCH_3). SEC (DMF system; PEG calibration): M_n = 2,000 g/mol, M_w = 2,260 g/mol, PDI = 1.13. MALDI-TOF-MS: M_n = 2,075 g/mol, M_w = 2,077 g/mol, PDI = 1.02.

Mono-terpyridine PEG$_{70}$ (9)
Yield: 5 g (94%). ^{1}H-NMR (400 MHz, CD_3COCD_3, 25 °C): δ (ppm) = 8.71 (m, 4H, H^6, $H^{6''}$, H^3, $H^{3''}$), 8.12 (s, 2H, $H^{3'}$, $H^{5'}$), 7.98 (td, 2H, J = 7.8, 1.6 Hz; H^4, $H^{4''}$), 7.46 (td, 2H, J = 8.0, 2.0 Hz; H^5, $H^{5''}$), 4.44 (m, 2H, tpyOCH_2), 3.96 (m, 2H, tpyOCH$_2$CH_2), 3.62-3.48 (m, 280H, PEG backbone), 3.31 (s, 3H, OCH_3). SEC (DMF system; PEG calibration): M_n = 3,300 g/mol, M_w = 3,650 g/mol, PDI = 1.11. MALDI-TOF-MS: M_n = 3,010 g/mol, M_w = 3,050 g/mol, PDI = 1.01.

Mono-terpyridine PEG$_{155}$ (10)
Yield: 4.6 g (90%). ^{1}H-NMR (400 MHz, CD_2Cl_2, 25 ˚C): δ (ppm) = 8.67 (m, 2H; H^6, $H^{6''}$), 8.61 (m, 2H; H^3, $H^{3''}$), 8.05 (s, 2H, $H^{3'}$, $H^{5'}$), 7.85 (m, 2H; H^4, $H^{4''}$), 7.33 (m, 2H; H^5, $H^{5''}$), 4.40 (m, 2H, tpyOCH_2), 3.93 (m, 2H, tpyOCH$_2$CH_2), 3.90-3.47 (m, 620H, PEG backbone), 3.37 (s, 3H, OCH_3). SEC (DMF system; PEG calibration): M_n = 7,000 g/mol, M_w = 7,400 g/mol, PDI = 1.05. MALDI-TOF-MS: M_n = 6,070 g/mol, M_w = 6,270 g/mol, PDI = 1.03.

Mono-terpyridine PEG$_{200}$ (11)
Yield: 4.6 g (93%). ^{1}H-NMR (400 MHz, CD_2Cl_2, 25 ˚C): δ (ppm) = 8.68 (m, 2H; H^6, $H^{6''}$), 8.61 (m, 2H; H^3, $H^{3''}$), 8.03 (s, 2H, $H^{3'}$, $H^{5'}$), 7.84 (m, 2H; H^4, $H^{4''}$), 7.33 (td, 2H; H^5, $H^{5''}$), 4.41 (m, 2H, tpyOCH_2), 3.95 (m, 2H, tpyOCH$_2$CH_2), 3.79-3.57 (m, 800H, PEG backbone), 3.57 (s, 3H, OCH_3). SEC (DMF system; PEG calibration): M_n = 9,500 g/mol, M_w = 9,550 g/mol, PDI = 1.02. MALDI-TOF-MS: M_n = 8,075 g/mol, M_w = 8,250 g/mol, PDI = 1.02.

General synthesis and purification of bis-terpyridine PEG (^tBuOK/THF route)

Powdered ^tBuOK (420.56 mg, 3.74 mmol, 6 eq.) and telechelic-PEG with M_n = 2,000 and 8,000 g/mol (5.00 g, 1 eq.) were stirred under argon in dry THF at 70 °C. After 30 minutes a 4-fold excess of 4'-chloro-2,2':6',2"-terpyridine **3** was added *via* a dropping funnel to the solution. The mixture was refluxed for 48 h, then poured into cold water and extracted with CH_2Cl_2. The purification was done using the same steps as in the case of *mono*-terpyridine PEG.

Bis-terpyridine PEG$_{44}$ (12)

Yield: 5.4 g (90%). ^{1}H-NMR (400 MHz, CD_2Cl_2, 25 °C): δ (ppm) = 8.68 (d, 2H, J = 5.2 Hz; H^6, H$^{6"}$), 8.63 (d, 2H, *J* = 8.4 Hz; H^3, H$^{3"}$), 8.06 (s, 2H, H$^{3'}$, H$^{5'}$), 7.87 (td, 2H, *J* = 1.9, 7.8 Hz; H^4, H$^{4"}$), 7.33 (td, 2H, *J* = 8.2, 2.1 Hz; H^5, H$^{5"}$), 4.39 (m, 2H, tpyOC*H$_2$*), 3.93 (m, 2H, tpyOCH$_2$C*H$_2$*), 3.49-3.34 (m, 176H, PEG backbone). SEC (DMF system; PEG calibration): M_n = 2,400 g/mol, M_w = 2,470 g/mol, PDI = 1.03. MALDI-TOF-MS: M_n = 2,396 g/mol, M_w = 2,409 g/mol, PDI = 1.02.

Bis-terpyridine PEG$_{180}$ (13)

Yield: 4.72 g (90%). ^{1}H-NMR (300 MHz, CDCl$_3$, 25 °C): δ (ppm) = 8.68 (m, 4H, H^6, H$^{6"}$), 8.61 (m, 4H, H^3, H$^{3"}$), 8.04 (s, 4H, H$^{3'}$, H$^{5'}$), 7.86 (m, 2H, H^4, H$^{4"}$), 7.34 (m, 4H, H^5, H$^{5"}$), 4.39 (m, 4H, tpyOC*H$_2$*), 3.93 (m, 4H, tpyOCH$_2$C*H$_2$*), 3.81-3.46 (m, 720H, PEG backbone). SEC (DMF system; PEG calibration): M_n = 8,400 g/mol, M_w = 8,600 g/mol, PDI = 1.07. MALDI-TOF-MS: M_n = 9,100 g/mol, M_w = 9,300 g/mol, PDI = 1.02.

Synthesis of methoxy-PTHF$_{60}$ (15)

THF was polymerized in a dry flask by the addition of methyl triflate (100 mL, 0.88 mmol) to dry THF (50 mL) at room temperature under argon. After 15 min of rigorous stirring, the polymerization was quenched by the addition of 50 mL H_2O followed by the extraction of the reaction mixture in CHCl$_3$ (200 mL). The organic solvent was dried with Na$_2$SO$_4$ and removed *in vacuo*. The PTHF was obtained as a white wax (3.31 g, 60%). ^{1}H-NMR (400 MHz, CDCl$_3$, 25 °C): δ (ppm) = 3.62 (m, 2H, C*H$_2$*), 3.48-3.39 (m, 240H, PTHF backbone), 3.35 (s, 3H, OC*H$_3$*), 1.72-1.55 (m, 240H, PTHF backbone), 2.83 (1H, O*H*). SEC (CHCl$_3$ system; PEG calibration): M_n = 4,350 g/mol, M_w = 5,100 g/mol, PDI = 1.17. MALDI-TOF-MS: M_n = 3,900 g/mol, M_w = 4,000 g/mol, PDI = 1.02.

General synthesis and purification of mono-terpyridine PTHF$_{60}$ (16)

Compound **16** was synthesized and purified following the procedure described for *mono*-terpyridine PEG (^tBuOK/THF route; reflux temperature 65 °C). No precipitation was performed for the pure fractions of **16** collected from the BioBeads. Yield: 440 mg (83%). ^{1}H-NMR (400 MHz, CD_2Cl_2, 25 °C): δ (ppm) = 8.68 (m, 2H; H^6, H$^{6"}$), 8.62 (m, 2H; H^3, H$^{3"}$), 8.00 (s, 2H, H$^{3'}$, H$^{5'}$), 7.86 (m, 2H; H^4, H$^{4"}$), 7.34 (m, 2H; H^5, H$^{5"}$), 4.25 (m, 2H, tpyOC*H$_2$*), 3.62 (m, 2H, tpyOCH$_2$C*H$_2$*), 3.49-3.34 (m, 280H, PTHF backbone), 1.69-1.50 (m, 280H, PTHF backbone). 3.32 (s, 3H, OC*H$_3$*). SEC (CHCl$_3$ system; PEG calibration): M_n = 4,500 g/mol, M_w = 6,500 g/mol, PDI = 1.44. MALDI-TOF-MS: M_n = 3,800 g/mol, M_w = 3,870 g/mol, PDI = 1.01.

Synthesis of telechelic-PTHF$_{90}$ (17)

THF was polymerized in a dry flask by the addition of triflic anhydride (200 mL, 1.18 mmol) to dry THF (50 mL) at room temperature under argon. After 15 min of rigorous stirring the polymerization was quenched by the addition of 50 mL H_2O followed by the extraction of the reaction mixture in CHCl$_3$ (200 mL). The organic solvent was dried with Na$_2$SO$_4$ and removed *in vacuo*. The PTHF was obtained as a white wax (12.56 g, 65%). ^{1}H-NMR (400 MHz, CDCl$_3$, 25 °C): δ (ppm) = 3.63 (m, 2H, C*H$_2$*), 3.53-3.35 (m, 360H, PTHF backbone), 1.73-1.48 (m, 360H, PTHF backbone), 2.53 (2H, O*H*). SEC (CHCl$_3$ system; PEG calibration): M_n = 5,800 g/mol, M_w = 7,000 g/mol, PDI = 1.2. MALDI-TOF-MS: M_n = 5,330 g/mol, M_w = 5,400 g/mol, PDI = 1.01.

General synthesis and purification of bis-terpyridine PTHF$_{90}$ (18)

Compound **18** was synthesized and purified following the procedure described for *bis*-terpyridine PEG (^tBuOK/THF route; reflux temperature 65 °C). No precipitation was performed for the pure fractions of **18** collected from the BioBeads. Yield: 2.2 g (73%). ^{1}H-NMR (400 MHz, CD_2Cl_2, 25 °C): δ (ppm)

= 8.69 (m, 2H; H^6, H$^{6"}$), 8.61 (m, 2H; H^3, H$^{3"}$), 8.00 (s, 2H, H$^{3'}$, H$^{5'}$), 7.84 (m, 2H; H^4, H$^{4"}$), 7.33 (m, 2H; H^5, H$^{5"}$), 4.25 (m, 2H, tpyOC*H$_2$*), 3.64 (m, 2H, tpyOCH$_2$C*H$_2$*), 3.50-3.29 (m, 380H, PTHF backbone), 1.67-1.55(m, 380H, PTHF backbone). SEC (CHCl$_3$ system; PEG calibration): M$_n$ = 7,300 g/mol, M$_w$ = 8,100 g/mol, PDI = 1.11 MALDI-TOF-MS: M$_n$ = 6,500 g/mol, M$_w$ = 6,600 g/mol, PDI = 1.01.

Synthesis of PEtOx$_{50}$ (19)
19 was prepared and fully characterized by Dr. David Fournier as described in literature.[38,39]

Synthesis of mono-terpyridine PEtOx$_{50}$ (20)
For the synthesis see the *mono*-terpyridine PEG (*^{t}*BuOK/THF route). Reflux temperature 60 °C. Yield of **20**: 3.2 g (90%). ^{1}H-NMR (400 MHz, CD$_3$Cl, 25 °C): δ (ppm) = 8.61 (m, 4H; H^6, H$^{6"}$, H^3, H$^{3"}$), 7.95 (s, 2H, H$^{3'}$, H$^{5'}$), 7.80 (m, 2H; H^4, H$^{4"}$), 7.29 (m, 2H; H^5, H$^{5"}$), 4.39 (m, 2H, tpyOC*H$_2$*), 3.68 (s, 3H, C*H$_3$*), 3.43-3.31 (m, 240H, PEtOx backbone), 2.38-2.15 (m, 120 H, PEtOx backbone), 1.06 (s, 180 H, C*H$_3$*). SEC (DMF system; PEG calibration): M$_n$ = 5,400 g/mol, M$_w$ = 4,500 g/mol, PDI = 1.20. MALDI-TOF-MS: M$_n$ = 4,600 g/mol, M$_w$ = 4,800 g/mol, PDI = 1.04.

Synthesis of mono-terpyridine PDMS (22)
Powdered KOH (168 mg, 3 mmol) and PDMS-(CH$_2$)$_3$OH with M$_n$ = 5 000 g/mol (3.00 g, 0.6 mmol) were stirred under argon in dry DMSO at 120 °C. After 30 minutes a 2.2 fold excess of 4'-chloro-2,2':6',2"-terpyridine was added (3.53 mg, 1.32 mmol). The reaction mixture was refluxed for 48 h, then poured into cold water and extracted with CH$_2$Cl$_2$. The combined organic layers were dried with Na$_2$SO$_4$ and removed *in vacuo*. The crude compound was further purified by preparative size exclusion chromatography (BioBeads SX-1, THF) yielding 740 mg of **22** (25%). ^{1}H-NMR (400 MHz, CD$_2$Cl$_2$, 25 °C): δ (ppm) = 8.64 (m, 4H; H^6, H$^{6"}$, H^3, H$^{3"}$), 8.08 (s, 2H, H$^{3'}$, H$^{5'}$), 7.90 (m, 2H; H^4, H$^{4"}$), 7.39 (m, 2H,; H^5, H$^{5"}$), 4.40 (m, 2H, tpyOC*H$_2$*CH$_2$CH$_2$), 2.28 (m, 2H, tpyOCH$_2$C*H$_2$*CH$_2$), 1.34 (m, 2H, tpyOCH$_2$CH$_2$C*H$_2$*), 0.26-0.02 (m, 370H, PDMS backbone). IR (ATR): 2 884, 2 741 (CH$_2$), 1 601, 1 583, 1 540, 1 565 (tpy), 1 240, 1 010, 780 (Si-O-Si). SEC (DMA system; PEG calibration): M$_n$ = 5,700 g/mol, M$_w$ = 6,700 g/mol, PDI = 1.17.

General synthesis of bis-terpyridine Pluronics$^®$
Analog to *bis*-terpyridine PEG **12-13** (KOH/DMSO route). Powdered KOH (4 eq.) and telechelic Pluronic$^®$ (3.00 g, 1 eq.) in dry DMSO at 60 °C.

Bis-terpyridine PEG$_{10}$-PPG$_{30}$-PEG$_{10}$ (23)
Yield of **23**: 1.2 g (83%). ^{1}H-NMR (400 MHz, CD$_2$Cl$_2$, 25 °C): δ (ppm) = 8.68 (m, 2H; H^6, H$^{6"}$), 8.62 (m, 2H; H^3, H$^{3"}$), 8.06 (s, 2H, H$^{3'}$, H$^{5'}$), 7.86 (m, 2H; H^4, H$^{4"}$), 7.34 (m, 2H; H^5, H$^{5"}$), 4.39 (m, 2H, tpyOC*H$_2$*), 3.92 (m, 2H, tpyOCH$_2$C*H$_2$*), 3.75-3.29 (m, 110H, PEG backbone and –C*H* backbone), 1.22-1.07 (m, 30H, CH$_3$ backbone). SEC (DMA system; PS calibration): M$_n$ = 3,600 g/mol, M$_w$ = 4,400 g/mol, PDI = 1.23.

Bis-terpyridine PPG$_{14}$-PEG$_{24}$-PPG$_{14}$ (24)
Yield of **24**: 1.1 g (80%). ^{1}H-NMR (400 MHz, CD$_2$Cl$_2$, 25 °C): δ (ppm) = 8.68 (m, 2H; H^6, H$^{6"}$), 8.62 (m, 2H; H^3, H$^{3"}$), 8.06 (s, 2H, H$^{3'}$, H$^{5'}$), 7.87 (m, 2H; H^4, H$^{4"}$), 7.35 (m, 2H; H^5, H$^{5"}$), 4.92 (m, 2H, tpyOC*H$_2$*-), 3.83-3.37 (m, 130H, PEG backbone and –C*H* backbone), 1.17-1.07 (m, 28H, CH$_3$ backbone). SEC (DMA system; PS calibration): M$_n$ = 3,300 g/mol, M$_w$ = 4,100 g/mol, PDI = 1.24.

Synthesis of PNIPAM (27)
The polymerization was performed using the previously optimized polymerization conditions.[40] NIPAM **25** (5 g, 44.19 mmol, 75 eq.), CBDB (1 eq.) and AIBN (0.25 eq.) were added into a round-bottom flask with a mixture of toluene and anisole (19 mL and 1 mL). The reaction mixture was bubbled for 30 min with argon. Subsequently, the flask was immersed in a preheated oil bath at 80 °C. After 7 hours the polymerization was stopped with a conversion of 39% as determined by ^{1}H-NMR spectroscopy. The pink resulting polymer was further purified by precipitation (3 times) from toluene into *n*-hexane yielding in 1.2 g of **26** (80%). SEC (DMA system; PS calibration): M$_n$ = 5,100 g/mol,

M_w = 6,000 g/mol, PDI = 1.18. The cleavage of the end chain RAFT agent was done at room temperature in dichloromethane with hexylamine. After 30 minutes the color changed from pink to yellow indicating the success of the reaction. The cleaved polymer was precipitated into hexane yielding in 1.0 g (83%). SEC (DMA system; PS calibration): M_n = 4,500 g/mol; M_w = 5,400 g/mol, PDI = 1.20. ^{1}H-NMR (400 MHz, CD$_2$Cl$_2$, 25 ˚C): δ (ppm) = 3.99-3.85 (bs, 30H, -C*H*), 2.43-1.93 (m, 30H, -C*H* backbone), 1.87-1.63 (m, 60H, -C*H$_2$* backbone), 1.15 (s, 180H, -C*H$_3$*).

Synthesis of PNIPAM imidazolide (28).

The PNIPAM **27** (881 mg, 0.259 mmol) was treated with *N,N'*-carbonyldiimidazole (1.104 g, 6.8 mmol) for 16 h in dried dichloromethane (15 mL) at room temperature. Precipitation of the resulting crude product into diethyl ether yielded 760 mg of the imidazolide activated PNIPAM (84%). ^{1}H-NMR (400 MHz, CD$_2$Cl$_2$, 25 ˚C): δ (ppm) = 7.91 (s, 1H), 7.51 (s, 1H), 7.15 (s, 2H), 3.97-3.85 (bs, 30H), 2.31-2.01 (m, 30H, -C*H* backbone), 1.87-1.63 (m, 60H, -C*H$_2$* backbone), 1.12 (s, 180H, -C*H$_3$*).

Synthesis of mono-terpyridine PNIPAM (30)

The PNIPAM imidazolide **28** (760 mg, 0.223 mmol) was treated with amino-terpyridine **29** (77.71 mg, 0.223 mmol) for 72 h in dried THF (15 mL) under reflux. The crude compound was further purified by preparative size exclusion chromatography (BioBeads SX-1, dichloromethane) yielding 200 mg of **30** (30%).^{1}H-NMR (400 MHz, CDCl$_3$, 25 ˚C): δ (ppm) = 8.67 (d, 2H, J = 4 Hz; H^6, H$^{6''}$), 8.60 (d , 2H, J = 8 Hz; H^3, H$^{3''}$), 7.99 (s, 2H, H$^{3'}$, H$^{5'}$), 7.86 (t, 2H, J = 7.6 Hz; H^4, H$^{4''}$), 7.35 (t, 2H, J = 6.2 Hz; H^5, H$^{5''}$), 4.23 (m, 2H, H^a), 3.97-3.85 (bs, 30H), 3.40 (m, 2H, H^e), 1.87-1.63 (m, 30H, -C*H$_2$* backbone), 1.80 (m, 2 H, H^b), 1.52-1.57 (m, 4 H, H^{c,d}), 2.34-2.02 (m, 60H, -C*H* backbone), 1.12 (s, 180H, -C*H$_3$*). SEC (DMA system; PS calibration): M_n = 6,400 g/mol, M_w = 7,800 g/mol, PDI = 1.21. MALDI-TOF-MS: M_n = 5,600 g/mol, M_w = 5,200 g/mol, PDI = 1.07.

2.6 References

1   F. H. Burstall, *J. Chem. Soc.* **1938**, 1662.

2   K. Nakamaru, *Bull. Chem. Soc. Jpn.* **1982**, *55*, 2697.

3   E. C. Constable, *Adv. Inorg. Chem. Radiochem.*, **1986**, *30*, 69.

4   P. R. Andres, U.S. Schubert, *Adv Mater.* **2004**, *16*, 1043.

5   J. M. Pollino, M. Weck, *Chem. Soc. Rev.* **2005**, *34*, 193.

6   E. C. Constable, *Chem. Soc. Rev.* **2007**, *36*, 246.

7   F. Kröhnke, *Synthesis* **1976**, *1*.

8   K. T. Potts, M. J. Cipullo, P. Ralli, G. Theodoridis, *J. Org. Chem.* **1982**, *47*, 3027.

9   U. S. Schubert, C. Eschbaumer, C. H. Weidl, *Des. Monomers Polym.* **1999**, *2*, 185; G. S. Hanan, U. S. Schubert, D. Volkmer, E. Riviere, J. M. Lehn, N. Kyritsakas, J. Fischer, *Can. J. Chem.* **1997**, *75*, 169; G. Ulrich, S. Bedel, C. Picard, P. Tisnes, *Tetrahedron Lett.* **2001**, *42*, 6113.

10   N. Belfrekh, C. Dietrich-Buchecker, J.-P. Sauvage, *Tetrahedron Lett.* **2001**, *42*, 2779; C. J. Aspley, J. A. G. Williams, *New J. Chem.* **2001**, *25*, 1136; U. Lehmann, A. D. Schlüter, *Eur. J. Org. Chem.* **2000**, 3483.

11   E. C. Constable, M. D. Ward, *J. Chem. Soc., Dalton Trans.* **1990**, 1405.

12   U. S. Schubert, S. Schmatloch, A. A. Precup, *Des. Monomers Polym.* **2002**, *5*, 211.

13   K. T. Potts, D. Konwar, *J. Org. Chem.* **1991**, *56*, 4815.

14   P. R. Andres, H. Hofmeier, B. G. G. Lohmeijer, U. S. Schubert, *Synthesis* **2003**, 2865-2871.

15   G. R. Newkome, F. Cardullo, E. C. Constable, C. N. Moorfield, A. M. W. C. Thomson. *Chem. Commun.* **1993**, 925.

16   P. R. Andres, *PhD thesis*, Eindhoven Technical University, **2004**.

17   J. M. Harris, S. Zalipsky, Poly(ethylene glycol): Chemistry and Biological Applications ACS Symp. Series, **1997**.

18   K. Bhowmick, H. L. Stephens, Handbook of Elastomers, Second Edition, Marcel Dekker, Inc., **2001**.

19   M. Dubreuil, E. Goethals, *Macromol. Chem. Phys.* **1997**, *198*, 3077.

20   M. Dubreuil, N. Farcv, E. Goethals, *Macromol. Rapid. Commun.* **1999**, *20,* 383.

21   E. J. Goethals, P. Van Caeter, J. M. Geeraert, F. E. Du Prez, *Angew. Makromol. Chemie* **1994***, 223,* 1.

22   H. F. Mark, N. M. Bikales, C. G. Overberger, G. Mengers, *"Encyclopedia of polymer science and engineering"*, 2 ed., Wiley-Interscience New York, **1985**.

23.   K. Aoi, M. Okada, *Prog. Polym. Sci.* **1996**, *21*, 151; S. Kobayashi, H. Uyama, *J. Polym. Sci. Part A: Polym. Chem.* **2002**, *40*, 192.

24   S. J. Clarson, J. A. Semlyen, Polysiloxane Polymers, PTR Prentice Hall, New York **2003**.

25   P. Alexandridis, T. A. Hatton, *Colloids Surf. A* **1995**, *96*, 1.

26   Pluronic and Tetronic surfactants, Technical Brochure, BASF Performance Chemicals: Parsippany, NJ, **1996**.

27   G. Zhou, I. I. Harruna, C. W. Ingram, *Polymer* **2005**, *46*, 10672.

28   G. Zhou, I. I. Harruna, *Macromolecules* **2005**, *38,* 4114.

29   J. Chiefari, Y. K. Chong, F. Ercole, J. Krstina, J. Jeffery, T. P. T. Le, R. T. A. Mayadunne, G. F. Meijs, C. L. Moad, G. Moad, E. Rizzardo, San H. Thang, *Macromolecules* **1998**, *31,* 5559.

30   C.-Y. Hong, Y.-Z. You, C.-Y. Pan, *J. Polym. Sci.: Part A: Polym. Chem.* **2004**, *42*, 4873.

31   Q. Liu, P. Zhang, M. Lu, *J. Polym. Sci.: Part A: Polym. Chem.* **2005**, *43*, 2615.

32   D. L. Patton, M. Mullings, F. Timothy, R. Advincula, *Macromolecules* **2005**, *38*, 8597.

33   G. R. Newkome, E. He, *J. Mater. Chem.* **1997**, *7*, 1237.

34   P. R. Andres, R. Lunkwitz, G. R. Pabst, K. Boehn, D. Wouters, S. Schmatloch, U. S. Schubert, *Eur. J. Org. Chem.* **2003**, *19*, 3769.

35   G. Bouhadir, N. Legrand, B. Quiclet-Sire, S. Z. Zard, *Tetrahedron Lett.* **1999**, *40*, 277.

36   U. Sampath, W. C. Putnam, T. A. Osiek, S. Touami, J. Xie, D. Cohen, A. Cagnolini, P. Droege, D. Klug, C. L. Barnes, A. Modak, J. K. Bashkin, S. S. Jurisson, *J. Chem. Soc., Dalton Trans.* **1999**, 2049.

37   P. R. Andres, U. S. Schubert, *Synthesis* **2004**, *8*, 1229.

38   F. Wiesbrock, R. Hoogenboom, M. A. M. Leenen, M. A. R. Meier, U. S. Schubert, *Macromolecules* **2005**, *38*, 5025.

39   R. Hoogenboom, R. M. Paulus, M. W. M. Fijten, U. S. Schubert, *J. Polym. Sci., Part A: Polym. Chem.* **2005**, *43*, 1487.

40   M. W. M. Fijten, M. A. R. Meier, R. Hoogenboom, U. S. Schubert, *J. Polym. Sci.: Part A: Polym. Chem.*, **2004**, *42*, 5775.

Chapter III

Supramolecular polymers and block copolymers containing Ni(II), Fe(II) and Co(II) *bis*-terpyridine complexes

Abstract

The characterization of supramolecular nickel(II), iron(II) and cobalt(II) bis-terpyridine poly(ethylene glycol) complexes was done utilizing SEC. The main aspects concerning the equilibrium between complexed and uncomplexed species are discussed in detail. In addition, the synthesized Ni(II) chain extended supramolecular-polymer was analyzed by depth-sensing indentation proving an increase in elastic modulus in comparison to the uncomplexed starting material. Furthermore, the self-assembly of the amphiphilic metallo-supramolecular A-b-B-b-A triblock copolymers based on the Ni(II)tpy$_2$, Fe(II)tpy$_2$ and Co(II)tpy$_2$ connectivity is discussed. The influence of the different binding strength of metal ions with terpyridine ligands on the metallo-polycondensation reaction and the micellization behavior of those materials was analyzed. Micelles of the obtained block copolymers were prepared and studied by different techniques, namely dynamic light scattering (DLS), cryogenic transmission electron microscopy (cryo-TEM) and atomic force microscopy (AFM). Moreover, the stability of the Ni(II)-tpy$_2$ type of connectivity was tested by performing decomplexation reactions.

3.1 Introduction

Inspired by nature, supramolecular chemistry has become one of the most studied topics in chemistry in the last years. Nowadays, a variety of polymers containing supramolecular binding units are synthetically accessible (see, *e.g.*, Chapter 2). The combination of macromolecular and supramolecular chemistry opens ways to obtain new functional materials that can be designed for a specific application by applying state-of-the-art controlled and living polymerization techniques teamed up with organic synthesis for the introduction of functional supramolecular moieties into the polymer architecture. These supramolecular polymers can generally be defined as polymer chains of small molecules held together *via* reversible, non-covalent bonds.[1,2] The most outstanding examples of supramolecular polymers can be found in hydrogen bonded systems,[3-6] systems based on metal ligand interactions[7-9] and systems that exploit ionic interactions.[10-12] All of these non-covalent interactions have certain advantages and disadvantages. Concerning metal-ligand interactions, the adjustability of their binding strength in a rather broad range (approximately between 25 and 95% of a covalent C-C bond, with a bond energy of 350 kJ/mol)[13] as well as their directionality can be considered an advantage, whereas the toxicity of some transition metal ions is a definite disadvantage. Hydrogen bonding motifs, on the other hand, can generally be considered as less toxic, but span a considerably smaller range of binding strengths (approximately 1-20% of a covalent C-C bond).[13]

Terpyridine metal-complexes are widely applied building blocks in supramolecular and macromolecular chemistry. Generally, 2,2':6',2"-terpyridines (tpy) are tridentate ligands which can complex a variety of transition metal ions with a high binding constant (compared to phenanthroline or 2,2'-bipyridine ligands), leading to the formation of octahedral metal complexes without giving rise to enantiomers.[14,15] The various possibilities for the functionalization of terpyridine ligands in the 4'-position[16,17] allows a straightforward access to supramolecular monomers and polymers.[18,19] The success in controlling the formation of a certain supramolecular metal-containing structures lies in the careful choice of metal ion, ligand, and framework motifs.[20-24]

The main interest for these types of "supra-structures" is the possibility of various combinations between the mentioned ligand and a large range of metal ions characterized by a different binding strength and exchange rate.[19,25,26] This characteristic could be an important feature for the preparation of new "smart" materials, intelligent glues or electro-photoactive compounds. To be able to design and to control the reversibility of such systems, a detailed knowledge of the complexation processes and the stability of the mentioned metal complexes

are required. For a good understanding and control of the complexation process, several independent detailed characterization techniques for the prepared systems are essential.

In the literature various studies describe and investigate the stability of terpyridine metal complexes. However, these reports focus on calorimetric,[27] thermogravimetric,[28] matrix-assisted laser desorption/ionization time-of-flight mass spectrometry (MALDI-TOF-MS)[29] and kinetic aspects[30,31] of small terpyridine metal complexes; to the best of our knowledge no detailed size exclusion chromatography (SEC) studies regarding the behavior of terpyridine metal containing polymers with different metal species have been published so far.

To determine the molar mass of macromolecules, size exclusion chromatography (SEC) turned out to be one of the most used characterization tools in polymer science. In the case of reversible systems based on hydrogen-bonds or weak metal-ligand interactions (*e.g.* zinc(II) or cobalt(II) *bis*-terpyridine complexes), the main difficulty faced in the usage of size exclusion chromatography was the comparably low binding strength of such systems in solution leading to fragmentation during the SEC separation. For this reason a SEC method was developed and proved to be suitable for the evaluation of metal-containing supramolecular homo and block copolymers based on metal ions with high binding strength (*e.g.* Ru(II)).[32] The main aim of the present study was to gain an improved understanding of the stability of different metal terpyridine homopolymer complexes based on a poly(ethylene glycol) macroligand in solution during the SEC measurements. This will lead to a better understanding and characterization of supramolecular polymers and assemblies.

3.2 Ni(II), Fe(II) and Co(II) *bis*-terpyridine poly(ethylene glycol)

The *bis*-terpyridine complex formation occurs *via* a *mono*-complex as shown in Equations (3.1) and (3.2).[33-36] The equilibrium constants and the mass balances are strongly influenced by the binding strength of the metal ion and also by the stability of the *mono* and *bis*-complexes, as it is described in the following:

$$M + L \rightleftharpoons ML \quad \text{with} \quad K_1 = \frac{[ML]}{[M][L]} \qquad \textbf{Equation 3.1}$$

$$ML + L \rightleftharpoons ML_2 \quad \text{with} \quad K_2 = \frac{[ML_2]}{[ML][L]} = \frac{[ML_2]}{K_1[M][L]^2} \qquad \textbf{Equation 3.2}$$
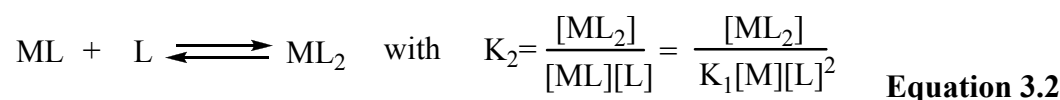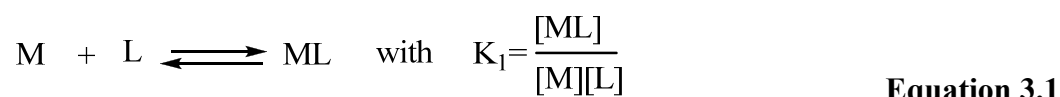
where [M], [L], [ML], and [ML$_2$] show the equilibrium concentrations of metal ion, ligand, *mono*-complex and *bis*-complex, respectively.

From previous studies it is known that Ru(II) ions form very stable complexes with terpyridine ligands, thereby offering the possibility of investigating the obtained species by optimized SEC methods.[32] Other transition metals ions do also form stable complexes with terpyridine units,[37] but no SEC studies of these species have been published so far to the best of our knowledge. For this reason model studies were carried out on low molar mass reference systems, namely metal(II) *bis*-terpyridine poly(ethylene glycol) complexes ($M_n \sim 4,000$ g/mol), with three different transition metal ions (Ni(II), Fe(II), Co(II)) to gain first insights into the behavior of the mentioned polymers, which are in equilibrium with their uncomplexed precursors as well as to maybe correlate their behavior to the stability of the metal(II) *bis*-terpyridine complex in solution during the SEC investigations. Once these important features for the polymeric model complexes have been elucidated, the application of the obtained knowledge to investigate chain-extended supramolecular polymers based on a *bis*-terpyridine poly(ethylene glycol) **12** ($M_n = 2,400$ g/mol) was targeted. For this purpose the metal ion characterized by the highest binding strength observed in this study should be used for SEC investigations.

3.2.1 Synthesis and characterization of Ni(II), Fe(II) and Co(II) *bis*-terpyridine poly(ethylene glycol)

First of all, the complexation of the *α*-terpyridine-*ω*-methyl-poly(ethylene glycol) named in our study *mono*-terpyridine PEG **8** (see Chapter 2) was performed with three different metal ions in low oxidation state: Ni(II), Fe(II) and Co(II), respectively (Scheme 3.1).[38] The selection of these transition metal ions was done in agreement with their relative high binding strength known from previous studies,[38] in order to study the differences which could result from the stability of the metal(II)-*bis*-terpyridine-PEG model complexes in solution during SEC measurements.
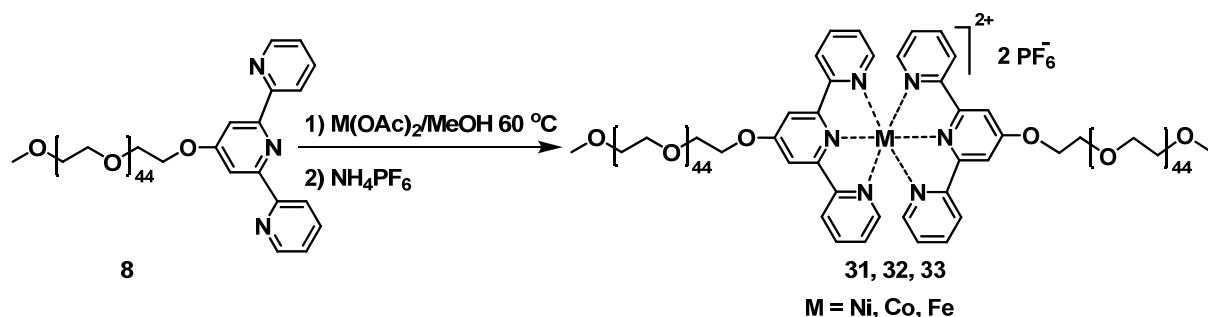
Scheme 3.1: *Schematic representation of the synthesis of Ni(II) bis-terpyridine-PEG **31**, Fe(II) bis-terpyridine PEG **32**, Co(II) bis-terpyridine PEG **33**.*

The model complex based on nickel(II) *bis*-terpyridine PEG hexafluorophosphate **31** was characterized by UV-Vis, ^{1}H-NMR and IR spectroscopy. The UV-Vis spectrum revealed a bathochromic shift of the ligand-centered (LC) π-π* absorption bands around 324 nm and 311 nm. The ^{1}H-NMR spectrum did not show any peaks in the aromatic region, due to the paramagnetic nature of the metal ion used. Nevertheless, signals for uncomplexed terpyridine could not be observed indicating a full complexation.

The ^{1}H-NMR spectrum of iron(II) *bis*-terpyridine PEG hexafluorophosphate **32** showed significant differences when compared to the spectrum of the starting material **8**. The upfield shift of the 6,6"-protons is characteristic for this type of complexes, due to the different chemical environment of the 6,6"-protons compared to the free ligand. From these investigations complete complexation of the free terpyridine ligands could be concluded. For the case of **32**, the UV-Vis spectrum revealed an intense absorption in the visible region, the color of the complex being intense purple. A distinct metal-to-ligand-charge-transfer band (MLCT) was detected at 556 nm.

The paramagnetic cobalt(II) *bis*-terpyridine PEG hexafluorophosphate complex **33** showed a Knight shift in ^{1}H-NMR due to the specific coupling of the electronic and nuclear spin, giving rise to proton shifts of up to 110 ppm from TMS.[39] The UV-Vis spectrum of complex **33** revealed also bathocromic shifts as already discussed for the Ni(II) complex. Moreover, complex **33** did not absorb in the visible region of the spectrum. IR spectra of the metallo-supramolecular polymers are similar to the model complexes described earlier.[38]

3.2.2 SEC stability studies of Ni(II), Fe(II) and Co(II) *bis*-terpyridine poly(ethylene glycol)

In a next step the stability of the prepared homopolymer model complexes was investigated by SEC. For this study, samples were utilized with known concentration (0.22 mmol/mL in the SEC eluent) from each metal(II)-*bis*-terpyridine complex **31**, **32** and **33**, respectively. From the prepared solutions different volumes (equivalent to 0.0011 mmol, 0.0055 mmol, 0.0110 mmol, 0.0165 mmol and 0.0221 mmol, respectively) were injected into the SEC system with the intention to observe the equilibrium between complexed and uncomplexed species (by varying the concentration). The stability of the studied metal complexes was mainly based on a qualitative observation of the signal of the elution peaks of complexed and uncomplexed species by SEC with a RI detector since these types of measurements were more difficult to be performed by SEC with an UV-Vis detector.

3.2.2.1 SEC studies of Ni(II) *bis*-terpyridine poly(ethylene glycol)

For Ni(II) *bis*-terpyridine complexes high K_1 and K_2 values (log K_1= 10.7 and log K_2= 11.1) were reported in the literature[31] and since the second equilibrium constant is slightly larger than the first one we expected the equilibrium to be completely shifted to the *bis*-complexed form. From the RI-SEC detector no relationship between the concentration and the chromatographic results was observed (Figure 3.1) and a shift towards lower retention times (higher molar masses) was noticed compared to the starting material **8**, indicating the successful formation as well as the high complex stability of the investigated Ni(II)tpy$_2$ type connectivity.
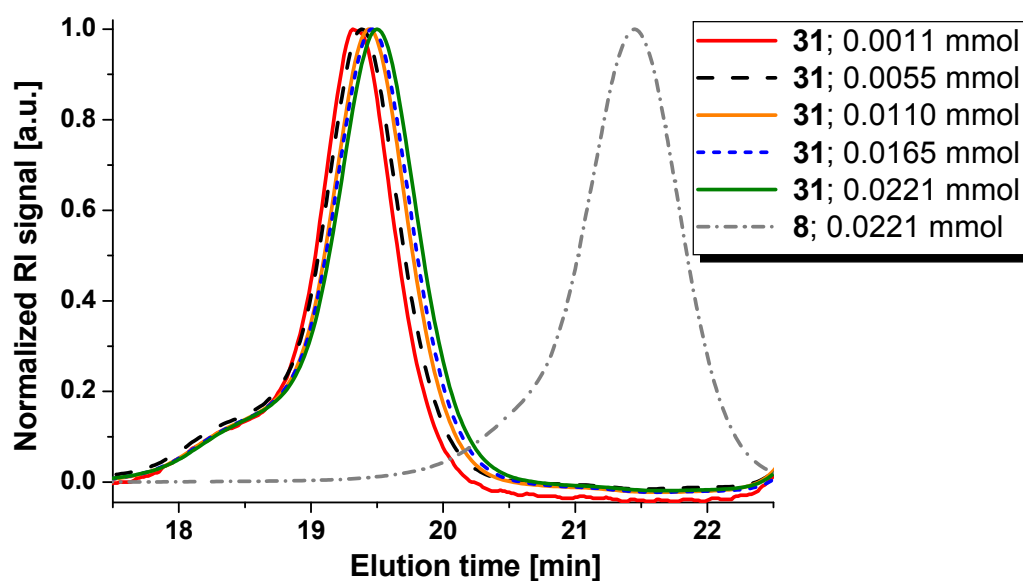
Figure 3.1: *SEC elution curves (RI detector) for the Ni(II) bis-terpyridine PEG **31** (different concentrations) and its corresponding starting material (mono-terpyridine PEG **8**).*

Moreover, the results obtained from the SEC-coupled in-line diode array detector of compound **31** demonstrated the integrity of the supramolecular assembly over the complete polymer distribution as indicated by the LC bands at 302, 314 and 324 nm, respectively (see Figure 3.2).
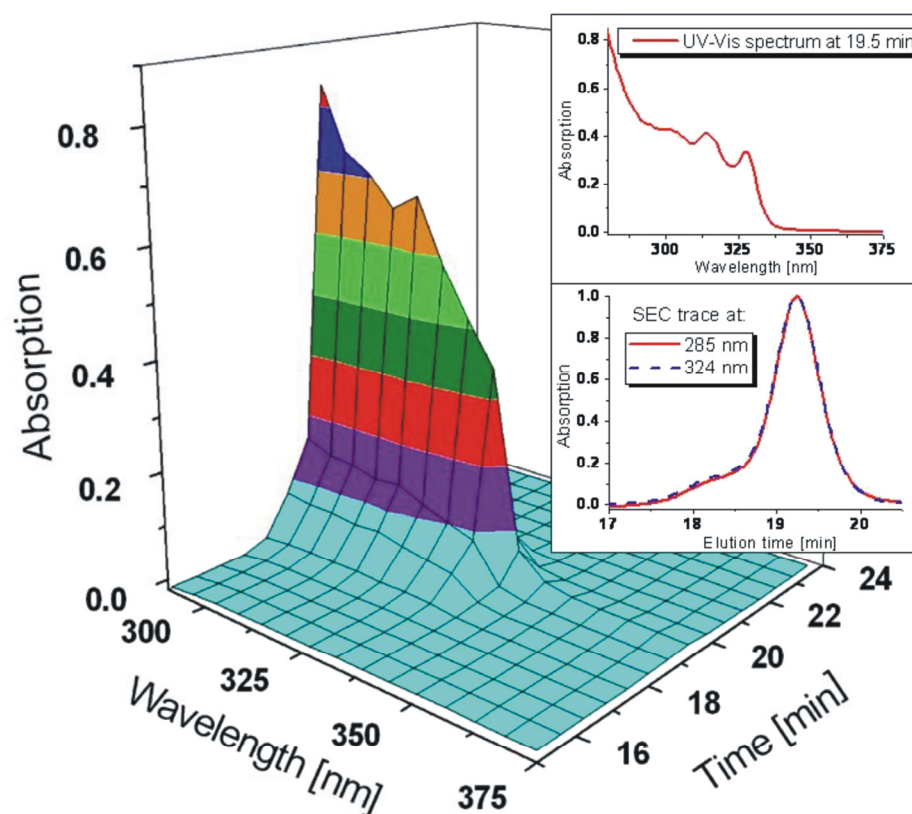
Figure 3.2: *SEC elution curves (PDA detector) for the Ni(II) bis-terpyridine PEG **31**.*

3.2.2.2 SEC studies of Fe(II) *bis*-terpyridine poly(ethylene glycol)

Taking into account that the binding constants for Fe(II) ions are slightly lower than for Ni(II) ions (log $\beta_{2(Ni)}$= 21.8; log $\beta_{2(Fe)}$= 20.9)[31] different results were expected from the SEC measurements in the case of Fe(II) *bis*-terpyridine PEG **32**. Moreover, for the case of Fe(II)tpy$_2$ systems, due to their increased lability, the possibility of oxidizing Fe(II) to Fe(III) is much higher compared to Ni(II)tpy$_2$ systems. By RI-SEC detector (Figure 3.3) it was observed that for lower concentrations of the Fe(II) *bis*-complex **32** the equilibrium is shifted to the uncomplexed species of **32**, namely **8**. If the concentration of the complex is increased, the equilibrium is shifted to the complexed compound **32** as it can also be expected considering Equations (3.1) and (3.2). From the RI-SEC plot the relationship between the concentration and the stability of the Fe(II) *bis*-terpyridine PEG **32** in solution could therefore be observed.
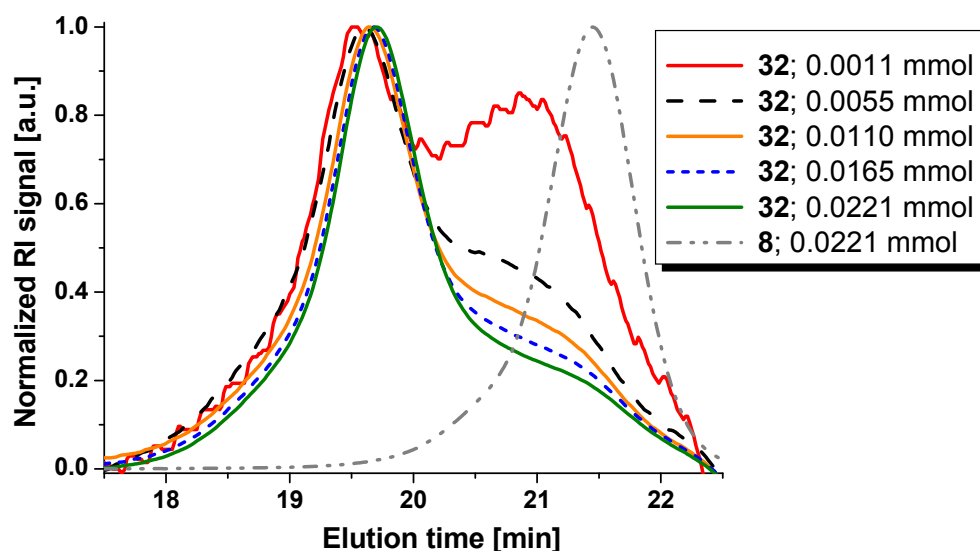
Figure 3.3: *SEC elution curves (RI detector) for the Fe(II) bis-terpyridine PEG 32 (different concentrations) and its corresponding starting material (mono-terpyridine PEG 8).*

The SEC-coupled in-line diode array detector showed the integrity of the Fe(II) *bis-*terpyridine PEG complex **32** characterized by the metal-to-ligand charge transfer (MLCT) bands at 556 nm (Figure 3.4). The molecular distribution demonstrated also the existence of the equilibrium between complexed and uncomplexed species (small shoulder for the SEC trace at 285 nm).
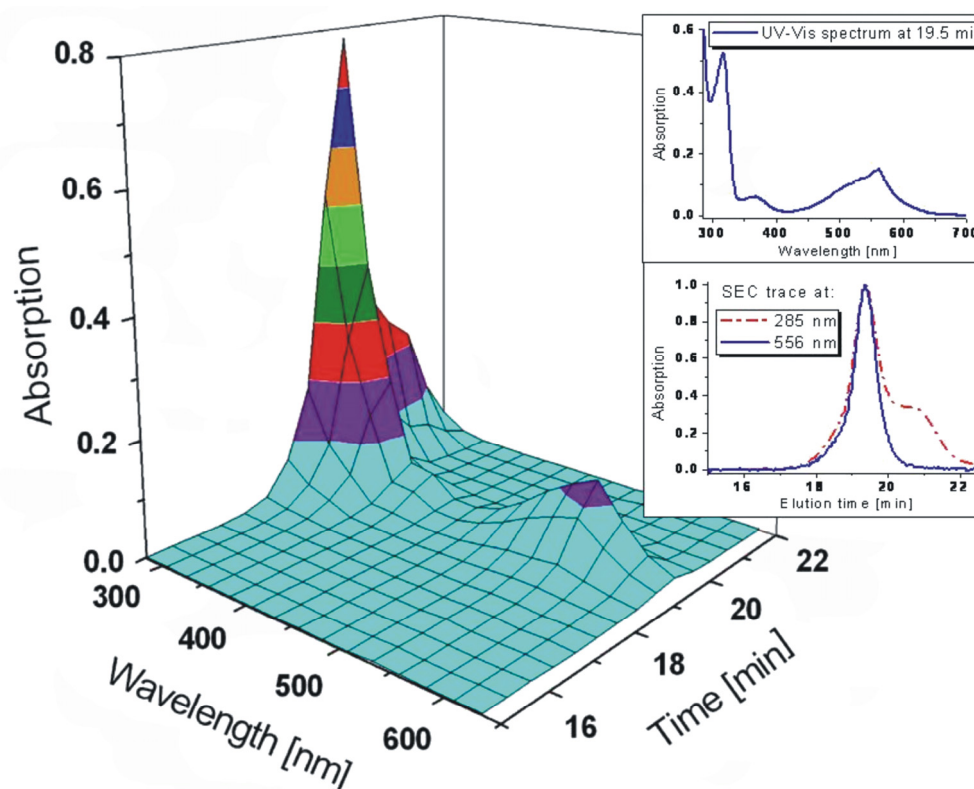
Figure 3.4: *SEC elution curves (PDA detector) for the Fe(II) bis-terpyridine PEG 32.*

3.2.2.3 SEC studies of Co(II) *bis*-terpyridine poly(ethylene glycol)

For the last case, Co(II) *bis*-terpyridine PEG **33**, the equilibrium constants are the smallest from the presented study (log $\beta_{2(Co)}$= 18.3)[31]. This implies that the stability of the complex during the SEC measurements would be lower than in the previous cases. From the RI-SEC plot (Figure 3.5) it can be observed that for lower concentrations the equilibrium is shifted to the uncomplexed starting material. Once the concentration of **33** increases, the equilibrium starts to shift to higher molar masses, namely to the *bis*-complex, in a similar fashion as observed for the iron system **32**. However, Figures 3.5 and 3.6 also clearly reveal that at the same concentration the measurements of complex **33** (Figure 3.5) show more free ligand **8** and less ML_2 species as in the case of complex **32** (Figure 3.3). This is another clear indication that the iron(II)tpy$_2$ connectivity has a higher binding strengths than the cobalt(II)tpy$_2$ connectivity.
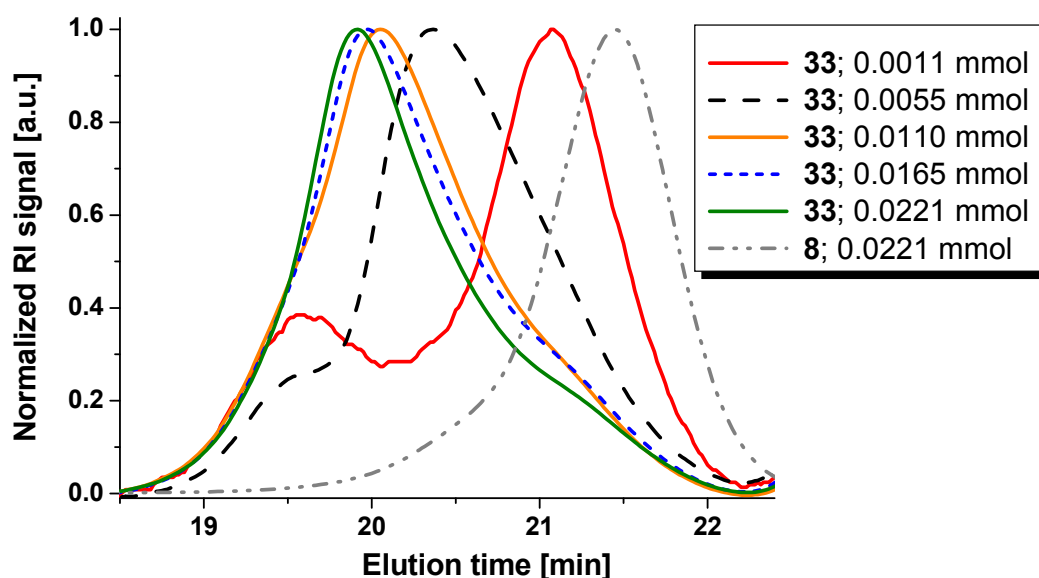
Figure 3.5: *SEC elution curves (RI detector) for the Co(II) bis-terpyridine PEG **33** (different concentrations) and its corresponding starting material (mono-terpyridine PEG **8**).*

From the SEC-coupled in-line diode array detector the existence of the LC bands at 327 nm can be observed, which proves the formation and the stability of the Co(II) *bis*-complex during the SEC measurements. The molecular distribution of **33** (Figure 3.6) showed also the equilibrium between complexed and uncomplexed species. Thus, the small shoulder for M_n at 285 nm could be attributed to possible decomplexed species.
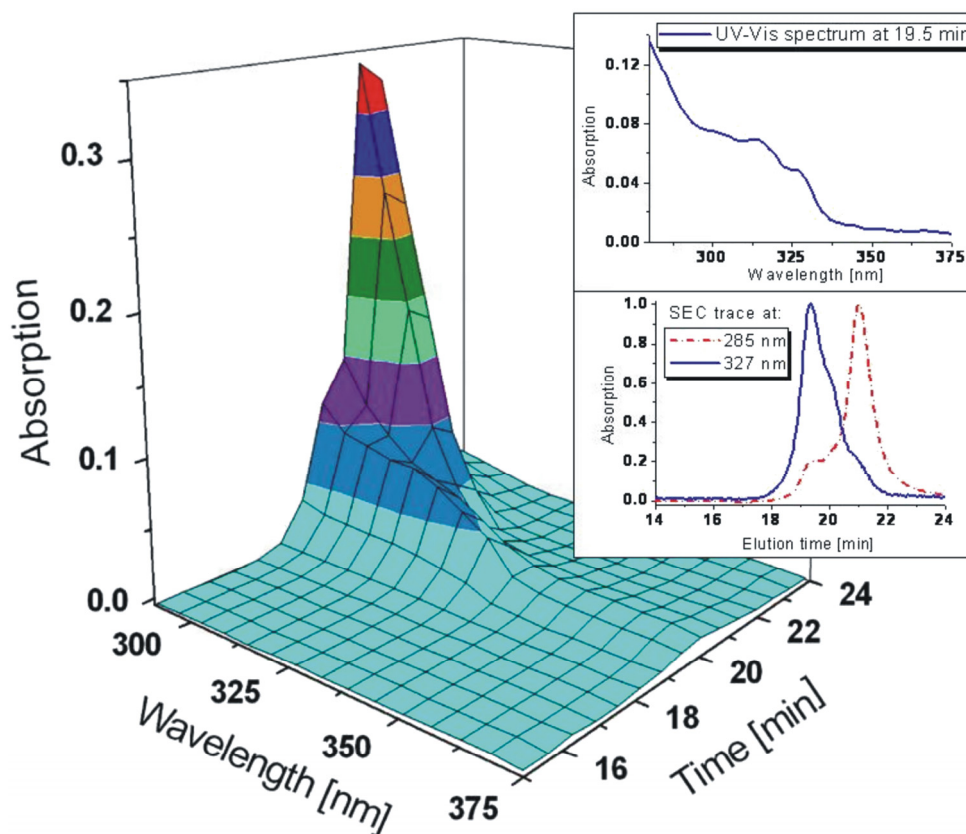
Figure 3.6: *SEC elution curves (PDA detector) for the Co(II) bis-terpyridine PEG **33**.*

3.2.2.3 Overview SEC studies: Ni(II), Fe(II) and Co(II) *bis*-terpyridine PEG

In conclusion, the present study revealed that the relative degree of stability of the three prepared metal complexes **31**, **32** and **33** during the SEC measurements (Figure 3.7 and 3.8) decreases from Ni(II) to Fe(II) and lastly to Co(II) ions. These results are in agreement with the metal binding strength published elsewhere.[31]
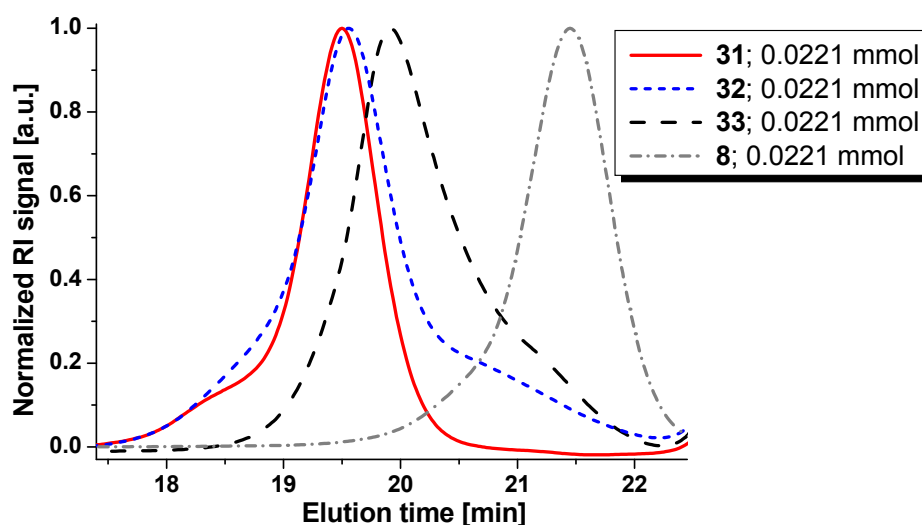
Figure 3.7: *Comparison of the SEC elution curves (RI detector) for Ni(II) bis-terpyridine PEG **31**, Fe(II) bis-terpyridine PEG **32**, Co(II) bis-terpyridine PEG **33** and its corresponding starting material (mono-terpyridine PEG **8**).*
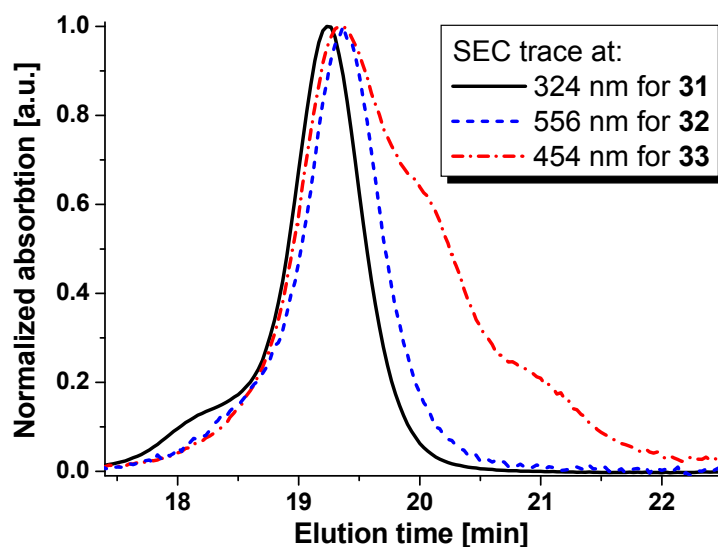
Figure 3.8: *Comparison of the SEC elution curves (UV-Vis detector) for Ni(II) bis-terpyridine PEG 31, Fe(II) bis-terpyridine PEG 32 and Co(II) bis-terpyridine PEG 33.*

3.2.3 Synthesis, optimization and SEC characterization of the Ni(II) chain extended polymer

Based on these results, we focused our further investigations on the most stable system based on the Ni(II)tpy$_2$ type of connectivity. Our interest was the investigation of one-step metallo-polymerization processes of *bis*-terpyridine PEG **12** with Ni(II) ions (Scheme 3.2).
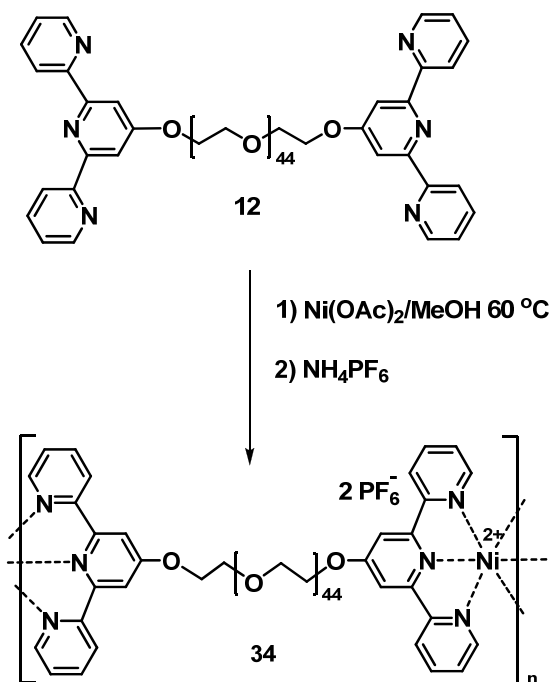
Scheme 3.2: *Schematic representation of the synthesis of the Ni(II) chain extended polymer 34.*

The preparation and characterization of the required ligand **12** was already discussed in Chapter 2. The optimization of the metallo-polymerization reaction was carried out in conical glass vials capped with a septum. All polymerization reactions were monitored by SEC, aiming for a high conversion and high molar mass. First of all several optimization reactions were performed in order to identify the best reaction conditions. In all these experiments the molar ratio between *bis*-terpyridine PEG **12** and $Ni(OAc)_2$ was kept constant at a 1:1 ratio, varying only the amount of solvent (CH_3OH) and the reaction time. From the SEC results it was observed that reaction times longer than 12 h did not influence the conversion of the reaction anymore. Regarding the concentration effect, it was noticed that the best conversion was achieved when the reagents had a good solubility from the start of the reaction, whereby high dilutions of the system led to a low conversion of the reactions (Table 3.1).

Table 3.1: *Optimization reactions for the polycondensation of 12 with Ni(OAc)$_2$ (molar ratio tpy/Ni(II)= 1:1) in MeOH at 60 ^{o}C; the conversions were estimated by peak integration of 12 and the corresponding Ni(II) polymer obtained by SEC measurements.*

c(12) (mmol/mL)	Conversion of 12 after 12 h (%)
0.208	66
0.138	72
0.104	43
0.083	22

After the evaluation of the optimization results for the polycondensation of **12** with $Ni(OAc)_2$ in CH_3OH, the optimal concentration was taken in order to prepare (on a larger scale) a chain extended polymer based on Ni(II) *bis*-terpyridine PEG. The crude polymer was subsequently subjected to counter ion exchange from CH_3COO^- to PF_6^- by refluxing the reaction mixture with an excess of NH_4PF_6. Further purifications were performed by column chromatography using BioBeads S-X1 in CH_2Cl_2. Figure 3.9 displays the SEC results for the purified chain extended polymer with a M_n of 28,600 g/mol (PEG calibration, DP = 28) clearly proving that it is possible to 1) prepare extended supramolecular polymers with a Ni(II)tpy$_2$ type of connectivity and 2) to investigate the formation of these polymers by size exclusion chromatography.
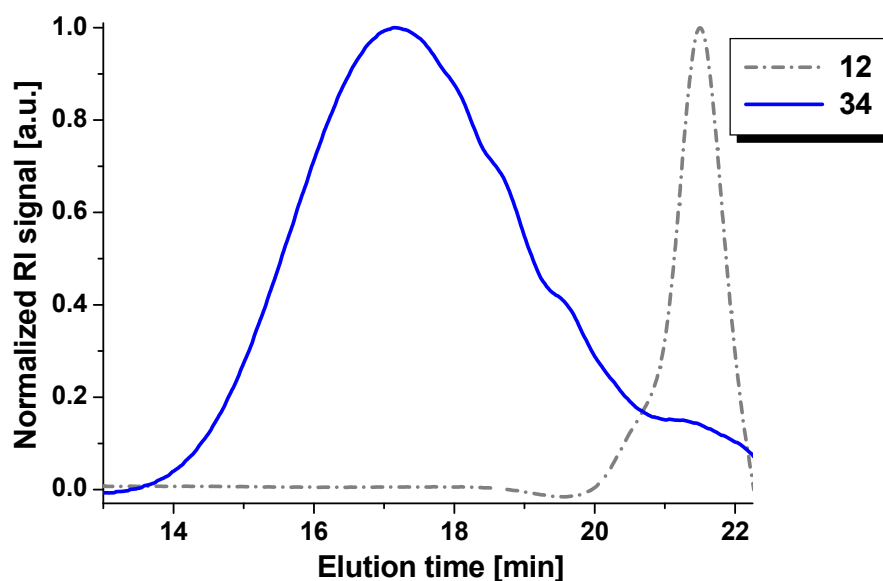
Figure 3.9: *SEC elution curves (RI detector) for the Ni(II) chain extended polymer **34** and the precursor polymer bis-terpyridine PEG **12**.*

3.2.4 Mechanical studies of the Ni(II) chain extended polymers

In order to show first indications that it is possible to also alter the polymer properties by supramolecular chain extension, depth sensing indentation studies were performed. The dropcasted Ni(II) chain-extended polymer **34** showed apparently crystalline regions (Figure 3.10 b) with amorphous regimes at the edges of the crystalline regions. For the *bis*-terpyridine PEG **12**, no pronounced crystals were observed (Figure 3.10 a).
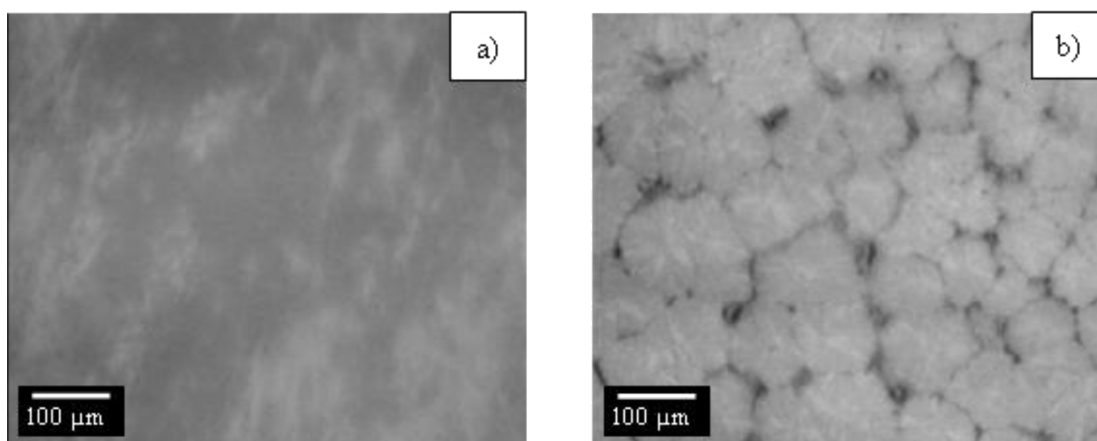
Figure 3.10: *(a) Morphology observed by optical microscopy polarized on the starting material **12**. (b) Morphology observed by optical microscopy on the Ni(II) chain extended polymer **34**.*

A typical load-displacement response for both materials is shown in Figure 3.11. Decreasing the humidity proved to be a successful approach to reduce the adhesion between the tip and the material that was impeding accurate measurements. The response of the materials during

the indentation experiment at 4.2% relative humidity revealed that the crystalline regions in the Ni(II) chain-extended polymer **34** had a higher E_r (0.67 ± 0.11 GPa) than the *bis*-terpyridine PEG **12** ($E_r = 0.44 \pm 0.06$ GPa). The standard deviation given here is somewhat larger than usually observed during depth-sensing indentation. This is due to non optimal surface conditions, for instance roughness. For some dropcast spots of chain extended polymer based on Ni(II) *bis*-terpyridine PEG **34**, only few crystallized regions were observed. The E_r of these crystalline regions was higher than measured on the morphology shown in Figure 3.10 b that consisted of the same material ($E_r = 0.84 \pm 0.13$ GPa). These crystalline regions were embedded in a featureless matrix, for which no modulus is stated as that material adhered too strongly to the tip, impeding accurate measurements. Crystallization and possibly entanglement length govern the mechanical properties. The metal complexes tend to crystallize, apart from the influence of the chain-extension on the crystallization (which is rather counterintuitive, as short chains are expected to crystallize more easily), the chain extension may also have a direct effect on E. On the other hand, the influence of the counter ion (PF_6^-) in the change of the morphology should not be neglected. Since the counter ion is charged and posses a relative large volume size, the arrangement of the final structure is also determined by the presence of the weak ionic interactions displayed by PF_6^-. The measurements provide a first clear indication that it is possible to change the material properties upon supramolecular chain extension with a Ni(II)tpy$_2$ type of connectivity.
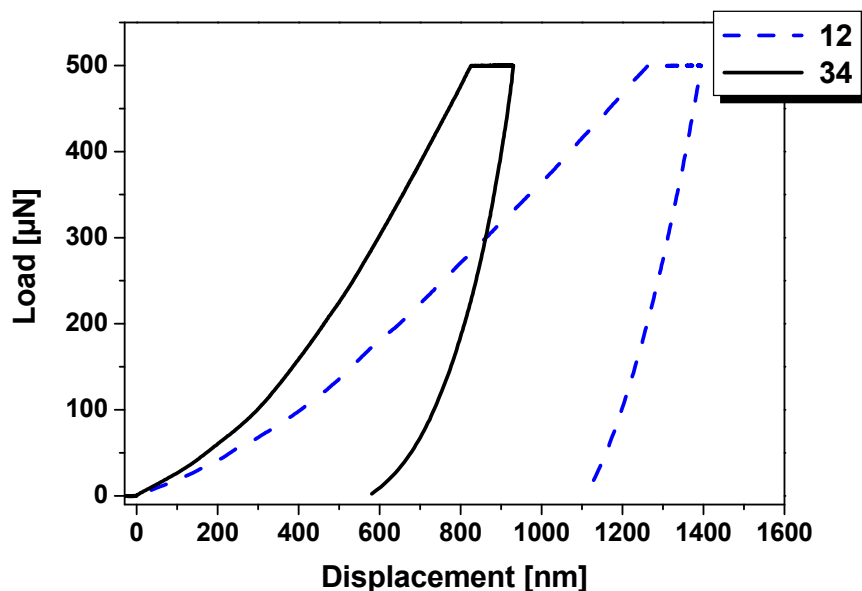
Figure 3.11: *Typical load-displacement responses at 4.2% relative humidity for both materials using nanoindentation; analysis of at least 9 load-displacement responses (several maximum loads) resulted for **12** in $E_r = 0.44 \pm 0.06$ GPa, and for the Ni(II) chain-extended polymer **34** in $E_r = 0.67 \pm 0.11$ GPa.*

3.3 Supramolecular self-assembled Ni(II), Fe(II) and Co(II) A-*b*-B-*b*-A triblock copolymers

Recently, it was shown that the polymerization of a *bis*-terpyridine monomer with RuCl₃ and a *mono*-terpyridine functionalized polymer can lead to supramolecular triblock copolymers in a one step procedure,[40] thereby expanding the range of accessible supramolecular polymer architectures. By varying the amount of the end capper in the polymerization reaction, different lengths (and molar masses) of the metallo-block copolymers could be easily achieved *via* an one step procedure. Moreover, the presence of the *mono*-terpridine functionalized polymer as an end capper decreases the possibility of ring formation, as it would be the case when only *bis*-terpyridine monomer would be polymerized with RuCl₃.

In this subchapter (3.3), the synthesis of A-*b*-B-*b*-A triblock copolymers based on a M(II)tpy₂ connectivity with three transition metal ions (studied in subchapter 3.2) characterized by different binding strengths[30,31] will be described in detail. As could already be seen before, the use of different metal ions offers the possibility of designing new materials with different stabilities, an aspect which could be used for the preparation of switchable systems. Finally, the micellization of the accordingly synthesized amphiphilic A-*b*-B-*b*-A triblock copolymers in a mixture of acetone and water was studied by dynamic light scattering (DLS), cryo-transmission electron microscopy (cryo-TEM) and atomic force microscopy (AFM). In order to prepare supramolecular, terpyridine containing A-*b*-B-*b*-A triblock copolymers, the polycondensation-like polymerization conditions of a *α,ω-bis*-terpyridine monomer with RuCl₃ were previously optimized in a parallel fashion with the appropriate screening techniques (an optimized SEC system and an UV-Vis plate reader).[32] Here, we apply a similar approach for the formation of A-*b*-B-*b*-A supramolecular triblock copolymers based on Ni(II)tpy₂, Fe(II)tpy₂ and Co(II)tpy₂ connectivities, and study the micellization of these new materials. The general chemical structure of the synthesized metallo-supramolecular A-*b*-B-*b*-A triblock copolymers consisting of terpyridine modified poly(ethylene glycol) **A** blocks and a poly(1,16-*bis*(2,2':6',2''-terpyridin-4'-yloxy)hexadecane) **B** central block, is depicted in Figure 3.12.
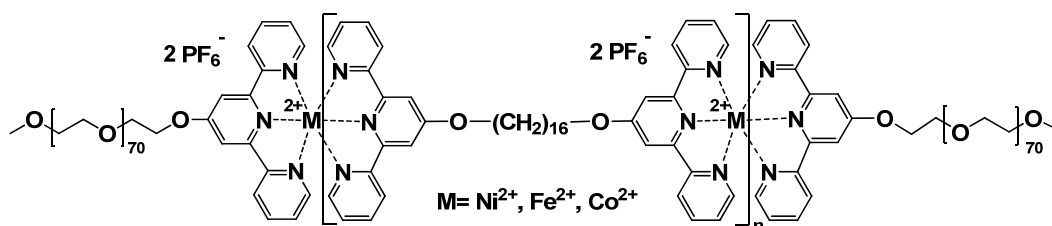
Figure 3.12: *Schematic representation of the M(II) A-b-B-b-A block copolymers.*

3.3.1 Synthesis, optimization and characterization of Ni(II) A-*b*-B-*b*-A supramolecular triblock copolymers

To gain an insight in the factors influencing the polycondensation reaction, optimization reactions were performed on the most stable system of the present study, namely Ni(II)tpy$_2$. As already shown in subchapter 3.2, nickel(II) ions bind stronger than iron(II) ions, whereas cobalt(II) ions offer the weakest supramolecular connectivity in this series.[41] First of all, Ni(II) homopolymer **35** was prepared by complexing ligand **9** (M_n = 3,000 g/mol), with Ni(OAc)$_2$ in refluxing MeOH (Scheme 3.3).[38,41]
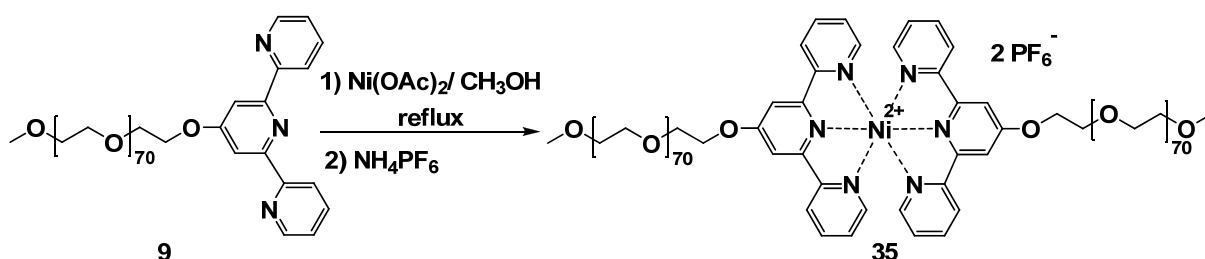
Scheme 3.3: *Schematic representation of the synthesis of Ni(II) bis-terpyridine poly(ethylene glycol) hexafluorophosphate 35.*

The main characterization technique for the Ni(II) homopolymer **35** (and all other nickel containing polymers) was SEC (Table 3.2) since ^{1}H-NMR spectroscopy could not detect any peaks in the aromatic region of these species due to the paramagnetic characteristic of Ni(II). Metallo-homopolymer **35** was used as a reference compound in the following investigations. Subsequently, the A-*b*-B-*b*-A triblock copolymer **37** based on Ni(II)tpy$_2$ was prepared (Scheme 3.4). Several synthetic procedures have been investigated. The DMA procedure (method B) with nickel(II) chloride, as described for the Ru(II)tpy$_2$ connectivity,[40] was less successful in the Ni(II)tpy$_2$ case and was leading to low molar mass block copolymers (as observed by SEC). Changing nickel(II) chloride to nickel(II) acetate but keeping the same solvent did not improve the polymerization results. In fact, it was observed from SEC measurements that no product was formed. One explanation could be related with the capacity of the solvent (DMA) to compete for the coordination,[25] since nickel ions are not binding to the terpyridine as strongly as ruthenium ions.[40] Moreover, the low solubility of Ni(II) chloride and later also acetate in the reaction mixture, as well as the influence of the used counter ions in the present polycondensation reactions should not be neglected and might be the cause for the unsuccessful polymerizations.[47] Taking into account previously gained knowledge regarding the chain extended polymerization based on Ni(II)tpy$_2$,[41] the reaction solvent

(DMA) was changed to methanol yielding in the formation of the desired triblock copolymer, confirming once again the crucial role of the solvent in the polymerization process.
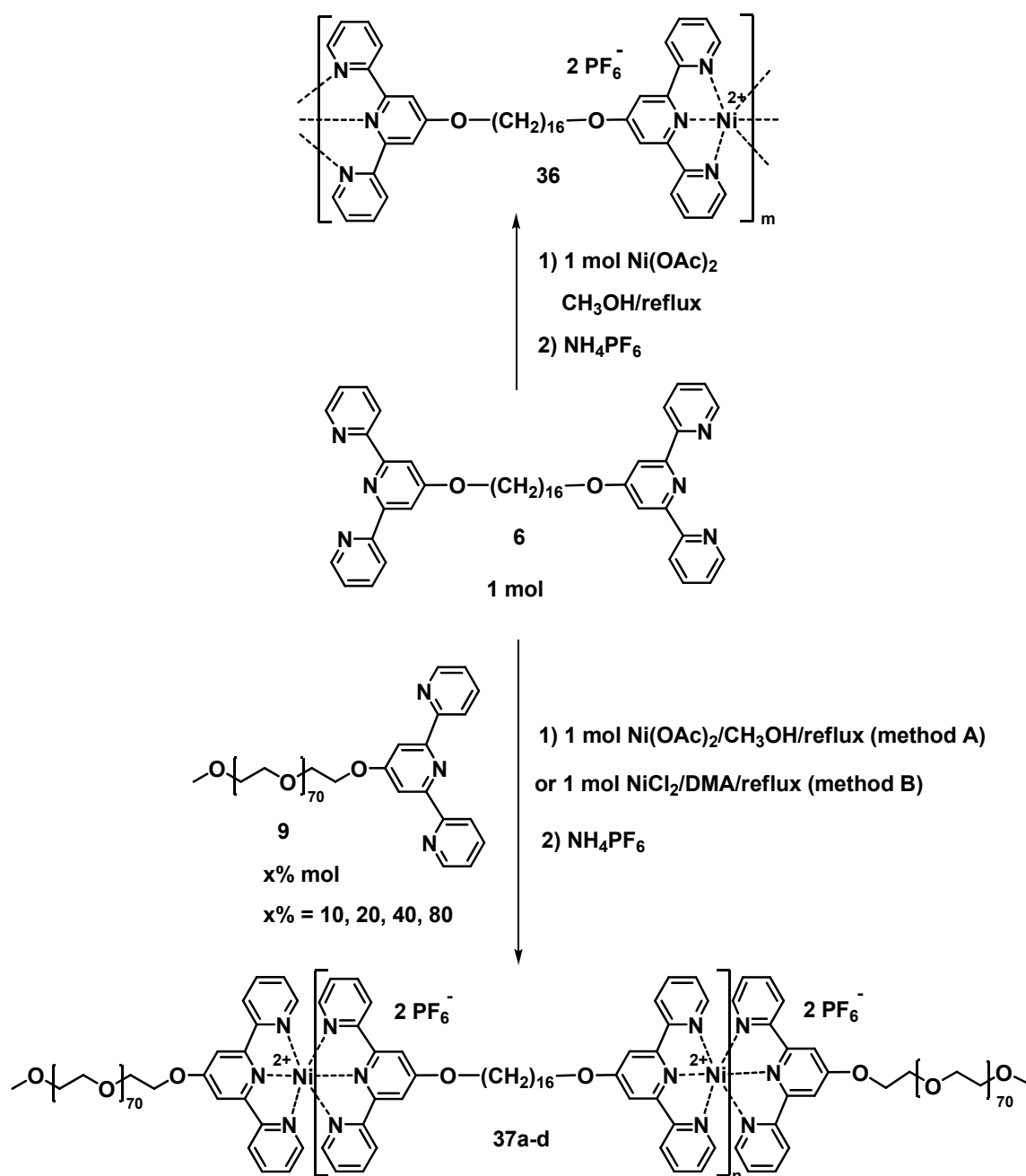
Scheme 3.4: *Schematic representation of the synthesis of the Ni(II) A-b-B-b-A triblock copolymers **37a-d** via methods A and B and the Ni(II) chain extended polymer **36** via method A.*

Since the "metallo-polymerization" of **6** would lead to the formation of chain extended polymers (compare **36**), the addition of a macromolecular chain stopper, such as **9**, should allow the formation of A-*b*-B-*b*-A architectures. Chain terminators are frequently used in technical polycondensation processes in order to control the molar masses.[43] Moreover, the

addition of various amounts of **9** should result in A-*b*-B-*b*-A copolymers with different lengths of the **B** block as it is known from classical polycondensation reactions.[43] As we were mainly interested in linear high molar mass A-*b*-B-*b*-A block copolymers, the addition of the chain terminator **9** could help us to reduce/limit the possibility of forming macrocycles.[43]

First of all, for the A-*b*-B-*b*-A triblock copolymer **37a** with 10% end capper **9**, the influence of the reaction time on the molar mass was studied. The polycondensation reaction was monitored during the first 12 hours. From SEC analysis it was observed that the metallo-polycondensation of the studied system first led to low molar mass that couple in time leading to higher molar mass block copolymers, in agreement with the results presented in the literature for typical chain growth polymerization reactions.[42,43] Moreover, SEC analysis also revealed (see Figure 3.13) that after 12 hours the molar mass did not increase anymore, and that much longer reaction times (*e.g.* 4 days) led to lower molar mass species that are most likely of macrocyclic nature,[44] in addition to the linear A-*b*-B-*b*-A triblock copolymers.
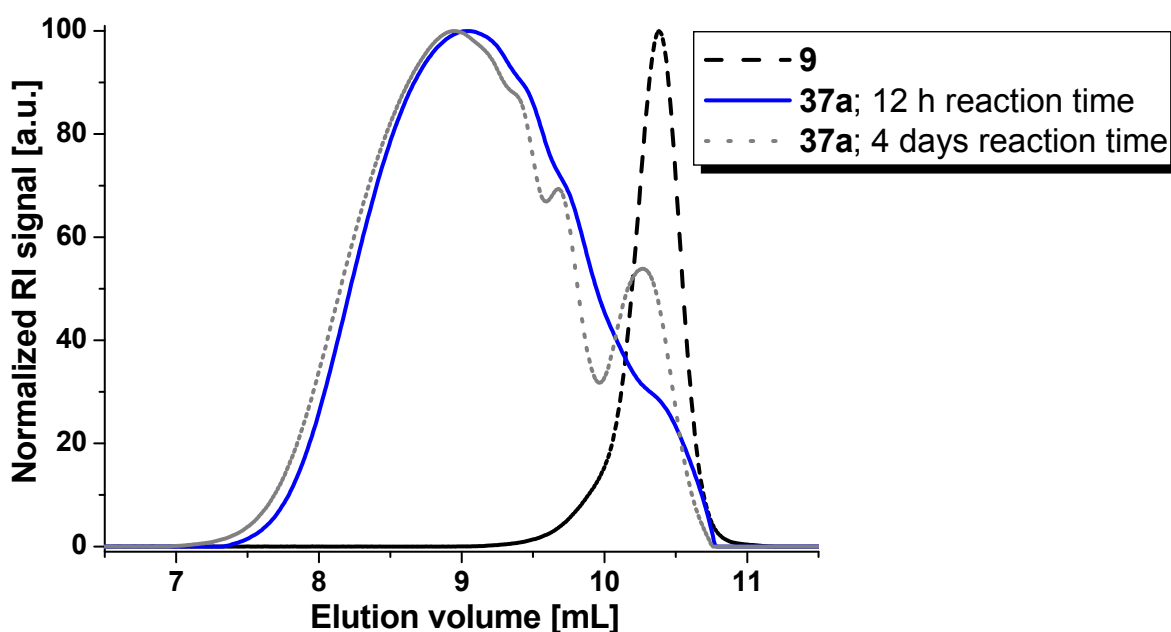
Figure 3.13: *SEC elution curves (RI detector) showing the influence of the reaction time on the molar mass of the A-b-B-b-A **37a** triblock copolymers (with 10% end capper **9**) in comparison to the starting material **9**.*

This observation is in agreement with the results presented in the literature for the preparation of polyesters *via* chain growth polymerizations.[45,46] This aspect might be due to the fact that this polycondensation is an equilibrium reaction and the proportion of rings may also vary with time being thermodynamically more favored.[34,47] By this assumption we can presume that during the polycondensation reaction the linear triblock copolymer might be first formed

and then, in time, due to the (possible) dynamic equilibrium between linear and cyclic macromolecules, rings are formed as well.[34] As we were interested mainly in the preparation of linear triblock copolymers, we decided to select the optimal reaction time of 12 hours, in terms of molar mass build up, for the rest of the polycondensation reactions.

The synthesis of **37a-d** with different molar ratios of the end capper **9** was thus performed in methanol for 12 h and the synthesized copolymers were characterized by SEC. Considering the composition of the triblock copolymers no proper GPC calibration standard could be found for these systems. However, to provide an indication of molar mass and polydispersity index, Table 3.2 shows the M_n values of the A-*b*-B-*b*-A triblock copolymers **37a-d** with different percentages of the end capper **9** calculated with a PEG calibration. As it can be seen from Table 3.2 and from the SEC traces in Figure 3.14, the highest M_n values were obtained by the addition of 10% of the end capper **9**. As expected, further increasing the amount of **9** in the polycondensation reaction led to the formation of shorter block copolymers with respectively lower M_n values (*e.g.* compare **37c** and **37d** to **36**).
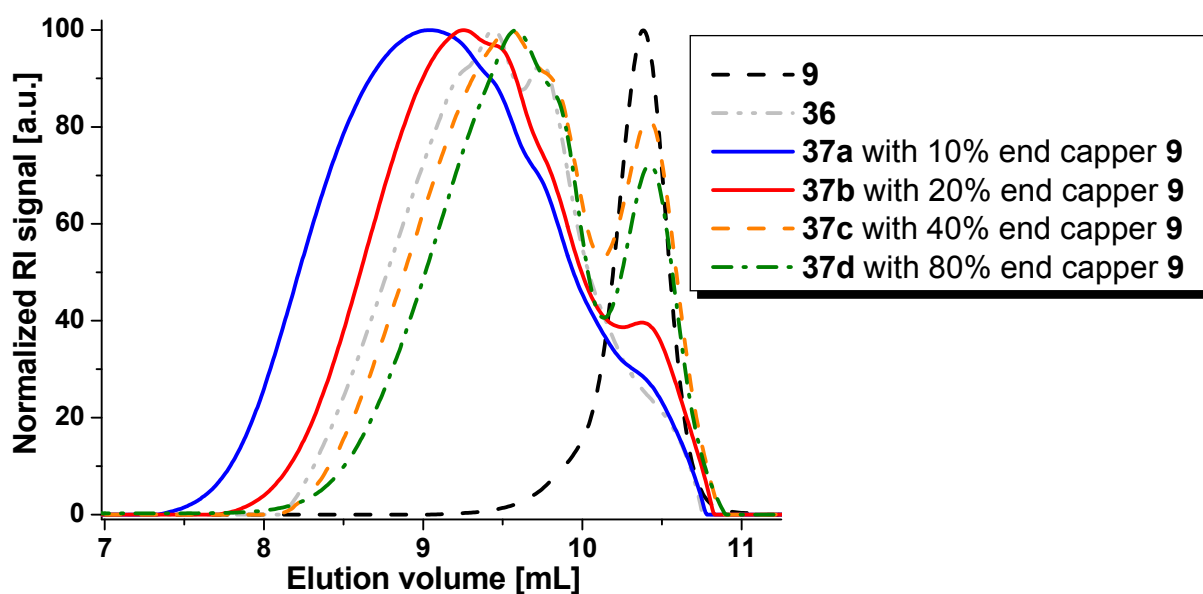
Figure 3.14: *SEC elution curves (RI detector) for the mono-terpyridine PEG **9** and the corresponding A-b-B-b-A **37a-d** triblock copolymers with different percentages of the end capper **9** after 12 h reaction time.*

Table 3.2: *Estimation of the molar mass values and polydispersity indexes for **9, 35** and crude A-b-B-b-A **37a-d** triblock copolymers (where **37a** is A-b-B-b-A with 10% end capper **9**; **37b** A-b-B-b-A with 20% end capper **9**; **37c** is A-b-B-b-A with 40% end capper **9** and **37d** is A-b-B-b-A with 80% end capper **9** using size exclusion chromatography with a PEG calibration.*

Compound	M_n [g/mol]	M_w [g/mol]	PDI
9	3,300	3,650	1.11
35	8,100	8,700	1.07
36	8,100	14,500	1.80
37a	12,350	24,000	1.94
37b	10,400	18,050	1.73
37c	7,300	12,900	1.76
37d	6,400	10,700	1.67

Further purification (BioBeads S-X1 in acetone and precipitation from acetone into dichloromethane) of the crude materials removed the macrocycles possibly formed during the polymerization reactions (Figure 3.15).
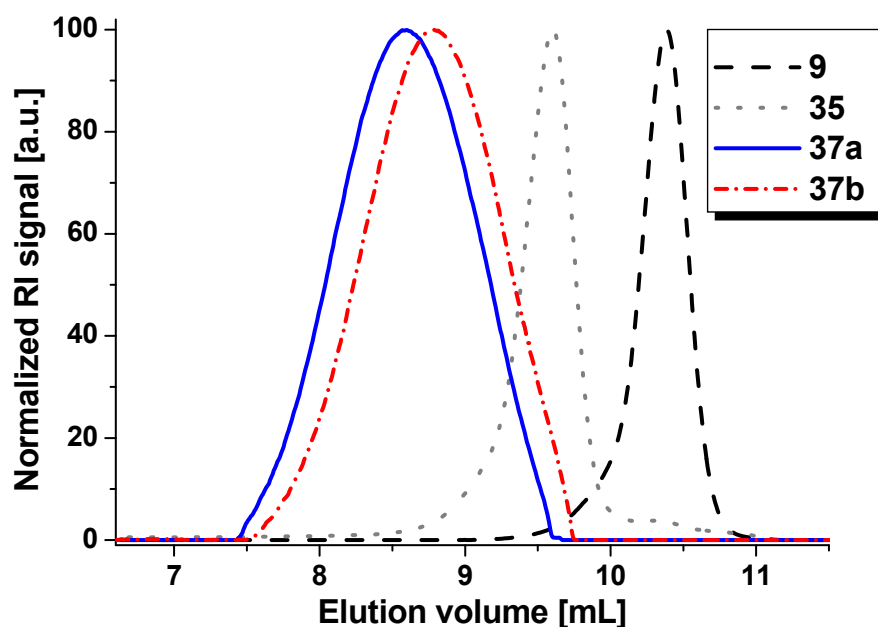
Figure 3.15: *SEC elution curves (RI detector) for the mono-terpyridine PEG **9**, Ni(II) homopolymer **35** and the purified A-b-B-b-A triblock copolymers **37a** with 10% end capper **9** and **37b** with 20% end capper **9**.*

The absence of aromatic protons in the ^{1}H-NMR spectrum revealed that no uncomplexed monomers were present in the final A-*b*-B-*b*-A triblock copolymers. Due to the fact that

Ni(II) is paramagnetic, no integration was possible on the terpyridine protons. Therefore, the estimation of the M_n values was done by SEC using a PEG calibration (Table 3.2). Furthermore, results obtained from the SEC-coupled in-line diode array detector demonstrated the integrity of the supramolecular assembly over the complete distribution as indicated by the ligand-centered (LC) π-π* absorption bands around 317 nm and 310 nm (Figure 3.16). The purified A-*b*-B-*b*-A triblock copolymer **37a** with the highest molar mass obtained in this study was further used for micellization studies (see 3.3.4).
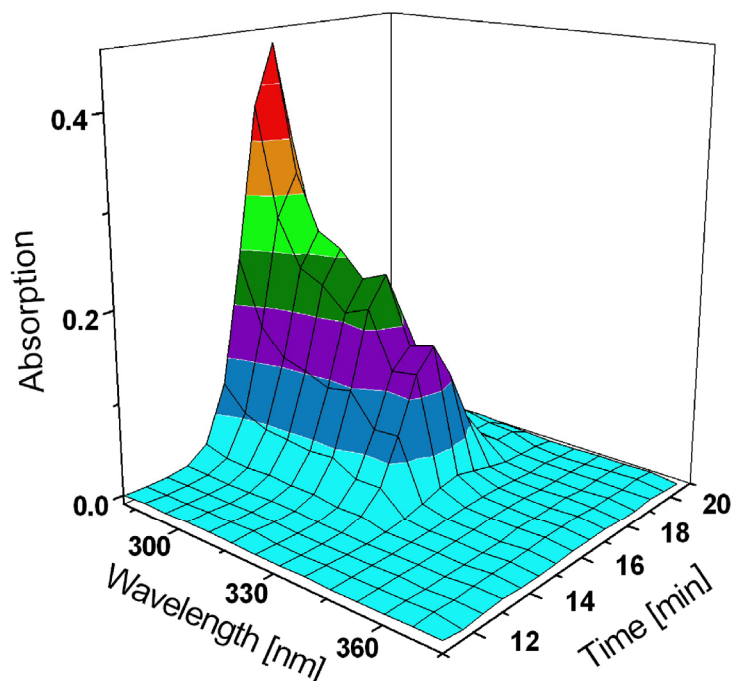
Figure 3.16: *SEC elution curve (PDA detector) for the purified A-b-B-b-A triblock copolymer 37a with 10% end capper 9.*

3.3.2 Synthesis, optimization and characterization of Fe(II) A-*b*-B-*b*-A supramolecular triblock copolymers

With the obtained knowledge regarding the synthesis, stability and characterization of A-*b*-B-*b*-A triblock copolymers **37a-d** based on Ni(II)tpy$_2$, we focused our attention on the preparation of A-*b*-B-*b*-A triblock copolymers based on the Fe(II)tpy$_2$ connectivity. For this system the two different synthetic approaches (methods A and B) have been studied and the results were compared. The first one followed the preparation of the triblock copolymer based on Ru(II)tpy$_2$ using 10% of the end capper[40] (see Experimental Part: method B) and the second one followed the successful synthesis of the triblock copolymer described earlier for Ni(II)tpy$_2$, also with 10% end capper (see Experimental Part: method A).
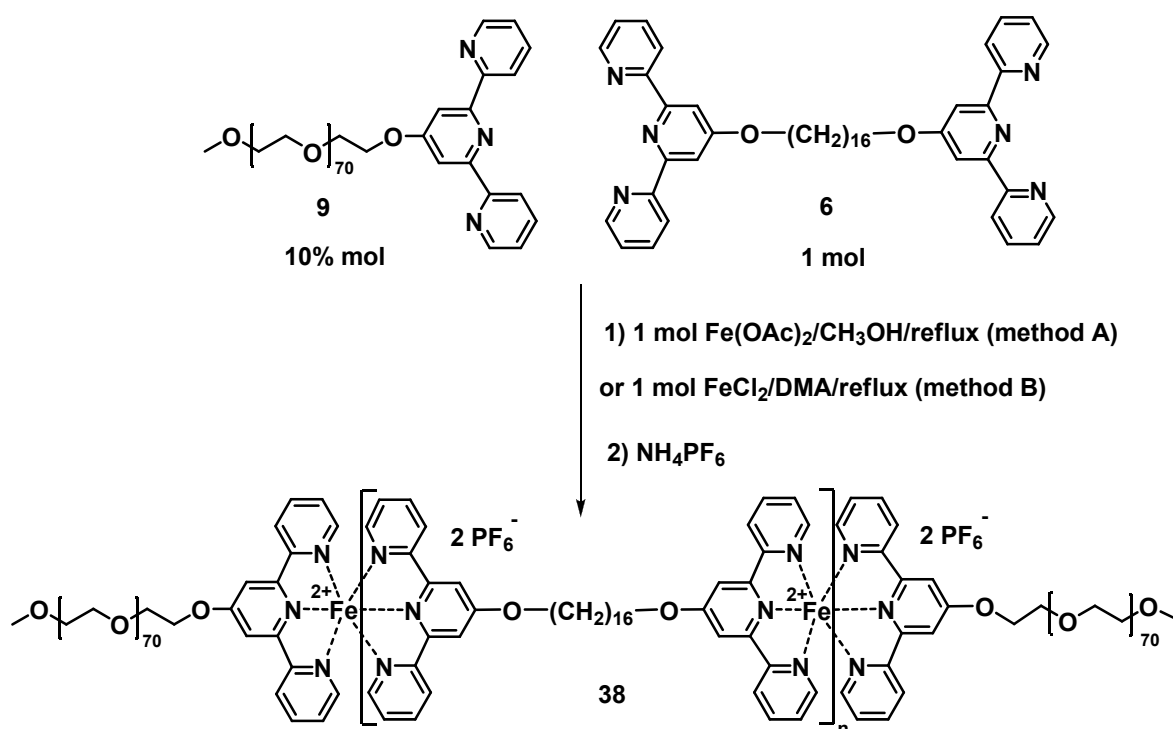
Scheme 3.5: *Schematic representation of the synthesis of the Fe(II) A-b-B-b-A triblock copolymers 38 via methods A and B.*

As a result of the weaker binding strength of the iron(II) *bis*-terpyridine complex, as compared to the analogous ruthenium and nickel complexes, it was unfortunately not possible to perform SEC investigations on such polymers.[41] For this reason the main characterization technique for the Fe(II)tpy$_2$ block copolymers was ^{1}H-NMR spectroscopy. For the purified A-*b*-B-*b*-A triblock copolymer based on Fe(II)tpy$_2$ **38** (prepared by the DMA approach) the ^{1}H-NMR spectrum (Figure 3.17) revealed similar degrees of polymerization as in the case of the ruthenium polymers described elsewhere.[40] Assuming that both ends of 1,16-*bis*(2,2':6',2"-terpyridin-4'-yloxy)hexadecane **6** were functionalized with PEG in order to obtain the A-*b*-B-*b*-A triblock copolymer structure, the ratio of signal intensities belonging to the PEG as well as 1,16-*bis*-(2,2':6',2"-terpyridin-4'-yloxy)hexadecane revealed a degree of polymerization of the central **B** block of approximately 40 units (compared to 33 units for the corresponding ruthenium containing polymer).[40] Therefore, the M$_n$ value of triblock copolymer **38** can be calculated to be 35 kDa if the PF$_6^-$ counter ions are omitted and 46.5 kDa if they are taken into account. Furthermore, almost full complexation was observed in the triblock copolymer **38** as revealed by a downfield shift of the methylene protons next to the terpyridine units (from 4.29 ppm (uncomplexed) to 4.72 ppm (complexed)) in the ^{1}H-NMR spectrum. Moreover, the existence of defect structures, such as *e.g.* **AB** type block copolymer or poly **B** structures, cannot be excluded.
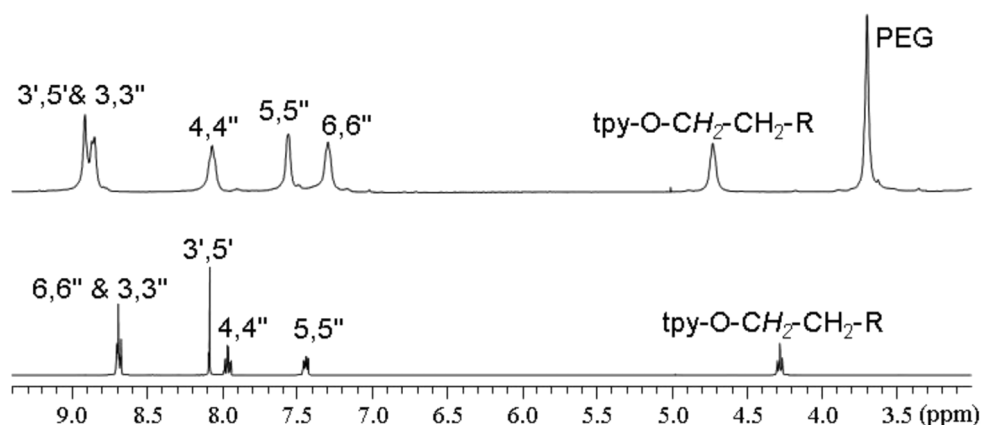
Figure 3.17: *Comparison between the ^{1}H-NMR spectra of monomer 6 (bottom) and Fe(II) A-b-B-b-A triblock copolymer 38 obtained via method B (top) in acetone-d$_6$.*

Moreover, the UV-Vis spectrum showed the typical metal-to-ligand-charge-transfer band of the iron(II)-*bis*-terpyridine type of connectivity in the visible region (560 nm) indicating that the anticipated connectivities are actually formed. This sample was further used in micellization studies.
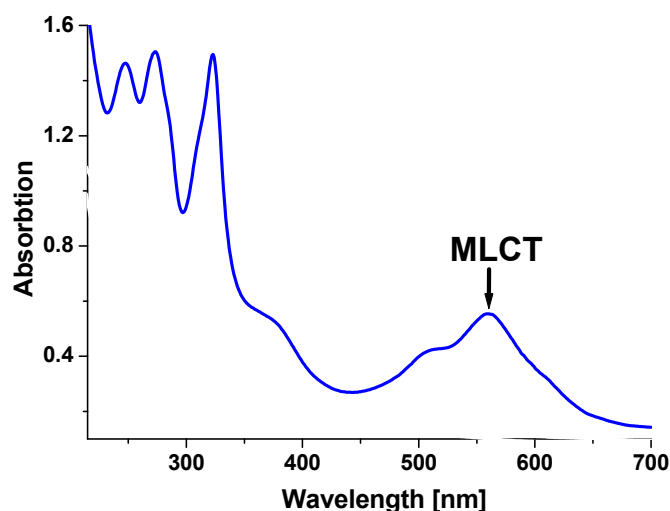
Figure 3.18: *Characteristic UV-Vis absorption of Fe(II) A-b-B-b-A 38 (measured in water).*

The second approach followed for the preparation of block copolymer **38** with 10% end capper **9** was the one also used for the synthesis of **37a**: in methanol with iron(II) acetate (see Experimental Part: method A). From the ^{1}H-NMR spectrum the degree of polymerization was found to be smaller (approximately 13 units for the **B** block) than with the DMA approach. One explanation could be the lower temperature in the methanol approach compared to the DMA approach, yielding lower molar masses. Unfortunately, the methanol approach does only allow reaction temperatures below 65 °C and at lower temperatures than 70 °C the reaction in DMA was not homogeneous, preventing a detailed comparison to study this effect.

For the case of the reaction performed in DMA, it could be possible that due to the higher temperature, the metallo-polymerization might take place with "opening and closing", named rearrangements, of the formed structures based on Fe(II)tpy$_2$ connectivity that yields in the chain extension of the desired metallo-system. One the other hand, the effect of the counter ions (acetate *vs.* chloride) should not be neglected also in this case.[44]

3.3.3 Synthesis, optimization and characterization of Co(II) A-*b*-B-*b*-A supramolecular triblock copolymers

The last system for our study was the A-*b*-B-*b*-A block copolymers based on the Co(II)tpy$_2$ connectivity using 10% end capper **9** as **A** block (Scheme 3.6).
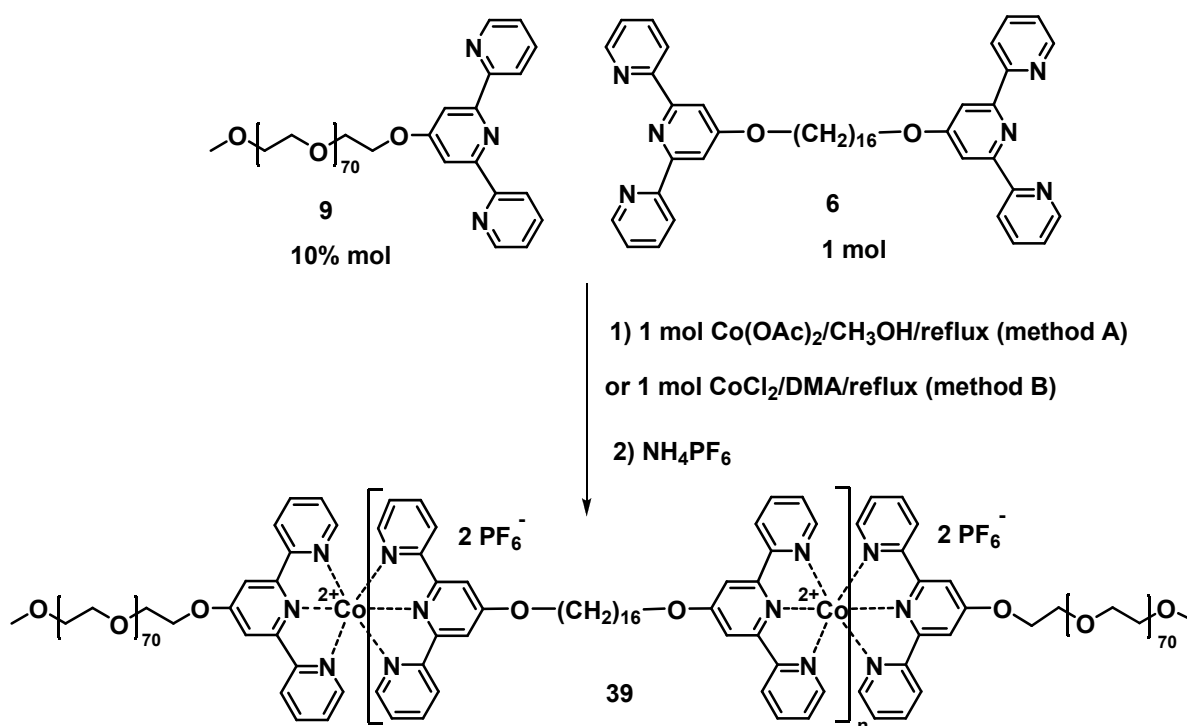
Scheme 3.6: *Schematic representation of the synthesis of the Co(II) A-b-B-b-A triblock copolymers 39 via method A and B.*

The two synthetic approaches have also been investigated and compared (see experimental: methods A and B). As a result of previous studies performed on the cobalt(II) *bis*-terpyridine homopolymer-complexes,[41] it is known that it is not possible to perform size exclusion chromatographic investigations with these copolymers due to the rather low stability of the Co(II) *bis*-terpyridine complex.[41] Therefore, the Co(II)tpy$_2$ block copolymers were characterized mainly by ^{1}H-NMR spectroscopy. It is known that paramagnetic complexes,

such as Ni(II) and Co(II), have unpaired electrons giving rise to two main effects in the ^{1}H-NMR spectrum. On the one hand, the local magnetic field at the protons is significantly different from the applied field due to the presence of unpaired electrons at the metal center. On the other hand, the recorded signals in the ^{1}H-NMR spectrum are broadened as a result of the interaction between the nuclear spins and the electron spins providing an efficient relaxation mechanism.[48] For Ni(II)tpy$_2$ the relaxation is very fast and the signals are broadened; therefore they cannot be observed anymore. For Co(II)tpy$_2$ the signals in the ^{1}H-NMR spectrum should normally reveal a Knight shift (up to 200 ppm from TMS).[30,39,49] In the case of the prepared Co(II) block copolymers **39** (methods A and B), no signals could, however, be observed in the mentioned region. The absence of the expected signals could be explained by a high molar mass of **39**, which would decrease the chain mobility and the diffusion rates during the ^{1}H-NMR measurements, inducing a broadening of the terpyridines signals, which normally appear at 100 ppm in a cobalt(II) *bis*-terpyridine model complex (Knight shift),[39,41] and thereby preventing their detection. From the comparison of the aliphatic region of the ^{1}H-NMR spectra for the two A-*b*-B-*b*-A block copolymers **39** prepared *via* method A and B, we concluded that the acetate approach (method A) led to a higher molar mass block copolymer (almost full conversion for the **B** block) in comparison with the DMA approach (less then 30% of the **B** block was incorporated into the synthesized triblock copolymer). The UV-Vis spectrum of **39** (obtained *via* method A) showed also the ligand-centered (LC) π-π* absorption bands in the visible region around 308 nm, 321 nm and 327 nm which are characteristic for the Co(II)tpy$_2$ connectivity. This sample was further used for micellization studies (see 3.3.4).
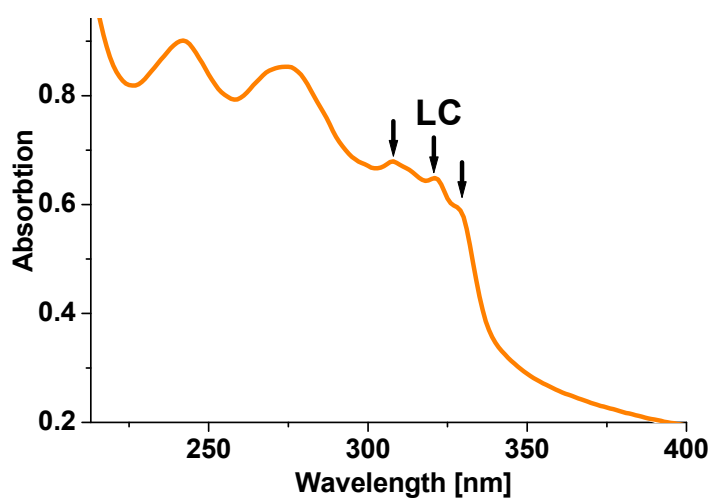
Figure 3.19: *Characteristic UV-Vis absorption spectrum of the Co(II) A-b-B-b-A **39** (measured in water).*

3.3.4 Self assembly investigations of the Ni(II), Fe(II) and Co(II) A-*b*-B-*b*-A block copolymers by DLS, cryo-TEM and AFM

In order to study the amphiphilic character of the supramolecular triblock copolymers **37a**, **38** and **39**, their ability to form micelles was investigated. Since the supramolecular block copolymers were not readily soluble in water the micelles were prepared by first dissolving the block copolymers **37a**, **38** and **39** (with the highest available molar masses) in acetone which represents a good solvent for both blocks, followed by the gradual addition of water which is a selective solvent for the PEG-containing block and a precipitant for the other block. Upon addition of water, the insoluble block collapses and aggregates are formed, shielded from the solvent by a corona of the PEG blocks. To transfer the micelles into pure water, we tried to remove the acetone by slow evaporation and by dialysis against water, but both methods lead to the precipitation of the copolymers. The micelles formed in an acetone/water (50/50) mixture were then characterized by dynamic light scattering (DLS), cryogenic transmission electron microscopy (cryo-TEM) and atomic force microscopy (AFM). The results are summarized in Table 3.3.

Table 3.3: *AFM, cryo-TEM and DLS average sizes of the prepared micelles containing A-b-B-b-A triblock copolymers **37a**, 38 and 39.*

A-*b*-B-*b*-A triblock copolymers	AFM R_h [nm]	Cryo-TEM R_h [nm]	DLS R_h [nm]	
			isolated chains	micelles and aggregate of micelles
37a	11.5	12	~10	56
38	12	14	~10	84
39	6.9 and 12	13	~10	100

The CONTIN analysis of the DLS results obtained on the micelles from the three copolymers revealed the presence of two different populations (Figure 3.19). The first population had a hydrodynamic radius of approximately ~10 nm for all three copolymers, and the second population had a R_h around 100 nm for the copolymer based on Co(II), around 84 nm for the copolymer based on Fe(II), and around 56 nm for the copolymer based on Ni(II). The first

population could correspond to isolated, non aggregated copolymer chains while the second one is attributed to micelles.
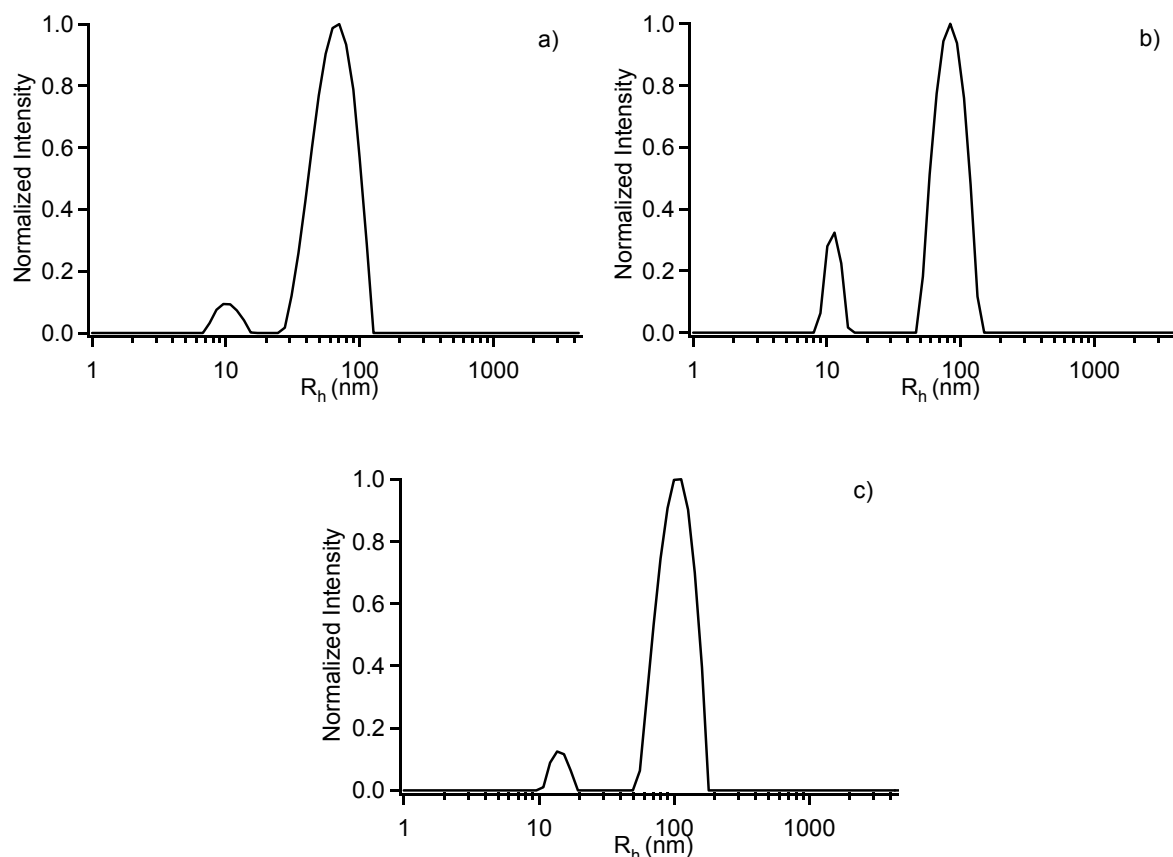
Figure 3.19: *CONTIN size distribution histograms obtained on the micelles prepared from the A-b-B-b-A triblock copolymers 37a, 38, 39 in an acetone/water mixture. a) copolymer 37a based on Ni(II)tpy$_2$, b) copolymer 38 based on Fe(II)tpy$_2$ and c) copolymer 39 based on Co(II)tpy$_2$.*

The micelles formed by the supramolecular triblocks were imaged by cryo-TEM and AFM. Figure 3.20 shows the micelles of the supramolecular triblock copolymers based on Ni(II)tpy$_2$, Fe(II)tpy$_2$ and Co(II)tpy$_2$ connectivity, imaged by cryo-TEM (left) and AFM (right). Spherical objects with a radius in the range of 10 to 14 nm were observed for all copolymers together with a few larger aggregates. However, the core radii measured by cryo-TEM seem rather small compared to the size associated to the second population of the CONTIN histogram as measured by DLS. These data confirmed that this second population observed in DLS experiments can be attributed not only to isolated micelles but to micelles and aggregates of micelles. In conclusion, the amphiphilic nature of the copolymers is clearly demonstrated by their ability to form micelles in water; however a more in-depth investigation is required to clarify the exact structure of those objects.
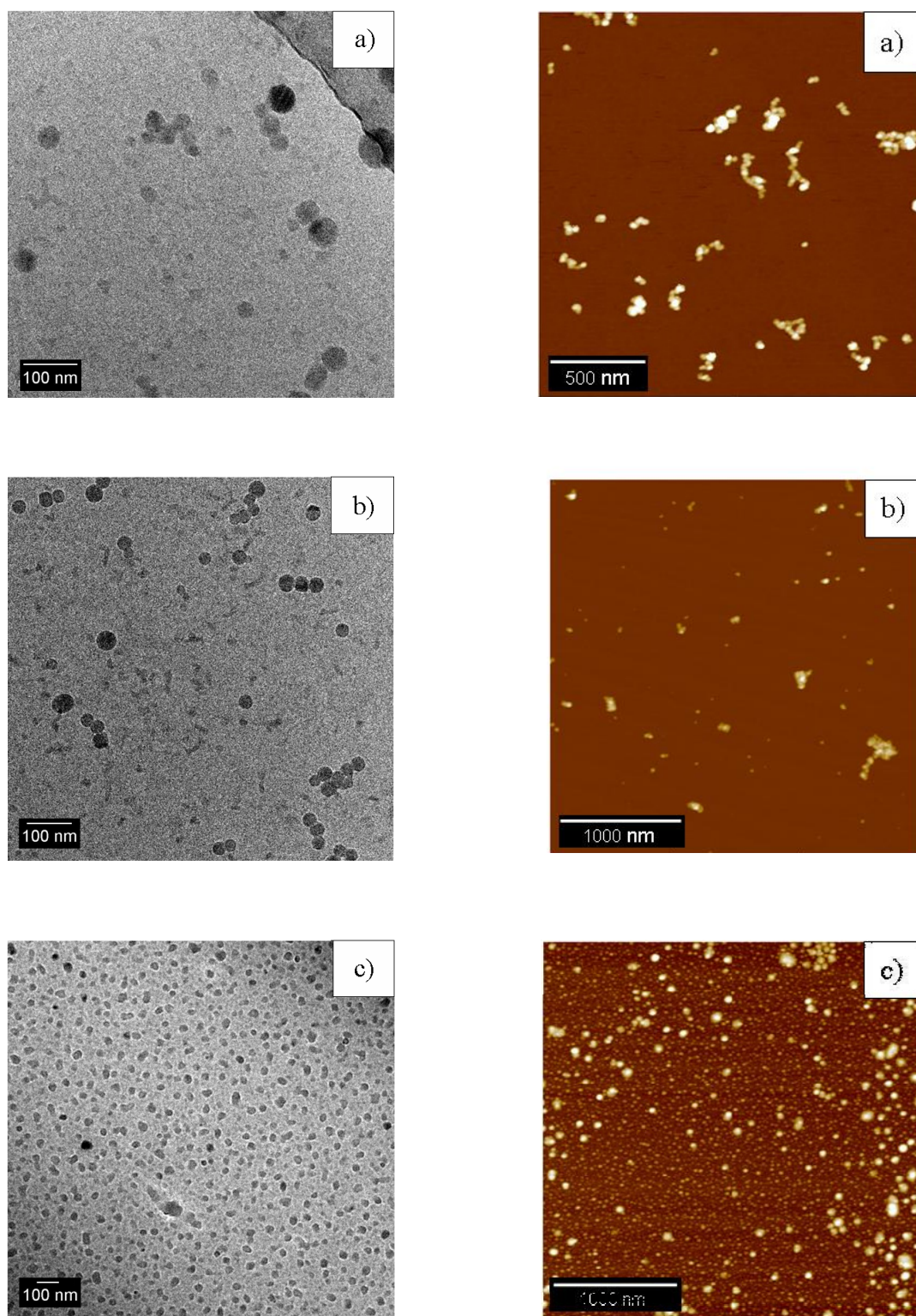
Figure 3.20: *Cryo-TEM (left) and AFM (right) pictures of micelles prepared from the A-b-B-b-A triblock copolymers **37a**, **38**, **39** in an acetone/water mixture: a) copolymer **37a** based on Ni(II)tpy₂, b) copolymer **38** based on Fe(II)tpy₂ and c) copolymer **39** based on Co(II)tpy₂.*

3.4 Depolymerization studies for Ni(II) A-*b*-B-*b*-A

For the A-*b*-B-*b*-A triblock copolymer **37a** (with 10% end capper **9** and PF_6^- as counter ion), the possibility to depolymerize the synthesized high molar mass polymers was studied. This aspect could be considered as a proof of the switchability of the designed $Ni(II)tpy_2$ system. As we already described in subchapter 3.2, the binding strength for Ni(II) ions is smaller then the binding strength for Ru(II) ions but larger than Fe(II) ions or Co(II) ions. Therefore, the $Ni(II)tpy_2$ connectivity could be an excellent switchable system regarding the decomplexation-complexation aspects (*e.g.* the stability of the $Ni(II)tpy_2$ complex *vs.* the possibility to open the $Ni(II)tpy_2$ complex). The depolymerization reactions were performed in parallel vials and monitored by SEC during the first 84 hours. Parameters such as *e.g.* temperature, polarity of the solvent and concentration of the reaction mixture (dilution effect) have been taken into consideration.

The first experiments were performed in MeOH stressing the dilution aspect, since the preparation of **37a** was best achieved in MeOH by using a high concentration of the polycondensation reactants. From SEC analysis we concluded that the decomplexation of the Ni(II) A-*b*-B-*b*-A is possible since the depolymerization reaction performed in MeOH at 63 ^{o}C with the reaction concentration $c_1 = 10$ mg/mL led to lower molar mass species after 12 h reaction time (see SEC curve **37a** (c_1) in Figure 3.21).
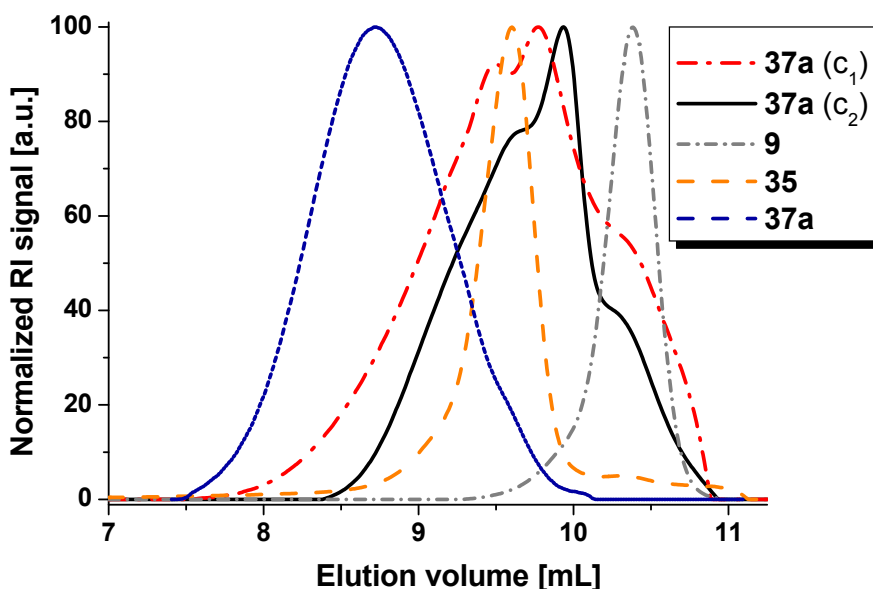
Figure 3.21: *SEC elution curves (RI detector) for the A-b-B-b-A **37a** triblock copolymer depolymerized in MeOH at 63 ^{o}C with reaction concentration c_1 respectivelly c_2, in comparison to mono-terpyridine PEG **9** and the corresponding Ni(II) model complex **35**.*

It was observed that longer depolymerization reaction times (more than 12 h) did not increase the quantity of the depolymerized species. By decreasing the concentration of the depolymerization experiment to $c_2 = 5$ mg/mL (performed in the same solvent) it was noticed that indeed the quantity of the depolymerized species could be slightly increased. Thus, from these experimental results we concluded that the dilution aspect together with the polarity of the utilized solvent might be important factors that can strongly influence the depolymerization process.

Therefore, MeOH was changed to DMF as reaction solvent that has a higher boiling point and polarity compared to methanol. The depolymerization reactions were performed at 153 ^{o}C. As it can be observed from SEC analysis, the first result of the depolymerization reaction (performed with the reaction concentration $c_1 = 10$ mg/mL) is that decomplexation also occurred although not so pronounced as in MeOH (see SEC curve for **37a** (c_1) in Figure 3.22).
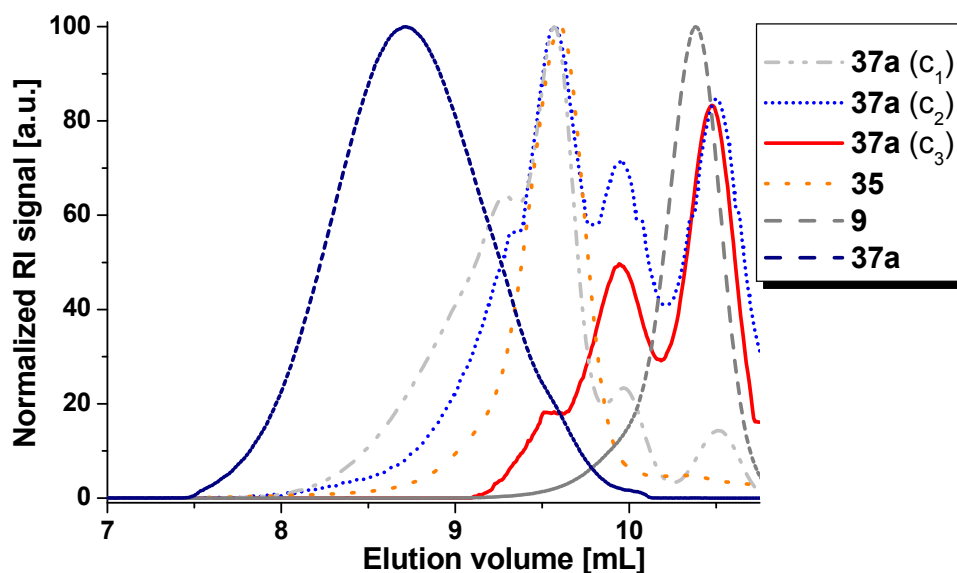
Figure 3.22: *SEC elution curves (RI detector) for the A-b-B-b-A **37a** triblock copolymer depolymerized in DMF at 153 ^{o}C after 12 h reaction with the reaction concentration c_1, c_2 respectively c_3, in comparison to mono-terpyridine PEG **9** and the corresponding Ni(II) model complex **35**.*

By decreasing the concentration of the depolymerization experiment to $c_2 = 5$ mg/mL it was found that the quantity of depolymerized species increased (as it can be seen from the shift of the SEC curve to higher elution time). A higher dilution (namely $c_3 = 3.33$ mg/mL) of the depolymerization reaction together with high temperature reflux (153 ^{o}C) showed that the triblock copolymer **37a** could be almost completely depolymerized (Figure 3.22). This result showed that by using a polar solvent with a high boiling point it is possible to depolymerize

the Ni(II)tpy connectivity without bringing into the system competitive chelating ligands or by changing the pH value of the systems as it is the case for Ru(II) or Fe(II)tpy connectivity.[50]

3.5 Conclusions

Three different metallo homopolymers, namely Ni(II), Fe(II) and Co(II) *bis*-terpyridine poly(ethylene glycol) **31**, **32** respectively **33**, have been synthesized and characterized. Detailed SEC studies were done in order to demonstrate the stability of the prepared terpyridine-metallo supramolecular polymers during the SEC measurements. Due to the different stabilities of the metallo-homopolymers in solution, the binding strength was found to decrease from Ni(II) to Fe(II) to Co(II). The *bis*-terpyridine functionalized poly(ethylene glycol) **12** led to a linear extended chain **34** *via* polycondensation reaction with Ni(OAc)$_2$. The obtained Ni(II) terpyridine chain extended polymer was purified and analyzed by SEC proving the high binding strength for Ni(II) ions and the high stability of the Ni(II)tpy$_2$ type of connectivity during the SEC measurements. The mechanical studies showed that the crystalline regions of the chain-extended material exhibited a higher E modulus than the non-chain extended material (which did not show such large crystalline regions). Furthermore, with the gained knowledge, metallo(II) A-*b*-B-*b*-A triblock copolymers were synthesized. The presented results clearly demonstrate that A-*b*-B-*b*-A triblock copolymers based on M(II)tpy$_2$ connectivity can be prepared with different metal ions *via* a simple one step polycondensation approach. The optimization studies were performed with different amounts of end capper for the case of Ni(II)tpy$_2$ connectivity leading to a variation in length of the Ni(II)tpy$_2$ A-*b*-B-*b*-A triblock copolymers. All the prepared metallo-triblock copolymers **37a**, **38** and **39** containing 10% end capper **9** are amphiphilic and were found to form micelles in acetone/water mixtures. The resulting micelles were analyzed by cryo-TEM, AFM and DLS and the results showed the formation of micelles as a proof of the amphiphilicity of the prepared block copolymers. In the future, it will be interesting to apply this knowledge for the synthesis and application of designed stimuli responsive micelles, since the strength of the metal-ligand interaction can be easily tuned due to the selection of the metal ion (and/or the exchange of counter ions).

3.6 Experimental part

Materials and instrumentation

Compounds **6**, **8**, **9** and **12** were synthesised as described in Chapter II. All reactions were performed under an inert atmosphere of argon using conical glass vials that can be capped with a septum. All chemicals were of reagent grade and used as received unless otherwise specified. Solvents were purchased from Biosolve. Ammonium hexafluorophosphate, Ni(II), Co(II) and Fe(II) acetate as well

as Ni(II), Co(II), Fe(II) chloride were purchased from Aldrich. Preparative size-exclusion chromatography was performed on BioBeads S-X1 columns using CH_2Cl_2, or acetone as eluent.

Instrumentation. Size exclusion chromatograms were measured on a Waters SEC system consisting of an isocratic pump, a solvent degasser, a column oven, a 2996 photodiode array (PDA) detector, a 2414 refractive index detector, a 717 plus autosampler, and a Styragel HT 4 GPC column with a precolumn installed. The eluent was *N,N*-dimethylformamide (DMF) with 5 mM NH_4PF_6 at a flow speed of 0.5 mL/min; PEG calibration was used. The column temperature was 50 °C. Nuclear magnetic resonance spectra were recorded on a Varian Gemini 400 MHz spectrometer at 298 K. Chemical shifts are reported in parts per million (δ) downfield from an internal standard, tetramethylsilane (TMS) in CD_2Cl_2, CD_3COCD_3 or CD_3CN. IR spectra were recorded on a Perkin Elmer 1600 FT-IR spectrometer. UV-Vis spectra were recorded on a Perkin Elmer Lamda-45 (1 cm cuvettes, H_2O). Depth sensing indentation was performed utilizing a Hysitron TriboIndenter equipped with a diamond Berkovich (id est: trigonal pyramid-geometry) indenter tip at reduced humidity (4.2 ± 0.4% RH). Loading to the maximum load (that was varied from 600 to 100 µN) was performed in 10 s, followed by 10 s hold at maximum load and unloading in 2 s. The unloading curves of the load-displacement responses were analyzed using the method proposed by Oliver and Pharr.[51] The reduced modulus E_r resulting from this analysis is for polymers somewhat higher (a small factor dependent on the Poisson's ratio) than the Young's modulus E. As the Poisson's ratio is not precisely known, the reduced modulus E_r is presented. The two materials *bis*-terpyridine PEG **12** and (tpy-PEG-tpyNi)$_n$ **34** were dissolved in dichloromethane (CH_2Cl_2) and dropcasted onto glass slides. After drying, the moduli of these materials were determined by depth-sensing indentation. Dynamic light scattering (DLS) experiments were performed on a Malvern CGS-3 equipped with a He-Ne laser (633 nm). The measurements have been performed at an angle of 90° and at a temperature of 25 °C. The viscosity of the 1:1 mixture of acetone and water was measured with a Cannon-Fenske viscometer (size 50). The density of the mixture was measured using a pycnometer (Brand) having a bulb volume of 10 cm³. The results were analyzed by the CONTIN method which is based on an inverse-Laplace transformation of the data and which provides access to a size distribution histogram for the analyzed micellar solutions. Cryogenic transmission electron microscopy (cryo-TEM) measurements were performed on a FEI Tecnai 20, type Sphera TEM operating at 200 kV (LaB6 filament). Images were recorded with a bottom mounted 1k × 1k Gatan CCD camera. A Gatan cryo-holder operating at −170 °C was used for the cryo-TEM measurements. R2/2 Quantifoil Jena grids were purchased from SPI. Cryo-TEM specimens were prepared applying 3 µL aliquots to the grids within the environmental chamber (22 °C, relative humidity 100%) of an automated vitrification robot (FEI Vitrobot Mark III). Excess liquid was blotted away (–2 mm offset, 2.5 s.) with filter paper within the environmental chamber of the Vitrobot. The grids were subsequently shot through a shutter into melting ethane placed just outside the environmental chamber. Vitrified specimens were stored under liquid nitrogen before imaging. Prior to blotting the grids were made hydrophilic by surface plasma treatment using a Cressington 208 carbon coater operating at 5 mA for 40 seconds. For conventional sample preparation 3 µL aliquots were applied to a 200 mesh carbon coated copper grid and subsequently excess liquid was quickly manually blotted away with filter paper. Atomic force microscopy (AFM) images were obtained using a Digital Instruments Nanoscope IV scanning force microscope in tapping mode using NCL type cantilevers (Si, 48 N/m, 190 kHz, Nanosensors). The samples were prepared by spin-coating a dilute solution of micelles on a siliconwafer.

Nickel(II) bis-{(α-terpyridine-ω-methyl-poly(ethylene glycol)} hexafluorophosphate (31)
The *mono*-terpyridine PEG **8** (150 mg, 0.066 mmol) and the metal salt Ni(OAc)$_2$ × H_2O (8.226 mg, 0.033 mmol) were stirred under reflux in 3 mL MeOH overnight. The reaction was followed by UV-Vis spectroscopy: when no more changes were observed in the UV-Vis spectrum, NH_4PF_6 (53.79 mg, 0.33 mmol, 10 fold excess) was added to the solution. Stirring was continued at least for another 30 minutes, after which the reaction mixture was cooled to room temperature and partitioned between dichloromethane and water. The organic layer was washed 3 times with water to remove excess salts, then dried over Na_2SO_4 and removed in vacuo. The crude product was purified by preparative size exclusion chromatography (BioBeads SX-1, CH_2Cl_2). Yield: 100 mg (33%). ^{1}H-NMR spectrum did not show any peaks in the aromatic region, due to the paramagnetic nature of the metal complex. Signals from uncomplexed terpyridine could not be observed. UV (H_2O): λ_{max} (ε) = (L mol^{-1} cm^{-1}):

324 (7 960), 311 (10 100), 299 (10 360), 272 (19 900), 243 (20 260). IR (ATR): ν/cm^{-1}: 2 884 (CH$_2$, CH$_3$), 1 614, 1 604, 1 573 (tpy), 1 279, 1 241, 1 146 (-CH$_2$-O-CH$_2$-), 840 (PF$_6$), 798, 752, 731, 700, 662 (CH$_2$). SEC (DMF system; PEG calibration): M$_n$ = 6,900 g/mol, M$_w$= 7,700 g/mol, PDI = 1.11.

General synthesis of cobalt(II) bis-{(α-terpyridine-ω-methyl-poly(ethylene glycol)} hexafluorophosphate (32) and iron(II) bis-{(α-terpyridine-ω-methyl-poly(ethylene glycol)} hexafluorophosphate (33)

The *mono*-PEG **8** (100 mg, 0.044 mmol) and the metal salt M(OAc)$_2$ × H$_2$O, with M = Co or Fe (0.022 mmol), were stirred under reflux in 3 mL MeOH overnight in a molar ratio 2:1. The reaction was followed by UV-Vis spectroscopy: when no more changes were observed in the UV-Vis spectrum, NH$_4$PF$_6$ (35.86 mg, 0.22 mmol, 10 fold excess) was added to the solution. Stirring was continued at least for another 30 minutes, after which the reaction mixture was cooled to room temperature and partitioned between dichloromethane and water. The organic layer was washed 3 times to remove excess salts, then dried over Na$_2$SO$_4$ and removed *in vacuo*. The crude product was purified by preparative size exclusion chromatography (BioBeads SX-1, CH$_2$Cl$_2$).

Iron(II) bis-{(α-terpyridine-ω-methyl-poly(ethylene glycol)} hexafluorophosphate (32)

Yield: 80 mg (40%). ^{1}H-NMR (400 MHz, CD$_2$Cl$_2$, 25 °C): δ (ppm) = 8.48 (s, 2H, H$^{3'}$, H$^{5'}$), 8.40 (d, 2H, J = 8.1 Hz; H^3, H$^{3"}$), 7.87 (m, 2H, H^4, H$^{4"}$), 7.20 (m, 2H, H^6, H$^{6"}$), 7.13 (d, 2H, J = 3.6 Hz; H^5, H$^{5"}$), 4.84 (m, 2H, tpyOCH_2), 4.15 (m, 2H, tpyOCH$_2$CH_2), 3.83–3.39 (m, PEG backbone), 3.34 (s, 3H, OCH_3). UV (H$_2$O): λ_{max} (ε) = (L mol^{-1} cm^{-1}): 556 (1 600), shoulder at 507 (1 468), 312 (4 510), 271 (6 500), 241 (7 130). IR (ATR): ν/cm^{-1}: 2 963, 2 888 (CH$_2$, CH$_3$), 1 616, 1 467, 1 413 (tpy), 1 360, 1 342, 1 259, 1 084, 1 058, 1 014 (-CH$_2$-O-CH$_2$-), 840 (PF$_6$), 838, 700, 662 (CH$_2$).

Cobalt(II) bis-{(α-terpyridine-ω-methyl-poly(ethylene glycol)} hexafluorophosphate (33)

Yield: 75 mg (37%). ^{1}H-NMR (400 MHz, CD$_3$CN, 25 °C): δ (ppm) = 110.82 (bs, 2H, H^6, H$^{6"}$), 73.81 (bs, 4H, H$^{3'}$, H$^{5'}$), 69.83 (bs, 4H, H^5, H$^{5"}$), 34.57 (bs, 4H, H^3, H$^{3"}$), 14.99 (m, 4H, tpyOCH_2), 9.35 (m, 2H, tpyOCH$_2$CH_2), 7.13 (m, 4H, CH$_2$OCH_2), 6.07 (bs, 4H, H^4, H$^{4"}$), 5.22 (m, 4H, CH_2OCH$_3$), 4.73 (m, 4H, CH$_2$OCH_2), 3.70–3.40 (m, PEG backbone), 3.30 (s, 3H, OCH_3). UV (H$_2$O): λ_{max} (ε) = (L mol^{-1} cm^{-1}): 453 (1 470), 306 (13 280), 272 (22 230), 240 (24 200). IR (ATR): ν/cm^{-1}: 2 884, 2 741 (CH$_2$, CH$_3$), 1 616, 1 572, 1 467 (tpy), 1 360, 1 342, 1 279, 1 241, 1 145 (-CH$_2$-O-CH$_2$-), 874 (PF$_6$), 798, 796, 752, 730, 700, 673, 661 (CH$_2$).

Synthesis of the nickel(II) chain extended polymer (34)

In a conical glass vial flushed with argon, *bis*-terpyridine PEG **12** (150 mg, 0.0625 mmol) and the metal salt Ni(OAc)$_2$ × H$_2$O (15.581 mg, 0.0625 mmol), were stirred under reflux in 750 μL MeOH overnight. A 10 fold excess of NH$_4$PF$_6$ (101.875 mg, 0.625 mmol) was added to the solution and the stirring was continued at least another 30 minutes, after which the reaction mixture was cooled to room temperature and partitioned between dichloromethane and water. The organic layer was washed 3 times to remove excess salts, then dried over Na$_2$SO$_4$ and removed *in vacuo*. The crude product was purified by preparative size exclusion chromatography (BioBeads SX-1, CH$_2$Cl$_2$). Yield: 225 mg (13%). SEC (DMF system; PEG calibration): M$_n$= 28,610 g/mol; M$_w$ = 39,430 g/mol; PDI = 1.37.

Synthesis of the nickel(II) bis-{(α-terpyridine-ω-methyl-poly(ethylene glycol)} hexafluorophosphate (35)

Compound **35** was prepared as described previously.[38,41] Yield: 42 mg (25%). Due to the paramagnetic metal complex the ^{1}H-NMR spectrum showed only the polymer backbone. In the aromatic region no signals from uncomplexed terpyridine molecules were observed, indicating full complexation of the starting material **9**. SEC (DMF system; PEG calibration): M$_n$ = 8,100 g/mol, M$_w$ = 8,700 g/mol, PDI = 1.07.

General synthesis of A-b-B-b-A triblock copolymers (37, 38 and 39)-Method A

M(OAc)$_2$ × H$_2$O (0.063 mmol), *mono*-terpyridine PEG **9** (variation of the end capper from 0% to 80% molar percentages in comparison to the M(OAc)$_2$ and monomer **6**) and 1,16-*bis*(2,2':6',2"-terpyridin-4'-yloxy)hexadecane **6** (43.26 mg, 0.06 mmol) were added to 300 μL MeOH in a conical glass vial and

capped with a septum. The polymerization was performed overnight at 65 °C. A 10 fold excess of NH_4PF_6 (15.686 mg, 0.63 mmol) in 2 mL MeOH was added to the solution and the stirring was continued for 1 hour, after which the solvent was evaporated. It was observed that this counter ion exchange had a significant effect on the solubility of the synthesized polymers; with acetate counter ions they were methanol soluble and acetone insoluble, while with hexafluorophosphate counter ions the reverse behavior was observed. The excess of NH_4PF_6 was removed by preparative size exclusion chromatography (BioBeads S-X1 in acetone). The pure compounds were obtained by precipitation from acetone into dichloromethane. <u>*Note*</u>: For Fe(II) and Co(II) A-*b*-B-*b*-A, only the reaction with 10% the end capper **9** was performed.

Synthesis of A-b-B-b-A triblock copolymers (37, 38 and 39) - Method B

$MCl_2 \times H_2O$ (0.315 mmol), 1,16-*bis*(2,2':6',2"-terpyridin-4'-yloxy)hexadecane **6** (0.3 mmol, 216.3 mg) and α-terpyridine-ω-methyl-poly(ethylene glycol) **9** (M_n = 3,000 g/mol, 0.03 mmol, 90 mg) were added to 1.5 mL of dimethylacetamide (DMA) in conical glass vials and capped with a septum. All components became readily dissolved after stirring the mixture for 3 minutes at 70 °C. The polymerization was performed overnight at 130 °C. The resulting product was purified as in the first approach after adding a 10 fold excess of NH_4PF_6 (see method A). <u>*Note*</u>: For Fe(II) and Co(II) A-*b*-B-*b*-A, only the reaction with 10% of end capper **9** was performed.

Micelle preparation of A-b-B-b-A triblock copolymers (37a, 38 and 39)

Since the block copolymers were not readily soluble in water, they were first dissolved in acetone (1 g/L). A water volume equal to half of the acetone volume was then added under stirring by steps of 50 μL, followed by the addition of the same water volume in one shot. The solutions were analyzed immediately without filtration.

Decomplexation of A-b-B-b-A triblock copolymer (37a)-MeOH approach

Experiment with the concentration c_1: 10 mg of **37a** were added together 1 mL of CH_3OH in a vial flushed with argon. The reaction mixture was refluxed at 63 °C for 12 h and then checked by SEC. Experiment with the concentration c_2: 10 mg of **37a** in 2 mL CH_3OH following the same procedure as in the previous experiment.

Decomplexation of A-b-B-b-A triblock copolymer (37a)-DMF approach

Experiment with the concentration c_1: 10 mg of **37a** were added together 1 mL of DMF in a vial flushed with argon. The reaction mixture was refluxed at 153 °C for 12 h and then checked by SEC. Experiment with the concentration c_2: 10 mg of **37a** were added together with 2 mL of DMF in a vial flushed with argon. Experiment with the concentration c_3: 10 mg of **37a** were added together 3 mL of DMF in a vial flushed with argon.

3.7 References

1   J.-M. Lehn, *Polym. Int.* **2002**, *51*, 825.

2   L. Brunsveld, B. J. B. Folmer, E. W. Meijer, R. P. Sijbesma, *Chem. Rev.* **2001**, *101*, 4071.

3   X. Yang, F. Hua, K. Yamato, E. Ruckenstein, B. Gong, W. Kim, C. Y. Ryu, *Angew. Chem. Int. Ed.* **2004**, *43*, 6471.

4   R. P. Sijbesma, F. H. Beijer, L. Brunsveld, B. J. B. Folmer, J. H. K. Ky Hirschberg, R. F. M. Lange, J. K. L. Lowe, E. W. Meijer, *Science* **1997**, *278*, 1601.

5   C. Schmuck, W. Wienand, *Angew. Chem. Int. Ed.* **2001**, *40*, 4363.

6   K. Yamauchi, J. R. Lizotte, T. E. Long, *Macromolecules* **2002**, *35*, 8745.

7   a) U. S. Schubert, C. Eschbaumer, *Angew. Chem. Int. Ed.* **2002**, *41*, 2892. b) C. A. Fustin, P. Guillet, U. S. Schubert, J. F. Gohy, *Adv. Mater.* **2007**, *19*, 1665.

8   J. B. Beck, J. M. Ineman, S. J. Rowan, *Macromolecules* **2005**, *38*, 5060.

9   H. Hofmeier, S. Schmatloch, D. Wouters, U. S. Schubert, *Macromol. Chem. Phys.* **2003**, *204*, 2197.

10   T. P. Russell, R. Jerome, P. Charlier, M. Foucart, *Macromolecules* **1988**, *21*, 1709.

11   Y. Guan, S.-H. Yu, M. Antonietti, C. Böttcher, C. F. J. Faul, *Chem. Eur. J.* **2005**, *11*, 1305.

12   Y. Sheng, B. Uwe, G. Tobias, L. Marina, F. Würthner, *J. Am. Chem. Soc.* **2004**, *126*, 8336.

13   A. J. Goshe, I. M. Steele, C. Ceccarelli, A. L. Rheingold, B. Bosnich, *Proc. Natl. Acad. Sci.* **2002**, *99*, 4823.

14   E. C. Constable, *Macromol. Symp.* **1995**, *98*, 503.

15   E. C. Constable, A. M. W. Cargill Thompson, *J. Chem. Soc. Dalton Trans.* **1992**, 3467.

16   U. S. Schubert, C. Eschbaumer, O. Hien, P. R. Andres, *Tetrahedron Lett.* **2001**, *42*, 4705.

17   M. Heller, U. S. Schubert, *Eur. J. Org. Chem.* **2003**, *6*, 47.

18   U. S. Schubert, C. Eschbaumer, *Macromol. Symp.* **2001**, *163*, 177.

19   U. S. Schubert, C. Eschbaumer, P. Andres, H. Hofmeier, C. H. Weidl, E. Herdtweck, E. Dulkeith, A. Morteani, N. Hecker, J. Feldmann, *Synth. Metals* **2001**, *121*, 1249.

20   B.-H. Ye, M.-L. Tong, X.-M. Chen, *Coord. Chem. Rev.* **2005**, *249*, 545.

21   S. Kelch, M. Rehahn, *Macromolecules* **1999**, *32*, 5818.

22   R. Dobrawa, F. Würthner, *Chem. Commun.* **2002**, *17*, 1878.

23   S. Schmatloch, A. M. J. van den Berg, A. S. Alexeev, H. Hofmeier, U. S. Schubert, *Macromolecules* **2003**, *36*, 9943.

24   B. G. G. Lohmeijer, U. S. Schubert, *J. Polym. Sci.: Part A: Polym. Chem.* **2003**, *41*, 1413.

25   R. Dobrawa, F. Würthner, *J. Polym. Sci.: Part A: Polym. Chem.* **2005**, *43*, 4981.

26   E. C. Constable, *Adv. Inorg. Chem. Radiochem.* **1986**, *30*, 69.

27   K. Kim, G. H. Nancollas, *J. Phys. Chem.* **1977**, *81*, 948.

28   U. S. Schubert, C. Eschbaumer, Q. An, T. Salditt, *J. Inclusion Phenom.* **1999**, *35*, 35.

29   M. A. R. Meier, B. G. G. Lohmeijer, U. S. Schubert, *J. Mass Spectrometry* **2003**, *38*, 502.

30   R. Hogg, R. G. Wilkins, *J. Chem. Soc.* **1962**, 341.

31   R. H. Holyer, C. D. Hubbard, S. F. A. Kettle, R. G. Wilkins, *Inorg. Chem.* **1966**, *5*, 622.

32   M. A. R. Meier, B. G. G. Lohmeijer, U. S. Schubert, *Macromol. Rapid Commun.* **2003**, *24*, 852.

33   P. A. Cock, C. E. Cottrell, R. K. Boyd, *Can. J. Chem.* **1972**, *50*, 402.

34   Y. Abe, G. Wada, *Bull. Chem. Soc. Jp.* **1981**, *54*, 3334.

35   H. P. Bennetto, E. F. Caldin, *J. Chem. Soc. A* **1971**, 2191.

36   G. U. Priimov, P. Moore, L. Helm, A. E. Merbach, *Inorg. React. Mech.* **2001**, *3*, 1.

37   R. Dobrawa, M. Lysetska, P. Ballester, M. Grune, F. Würthner, *Macromolecules* **2005**, *38*, 1315.

38   B. G. G. Lohmeijer, U. S. Schubert, *Macromol. Chem. Phys.* **2003**, *204*, 1072.

39   E. C. Constable, C. E. Housecroft, T. Kulke, C. Lazzarini, E. R. Schofield, Y. Zimmerman, *Dalton Trans.* **2001**, 2864.

40   M. A. R. Meier, D. Wouters, C. Ott, P. Guillet, C.-A. Fustin, J.-F. Gohy, U. S. Schubert, *Macromolecules* **2006**, *39*, 1569.

41   M. Chiper, M. A. R. Meier, J. M. Kranenburg, U. S. Schubert, *Macromol. Chem. Phys.* **2007**, *208*, 679.

42   H. R. Kricheldorf, M. Rabenstein, M. Maskos, M. Schmidt, *Macromolecules* **2001**, *34,* 713.

43   H. R. Kricheldorf, G. Schwarz, *Macromol. Rapid Commun.* **2003**, *24*, 359.

44   P. R. Andres, U. S. Schubert, *Synthesis* **2004**, *8*, 1229.

45   H. Kricheldorf, *Macromol. Symp.* **2003**, *199,* 1.

46   T. Yokosawa, H. Suzuki, *J. Am. Chem. Soc.* **1999,** *121,* 11573.

47   H.-G. Elias, *An Introduction to Polymer Science*, Wiley-VCH, **1997**.

48   P. J. Hore, *Nuclear magnetic resonance (Oxford chemistry primers, 32)*, Oxford University Press, Oxford, **1996**.

49   J. D. Epperson, L.- J. Ming, G. R. Baker, G. R. Newkome, *J. Am. Chem. Soc.* **2001**, *123,* 8583.

50   J.-F. Gohy, B. G. G. Lohmeijer, U. S. Schubert, *Chem. Eur. J.* **2003**, *9*, 3472.

51   W. C. Oliver, G. M. Pharr, *J. Mater. Res.* **1992**, *7*, 1564.

Chapter IV

Ruthenium(II) supramolecular assemblies

Abstract

*Different **AA, AB** and **ABA** ruthenium(II)-terpyridine supramolecular assemblies have been synthesized via Ru(II) terpyridine complexation, using mono-terpyridine end functionalized poly(ethylene glycol) as hydrophilic block **A** and various rigid-rod conjugated terpyridyl ligands as hydrophobic segment **B**. Those systems are reminiscent of **ABA** or **AB** block copolymer structures. Herein, we discuss the synthesis and characterization of these new **ABA** and **AB** Ru(II) supramolecular assemblies. Photophysical and electrochemical properties of the new **ABA** Ru(II) systems are discussed in detail. The aqueous self-assembly of the **ABA** triblock amphiphilic assemblies was studied by cryo-transmission electron microscopy, dynamic light scattering and atomic force microscopy demonstrating a significant influence of the various middle segments **B** on the size of the obtained micelles. Furthermore, to be able to synthesize linear high molar mass Ru(II) coordination polymers, **A_n**, the reaction conditions for the direct one-step metallo-polymerization of bis-terpyridine poly(ethylene glycol) with RuCl$_3$ in the presence of reducing agents were investigated. The optimization of the metallo-polymerization was monitored by SEC. For the highest molar mass Ru(II) coordination polymer obtained, full characterization was performed by various techniques including SEC, ^{1}H-NMR and UV-Vis spectroscopy, proving the formation and the stability of the designed structure.*

4.1 Introduction

The possibility of combining various functional ligands with a large range of transition metal ions has made metal-ligand coordination an important method in the field of supramolecular chemistry.[1-4] Metal-ligand interactions vary from very strong to very weak based on the combination of metal ion and ligand used. Most of these supramolecular "connections" are weaker than covalent bonds making them more labile and dynamical, providing the possibility of forming "switchable" systems under certain conditions (*e.g.* following an external trigger).[5-8] The architecture of supramolecular metal-containing polymers can be controlled by the geometry of the bridging ligands that influences the coordination of metal ions.[9-13] The extraordinary binding affinity towards most transition metal ions due to $d\pi\rightarrow p\pi^*$ bonding, together with the strong chelating effect, makes terpyridines (tpy) and their derivatives appealing building blocks for the design and the construction of supramolecular assemblies.[4,14-17] From the large range of transition metal ions, ruthenium(II) represents one of the most favorable ions in the engineering of robust terpyridine coordination assemblies, because it allows the direct synthesis of both heteroleptic as well as homoleptic systems.[18] Moreover, ruthenium(II) is characterized by high binding strengths towards terpyridine ligands and, consequently, the resulting ruthenium terpyridine structures are characterized by high stabilities compared to other metal ion terpyridine complexes. Literature provides examples where the ruthenium terpyridine connectivity could be opened only by the usage of harsh conditions (low pH, competitive ligands, temperature).[38] In addition, ruthenium terpyridine complexes possess interesting photophysical and electrochemical properties, which are strongly influenced by the electronic characteristics of the lateral substituents.[19-22]

Complexation of the terpyridine moiety could be achieved by several synthetic approaches summarized in literature.[4] In this chapter, the synthesis of a variety of ruthenium(II) supramolecular assemblies is based on two main synthetic strategies: (1) complexation of terpyridine macroligands with $RuCl_3$ ions followed by the reduction of Ru(III) to Ru(II) ions and addition of the second terpyridine ligand as well as (2) complexation of the terpyridine ligand with a $Ru(II)(DMSO)_4Cl_2$ precursor and subsequent attachment of the second terpyridine ligand under relatively mild conditions.

4.2 Ruthenium terpyridine complexation: synthetic strategies

4.2.1 Complexation *via* RuCl$_3$
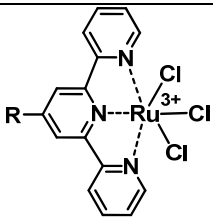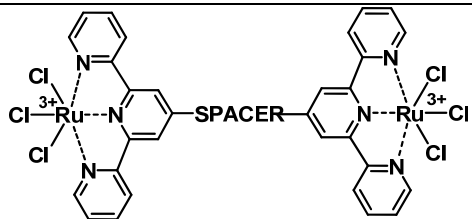
Homoleptic and heteroleptic Ru(II) terpyridine complexes can be prepared *via* the classical synthesis that starts from RuCl$_3 \times 3$ H$_2$O as displayed in Scheme 4.1. This synthetic approach consists of two defined steps. The first step deals with the preparation of the terpyridine-Ru(III)Cl$_3$ *mono*-complex which is generally synthesized by refluxing the commercially available RuCl$_3 \times 3$ H$_2$O together with the terpyridine ligand (in a molar ratio 1:1), which can be performed in various solvents such as MeOH, EtOH, ^{n}BuOH or DMF. Several Ru(III)Cl$_3$ terpyridine *mono*-complexes where synthesized by following the approach described in Scheme 4.1 and are summarized in Table 4.1. The obtained Ru(III)Cl$_3$ terpyridine *mono*-complex is characterized by a medium to high stability and could be stored under dry and inert conditions.
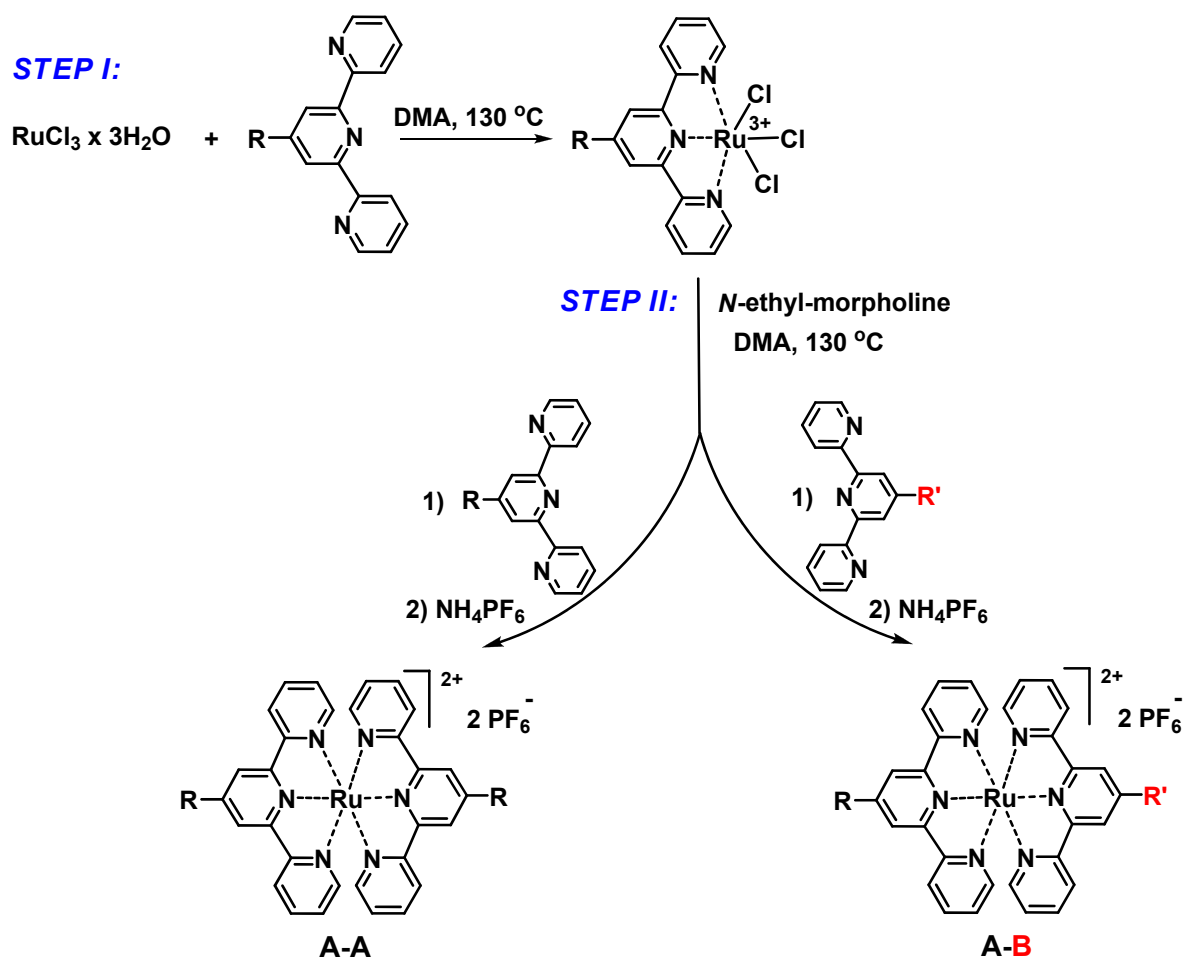
Scheme 4.1: *Schematic representation of the synthesis of the Ru(III)Cl$_3$ terpyridine mono-complex, the homoleptic **A-A** and the heteroleptic **A-B** Ru(II) bis-terpyridine complexes.*

The characterization of the synthesized Ru(III)Cl$_3$ terpyridine *mono*-complexes was performed by UV-Vis spectroscopy where a strong absorption band could be observed at about 490 nm. For this case ^{1}H-NMR spectroscopy can not be used as a reliable characterization tool since the Ru(III) ions are paramagnetic. Nevertheless, the absence of terpyridine signals provides an indication of the *mono*-complex formation for all synthesized compounds (Table 4.1).

Table 4.1: *Overview of the synthesized Ru(III)Cl$_3$ terpyridine mono-complexes **40-44**.*

	R
40	HO-(CH$_2$)$_3$-O-
41	MeO-PEG$_{200}$-O-
42	MeO-PTHF$_{90}$-O-

	SPACER
43	-O-PEG$_{180}$-O-
44	-O-PTHF$_{90}$-O-

The second step of the discussed approach is the formation of the Ru(II) *bis*-terpyridine complex. The reaction is performed with an equal molar ratio between the Ru(III)Cl$_3$ terpyridine *mono*-complex and the second terpyridine ligand. In order to convert Ru(III) into Ru(II) a reducing agent is required. For that reason the reaction is performed in the presence of *N*-ethyl-morpholine, which provides the essential electrons for the reducing process. Moreover, some of the utilized solvents, such as MeOH, EtOH or BuOH, are also contributing to the reduction of Ru(III) species to Ru(II).[18,23] This approach is further discussed in subchapter 4.5.

4.2.2 Complexation *via* Ru(DMSO)$_4$Cl$_2$

A different approach for the preparation of homo- and heteroleptic Ru(II) *bis*-terpyridine complexes is based on the use of a RuCl$_2$(DMSO)$_4$ precursor. This mild agent offers the opportunity of introducing Ru(II) species to the terpyridine moiety without the need of any further reducing steps. Moreover, the RuCl$_2$(DMSO)$_4$ precursor could be successfully used in the presence of some sensitive or (very) reactive groups (such as, *e.g.*, ethynyl) that might interact with Ru(III) species when the classical approach discussed in subchapter 4.2.1 is

used. The synthesis of the desired Ru(II) precursor was first reported by Evans *et al.* in 1973.[24]

The $RuCl_2(DMSO)_4$ precursor **45** is obtained as a mixture of stereoisomers (*cis* and *trans*) as described in Scheme 4.2. The isomers are separable, which is intensively applied in the research area of medicinal chemistry (for drug delivery systems) since $RuCl_2(DMSO)_4$ is known for its high antitumor activity.[25,26] However, for further complexation reactions this is not required.
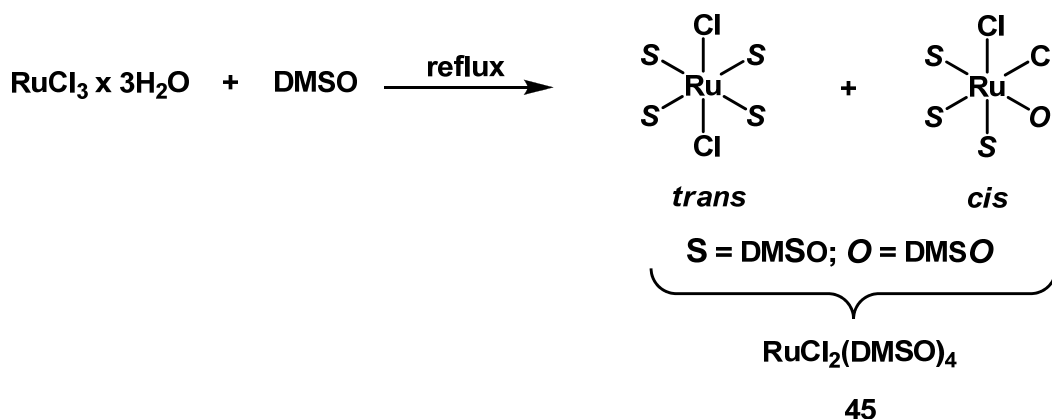
Scheme 4.2: *General representation of the synthesis of the Ru(II)(DMSO)₄Cl₂ precursor **45** (cis and trans isomers) (DM**S**O = **S**-bonded dimethyl sulfoxide; DMS**O** = **O**-bonded dimethylsulfoxide).*

The structure of the synthesized precursor **45** was proven by UV-Vis spectroscopy, elemental analysis and ^{1}H-NMR spectroscopy. Generally, the UV-Vis spectrum offers characteristic absorption bands for the different ruthenium species as depicted in Figure 4.1.
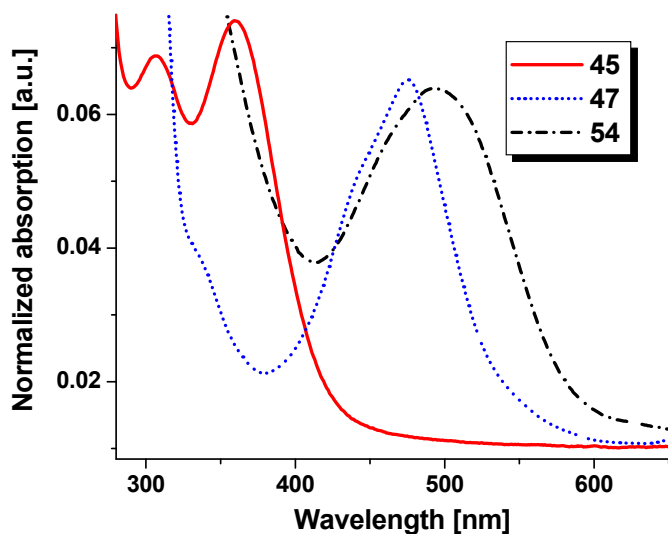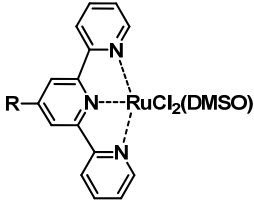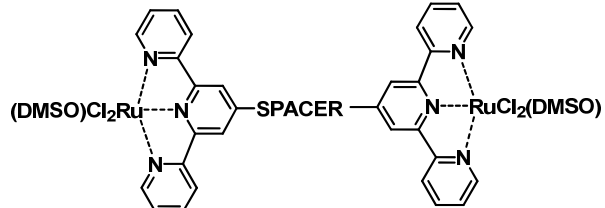
Figure 4.1: *Characteristic UV-Vis absorption spectra of the Ru(II)(DMSO)₄Cl₂ precursor **45** (solid line), the Ru(II)Cl₂DMSO chloro-terpyridine mono-complex **47** (short doted line) and the Ru(II) bis-chloro-terpyridine **54** (short dash dotted line) in DMSO.*

In order to chelate the terpyridine moiety with the Ru(II) species from the $RuCl_2(DMSO)_4$ precursor, the approach described in Scheme 4.3 is followed. A short overview of the synthesized structures *via* this route is offered in Table 4.2. In the first step, the $Ru(II)Cl_2DMSO$ terpyridine *mono*-complex is obtained as a mixture of *cis* and *trans* stereo-isomers as it was described by Ziessel *et al.*[49] The diasteroisomers could be separated by performing a recrystallization when R represents a small substituent and by preparative size exclusion chromatography (BioBeads) when R has a polymeric nature (for the polymeric case a convincing explanation of the successful separation by BioBeads could not be found). The prepared $Ru(II)Cl_2DMSO$ terpyridine *mono*-complex offers characteristic features in UV-Vis and ^{1}H-NMR spectroscopy. The UV-Vis spectrum displayed a red shift around 480 nm in comparison to the $RuCl_2(DMSO)_4$ precursor (Figure 4.1).
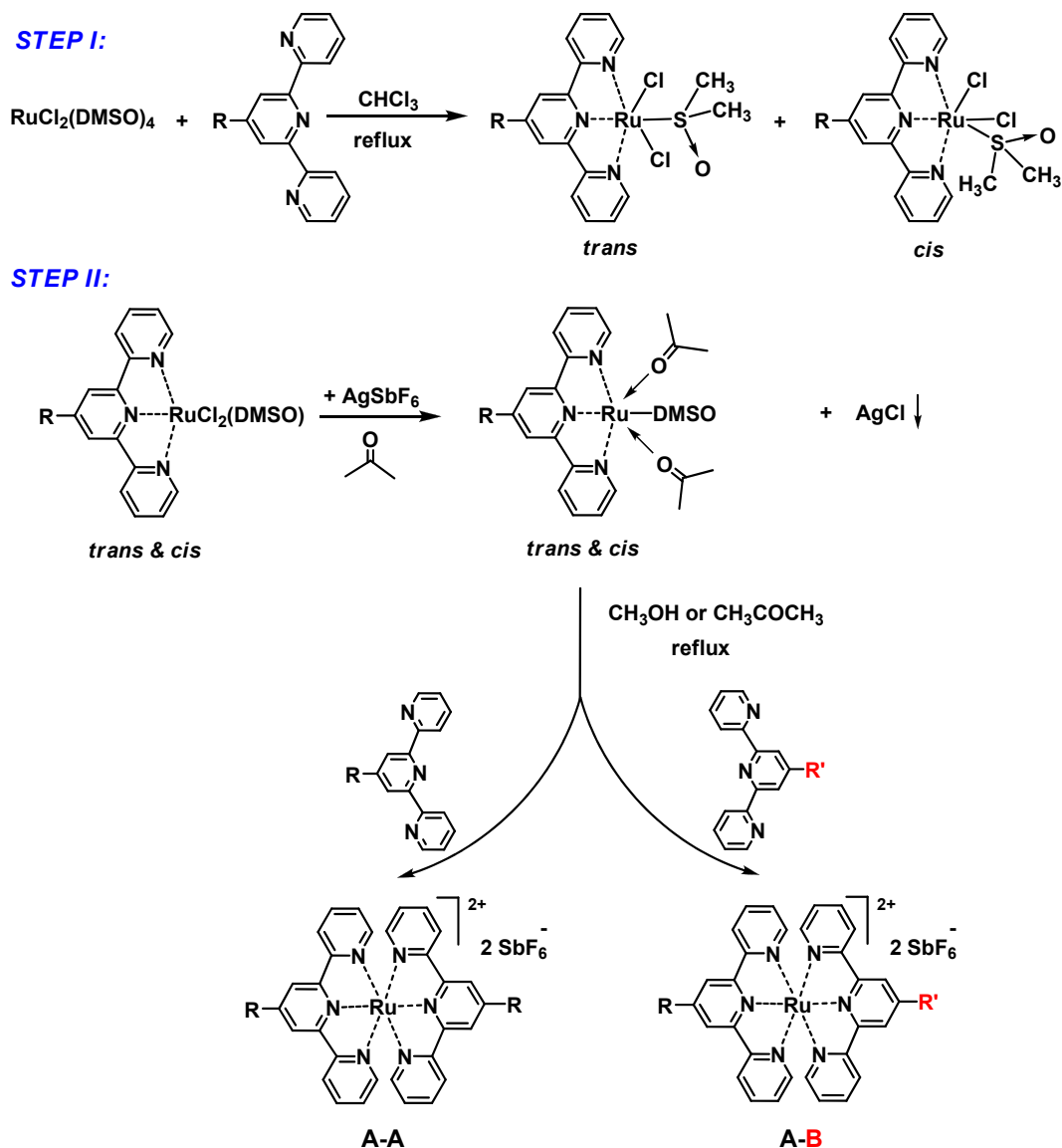
Scheme 4.3: *Schematic representation of the synthesis of a Ru(II)Cl₂DMSO terpyridine mono-complex and the homoleptic **A-A** and the heteroleptic **A-B** Ru(II) bis-terpyridine complexes.*

Table 4.2: *Overview of the synthesized Ru(II)Cl$_2$DMSO terpyridine mono-complexes **46-53**.*

	R
46	H-
47	Cl-
48	HO-(CH$_2$)$_3$-O-
49	MeO-PEG$_{12}$-O-
50	MeO-PEG$_{44}$-O-
51	MeO-PEG$_{70}$-O-
52	MeO-PEG$_{200}$-O-

	SPACER
53	-O-PEG$_{180}$-O-

Moreover, the isomers of the synthesized Ru(II)Cl$_2$DMSO terpyridine *mono*-complex displayed a different pattern in the ^{1}H-NMR spectrum, as described in literature.[49] Generally speaking, the *trans* isomer compared to the *cis* isomer has a deshielding effect of approximate Δ = 0.30 ppm on the 6,6" protons and a shielding of the 5,5" protons of approximately Δ = 0.25 ppm, due to the stereoelectronic effect of the DMSO and/or Cl ligands, compared to the uncomplexed terpyridine ligand (Figure 4.2).

The second step of this approach showed the formation of the Ru(II) *bis*-terpyridine complex. The reaction started with the activation of the Ru(II)Cl$_2$DMSO *mono*-terpyridine by dehalogenation with hexafluoroantimonate (AgSbF$_6$), whereby the reaction solvent coordinated to the vacant orbitals from the Ru(II) *mono*-complex forming a more reactive synthon. The reactive species subsequently reacted with the second terpyridine ligand that was added. A short overview of the synthesized structures is shown in Table 4.3. Furthermore, this approach will be discussed in detail in the following subchapters (4.3 and 4.4, respectively).
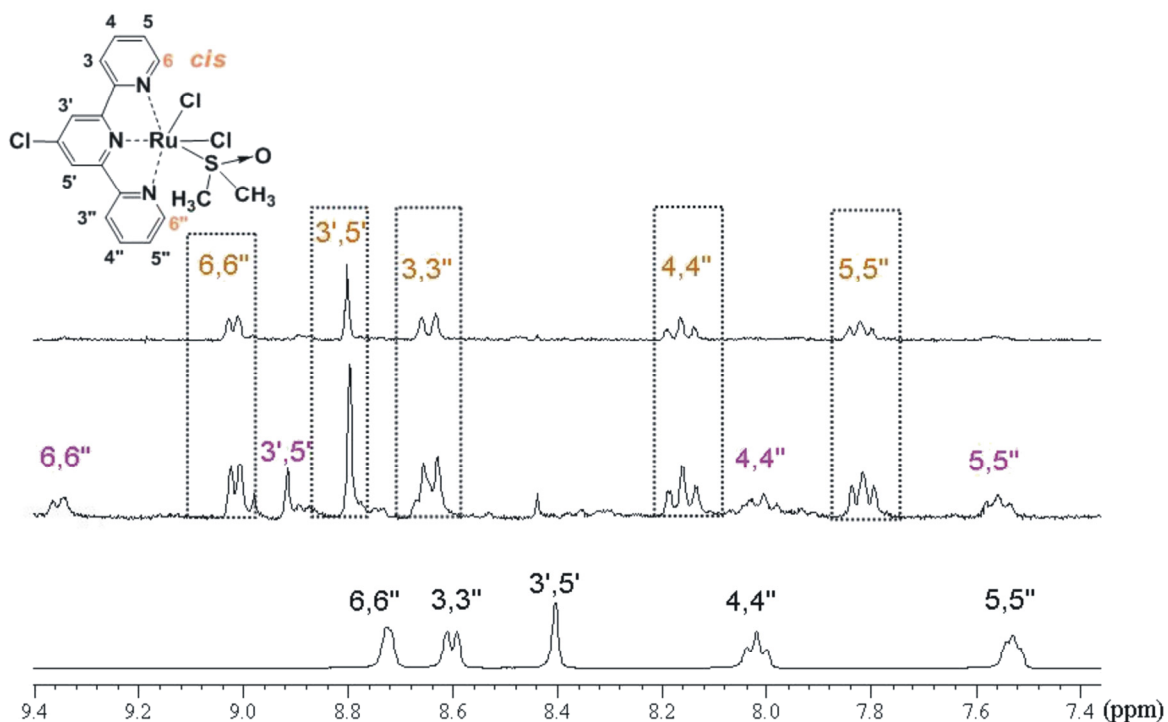
Figure 4.2: *^{1}H-NMR spectra of the chloro-terpyridine (bottom), the crude reaction mixture (cis and trans) isomers of Ru(II)Cl$_2$DMSO chloro-terpyridine mono-complex (middle) and the cis Ru(II) chloro-terpyridine mono-complex (top) in DMSO-d$_6$.*

Table 4.3: *Overview of the synthesized Ru(II) bis-terpyridine complexes 54-58.*

	R		R	R'
54	Cl-	**57**	H-	Cl-
55	HO-(CH$_2$)$_3$-O-	**58**	H-	MeO-PEG$_{200}$-O-
56	MeO-PEG$_{44}$-O-			

4.3 Coil-rod-coil ruthenium(II) ABA terpyridine triblock assemblies

Rigid rod-like ditopic terpyridyl ligands have been used as precursors for polymetallic architectures,[27-29] which could be potentially applied for the preparation of luminescent or electrochemical sensors.[30-34] In addition, examples of flexible terpyridine-containing metallo-supramolecular polymers have been reported in literature.[9,35-38] Due to the stiff structural design of the spacer, rigid-rod like ditopic terpyridyl ligands are leading to the formation of linear supramolecular metal-containing structures since cyclic structures can not be formed.[12,39,40] Furthermore, the addition of flexible side chains on the rigid spacer of the ditopic terpyridyl ligands can significantly improve the solubility of the substituted systems in comparison to the poorly soluble unsubstituted analogous compounds.[22,34] This type of conjugated rigid-rod like ditopic ligands can also be considered as promising candidates for the synthesis of block copolymers based on ruthenium(II) terpyridine complexes; structures which are susceptible to segregate into nanostructured materials (*e.g.* micelles in a selective solvent) when sufficiently different blocks are chosen. In the present subchapter, we focus on the synthesis and characterization of new coil-rod-coil macromolecular architectures based on ruthenium(II) terpyridine complexes that resemble **ABA** triblock copolymers. Several examples of **AB**, **ABA** and **ABC** block copolymers based on Ru(II) *bis*-terpyridine connectivities were already described in literature.[41-44] These types of metallo-supramolecular block copolymers have proven to be attractive precursors for complex self-assembled architectures.[45,46] However, rigid building blocks were not yet included in terpyridine Ru(II) based copolymers. In this work, **A** is a *mono*-terpyridine end-functionalized poly(ethylene glycol), a water soluble random coil polymer, and **B** is a rigid conjugated segment end-capped at both ends by terpyridyl ligands. For the preparation of the hydrophobic segments **60a-d**, terpyridine units were introduced onto both ends of the rigid conjugated chains *via* several routes, as reported previously.[22] The resulting ligands **60a-d** were assembled into **ABA** supramolecular structures **61a-d** *via* Ru(II) complexation of *mono*-terpyridine PEG **8**. Besides the synthesis and characterization, the aqueous micellization of those coil-rod-coil amphiphilic **ABA** triblock assemblies is described and studied by cryo-transmission electron microscopy (cryo-TEM), atomic force microscopy (AFM) and dynamic light scattering (DLS).

4.3.1 Synthesis and characterization of the Ru(II)Cl$_2$DMSO *mono*-terpyridine PEG *mono*-complex and Ru(II) *bis*-terpyridine PEG (model complex)

The complexation approach *via* Ru(DMSO)$_4$Cl$_2$ was adopted as an alternative and more advantageous method to coordinate Ru(II) ions to the terpyridine moiety of both chelating blocks (**A** and **B**) in comparison to the RuCl$_3$ route which usually requires the presence of a reductive agent and sometimes more harsh reaction conditions as briefly discussed before.[5,18,47] To the best of our knowledge, the Ru(DMSO)$_4$Cl$_2$ route has not been described previously for the construction of metallo-supramolecular polymers and this combination might overcome some of the difficulties met in the RuCl$_3$ procedure. On the other hand, the presence of a bulky counter ion, such as SbF$_6^-$, from the beginning of the reaction makes the complexation step more straightforward since there is no need of a counter ion exchange at the end of the complexation process to make the complex soluble in organic solvents, as it is the case when chloride anions are used (exchange from Cl$^-$ to PF$_6^-$ or other bulky ions).
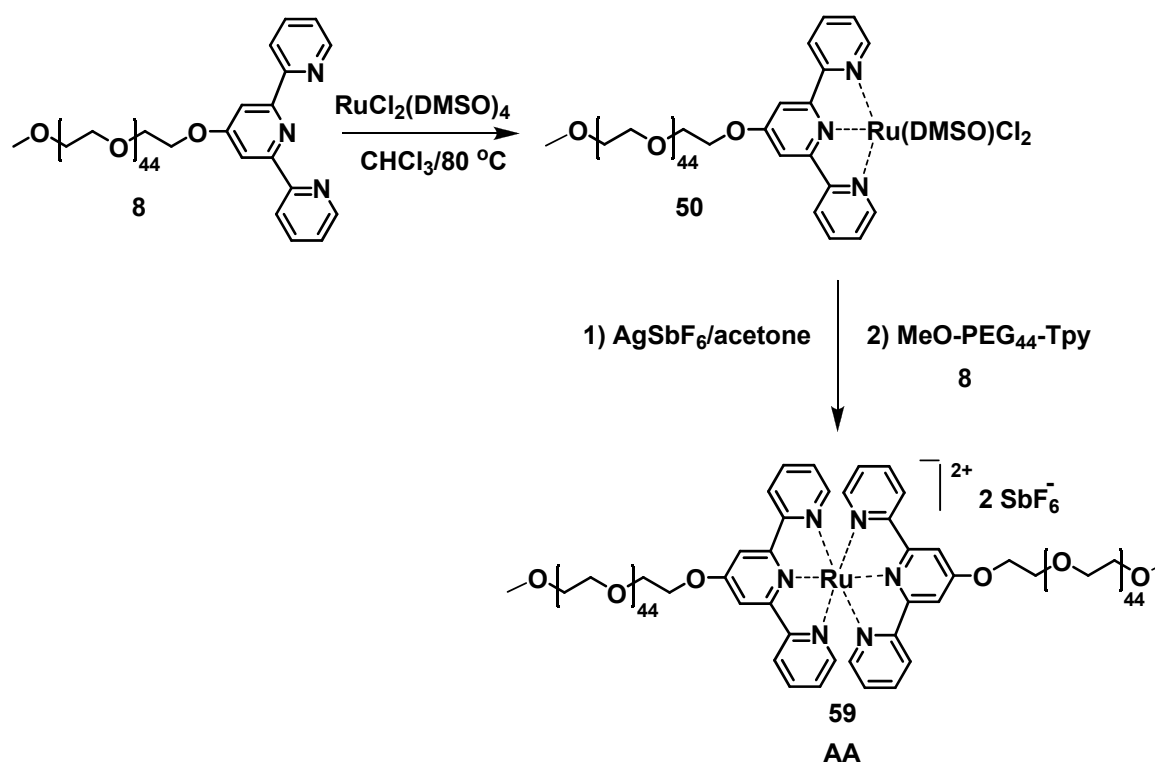
Scheme 4.4: *Schematic representation of the synthesis of the Ru(II)Cl$_2$DMSO mono-complex macroligand 50 and the Ru(II) model complex 59.*

The synthesis procedure starts from *mono*-terpyridine PEG **8** (prepared and characterized in Chapter 2) that was used to synthesize the *mono*-complex macroligand **50** which represents the key building block[48,49] in the preparation of the desired **ABA** triblock assemblies **61a-d**. By treating *mono*-terpyridine PEG **8** with Ru(DMSO)$_4$Cl$_2$ **45** in chloroform, followed by

overnight reflux conditions, the *mono*-complex macroligand **50** was synthesized (Scheme 4.4). The crude reaction mixture was purified by preparative size exclusion chromatography (BioBeads SX-1, CH_2Cl_2), followed by precipitation from dichloromethane into diethyl ether yielding a red-brownish powder. The UV-Vis spectrum of **50** revealed the characteristic metal-to-ligand charge transfer (MLCT) band of the *mono*-complex at 477 nm proving the successful incorporation of Ru(II) into the *mono*-terpyridine functionalized polymer **8**. The ^{1}H-NMR spectrum of **50** revealed a clear shift for the complexed terpyridine protons due to the presence of the $Ru(II)Cl_2DMSO$ group. The 6,6" terpyridine protons, which were detected at 8.68 ppm in the uncomplexed ligand **8**, were strongly shifted to lower magnetic field (9.21 ppm) in the *mono*-complex macroligand **50**, confirming the formation of the $Ru(II)Cl_2DMSO$ *mono*-complex macroligand **50** (Figure 4.3).[49] The SEC trace (Figure 4.4) showed a monomodal distribution for the prepared *mono*-complex macroligand **50** with a slightly increased molar mass in comparison to the uncomplexed starting material **8**. In addition, SEC analysis with in-line diode array detector displayed the characteristic absorption band for the $Ru(II)Cl_2DMSO$ *mono*-terpyridine *mono*-complex at 477 nm over the complete molar mass distribution as a proof for the stability of the Ru(II) terpyridine species (Figure 4.5 left).

Prior to the synthesis of the **ABA** triblock assemblies based on Ru(II) connectivity, the symmetric Ru(II) complex **59** based on *mono*-terpyridine PEG **8** was prepared and characterized. Taking into account that the metal complexation of telechelic ligands (*e.g.* **60a-d**) can, in theory, also lead to the formation of defect structures such as **AA** or **AB** (apart from the desired **ABA**), complex **59** represents a model compound for the corresponding **ABA** supramolecular triblock assemblies **61a-d**. Comparison of the characteristics of the **ABA** triblock assemblies with the model complex (*e.g.* ^{1}H-NMR signals or SEC curves) represents a very helpful method to evaluate the success of the reactions and the purity of the obtained supramolecular systems.

The model complex **59** was synthesized starting from the *mono*-complex macroligand **50**, which was first treated with $AgSbF_6$ in acetone followed by the addition of *mono*-terpyridine PEG **8** (Scheme 4.4). Further purification of the crude product performed by size exclusion chromatography (BioBeads S-X1, CH_2Cl_2) yielded the pure model complex **59** that was characterized by ^{1}H-NMR and UV-Vis spectroscopy as well as SEC. The ^{1}H-NMR spectrum of **59** revealed the characteristic fingerprint for the complexed terpyridine protons: a strong upfield shift of the 6,6"-signal in the *bis*-terpyridine complex, due to the different chemical environment of the 6,6"-protons, compared to the free ligand **8** and the *mono*-complex macroligand **50** (Figure 4.3).
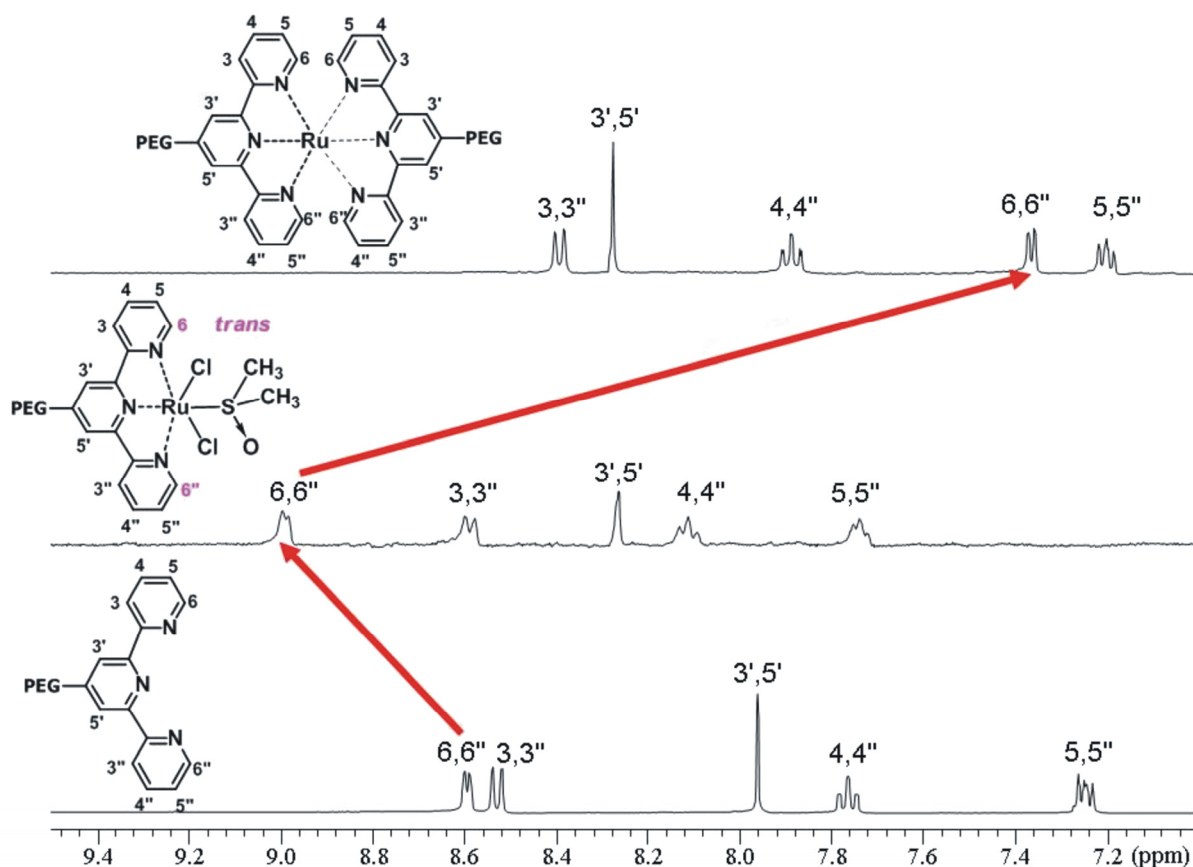
Figure 4.3: *^{1}H-NMR spectra of the mono-terpyridine PEG **8** (bottom), the trans isomer Ru(II)Cl$_2$DMSO mono-terpyridine mono-complex **50** (middle) and the Ru(II) bis-terpyridine PEG **59** (top) in CD$_2$Cl$_2$.*

In addition, the UV-Vis spectrum showed a bathochromic shift from 477 nm to 490 nm of the metal-to-ligand charge-transfer (MLCT) transitions. The SEC analysis with RI detector of **59** displayed, as expected, an increased molar mass in comparison to the starting materials **8** and **50** (Figure 4.4).
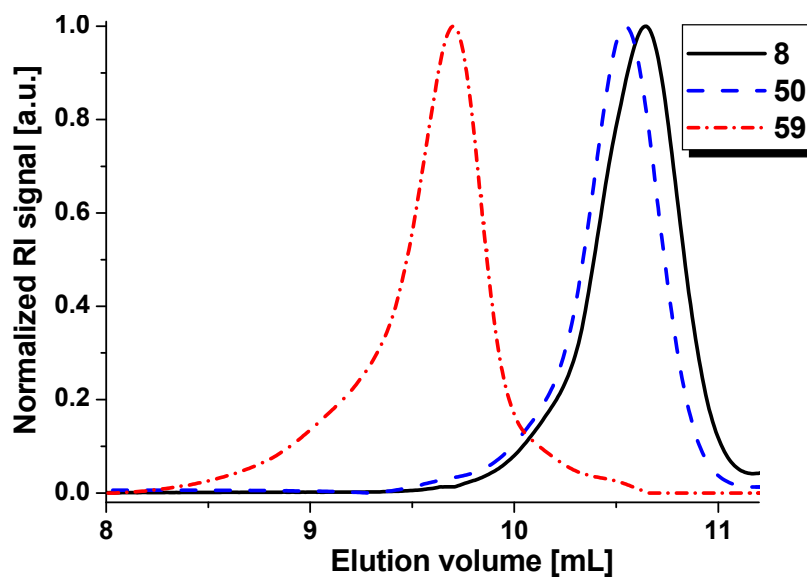
Figure 4.4: *SEC elution curves (RI detector) of the mono-terpyridine PEG **8** in comparison to the Ru(II)Cl₂DMSO mono-complex macroligand **50** and the Ru(II) model complex **59**.*

Moreover, SEC analysis with an in-line diode array detector displayed the characteristic MLCT band for the Ru(II) *bis*-terpyridine complexes at 490 nm over the complete molar mass distribution (Figure 4.5 right).
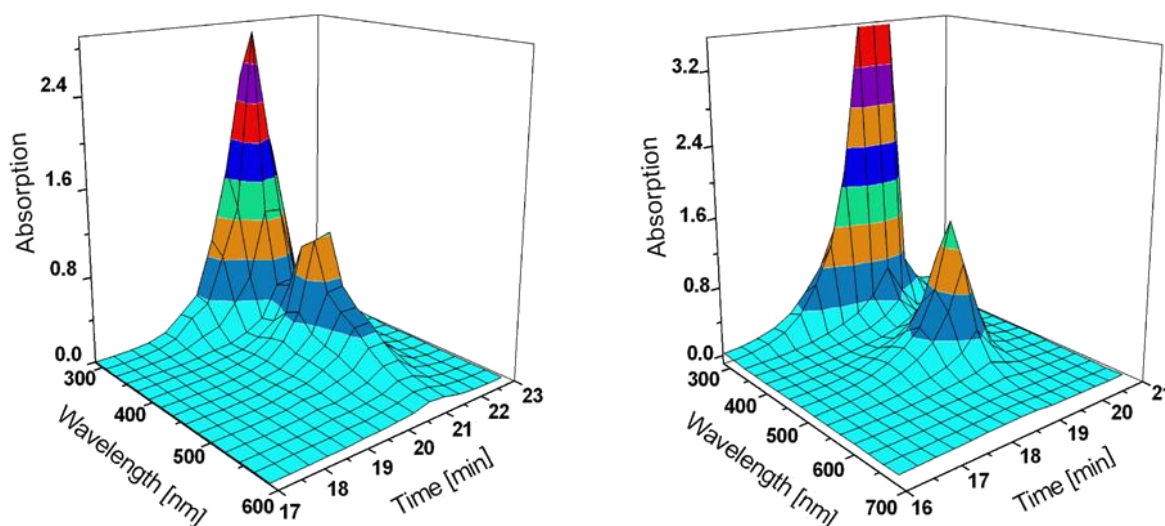
Figure 4.5: *Comparison of the SEC elution curves (photo diode array detector) of the Ru(II)Cl₂DMSO mono-terpyridine PEG mono-complex **50** (left) and Ru(II) bis-terpyridine PEG **59** (right).*

4.3.2 Synthesis and characterization of the Ru(II) ABA triblock assemblies

The desired **ABA** triblock resembling copolymers **61a-d** consist of a hydrophilic random coil block **A** based on *mono*-terpyridine PEG **8** with $M_n = 2,200$ g/mol and a hydrophobic segment **B** based on various rigid-rod like *bis*-terpyridine ligands **60a-d** (Scheme 4.5 and Figure 4.6). Even if the rigid building block does not consist of monomer units, we will discuss the structures **61a-d** as being **ABA** triblock assemblies. Since the mentioned building blocks carry terpyridine chelating units, their metal complexation could be achieved *via* a stepwise Ru(II) terpyridine complexation leading to the formation of well-defined **ABA** triblock copolymers architectures.
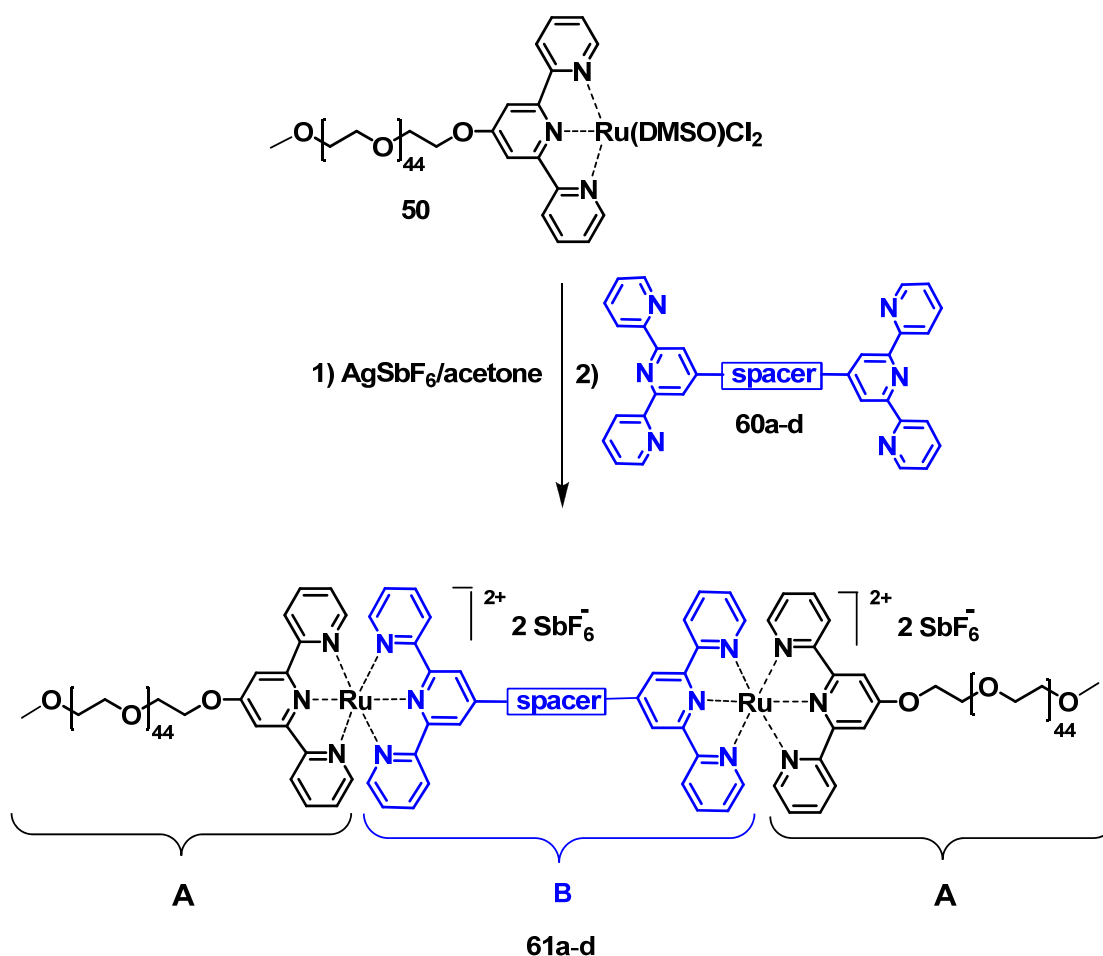
Scheme 4.5: *Schematic representation of the synthesis of the **ABA** triblock assemblies 61a-d.*

To synthesize the **ABA** triblock assemblies, the general synthetic strategy described in Scheme 4.5 was followed. In the first step macroligand *mono*-complex **50** was treated with AgSbF$_6$ resulting in dehalogenation and coordination of acetone ligands to the metal sphere to generate a more reactive ruthenium(II) synthon. In the second step, after the removal of the formed AgCl by filtration, the intermediate was reacted with the conjugated ditopic

terpyridine ligands **60a-d**. The obtained crude products were purified by preparative size exclusion chromatography (BioBeads SX-1, CH₂Cl₂) where the by-products, such as **AA** and **AB** structures, could be successfully removed. The purified triblock assemblies **61a-d** were obtained as red-brownish solids in yields between 25-50%. They were characterized by SEC, ¹H-NMR, UV-Vis and emission spectroscopy as well as cyclic voltammetry, as described in the following.
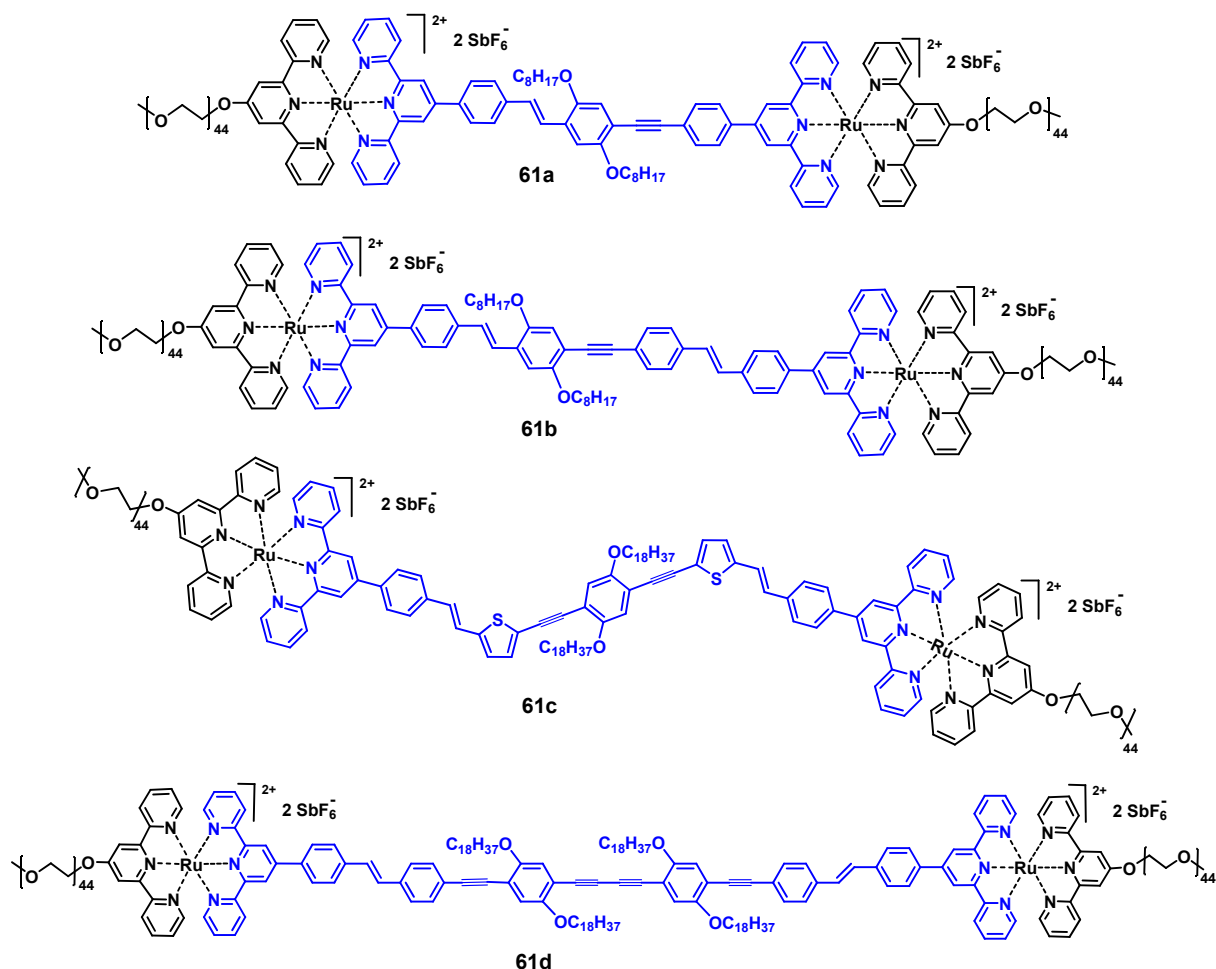
Figure 4.6: *Schematic representation of the chemical structures of the synthesized* **ABA** *triblock assemblies* **61a-d**.

From the results of size exclusion chromatography (SEC, see Figure 4.7) it is evident that the purified **ABA** triblocks assemblies **61a-d** had higher molar masses than the starting material **8**, the *mono*-complex macroligand **50** and the model complex **59**, while a monomodal molecular weight distribution was retained. The hydrodynamic volumes of the synthesized **ABA** triblock assemblies seem to be influenced by the different structures of segment **B**. For the **ABA** triblock assemblies **61a** and **61b**, SEC analysis revealed a narrow molar mass distribution while for **61c** and **61d** the molar mass distributions are more broadened.
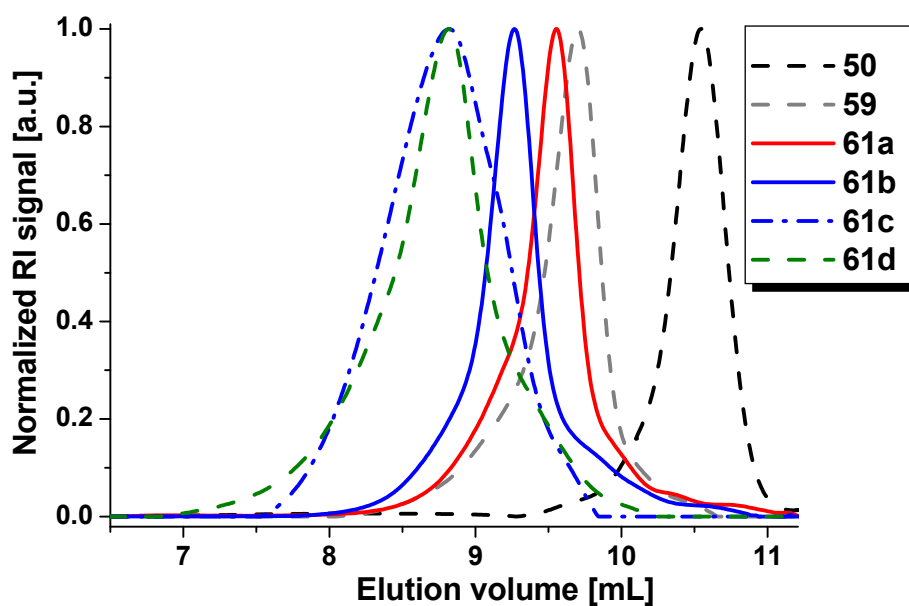
Figure 4.7: *SEC elution curves (RI detector) of the **ABA** triblock assemblies **61a-d** in comparison to the Ru(II)Cl$_2$DMSO mono-complex macroligand **50** and the model complex **59**.*

The results obtained from the SEC with in-line diode array detector of the purified **ABA** triblock assemblies **61a-d** (Figure 4.8) clearly demonstrated the presence and the stability of the supramolecular moieties over the complete molar mass distribution as indicated by the MLCT band around 500 nm, which is characteristic for the Ru(II) *bis*-terpyridine complexes.
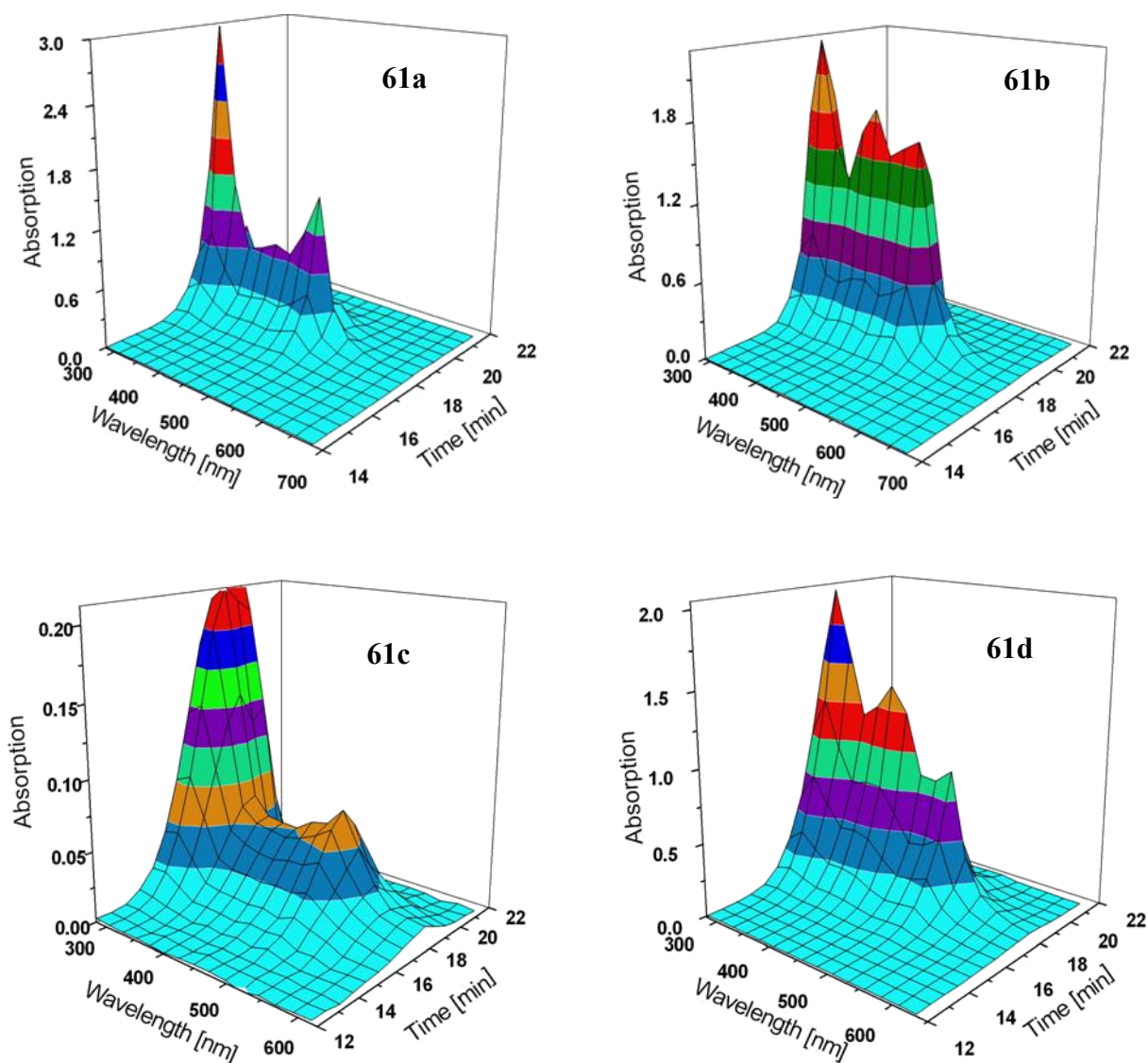
Figure 4.8: *SEC elution curves (photo diode array) of the **ABA** triblock assemblies **61a-d**.*

The ^{1}H-NMR spectra for the **ABA** synthesized triblock assemblies **61a-d** revealed clear shifts, similar to the model complex, for the complexed terpyridine protons as well as the expected integral ratios proving the successful formation of the desired **ABA** triblock assemblies. The assignments for the aromatic protons were based on two-dimensional [1]H-^{1}H correlation spectroscopy (^{1}H-^{1}H COSY) as depicted in Figure 4.9. The signals between 4 and 5 ppm could be attributed to the proton signals of the methylene groups next to the terpyridines (α-methylenes) and the strong signal around 3.7 ppm to the other methylene protons of the PEG backbone (see Experimental Part).
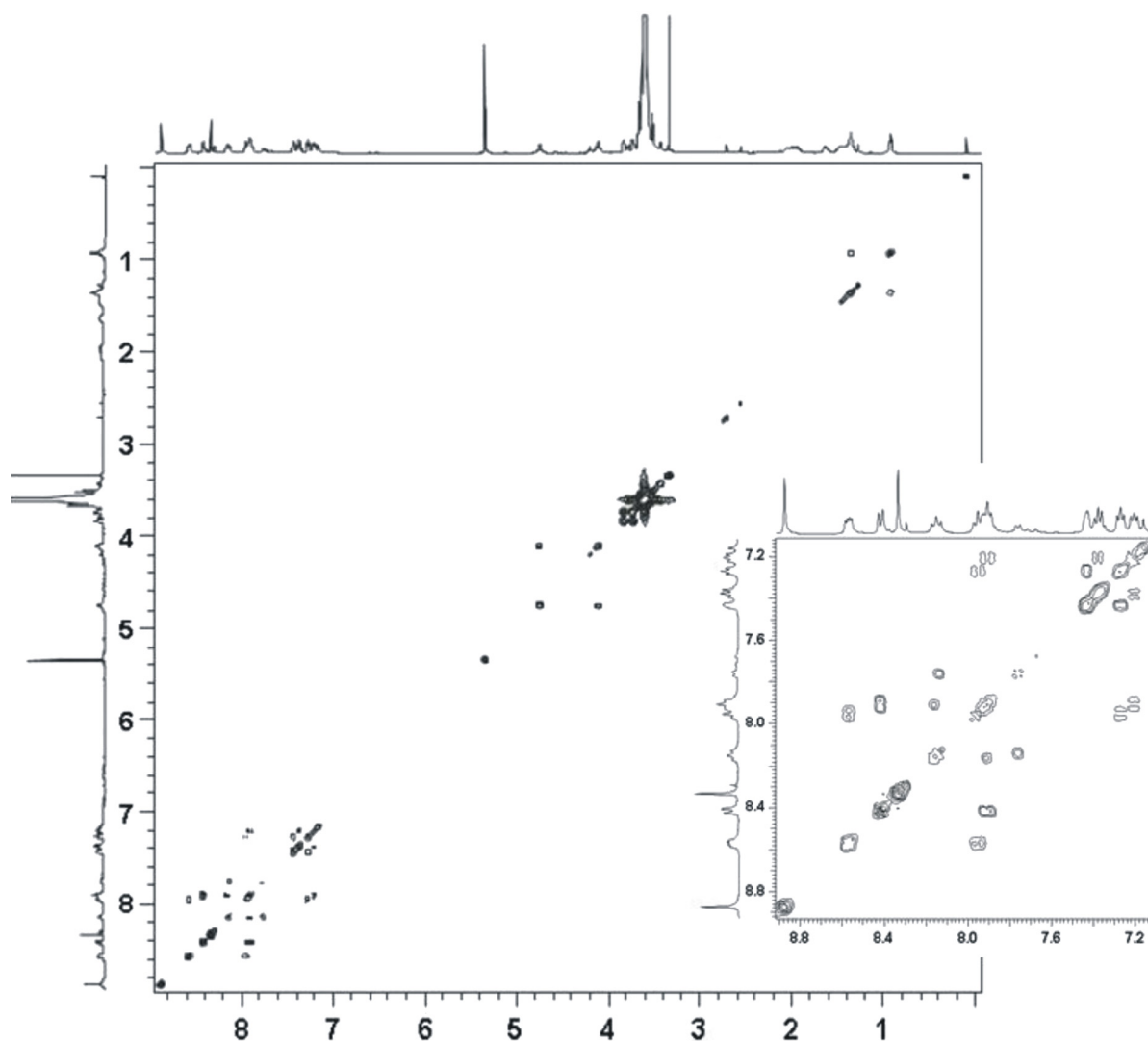
Figure 4.9: *Representative ^1H-^1H COSY NMR of the **ABA** triblock assembly **61a** in CD$_3$CN.*

4.3.3 Photophysical and electrochemical investigations of the Ru(II) ABA triblock assemblies

The photophysical properties of the rigid conjugated ditopic spacers **60a-d** and their corresponding supramolecular triblock copolymers **61a-d** were investigated by the absorption maxima, λ_a, the optical band gap energy, E_g^{opt} (estimated from low energy edge of the absorption spectra), the emission maxima, λ_{em} and the fluorescence quantum yields, Φ_{fl}. In order to allow a direct comparison between the complexed and uncomplexed studied structures (including the ditopic ligands **60a-d**, prepared and characterized elsewhere), all results are summarized in Table 4.4.

Table 4.4: *Comparison of the photophysical and electrochemical properties of the bis-terpyridine ligands **60a-d** and the Ru(II) **ABA** triblock assemblies **61a-d**.*

Compound	$\lambda_{abs, max}$ [nm][a]	E_g^{opt} [eV][b]	$\lambda_{em, max}$ [nm][a]	Φ_{fl} [%][c]	E^o [V][d]
60a	281, 326, 394	2.72	459	81	-
60b	339, 371, 419	2.78	490	68	-
60c	280, 424	2.56	487	54	-
60d	284, 348, 406	2.72	458	60	-
61a	272, 306, 498	2.27	540	-	1.194
61b	273, 306, 356, 498	2.26	538	-	1.203
61c	271, 303, 492	2.26	518	-	1.201
61d	272, 305, 401, 491	2.29	471	-	1.183

[a]*The absorption and emission spectra of **60a-d** have been recorded at room temperature in CHCl$_3$.[22] The absorption and emission spectra of **61a-d** have been recorded at room temperature in CH$_3$CN. For all spectra a concentration of 10^{-5} M was used. Photoluminescence spectra were obtained at an excitation wavelength of $\lambda_{ex} = 400$ nm.* [b]*Optical band gaps were estimated from the absorption spectra in solution by extrapolating the tails of the lower energy peaks.* [c]*Quantum yields were measured using quinine sulfate ($\Phi_{fl} = 55\%$) as a reference.[58]* [d]*All CV spectra were recorded in CH$_2$Cl$_2$ (freshly distilled from CaH$_2$) containing 0.1 M n-Bu$_4$NPF$_6$ vs. Ag/Ag$^+$ reference electrode. The shown data refers to the oxidation potential Ru(II)/Ru(III).*

The absorption spectra of the *bis*-terpyridine ligands **60c-d** and the binuclear Ru(II) **ABA** complexes **61c-d** are depicted in Figure 4.10.
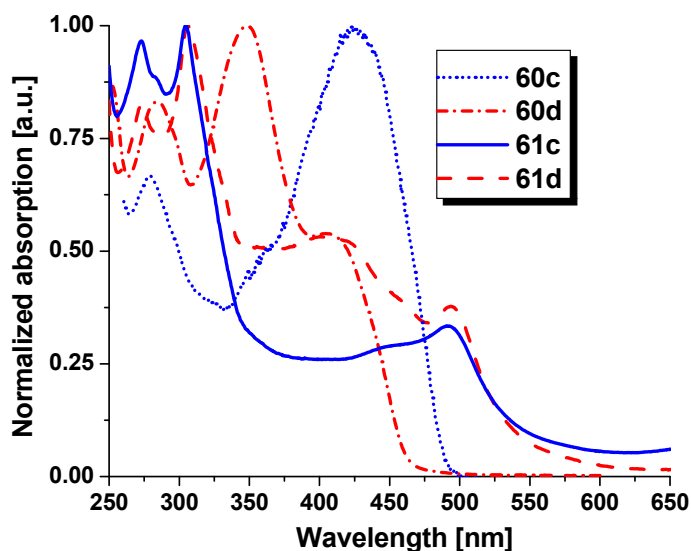
Figure 4.10: *Representative comparison of the normalized absorption spectra of bis-terpyridine ligands **60c-d** and their corresponding **ABA** triblock assemblies **61c-d**. The spectra were recorded at a concentration of 10^{-5} M in CHCl$_3$ (**60c-d**) and CH$_3$CN (**61c-d**), respectively.*

All absorption spectra of the uncomplexed ligands **60a-d** in chloroform showed a sharp band around 280 nm corresponding to the terpyridine moieties. The very intense broad band in the visible region (350-450 nm) can be attributed to the π-π* electronic transitions of the conjugated backbone between the terminal terpyridine units. The strongest bathochromic shift was observed for the thiophene-containing derivative **60c**.[22] In the UV-Vis spectra of the Ru(II) **ABA** complexes **61a-d** (recorded in acetonitrile) a set of absorption bands below λ = 300 nm is present and assigned to the π→π* transitions of the complexed terpyridines. In comparison to **60a-d**, the intensity of the spacer-based π→π* transitions (around 400 nm) decreased significantly. The metal-to-ligand charge transfer (MLCT) band at around 495 nm is characteristic for octahedral Ru(II) *bis*-terpyridine complexes.[3] The MLCT absorption of compounds **61c-d** is shifted to slightly lower wavelength. Upon complexation with Ru(II), the highest occupied molecular orbital (HOMO) of the *bis*-terpyridine ligands **60a-d** is lowered in these cases because of the relatively electron-poor nature of the spacer units. The difference Δ_0 to the energy level of the lowest unoccupied molecular orbital (LUMO) is increased resulting in a shift of the MLCT band towards lower wavelengths.[50] Due to the electronic nature (increased electron density of the spacer) this effect is least pronounced for the thiophene containing materials **60c** and **61c**.

While luminescence studies at low temperature and in the solid state will be the focus of future work, we investigated within this thesis the emission properties of the Ru(II) **ABA** triblock copolymers **61a-d** at room temperature. The photoluminescence spectra of **60c** and **61c** are depicted in Figure 4.11.
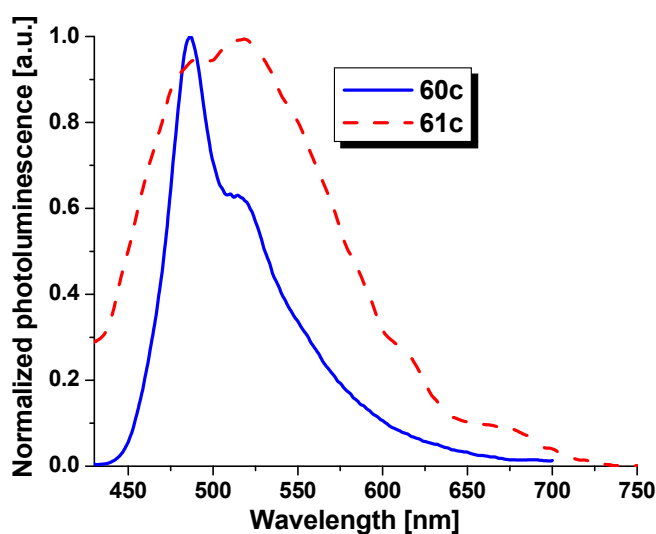
Figure 4.11: *Comparison of the normalized emission spectra of the bis-terpyridine ligand **60c** and the corresponding Ru(II) **ABA** triblock assembly **61c**. Spectra were recorded at a concentration of 10^{-5} M in CHCl$_3$ (**60c**) or CH$_3$CN (**61c**), respectively, with an excitation at $\lambda_{ex}= 400$ nm.*

The emission spectra were recorded after excitation at $\lambda_{ex} = 400$ nm. We previously reported that the emission of the rigid-rod ditopic terpyridyl ligands **60a-d** covered the blue range (425-500 nm) with high quantum yields up to 85%.[22] A broadening of the emission of the supramolecular materials **61a-d**, with their maxima shifted to 470-550 nm in comparison to **60a-d**, was observed. However, the quantum yield Φ_{fl} of the complexes **61a-d** is dramatically decreased by a factor of 8 to 10. This led us to the conclusion that the major part of the excitons formed upon excitation of the ligand was transferred to the complex.[50] Since the conjugated systems were emitting in the range where the complex absorbs, this energy transfer may be assigned to be of the Förster-type.[51] In full agreement with the literature,[52] only very weak emission of the complexes at room temperature (around 650 nm) was observed. Thus, the transfer of energy from the π-conjugated spacer to the complex causes a strong quenching of luminescence.

The redox behavior of the synthesized Ru(II) **ABA** triblock copolymers **61a-d** and the model complex **59** has been studied in dichloromethane by cyclic voltammetry (CV) (Figure 4.12 and Table 4.4).
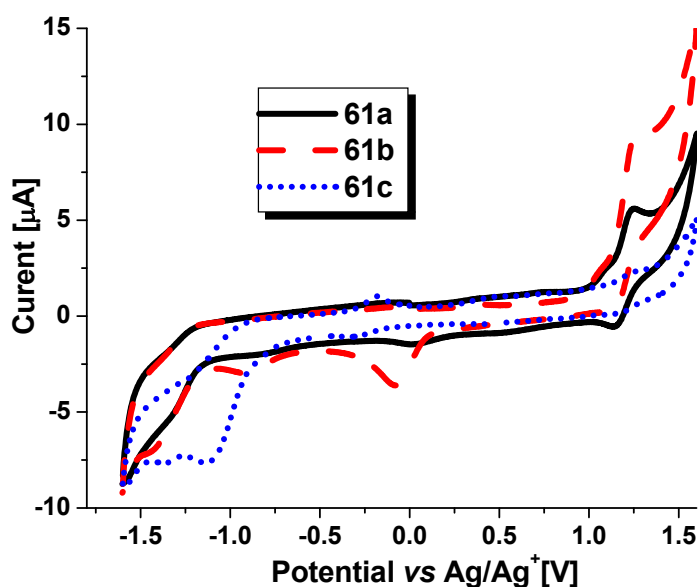
Figure 4.12: *Representative electrochemical properties of Ru(II) **ABA** triblock assemblies 61a (solid line), 61b (dashed line) and 61c (short doted line, respectively. All spectra were recorded in CH₂Cl₂ (freshly distilled from CaH₂), containing 0.1 M n-Bu₄NPF₆.*

The oxidation potentials are in agreement with the literature data for Ru(II) *bis*-terpyridine complexes[53] showing that the electrochemical properties were mainly ruled by the metal complex and not by the ligand itself. For the **ABA** triblock assemblies **61a-d** the Ru(II/III) wave was enlarged in comparison to the model complex **59** due to the fact that the two Ru(II)

centers were oxidized approximately at the same potential. The presence of a single broadened wave supported the idea that these metal centers were not in electronic interaction but were influenced by the chain length of the spacer.

4.3.4 Micellization of the Ru(II) ABA triblock assemblies

The synthesized amphiphilic Ru(II) **ABA** triblock assemblies **61a-d** were not directly soluble in water due to the rather low hydrophilic content. Therefore, the **ABA** triblock assemblies were first dissolved in *N,N*-dimethylformamide (DMF), which is a good solvent for all blocks, followed by the slow addition of water to trigger micellization. Upon addition of water to the DMF solution of the triblock assemblies **61a-d**, aggregation of the block was expected to induce the formation of self-assembled structures with the hydrophobic segment **B** in the core of the micelles and the hydrophilic block **A** as stabilizing corona. Subsequently, the organic solvent was removed by dialysis[43,54] leading to the formation of kinetically frozen aggregates, which mirror the self-assembly state in the initial DMF/water mixture.[55] The final micelles in pure water are thus locked structures with a rigid core in which no unimer-micelle equilibrium is present. Such systems have been previously referred to as "kinetically frozen micelles".[55] From previous studies performed on "metallo-supramolecular micelles" based on the Ru(II) terpyridine connectivity and from the hydrophobic character of the Ru(II) *bis*-terpyridine complex with SbF_6^- counter ions, we assumed that the Ru(II) *bis*-2,2':6',2''-terpyridine-complexes will be located at the core-corona interface.[44] Taking into account that Ru(II) ions are characterized by a high binding strength towards terpyridine ligands and that the Ru(II) *bis*-terpyridine complexes are known to be inert complexes, we can expect that the amphiphilic **ABA** triblock assemblies will stay intact during the micellization studies. Cryogenic transmission electron microscopy (cryo-TEM) and dynamic light scattering (DLS) were utilized to characterize the formed micelles by the self-assembly of the **ABA** triblock assemblies **61a-d**. The DLS results (Figures 4.13-4.16, right) revealed the presence of two different populations of objects. This observation is in agreement with previous studies performed on metallo-supramolecular micelles with a PEG corona, which have shown that such micelles have a rather strong tendency to form multimicellar large aggregates.[54,56] Moreover, a previous investigation on metallo-supramolecular micelles combining DLS and cryo-TEM revealed that the first population observed in the CONTIN histogram could not be attributed to only individual micelles but rather corresponded to individual micelles plus small clusters of micelles (*e.g.* dimers, trimers, tetramers, etc. of individual micelles).[56] This situation results from a limitation of the CONTIN analysis that is not able to resolve

individual micelles from small clusters. On the other hand, the second population could be attributed to large aggregates of micelles.[56] The same situation prevails in the present study and it is therefore not possible to correlate the DLS results (Figures 4.13-4.16, right) to data obtained by imaging techniques (*e.g.* cryo-TEM). Cryo-TEM revealed that spherical micelles are obtained for all triblock assemblies **61a-d** (Figures 4.13-4.16, left). For the reason discussed above, the size of the micellar core (R), measured from the images, does not correlate well with the R_h obtained by DLS for the first population (Table 4.5). Moreover, large aggregates can not be observed by cryo-TEM since only a very thin slice of the prepared probe is measured. Although their **B** middle blocks are very short, the **ABA** triblock assemblies investigated in this study can be seen as coil-rod-coil triblock assemblies.
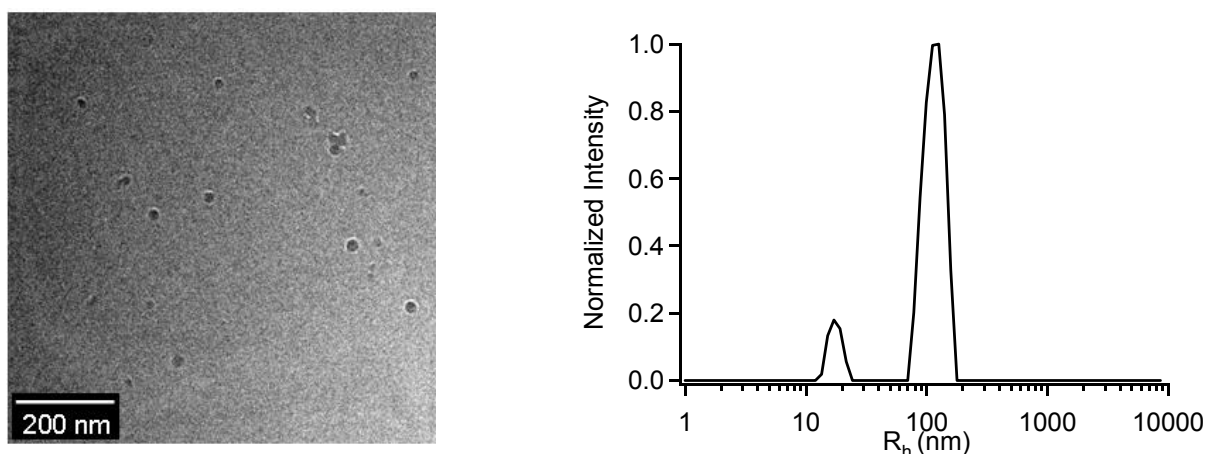
Figure 4.13: *Cryo-TEM (left) and DLS (right) for the micelles obtained from **ABA** triblock assemblies **61a**.*
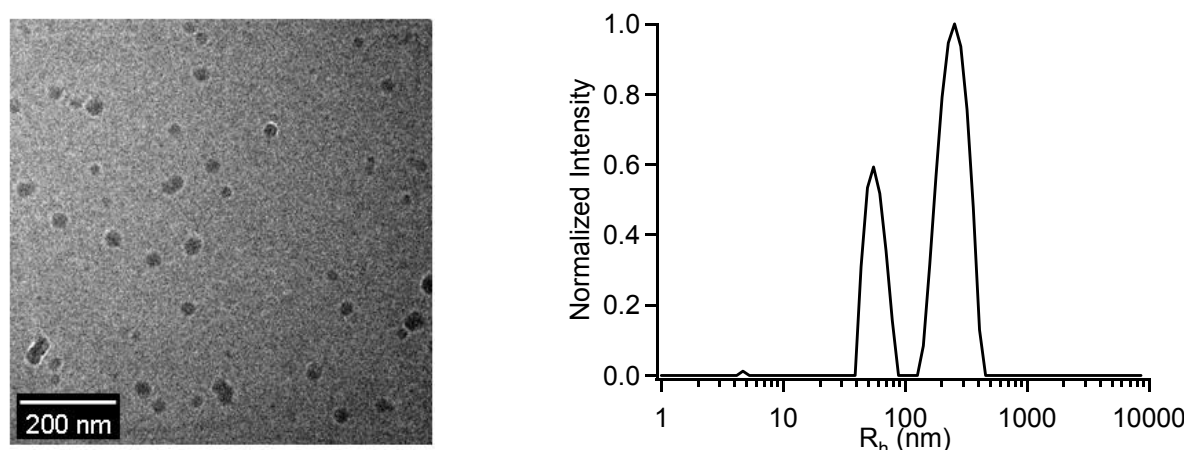
Figure 4.14: *Cryo-TEM (left) and DLS (right) for the micelles obtained from the **ABA** triblock assemblies **61b**.*
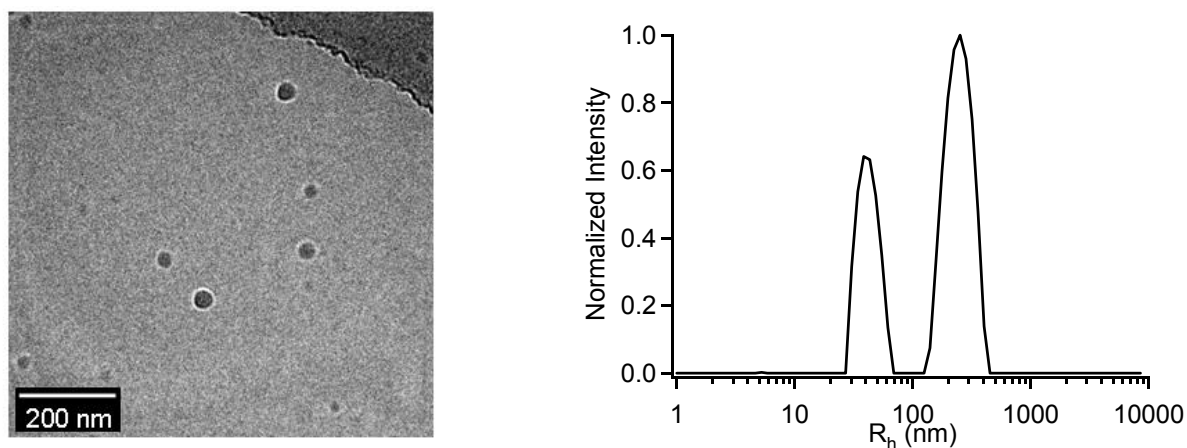
Figure 4.15: *Cryo-TEM (left) and DLS (right) for the micelles obtained from **ABA** triblock assemblies **61c**.*
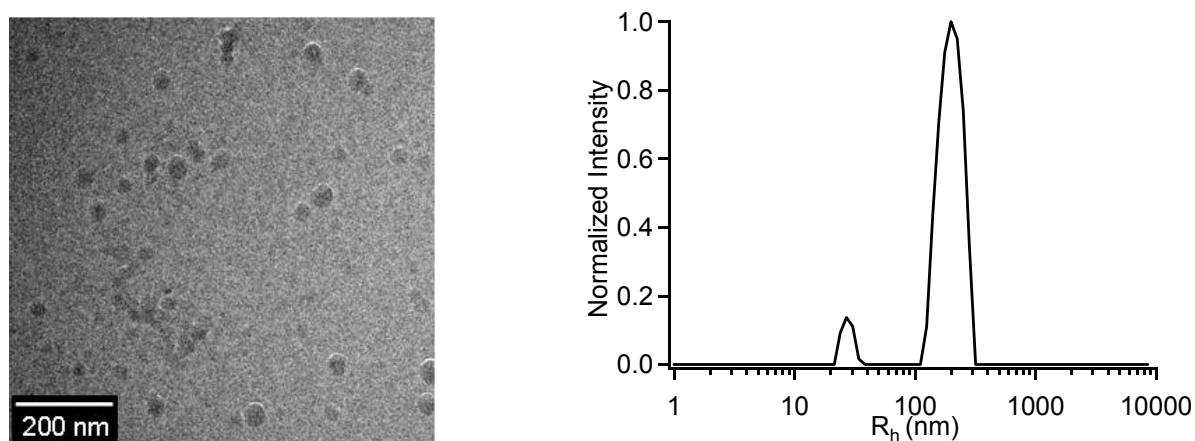
Figure 4.16: *Cryo-TEM (left) and DLS (right) for the micelles obtained from **ABA** triblock assemblies **61d**.*

Compared to block copolymers only composed of coiled blocks, the self-assembly of coil-rod-coil block copolymers is no longer solely determined by phase-separation between the blocks, but can also be affected by other processes, *e.g.* the aggregation of the rod-like segments into (liquid-) crystalline domains.[57] Such phenomena are able to lead to micelles with peculiar morphologies, including vesicles, tubules, etc.[57] The method used for micelle preparation obviously impedes any aggregation of the rigid **B** segments in crystalline domains since only spherical micelles have been formed in agreement with the composition of the investigated **ABA** triblock assemblies that contain a minor volume fraction of insoluble **B** segments.

Table 4.5: *AFM, cryo-TEM and DLS average sizes of the prepared micelles containing Ru(II)*
*ABA triblock assemblies **61a-d**.*

ABA triblock assemblies	AFM D [nm]	Cryo-TEM D [nm]	DLS R_h [nm]	
			micelles	aggregates
61a	5.2	9.5	19	120
61b	5.8	14	47	250
61c	6 and 60	16	42	257
61d	5.4	13	25	188

The synthesized amphiphilic Ru(II) **ABA** triblock assemblies **61a-d** were also studied by AFM. In all cases AFM showed the existence of individual spherical micelles and also the presence of aggregates (Figure 4.17).
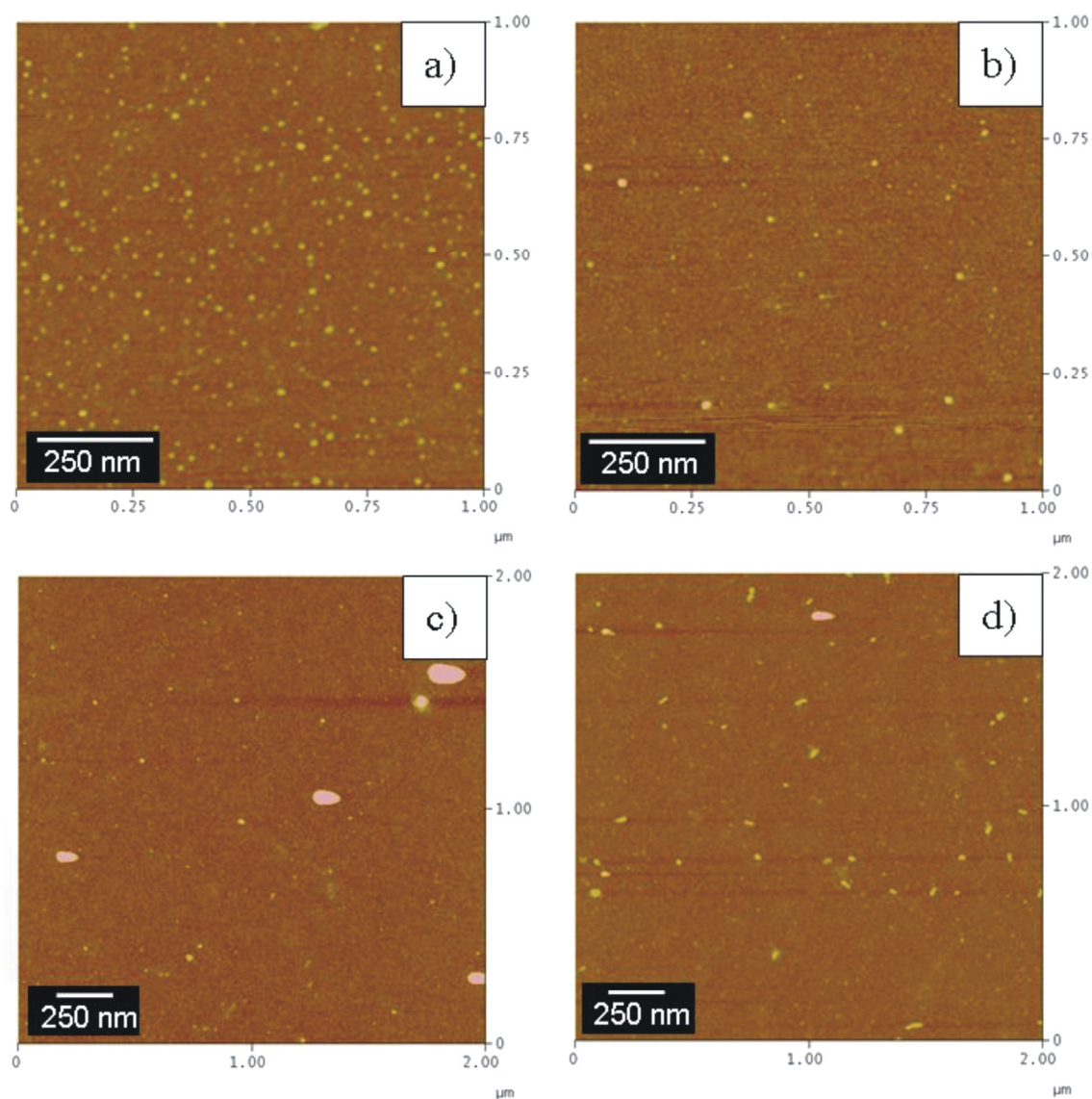
Figure 4.17: *AFM pictures (height images) for the micelles obtained from **ABA** triblock assemblies **61a-d**.*

The size of the micellar core (D), measured as the height of the objects observed in the AFM images, did not correlate well with the R_h obtained by cryo-TEM and DLS (Table 4.5). The explanation might be related to the sample preparation method (drying step) for the AFM analysis that resulted in dehydration and collapse of the PEG corona.

In order to establish the influence of the solvent on the self assembly of the synthesized Ru(II) **ABA** triblock assemblies, preliminary micellization studies were performed in THF/water mixture without dialysis for **61a** and **61b**. The use of the THF/water solvent mixture might prevent the formation of kinetically frozen micelles and, thus, might allow the formation of a crystalline core. The **ABA** triblock assembly **61a** seems to form worm like micelles, structures proven by TEM (where the length of the rods was about 80 nm) and AFM (Figure 4.18). The formation of such non-spherical structures was also proven by DLS where a defined population with R_h of 105 nm was observed (Figure 4.18).
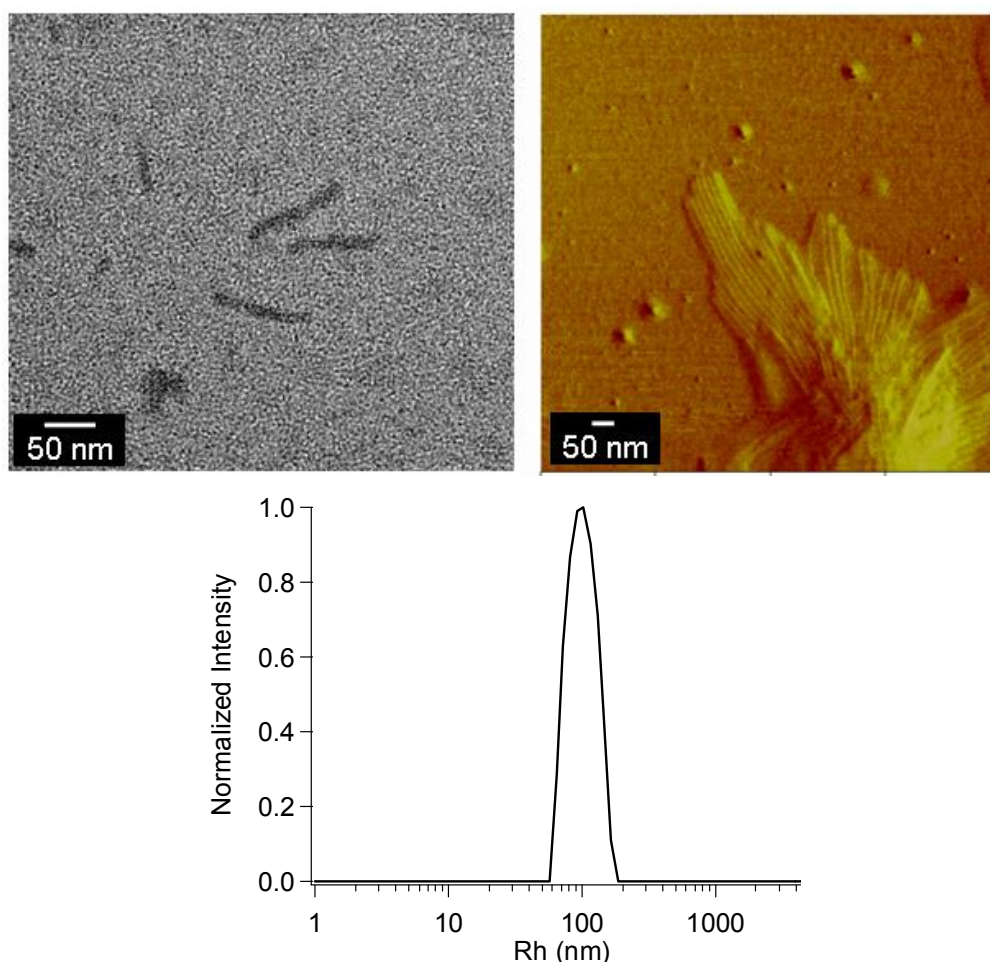
Figure 4.18: *TEM (top left) and AFM (top right) and DLS (bottom) for the micelles obtained from ABA triblock assemblies 61a.*

The second investigated structure, namely **61b**, revealed the formation of well defined structures which might be vesicles or toroids with an outer radius of about 30 nm and an inner

radius of about 14 nm (Figure 4.19 left). DLS results showed a single and extremely well defined population with a R_h of 145 nm (Figure 4.19 right).
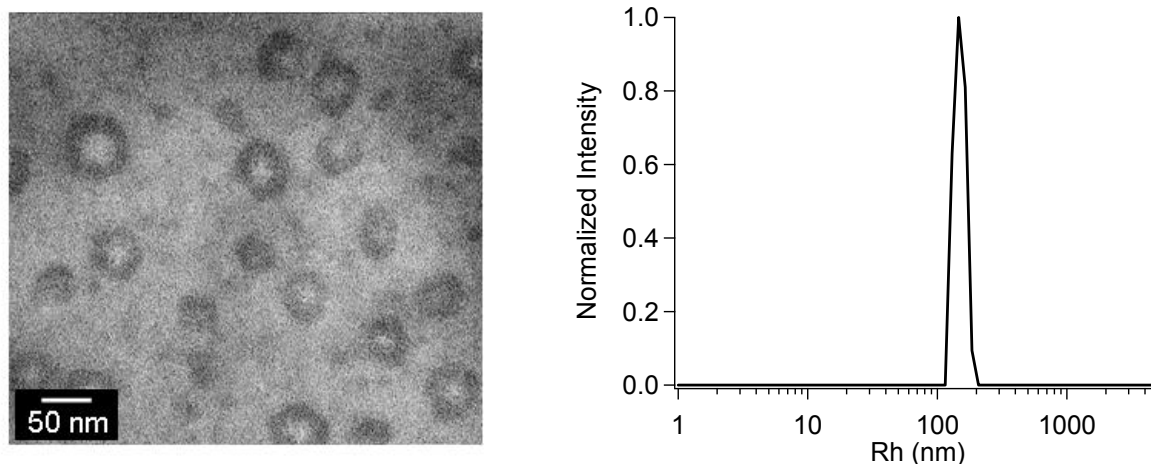
Figure 4.19: *TEM (left) and DLS (right) pictures for the micelles obtained from **ABA** triblock assemblies **61b**.*

4.4 Star-shaped rod-coil AB ruthenium(II) terpyridine supramolecular assemblies

Following the work described in section 4.3, synthetic efforts were focused on the preparation of star-shaped Ru(II) **AB** diblock amphiphilic assemblies. For this study block **A** is *mono*-terpyridine PEG **8** with M_n = 2,200 g/mol and **B** is a hydrophobic segment represented by organic molecules with well-defined size and structure based on *tris*-terpyridine **62** with a conjugated rigid rod core and *tetra*-terpyridine **64** with a conjugated rigid-rod core, respectively. Previous studies performed on the self-assembly of defined organic molecules and polymers, showed that a wide variety of objects with nanoscale or micrometer-scale morphologies such as, *e.g.*, micelles, vesicles, ribbons, films, fibers, tubules could be generated by a simple variation of the solvent (see also section 4.3.4).[58,59] Therefore, the designed Ru(II) **AB** diblock amphiphilic assemblies **63** and **65** represent appealing structures for self-assembly studies performed in various solvents.

4.4.1 "Tri-star" rod-coil AB ruthenium (II) terpyridine assemblies: synthesis and characterization

The synthesis of the "tri-star" Ru(II) **AB** diblock assemblies was performed by activating in the first step the Ru(II)Cl$_2$DMSO *mono*-terpyridine macroligand **50** (see 4.3.1) with AgSbF$_6$ in acetone under reflux followed by the subsequent addition of the *tris*-terpyridine ligand **62** with a conjugated rigid rod core (Scheme 4.6). The molar ratio between **50** and **62** was 3:1,

since segment **B** has three available terpyridine units per molecule for the metallo-complexation process.
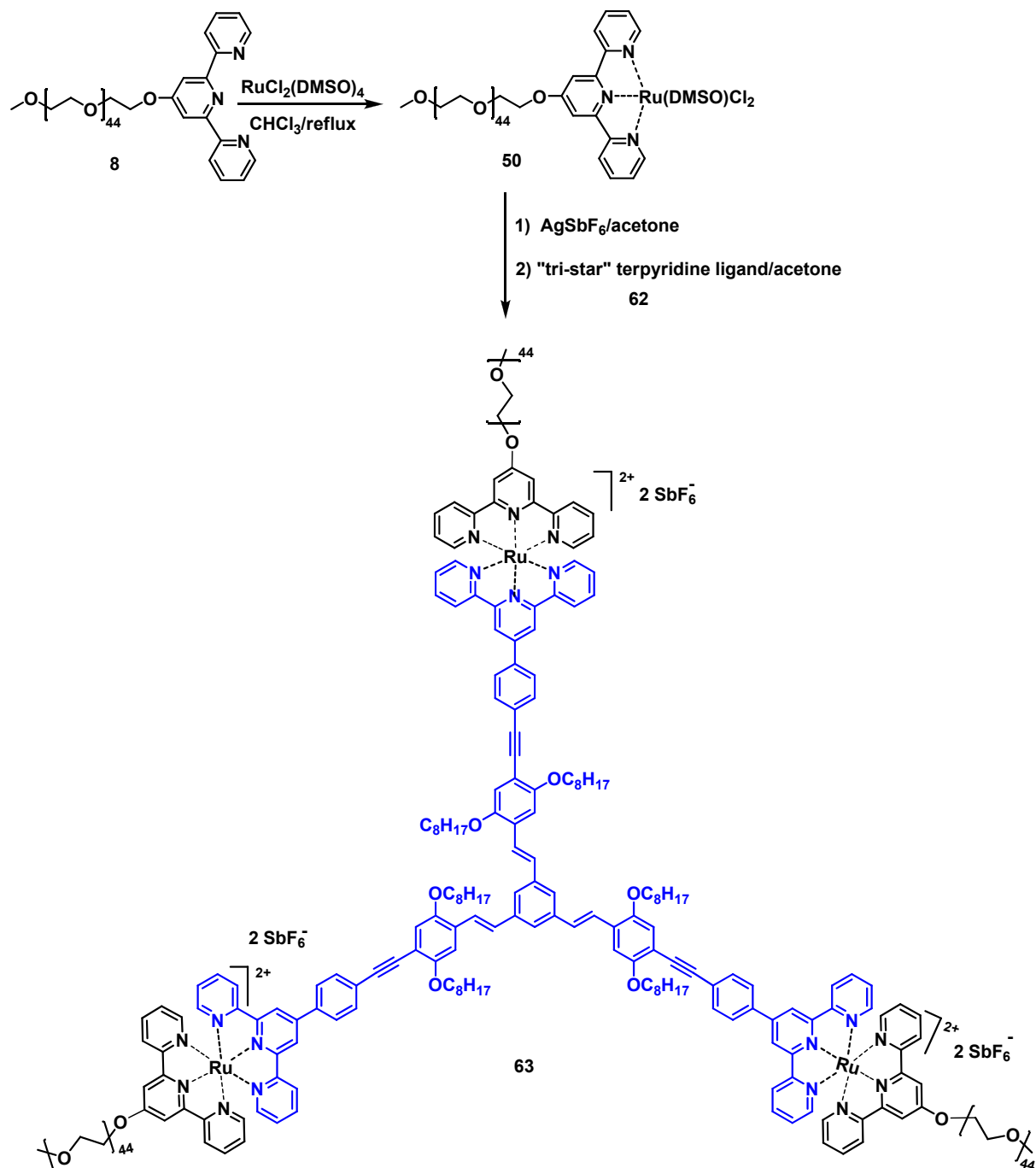
Scheme 4.6: *Schematic representation of the synthesis of the mono-complex macroligand **50** and the "tri-star" Ru(II) **AB** diblock assemblies **63**.*

Purification of the crude reaction product was performed by repetitive fractionation by preparative size exclusion chromatography (BioBeads S-X1 in acetone). The collected fractions were firstly checked by SEC with a RI detector aiming for a higher and monomodal

molar mass distribution of the resulting "tri-star" Ru(II) **AB** diblock assembly in comparison to the starting material **50** and the model complex **59**. Figure 4.20 displays three isolated fractions of the Ru(II) **AB** diblock "tri-star" **63F₁-F₃** in comparison to the Ru(II)Cl₂DMSO *mono*-terpyridine macroligand **50** and the Ru(II) model complex **59**.
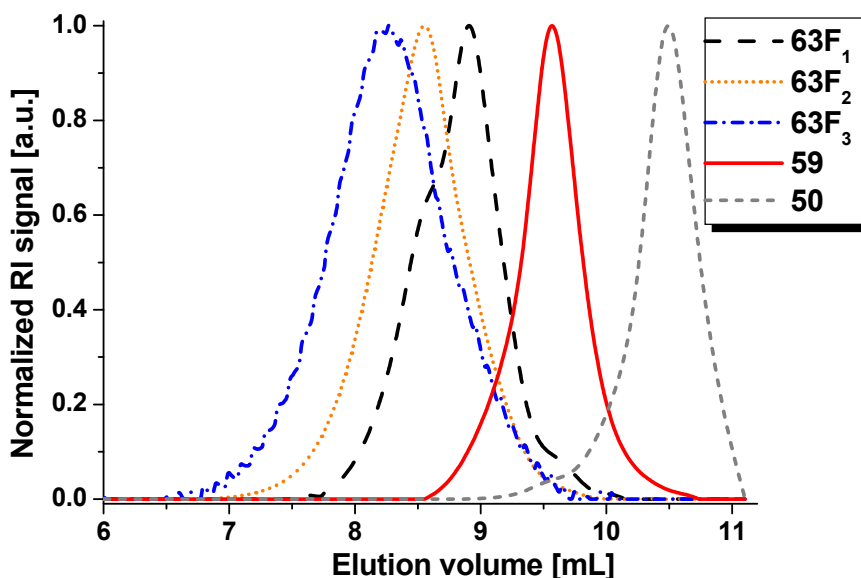
Figure 4.20: *SEC elution curves (RI detector) of the "tri-star" Ru(II) **AB** diblock **63F₁-F₃** in comparison to the Ru(II)Cl₂DMSO mono-complex macroligand **50** and the Ru(II) model complex **59**.*

Thus, fraction **63F₁** displayed the highest molar mass from the analyzed fractions. This feature could be attributed to the full complexation of all three arms of **62** (which has three terpyridine moieties) with the *mono*-terpyridine macroligand **50**. Following the same reasoning, fraction **63F₂** might be attributed to the two complexed arms of the Ru(II) **AB** assemblies and **63F₃** might be represented by the one complexed arm of the Ru(II) **AB** diblock species. However, it should be noted that the used PEG had a defined molar mass distribution and, thus, the observed differences in molar mass might be related to the molar mass of the attached PEG chains. Furthermore, SEC with an in-line diode array detector proved the existence and the stability of the Ru(II)tpy₂ connectivity from the analyzed fractions **63F₁-F₃** as revealed by the monomodal distribution of the M_n correlated with the UV-Vis absorption around 500 nm. The molar mass of the fractions could not be calculated from SEC since the analyzed structures contain multiple charges and their hydrodynamic volume (tri-star) is very different compared to the neutral linear polymers used for SEC

calibrations. Therefore, from SEC results no definitive conclusions regarding *mono-*, *di-* or *tri*-Ru(II) functionalization of the ligand **62** could be drawn.

^{1}H-NMR spectra of the studied fractions **63F$_1$-F$_3$** showed in all cases the same type of shifts for the aromatic protons (compared to ligand **62**), which proved the formation of the Ru(II) *bis*-terpyridine connectivity between the two terpyridine blocks **50** and **62**. Two dimensional ^{1}H-^{1}H COSY NMR was used for the assignment of the complexed terpyridine protons *via* the cross-peaks (see Experimental Part). No uncomplexed signals could be observed in the terpyridine region of **63F$_1$-F$_3$**, which indicate that full complexation occurred in all three fractions: **63F$_1$**, **63F$_2$** and **63F$_3$** respectively. Moreover, full complexation was further confirmed for **63F$_1$** by addition of Fe(II) acetate that did not result in the characteristic Fe(II) *bis*-terpyridine MLCT band at 590 nm. Furthermore, the CH$_2$ signals of the PEG backbone and the signals belonging to the alkyl groups of the core could be distinguished. In order to determine the "degree of complexation" for the isolated fractions **63F$_1$-F$_3$**, the integrals of the terpyridine protons and CH$_2$- (situated next to the PEG polymer backbone) were compared demonstrating that **63F$_1$** was fully complexed while **63F$_2$** and **63F$_3$** revealed a lower integral for the PEG signal indicating partially complexation of the three arm star **62**. These opposite results revealed that all present terpyridines are complexed but not all terpyridines still bear the PEG chain.

The isolated fractions of Ru(II) **AB** diblock assemblies **63F$_1$-F$_3$** were also investigated by UV-Vis absorption spectroscopy (Figure 4.21). In order to allow a clear comparison between the uncomplexed and Ru(II) complexed species, Figure 4.21 also display the absorption of segment **B**, the *tris*-terpyridine **62** with conjugated rigid rod core spacer (the synthesis and characterization is reported elsewhere[60]). All absorption spectra were measured in acetonitrile and showed characteristic bands for the terpyridine moiety at 280 nm. The uncomplexed ligand **62** exhibited a strong absorption at 400 nm which is assigned to the π-π* transition from the conjugated spacer decorated by the terpyridine units. In comparison to the uncomplexed ligand **62**, all three analyzed fractions of the Ru(II) **AB** diblock assemblies **63F$_1$-F$_3$** showed MLCT bands around 500 nm corresponding to the typical absorption of the octahedral Ru(II) *bis*-terpyridine complexes. Moreover, the formation of the Ru(II) *bis*-terpyridine connectivity in **63F$_1$-F$_3$** is proven by the considerably decreased intensity of the π-π* transition belonging to the conjugated spacer due to quenching by the Ru(II) *bis*-terpyridine complex as was also discussed in section 4.3.3. On the other hand, fraction **63F$_3$** of the Ru(II) **AB** diblock assemby revealed weaker absorption bands in comparison to **63F$_1$** and **63F$_2$**, which indicated that indeed fraction **63F$_3$** contained a lower quantity of the Ru(II)

bis-terpyridine species (due to incomplete complexation of the terpyridine moieties of ligand **62**).
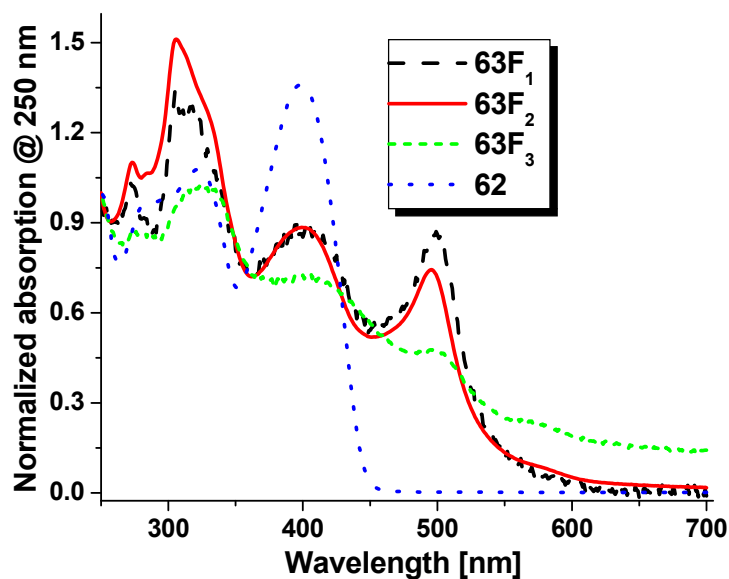
Figure 4.21: *Comparison of the normalized absorption spectra of tris-terpyridine ligand **62** and its corresponding "tri-star" Ru(II) **AB** diblock assemblies **63F₁-F₃**. All spectra were recorded at a concentration of 10^{-5} M in CH_2Cl_2 (**62**) and CH_3CN (**64**), respectively.*

4.4.2 "Tetra-star" rod-coil AB ruthenium (II) terpyridine assembly: synthesis and characterization

The synthesis of the "tetra-star" Ru(II) **AB** diblock assembly was performed in the same fashion as the "tri-star" Ru(II) **AB** diblock assembly (see 4.4.1). The synthesis started with the activation of the Ru(II)Cl₂DMSO *mono*-terpyridine macroligand **50** with AgSbF₆ in acetone under reflux, followed by the subsequent addition of the *tetra*-terpyridine bearing a conjugated rigid rod core spacer **64**. The molar ratio between **50** and **64** was 4:1, taking into account that segment **B** had four terpyridine moieties per molecule. The structure of the desired "tetra-star" Ru(II) **AB** diblock **65** is depicted in Figure 4.22.
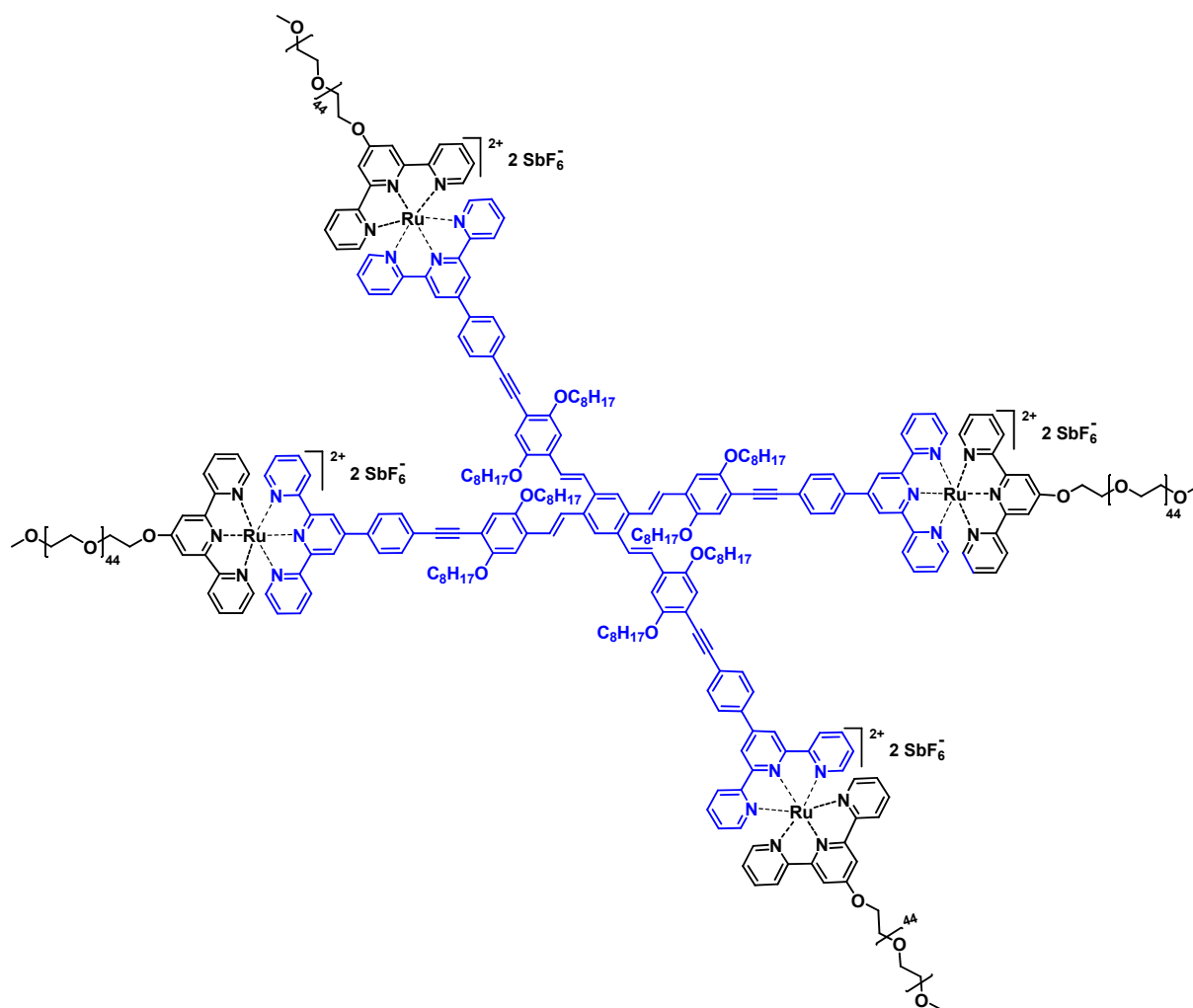
Figure 4.22: *Schematic representation of the structure of the synthesized "tetra-star" Ru(II) **AB** diblock assembly **65**.*

The reaction product required extensive purification by preparative size exclusion chromatography (BioBeads S-X1 in acetone). Figure 4.23 displays the SEC traces of the purified "tetra-star" Ru(II) **AB** diblock assembly **65**, the Ru(II)Cl$_2$DMSO *mono*-terpyridine macroligand **50** and the Ru(II) model complex **59**. As it can be observed, **65** is characterized by a monomodal distribution of higher molar mass in comparison to its precursor **50** and the model complex **59**. Nevertheless, **65** displays a small shoulder at lower elution time that might correspond to minor impurities such as, *e.g.*, the model complex **59** or defect structures. Repetitions of the SEC analysis revealed always the same distribution of the SEC curve. Moreover, the molar mass of **65** could not be calculated from SEC since the analyzed structure had incorporated many charges and had a very different hydrodynamic volume (tetra-star) than the neutral linear polymers used for SEC calibrations. Moreover, SEC with an in-line diode array detector proved that the synthesized structure **65** is stable during the SEC

measurement as demonstrated by a monomodal molar mass distribution together with the UV-Vis absorption around 500 nm.
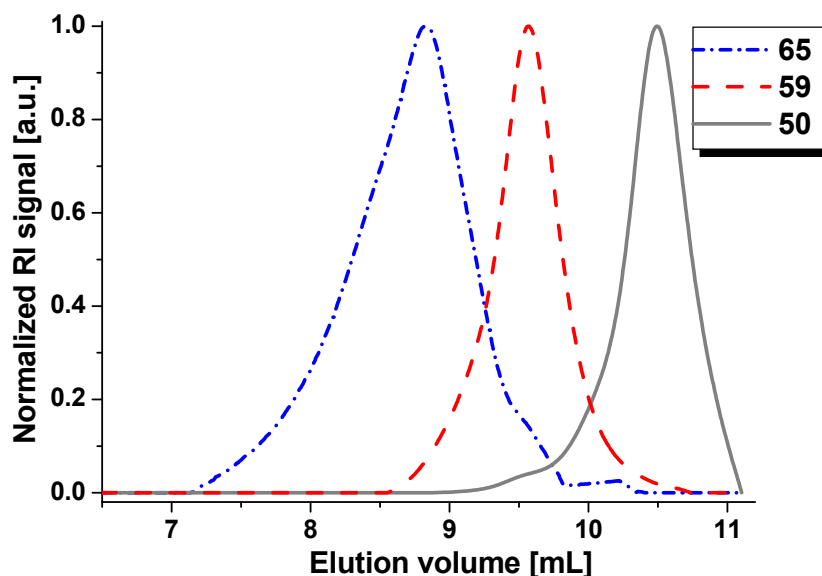
Figure 4.23: *SEC elution curves (RI detector) of the "tetra-star" Ru(II) **AB** diblock assembly **65** in comparison to the mono-complex macroligand **50** and the model complex **59**.*

The ^{1}H-NMR spectrum of **65** revealed clear shifts of the terpyridine protons (in comparison to **50** and **64**). The proton assignments were performed *via* the cross-peaks of the 2-dimensional ^{1}H-^{1}H-COSY NMR (see Experimental Part) which proved the formation of the Ru(II)tpy$_2$ connectivity between the starting materials **50** and **64**.

The isolated fraction of the Ru(II) **AB** diblock "tetra-star" assembly **65** was investigated by UV-Vis absorption spectroscopy (Figure 4.24) in comparison to the uncomplexed ligand **B** based on *tetra*-terpyridine **64** bearing a conjugated rigid rod core spacer (the synthesis and characterization were reported elsewhere[60]). Both absorption spectra displayed the characteristic bands for the terpyridine moiety: 290 nm in the case of the uncomplexed ligand **64** and 307 nm for the Ru(II) **AB** "tetra-star" **65** which proved the formation of the Ru(II) complexes. Following the same behavior as the "tri-star" ligand **62**, the uncomplexed ligand **64** exhibited a strong absorption at 410 nm which belongs to the π-π* transition from the conjugated spacer between the terpyridine units. The "tetra-star" Ru(II) **AB** diblock assembly **65** showed a characteristic MLCT band around 498 nm that corresponded to the typical absorption of the octahedral Ru(II) *bis*-terpyridine complexes. Moreover, compound **65** also displayed a considerable decreased intensity of the π-π* transition belonging to the conjugated

spacer between the terpyridine units due to the influence of the Ru(II) *bis*-terpyridine species in the synthesized molecule.
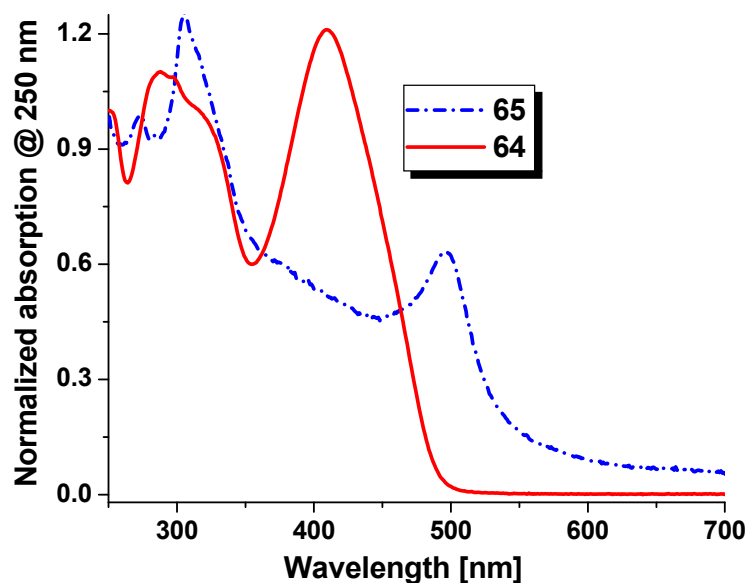
Figure 4.24: *Comparison of the normalized absorption spectra of tetra-terpyridine ligand **64** and its corresponding **AB** diblock assembly **65**. The spectra were recorded at a concentration of 10^{-5} M in CH$_2$Cl$_2$ (**64**) or CH$_3$CN (**65**), respectively.*

4.5 Ruthenium(II) supramolecular polymerization of *bis*-terpyridine poly(ethylene glycol): new insights on synthesis and optimization

In order to obtain linear and high molar mass Ru(II) coordination polymers, we investigated the reaction conditions for the direct one-step metallo-polymerization of *bis*-terpyridine poly(ethylene glycol) **13** with RuCl$_3$ in the presence of reducing agents. Previous work performed on Ru(II) poly(ethylene glycol) coordination polymers required an activation step for the Ru(III) precursor which, subsequently, was used as a key building block for synthesizing high molar mass species.[35] In the following, we report on the optimization and synthesis of soluble linear coordination polymers based on *bis*-terpyridine poly(ethylene glycol) *via* direct Ru(II) complexation in an one-step reaction, which is a straightforward and improved approach in comparison to what has been described previously.[69] The optimization of the metallo-polymerization was monitored by SEC. For the highest molar mass Ru(II) coordination polymer **66** obtained in this study, full characterization was performed by ^{1}H-NMR and UV-Vis spectroscopy as well as SEC proving the formation and the stability of the designed structure.

4.5.1 Intro: metallo-chain extended polymers

Metallo-supramolecular polymers are a known example of supramolecular chemistry where the new designed structures can successfully combine in one material the properties of polymers with the characteristic features offered by metal-ligand coordination.[40,61,62] The main interest for metallo-terpyridine "supra-structures" is the large possibility of potential combinations between the various polymers bearing terpyridine moieties and transition metal ions characterized by different binding strengths and exchange rates.[38,39,63,64,67] In this way, new materials with tunable properties can be synthesized as was *e.g.* demonstrated by Newkome and co-workers who prepared large, well-defined "hexagonal gasket" metallocycles.[65]

In metallo-polycondensation type polymerization reactions, each chelating monomer is linked by transition metal ions *via* coordinative bonds in the main chain. This concept requires telechelic monomers capable to condensate continuously by metallo-complexation. Using appropriate conditions, the metallo-coordinative polymerization can yield supramolecular structures with molar mass distributions comparable to covalently bonded polymers prepared by polycondensation. By varying the transition metal ion, it is possible to synthesize labile or inert metallo-supramolecular polymers; the characterization should be adjusted accordingly to their stabilities.[66,67] Another important issue in metallo-coordination polymerization is the solubility of the resulting supra-polymers, since it is known that their potential insolubility might obstruct their analysis as well as potential applications.[5] Thus, by using water soluble chelating monomers in combination with water soluble metal complexes the solubility issue could be tactfully solved or avoided.

From the large range of transition metal ions, ruthenium chemistry offers attractive features regarding the synthesis of homo and heteroleptic terpyridine systems. Moreover, ruthenium terpyridine complexes exhibit interesting optical and photophysical properties and their stability is much higher in comparison to other metal ions such as, *e.g.*, Fe(II) or Co(II).[67] In fact, they are rather inert and can only be opened using harsh oxidizing conditions.[37] Coordination polymers with a rigid or flexible terpyridine linker have been already reported for Ru(II)[9,41,42,68,69] and other transition metal ions. Depending on the structure of the utilized chelating monomers by metallo-polymerization, various architectures are accessible.

4.5.2 Synthesis, optimization and characterization

In order to perform metallo-polycondensation reactions, the telechelic monomer bearing chelating units has been first synthesized. The selected *bis*-terpyridine PEG **13** monomer with

M_n = 8,400 g/mol was prepared and characterized as described in Chapter 2. Generally, as it was mentioned in the beginning of this chapter, the preparation of Ru(II) *bis*-terpyridine complexes requires two steps: the first reaction step deals with the preparation and isolation of a Ru(III)Cl$_3$ *mono*-complex which, in the second step, is subsequently reduced to Ru(II) and further reacted with another terpyridine ligand in order to create Ru(II) *bis*-terpyridine complexes. The novelty of the present complexation approach consists in the one pot reaction performed without any preliminary activation of the Ru(III)Cl$_3$ precursor or isolation of the Ru(III)Cl$_3$ *mono*-complex which could be possibly formed as reaction intermediate.[69,70]
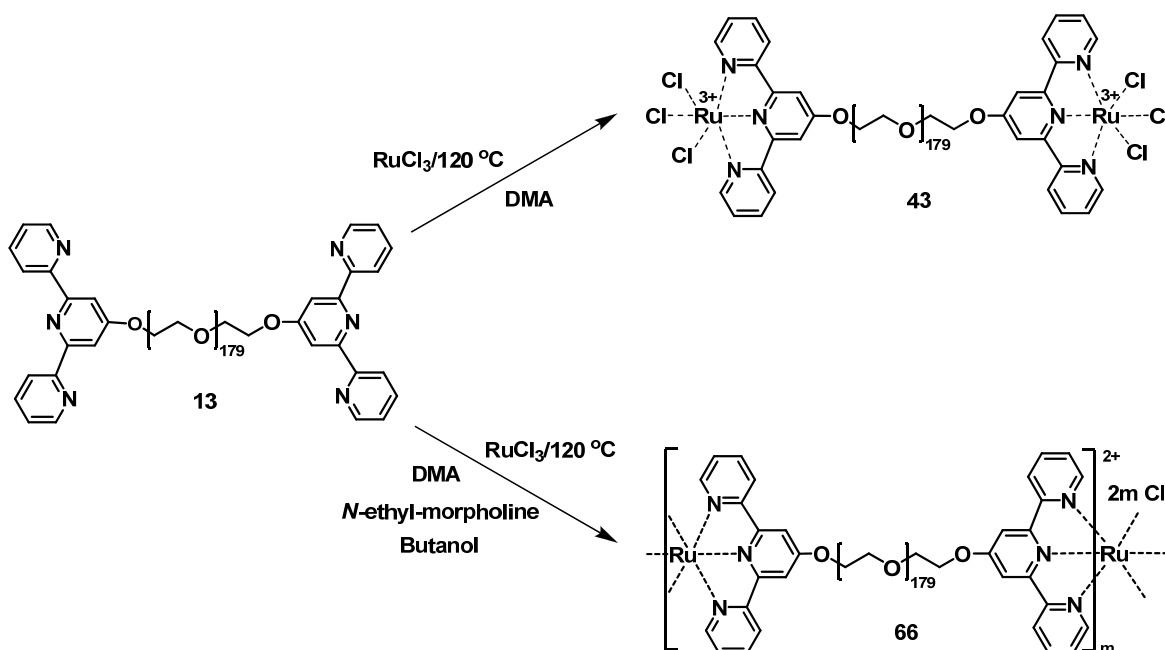
Scheme 4.7: *Schematic representation of the synthesis of compounds 43 and 66.*

To prepare Ru(II) *bis*-terpyridine coordination polymers, the polycondensation conditions of monomer **13** with RuCl$_3$ had to be initially optimized for the one step procedure. The most successful synthesis of **66** was performed in *n*-butanol with *N*-ethyl-morpholine at 117 °C, using equivalent amounts (molar ratio 1:1) of monomer **13** and RuCl$_3$ (Scheme 4.7). The replacement of *n*-butanol with other solvents (*e.g.* methanol, ethanol or dimethylformamide) was investigated but the results were less promising. Furthermore, a detailed optimization reaction was monitored by SEC during the first 36 hours for the *n*-butanol and *N*-ethyl-morpholine procedure (Figure 4.25). The SEC comparison for **66** samples taken at various reaction times, Ru(III)Cl$_3$ *mono*-complex **43** and monomer **13** (Figure 4.25) showed that the construction of **66** occured without the formation of pure Ru(III)Cl$_3$ *mono*-complex **43** as intermediate. Since **43** was prepared as a model compound for this study *via* a different approach (DMA at 120 °C; see Experimental Part) we presume that due to the presence of the

reducing agents (*n*-butanol and *N*-ethyl-morpholine) from the beginning of the complexation process, the Ru(III)Cl$_3$ *mono*-complex was directly reduced to Ru(II) to start the metallo-polycondensation reaction in the one-step approach.

An important factor in the polycondensation reaction is the concentration of the reaction mixture. Since *bis*-terpyridine PEG **13** has a very flexible chain, the formation of rings during the Ru(II) polycondensation process might be possible.[71] Therefore, to minimize the probability of ring formation, the optimization reactions were performed with low amount of solvents (see Experimental Part). The SEC investigation (Figure 4.25) revealed that the Ru(II) polycondensation of the studied system first occured with the formation of low molecular weight species and these couple in time yielding higher molar mass homopolymers, as expected for typical chain growth polymerization or metallo-polymerization reactions.[72-74] From the SEC curves (Figure 4.25) it can be observed that the highest molar mass is achieved after 24 hours. Longer reaction times led to slightly lower molar mass Ru(II) chain extended polymers (Figure 4.25, comparison of the reaction after 24 hours and 36 hours, respectively). This might be explained by the fact that the polycondensation reaction is an equilibrium process and, therefore, the proportion of rings varies with time being thermodynamically more favored.[73,75]
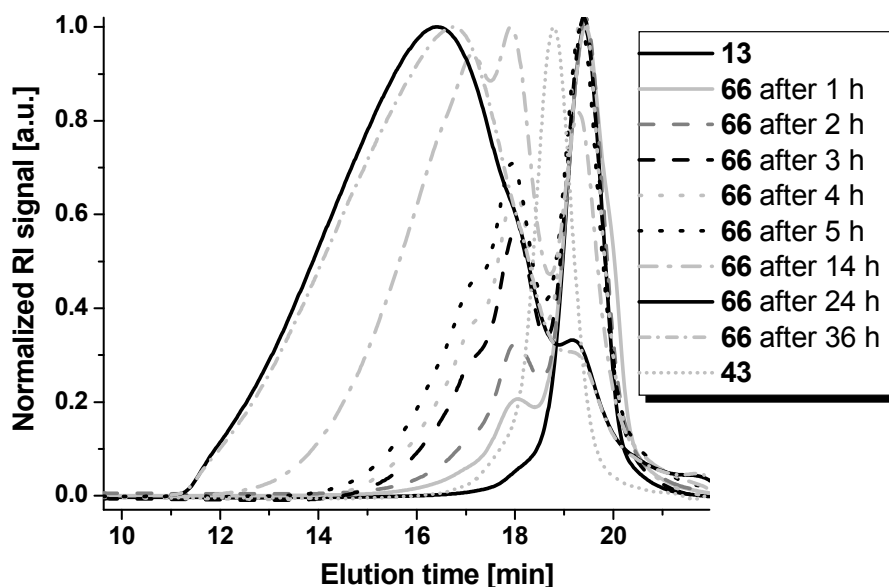
Figure 4.25: *Selected SEC elution curves (RI detector) showing the influence of the reaction time on the molar masses of the Ru(II) bis-terpyridine-poly(ethylene glycol) coordination polymer **66** in comparison to the monomer **13** and the Ru(III)Cl$_3$ mono-complex **43**.*

With this characteristic feature for chain growth polymerization, we could assume that during the metallo-polycondensation reaction the linear species might be first formed and then, in

time, due to an existent dynamic equilibrium between linear and cyclic species, the proportion of rings is favorably increased.[73] However, it should be noted that Ru(II) *bis*-terpyridine complexes are generally considered to be inert so the exchange reactions will be extremely slow. The conversion of the reaction (calculated by SEC) was 81% after 14 hours reaction time and was larger than 95% after 24 hours.

The purification of crude **66** (prepared by metallo-polymerization for 24 hours) was performed by BioBeads S-X1 in dichloromethane, to remove the potentially present small macrocycles and some remaining unreacted monomer **13**. The purified fraction of **66** exhibited a monomodal molar mass distribution which was shifted to shorter retention times in comparison to the starting material **13** (Figure 4.26). The broad distribution of the SEC curve for **66** is a normal observation for a metallo-polycondensation reaction, (PDI = 2.30).
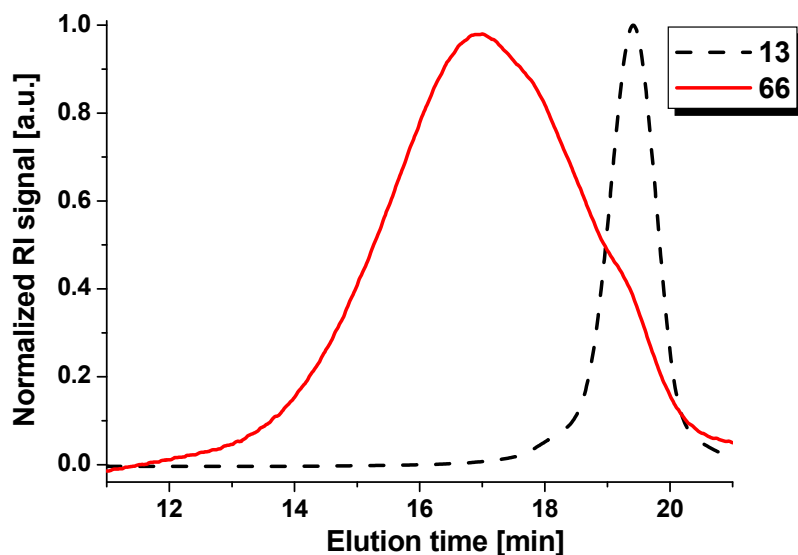
Figure 4.26: *SEC elution curves (RI detector) showing the purified Ru(II) bis-terpyridine-poly(ethylene glycol) 66 in comparison to the chelating monomer 13.*

Figure 4.27 displays the SEC chromatogram of the purified Ru(II) coordination polymer **66** obtained with a photodiode array detector revealing the characteristic Ru(II) *bis*-terpyridine metal-to-ligand charge transfer (MLCT) band of the complex at 490 nm over the whole polymer distribution demonstrating that indeed the expected Ru(II) *bis*-terpyridine metallo-supramolecular polymer was formed.
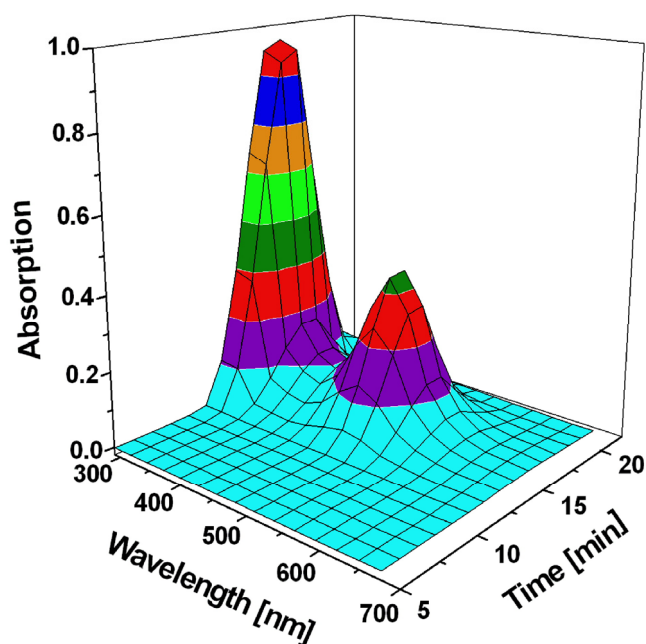
Figure 4.27: *SEC elution curve (PDA detector) for the purified Ru(II) bis-terpyridine-poly(ethylene glycol) coordination polymer 66.*

The ^{1}H-NMR spectrum of **66** confirmed full complexation of the telechelic monomer **13** (Figure 4.28). All signals in the aromatic region could be assigned to the complexed terpyridine protons and the chemical shifts were in agreement with the literature data.[69]
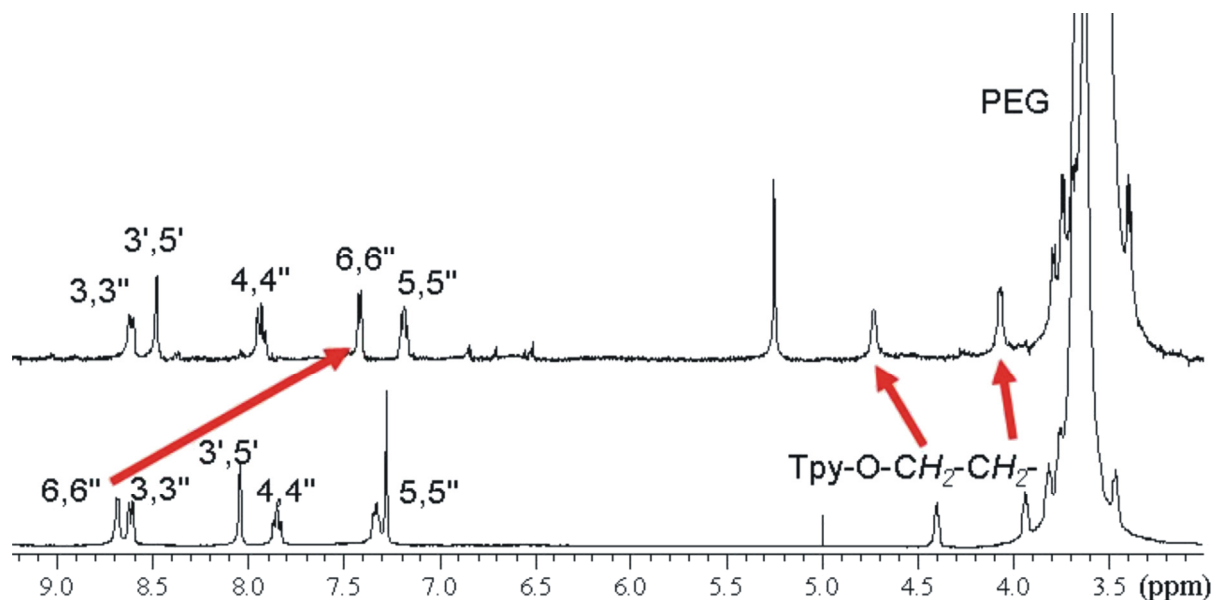
Figure 4.28: *^{1}H-NMR spectra of the macro-monomer 13 in CD₃Cl (bottom) and the purified Ru(II) bis-terpyridine-poly(ethylene glycol) coordination polymer 66 in CD₂Cl₂ (top).*

Signals of free terpyridine ligands were not detected in the ^{1}H-NMR spectrum which indicated that the purification step was efficient in removing the possible traces of unreacted

macro-monomer **13**. Additionally, the ¹H-NMR spectrum revealed signals between 6.5-7 ppm which might belong to the excess of the utilized counter ion PF$_6^-$, proving the poly-charged character of **66**. Furthermore, the absence of free terpyridine signals indicated the formation of high molar mass polymers (or cycles) since no end-groups could be detected. As a result, it was not possible to estimate the molar mass from ¹H-NMR spectroscopy.

UV-Vis spectra recorded in dichloromethane revealed the characteristic absorption bands for all analyzed compounds (Figure 4.29). Thus, *mono*-complex **43** displayed a strong absorption at 400 nm due to the presence of Ru(III)Cl$_3$ species in comparison to **66**, which presents a characteristic MLCT band at 490 nm proving the formation of the Ru(II) *bis*-terpyridine complex. The absence of the absorption band at 400 nm in the final product **66** indicated once more that all Ru(III) ions were reduced to Ru(II) during the direct one-step metallo-polycondensation. For the uncomplexed chelating monomer **13**, UV-Vis spectroscopy revealed the specific π-π* absorption bands for the terpyridine moiety at 278 nm.
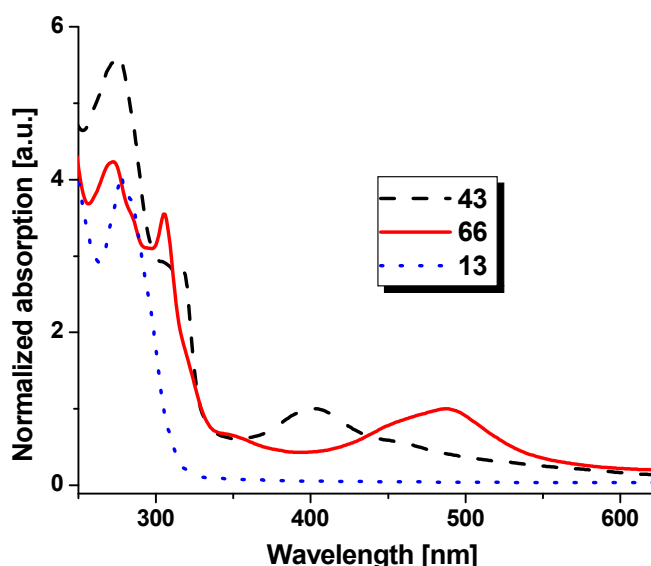
Figure 4.29: *UV-Vis spectra for **43** containing Ru(III)Cl$_3$ species (note the characteristic band at 400 nm), **66** containing Ru(II) species (note the characteristic band at 490 nm) and monomer **13**.*

4.6 Conclusions

This chapter described the synthesis and characterization of the various Ru(II) terpyridine supramolecular assemblies. The Ru(II) **ABA** triblock assemblies **61a-d** were prepared by Ru(II) complexation using as hydrophilic block *mono*-terpyridine end functionalized PEG **8** and as hydrophobic segment different rigid-rod conjugated ditopic terpyridyl ligands **60a-d**. The Ru(II) complexation of the utilized chelating ligands followed, for the first time, a

different route using a Ru(II)Cl$_2$DMSO precursor in comparison to what has been described previously. The photophysical and electrochemical properties of the synthesized materials **61a-d** were studied in solution and compared to the uncomplexed rigid-rod conjugated ditopic ligands **60a-d**. The results revealed that there is a strong influence of the metal-complex on the photophysical properties of the designed structures **61a-d**: typical UV-Vis absorption accompanied by strong quenching of the luminescence at room temperature. Furthermore, due to their amphiphilic properties, the synthesized Ru(II) supramolecular **ABA** triblock assemblies **61a-d** self-assembled in aqueous solution. Spherical micelles that are clustering into larger structures were obtained for all **ABA** triblock assemblies as observed by AFM, cryo-TEM and DLS. Future work should be focused on detailed morphology studies of the **ABA** triblock assemblies in different solvents as preliminary results showing the formation of non spherical aggregates were already discussed in this chapter. For the same structures, an interesting aspect to be investigated in detail, would be the influence of the counter ions on the phase separation. Following the same trend, "tri-star" and "tetra-star" **AB** diblock assemblies were prepared *via* Ru(II) complexation. The novel synthesized structures were characterized by means of ^{1}H-NMR and UV-Vis spectroscopy as well as SEC proving the formation of the Ru(II)tpy$_2$ connectivity. These structures have significant potential for self-assembly studies performed in different solvents.

Moreover, the optimization and synthesis of the Ru(II) *bis*-terpyridine PEG polymers is described in a direct one step procedure. In comparison to what has been published before, this new synthetic approach significantly simplifies the metallo-polymerization process by excluding the activation step. Optimization reactions were performed in order to identify the best reaction conditions such as, *e.g.*, temperature, amount and nature of reaction solvents, *etc.*, to construct high molar mass metallo-supramolecular polymers. Subsequently, the purified Ru(II) coordination polymer was characterized by ^{1}H-NMR and UV-Vis spectroscopy as well SEC proving the formation of the desired structure. Future work could be focused on morphology studies of the synthesized Ru(II) coordination polymers. In addition, this direct approach would be also applicable to other polymer building blocks.

4.7 Experimental Section

Materials and instrumentation

Solvents were purchased from Biosolve and all other compounds were obtained from Sigma-Aldrich or Fluka and used as received unless otherwise specified. AgSbF$_6$ was purchased from Aldrich. Ru(DMSO)Cl$_2$ was prepared according to a literature procedure.[24] Compounds **8** and **13** were synthesized as described in Chapter II. The preparation and full characterization of the rigid-rod terpyridine ligands **60a-d**, **62** and **64** is described elsewhere.[22,60] Preparative size exclusion

chromatography was performed on BioBeads S-X1 columns using dichloromethane or tetrahydrofuran as eluents. All reactions were performed under an inert atmosphere of argon using closed conical glass vials that can be capped with a septum or by employing the usual Schlenk techniques.

Instrumentation. Size exclusion chromatograms were measured on a Waters SEC system consisting of an isocratic pump, a solvent degasser, a column oven, a 2996 photodiode array (PDA) detector, a 2414 refractive index detector, a 717 plus autosampler, and a Styragel HT 4 GPC column with a precolumn installed. The eluent was *N,N*-dimethyl-formamide (DMF) with 5 mM NH_4PF_6 as additive at a flow speed of 0.5 mL/min. Narrowly distributed linear PEG and PMMA standards were used for calibration to calculate M_n and PDI. The column temperature was 50 °C. Nuclear magnetic resonance spectra were recorded on a Varian Gemini 400 MHz spectrometer at 298 K. Chemical shifts are reported in parts per million (δ) downfield from an internal standard, tetramethylsilane (TMS) in CD_2Cl_2 or DMSO-d_6. UV-Vis spectra were recorded on a Perkin Elmer Lamda-45 (1 cm cuvettes, $CHCl_3$ or CH_3CN). Emission spectra were recorded on a Perkin Elmer LS50B luminescence spectrometer (1 cm cuvettes, CH_3CN). Electrochemical experiments were performed using an Autolab PGSTAT30 model potentiostat. A standard three electrode configuration was used, with a platinum-disk working electrode, a platinum-rod auxiliary electrode, and Ag/AgCl reference electrode. Ferrocene was added at the end of each experiment as an internal standard. The oxidation potentials are quoted *versus* the ferrocene/ferrocenium couple (F_c/F_c^+). The solvent used was CH_2Cl_2 (freshly distilled from CaH_2), containing 0.1 M *n*-Bu_4NPF_6. The scan rate was 100 mV/s. Dynamic light scattering (DLS) experiments were performed on a Malvern CGS-3 equipped with a He-Ne laser (633 nm, 22 mW) and an ALV-5000/EPP correlator. The measurements have been performed at an angle of 90° and at a temperature of 25 °C. The results were analyzed by the CONTIN method which is based on an inverse-Laplace transformation of the data and which provides access to a size distribution histogram for the analyzed micellar solutions. Cryogenic transmission electron microscopy (cryo-TEM) measurements were performed on a FEI Tecnai 20, type Sphera TEM operating at 200 kV (LaB6 filament). Images were recorded with a bottom mounted 1k × 1k Gatan CCD camera. A Gatan cryo-holder operating at –170 °C was used for the cryo-TEM measurements. R2/2 Quantifoil Jena grids were purchased from SPI. Cryo-TEM specimens were prepared applying 3 μL aliquots to the grids within the environmental chamber (22 °C, relative humidity 100%) of an automated vitrification robot (FEI Vitrobot Mark III). Excess liquid was blotted away (–2 mm offset, 2.5 s) with filter paper within the environmental chamber of the Vitrobot. The grids were subsequently shot through a shutter into melting ethane placed just outside the environmental chamber. Vitrified specimens were stored under liquid nitrogen before imaging. Prior to blotting, the grids were made hydrophilic by surface plasma treatment using a Cressington 208 carbon coater operating at 5 mA for 40 seconds. AFM measurements were performed on a Solver LS produced by NT-MDT Russia. The cantilever used was an NSG01s, produced by NT-MDT Russia.

General procedure for the synthesis of the RuCl₃ mono-terpyridine-R mono-complexes (40-42)

In a flask preliminary flushed with argon, a mixture of $RuCl_3 \times 3\ H_2O$ (33.6 mg, 0.16 mmol) and dry degassed DMA (15 mL) was heated under argon at 120 °C for 30 minutes. A 1/3 fold of *mono*-terpyridine-R in 10 mL dry degassed DMA was added slowly to the reaction mixture. The reflux was continued overnight.

RuCl₃ (4'-3-hydroxypropyl-2,2':6',2''-terpyridine) mono-complex (40)

Purification was done by washing the brown-reddish precipitate with water and then with methanol. Yield: 60%. UV-Vis (CH_2Cl_2): λ_{max} (ε) = (L mol^{-1} cm^{-1}): 400 (8 500), 318 (17 200), 290 (17 800). The ^{1}H-NMR spectrum displayed only the protons of the alkyl chain due to the paramagnetic nature of Ru(III) complex.

RuCl₃ MeO-PEG₂₀₀ mono-terpyridine mono-complex (41)

The reaction mixture was allowed to cool to room temperature followed by a partitioning between water and CH_2Cl_2. The organic layer was separated and dried over Na_2SO_4. After removing the solvents in vacuum, the crude product was passed over a BioBeads S-X1 column in CH_2Cl_2. Yield: 75%. UV-Vis (CH_2Cl_2): λ_{max} (ε) = (L mol^{-1} cm^{-1}): 400 (8 200), 318 (17 900), 309 (17 500). SEC (DMF

system; PEG calibration): M_n = 9,350 g/mol, M_w = 10,200 g/mol, PDI = 1.09. The ^{1}H-NMR spectrum displayed only the protons of the polymer backbone due to the paramagnetic nature of Ru(III) complex.

RuCl₃ MeO-PTHF₉₀ mono-terpyridine mono-complex (42)
Purification was done analogue to **41**. Yield: 90%. UV-Vis (CH₂Cl₂): λ_{max} (ε) = (L mol^{-1} cm^{-1}): 402 (8 200), 318 (17 500), 274 (17 100). SEC (DMF system; PEG calibration): M_n = 7,300 g/mol, M_w = 8,200 g/mol, PDI = 1.12. The ^{1}H-NMR spectrum displayed only the protons of the polymer backbone due to the paramagnetic nature of Ru(III) complex.

General procedure for the synthesis of the RuCl₃ bis-terpyridine-R mono-complexes (43-44)
In a flask preliminary flushed with argon, a mixture of 1 eq. RuCl₃ in dry degassed DMA (15 mL) was heated under argon at 120 °C for 30 minutes. A 1/3 fold of **13** or **18** in 10 mL dry degassed DMA was added slowly to the reaction mixture and reflux was continued overnight.

RuCl₃ PEG₁₈₀ bis-terpyridine mono-complex (43)
Purification was done analogue to **41**. Yield: 70%. UV-Vis (CH₂Cl₂): λ_{max} (ε) = (L mol^{-1} cm^{-1}): 400 (8 100), 318 (17 600), 304 (17 200). SEC (DMF system; PEG calibration): M_n = 9,000 g/mol, M_w = 9,600 g/mol, PDI = 1.06. The ^{1}H-NMR spectrum displayed only the protons of the polymer backbone due to the paramagnetic nature of Ru(III) complex.

RuCl₃ PTHF₉₀ bis-terpyridine mono-complex (44)
Purification was done analogue to **41**. Yield: 90%. UV-Vis (CH₂Cl₂): λ_{max} (ε) = (L mol^{-1} cm^{-1}): 402 (8 200), 318 (17 700), 304 (17 200). SEC (DMF system; PEG calibration): M_n = 7,300 g/mol, M_w = 8,200 g/mol, PDI = 1.12. The ^{1}H-NMR spectrum displayed only the protons of the polymers backbone due to the paramagnetic nature of Ru(III) complex.

Ru(II)Cl₂DMSO 4'-terpyridine mono-complex (46) and Ru(II)Cl₂DMSO 4'-chloro-terpyridine mono-complex (47)
Compounds **46** and **47** were synthesized and characterized according to literature procedure.[49]

Synthesis of Ru(II)Cl₂DMSO (4'-3-hydroxypropyl-2,2':6',2''-terpyridine) mono-complex (48)
Compounds **48** was synthesized and purified according to a literature procedure.[49] Yield: 60%. ^{1}H-NMR (400 MHz, DMSO-d_6, 25 °C): δ (ppm) = 9.33 (d, 2H, J = 4 Hz; H^6, H$^{6''}$), 8.60 (d, 2H, J = 8 Hz; H$^{3'}$, H$^{3''}$), 8.32. (s, 2H, H$^{3'}$, H$^{5'}$), 7.94 (t, 2H, J = 4 Hz; J = 8 Hz; H^4, H$^{4''}$), 7.47 (t, 2H, J = 4 Hz; J = 8 Hz; H^5, H$^{5''}$), 4.69 (t, J = 6.0 Hz; 2H, H$^\gamma$), 4.48 (t, J = 6.0 Hz; 2H, H$^\alpha$), 3.43 (m, 2 H, H$^\beta$). UV-Vis (CH₂Cl₂): λ_{max} (ε) = (L mol^{-1} cm^{-1}): 482 (4 200), 404 (8 700), 304 (16 100).

General synthesis of Ru(II)Cl₂DMSO MeO-PEG-terpyridine mono-complexes (49-52)
A mixture of Ru(DMSO)₄Cl₂ (261 mg, 540 mmol) and MeO-PEG *mono*-terpyridine (450 mmol) in argon degassed CHCl₃ (10 mL) was refluxed overnight. During this time the solution turned brown. After being cooled to ambient temperature, the solution was concentrated *in vacuo*. The crude product was further purified by preparative size exclusion chromatography accordingly to their molar mass (BioBeads SX-3 or SX-1, CH₂Cl₂), followed by precipitation from dichloromethane into diethyl ether.

Ru(II)Cl₂DMSO MeO-PEG₁₂-terpyridine mono-complex (49)
Yield: 88%. ^{1}H-NMR (400 MHz, DMSO-d_6, 25 °C): δ (ppm) = 8.98 (d, 2H, J = 4 Hz; H^6, H$^{6''}$), 8.58 (d, 2H, J = 4 Hz; H^3, H$^{3''}$), 8.26 (s, 2H, H$^{3'}$, H$^{5'}$), 8.11 (t, 2H, J = 4 Hz; J = 8 Hz; H^4, H$^{4''}$), 7.37 (t, 2H, J = 4 Hz; J = 8 Hz; H^5, H$^{5''}$), 4.47 (m, 2H, tpyOCH_2), 3.86(m, 2H, tpyOCH₂CH_2), 3.66-3.47 (m, 48H, PEG-backbone), 3.24 (s, 3H; OCH_3). UV-Vis (CHCl₃): λ_{max} (ε) = (L mol^{-1} cm^{-1}): 480 (4 200), 400 (8 700), 310 (16 100).

Ru(II)Cl₂DMSO MeO-PEG₄₄-terpyridine mono-complex (50)
Yield: 80%. ^{1}H-NMR (400 MHz, DMSO-d_6, 25 °C): δ (ppm) = 9.21 (m, 2H, H^6, H$^{6''}$), 8.17 (m, 2H, H^3, H$^{3''}$), 8.20 (s, 2H, H$^{3'}$, H$^{5'}$), 7.98 (m, 2H, J = 4 Hz; H^4, H$^{4''}$), 7.45 (m, 2H, H^5, H$^{5''}$), 4.33 (m, 2H,

tpyOCH_2), 3.87(m, 2H, tpyOCH$_2$CH_2), 3.77-3.52 (m, 176H, PEG-backbone), 3.24 (s, 3H; OCH_3). UV-Vis (CHCl$_3$): λ_{max} (ε) = (L mol^{-1} cm^{-1}): 477 (4 200), 402 (8 700), 309 (16 100). SEC (RI detector; PEG calibration): M_n = 2,500 g/mol, M_w= 2 800 g/mol, PDI = 1.12.

Ru(II)Cl$_2$DMSO MeO-PEG$_{70}$-terpyridine mono-complex (51)

Yield: 85%. ^{1}H-NMR (400 MHz, DMSO-d_6, 25 °C): δ (ppm) = 9.02 (m, 2H, H^6, H$^{6"}$), 8.60 (m, 2H, H^3, H$^{3"}$), 8.28 (s, 2H, H$^{3'}$, H$^{5'}$), 8.08 (m, 2H, H^4, H$^{4"}$), 7.35 (m, 2H, H^5, H$^{5"}$), 4.44 (m, 2H, tpyOCH_2), 3.80 (m, 2H, tpyOCH$_2$CH_2), 3.66-3.47 (m, 280H, PEG-backbone), 3.20 (s, 3H; OCH_3). UV-Vis (CHCl$_3$): λ_{max} (ε) = (L mol^{-1} cm^{-1}): 477 (4 200), 402 (8 700), 309 (16 100). SEC (RI detector; PEG calibration): M_n = 3,500 g/mol, M_w = 3,900 g/mol, PDI = 1.11.

Ru(II)Cl$_2$DMSO MeO-PEG$_{200}$-terpyridine mono-complex (52)

Yield: 85%. ^{1}H-NMR (400 MHz, DMSO-d_6, 25 °C): δ (ppm) = 9.35 (m, 2H, H^6, H$^{6"}$), 8.70 (m, 2H, H^3, H$^{3"}$), 8.30 (s, 2H, H$^{3'}$, H$^{5'}$), 7.98 (m, 2H, H^4, H$^{4"}$), 7.50 (m, 2H, H^5, H$^{5"}$), 4.34 (m, 2H, tpyOCH_2), 3.84-3.37 (m, 800H, PEG-backbone), 3.07 (s, 3H; OCH_3). UV-Vis (CHCl$_3$): λ_{max} (ε) = (L mol^{-1} cm^{-1}): 479 (4 300), 405 (8 800), 310 (16 500). SEC (RI detector; PEG calibration): M_n = 8,500 g/mol, M_w = 9,100 g/mol, PDI = 1.07.

Synthesis of Ru(II)Cl$_2$DMSO bis-terpyridine PEG$_{180}$ mono-complex (53)

Analog to **49-52**. Molar ratio Ru(DMSO)$_4$Cl$_2$ to *bis*-terpyridine PEG$_{180}$ was 1:3. Yield: 80%. ^{1}H-NMR (400 MHz, DMSO-d_6, 25 °C): δ (ppm) = 9.20 (m, 4H, H^6, H$^{6"}$), 8.73 (m, 4H, H^3, H$^{3"}$), 8.32 (s, 4H, H$^{3'}$, H$^{5'}$), 7.80 (m, 4H, H^4, H$^{4"}$), 7.53 (m, 4H, H^5, H$^{5"}$), 4.33 (m, 2H, tpyOCH_2), 3.84-3.37 (m, 720H, PEG-backbone). UV-Vis (CHCl$_3$): λ_{max} (ε) = (L mol^{-1} cm^{-1}): 480 (4 300), 403 (8 800), 311 (16 500). SEC (RI detector; PEG calibration): M_n = 9,100 g/mol, M_w = 9,800 g/mol, PDI = 1.07.

Ru(II) bis-4'-chloro-terpyridine complex (54)

Compounds **54** was synthesized and characterized according to a literature procedure.[49,76]

Synthesis of Ru(II) bis-(4'-3-hydroxypropyl-2,2':6',2"-terpyridine) complex (55)

Analog to **54**. Yield: 38%. ^{1}H-NMR (400 MHz, CD$_3$CN, 25 °C): δ (ppm) = 8.48 (d, 4H, J = 8 Hz; H^3, H$^{3"}$), 8.33 (s, 4H; H$^{3'}$, H$^{5'}$), 7.90 (t, 4H, J = 7.2 Hz, 4.4 Hz; H^4, H$^{4"}$), 7.40 (d, 4H, J = 4 Hz; H^6, H$^{6"}$), 7.16 (t, 4H, J = 6.6 Hz, 4.6 Hz; H^5, H$^{5"}$), 4.65 (m, 4H, H$^\gamma$), 3.92 (m, 4H, H$^\alpha$), 2.65 (m, 2 H, H$^\beta$). SEC (RI detector; PMMA calibration): M_n = 1,400 g/mol, M_w = 1,600 g/mol; PDI = 1.14.

Synthesis of Ru(II) bis-terpyridine PEG$_{44}$ (56)

A suspension of MeO-PEG$_{44}$ *mono*-terpyridine-RuCl$_2$(DMSO) (100 mg, 0.04 mmol) **50** and AgSbF$_6$ (27.27 mg, 0.08 mmol) was heated under refluxed overnight in acetone, followed by filtration to remove the formed AgCl. The [MeO-PEG$_{44}$ *mono*-terpyridine Ru(II)(DMSO)(COMe$_2$)$_2$]$^{2+}$ (SbF$_6^-$)$_2$ solution was subsequently added to a solution of the MeO-PEG$_{44}$ *mono*-terpyridine **8** (68.1 mg, 0.03 mmol) in acetone. The reaction mixture was heated under reflux for 48 h. After cooling to ambient temperature, the reaction mixture was filtered through celite and then purified by preparative size exclusion chromatography (BioBeads SX-1, CH$_2$Cl$_2$). Yield: 38%. ^{1}H-NMR (400 MHz, CD$_2$Cl$_2$, 25 °C): δ (ppm) = 8.39 (d, 4H, J = 8 Hz; H^3, H$^{3"}$), 8.27 (s, 4H; H$^{3'}$, H$^{5'}$), 7.88 (t, 4H, J = 7.6 Hz, 3.6 Hz; H^4, H$^{4"}$), 7.35 (d, 4H, J = 4 Hz; H^6, H$^{6"}$), 7.19 (t, 4H, J = 6.6 Hz, 3.6 Hz; H^5, H$^{5"}$), 4.73 (m, 4H, tpyOCH_2), 4.12 (m, 4H, tpyOCH$_2$CH_2), 3.78-3.52 (m, 90H; PEG-backbone), 3.36 (s, 6H; OCH_3). UV-Vis (CHCl$_3$): λ_{max}: 267, 305, 486. SEC (RI detector; PEG calibration): M_n = 9,400 g/mol, M_w = 10,000 g/mol, PDI = 1.05.

Synthesis of Ru(II) (4'-3-hydroxypropyl-2,2':6',2"-terpyridine) (2,2':6',2"-terpyridine) complex (57)

Compound **57** was synthesized and characterized according to a literature procedure.[49,77]

Synthesis of Ru(II) (MeO-PEG$_{200}$-4'-terpyridine) (2,2':6',2"-terpyridine) complex (58)

Analog to **56**. Yield: 49%. ^{1}H-NMR (400 MHz, CD$_2$Cl$_2$, 25 °C): δ (ppm) = 8.70 (m, 4H, H^3, H$^{3"}$), 8.63 (s, 2H, H$^{3'}$, H$^{5'}$), 8.47 (s, 2H, H$^{3'}$, H$^{5'}$), 7.98 (m, 4H, H^4, H$^{4"}$), 7.90 (m, 4H, H^6, H$^{6"}$), 7.36 (m, 4H, H^5, H$^{5"}$), 4.76 (m, 2H, tpyOCH_2), 4.11 (m, 2H, tpyOCH$_2$CH_2), 3.90-3.42 (m, 200H, PEG-backbone), 3.37

(s, 3H; OCH_3). UV-Vis (CHCl$_3$): λ_{max}: 270, 303, 402, 489. SEC (RI detector; PEG calibration): M_n = 8,100 g/mol, M_w = 8,400 g/mol, PDI = 1.06.

General synthesis of the Ru(II) ABA triblock assemblies (61a-d)

A suspension of MeO-PEG$_{44}$-RuCl$_2$(DMSO) (0.1 mmol) **50** and AgSbF$_6$ (0.3 mmol) was heated under reflux overnight in acetone, followed by filtration to remove the formed AgCl. The [MeO-PEG$_{44}$-Ru(II)(DMSO)(COMe$_2$)$_2$]$^{2+}$ (SbF$_6^-$)$_2$ solution was then added to a solution of the ditopic ligand **60a-d** (0.03 mmol) in acetone. The reaction mixture was heated under reflux for 48 h. After cooling to ambient temperature, the reaction mixture was filtered through celite and then purified by preparative size exclusion chromatography (BioBeads SX-1, CH$_2$Cl$_2$).

61a: Yield: 25%. ^{1}H-NMR (400 MHz, CD$_2$Cl$_2$, 25 ˚C): δ (ppm) = 8.87 (s, 4H), 8.57 (m, 4H), 8.41 (d, 4H, J = 4 Hz), 8.33 (s, 4H), 8. 15 (m, 4H), 7.97-7.87 (m, 10H), 7.76 (d, 2H, J = 4 Hz), 7.69 (d, 2H), 7.43-7.34 (m, 9H), 7.27 (t, 4H, J = 2 Hz), 7.20 (t, 4H, J = 4 Hz), 7.16 (s, 1H,), 4.75 (m, 4H), 4.19 (m, 2H), 4.11 (m, 6H), 3.84-3.40 (m, 90H), 3.34 (s, 6H), 1.97 (m, 4H), 1.60 (m, 4H), 1.23-1.45 (m, 16H), 0.91 (m, 6H). UV-Vis (CHCl$_3$): λ_{max}: 272, 306, 489. SEC (RI detector; PEG calibration): M_n = 11,000 g/mol, M_w = 11,300 g/mol, PDI = 1.02.

61b: Yield: 50%. ^{1}H-NMR (400 MHz, CD$_2$Cl$_2$, 25 ˚C): δ (ppm) = 8.89 (s, 4H), 8.56 (m, 4H), 8.41 (m, 4H), 8.34 (s, 4H), 8.17 (m, 4H), 7.98-7.90 (m, 10H), 7.65 (m, 2H), 7.42 (m, 2H), 7.37 (m, 2H), 7.28 (m, 4H), 7.21 (m, 4H), 7.16 (s, 1H), 4.76 (m, 4H), 4.19 (m, 2H), 4.11 (m, 6H), 3.77-3.42 (m, 90H), 3.34 (s, 6H), 1.97 (m, 4H,), 1.66 (m, 4H), 1.17-1.31 (m, 16H), 0.85 (m, 6H). UV-Vis (CHCl$_3$): λ_{max}: 273, 306, 356, 498. SEC (RI detector; PEG calibration): M_n = 9,700 g/mol, M_w = 10,700 g/mol, PDI = 1.10.

61c: Yield: 20%; ^{1}H-NMR (400 MHz, CD$_2$Cl$_2$, 25 ˚C): δ (ppm) = 8.87 (s, 4H), 8.80 (s, 4H). 8.74 (m, 4H), 8.40 (m, 4H), 7.93 (m, 4H), 7.89 (m, 4H), 7.61 (m, 4H), 7.37 (m, 4H), 7.29 (m, 2H), 7.18 (m, 2H), 6.99 (m, 4H), 4.76 (m, 4H), 4.11 (m, 4H), 3.91-3.37 (m, 90H), 3.35 (s, 6H) 1.65 (m, 4H), 1.44 (m, 4H), 1.12-1.35 (m, 56H), 0.89 (m, 6H). UV-Vis (CHCl$_3$): λ_{max}: 271, 303, 492. SEC (RI detector; PEG calibration): M_n = 11,500 g/mol; M_w = 13,400 g/mol; PDI = 1.16.

61d: Yield: 39%; ^{1}H-NMR (400 MHz, CD$_2$Cl$_2$, 25 ˚C): δ (ppm) = 8.90 (s, 4H), 8.55 (m, 4H). 8.42 (m, 4H), 8.34 (s, 4H), 8.16 (m, 4H), 7.94 (m, 4H), 7.89 (m, 4H), 7.61(m, 4H), 7.42 (m, 7H), 7.39 (m, 2H), 7.28 (m, 2H) 7.21 (m, 3H), 7.00 (m, 3H), 4.76 (m, 4H), 3.66-3.46 (m, 90H), 3.35 (s, 6H), 3.84 (m, 8H), 1.85 (m, 8H), 1.72 (m, 8H), 1.59 (m, 8H), 1.17-1.43 (m, 104H), 0.87 (m, 12H). UV-Vis (CHCl$_3$): λ_{max}: 272, 303, 401, 491. SEC (RI detector; PEG calibration): M_n = 12,200 g/mol, M_w = 13,400 g/mol, PDI = 1. 02.

Micelle preparation of Ru(II) ABA triblock assemblies (61a-d)

Experiment 1: The **ABA** triblock assemblies **61a-d** were dissolved in DMF (2 g/L). In a next step, a water volume equal to half the DMF volume was added under stirring by steps of 50 µL, followed by the addition of the same water volume in one shot. Afterwards the solution was dialyzed against water to remove the DMF. The final concentration was about 0.6 g/L. The solutions have been filtered through 1 µm filters before the DLS measurements. For cryo-TEM measurements the solutions have been prepared in the same fashion without further filtration. **Experiment 2:** The **ABA** triblock assemblies **61a** and **61b** were dissolved in THF (1g/L), a water volume equal to the THF volume was added dropwise under stirring. The solutions have not been filtered before the measurements.

Synthesis of Ru(II) AB diblock "tri-star" (63)

Analog to **56** using the following 3 eq. MeO-PEG$_{44}$-RuCl$_2$(DMSO) **50**, 4 eq. AgSbF$_6$ and 1 eq. *tris*-terpyridine ligand **62** (0.03 mmol). Final purification was done by preparative size exclusion chromatography (BioBeads SX-1, acetone).

63F$_1$: Yield: 15%. ^{1}H-NMR (400 MHz, CD$_3$CN, 25 ˚C): δ (ppm) = 9.07 (s, 6H, H$^{3'}$, H$^{5'}$), 8.70 (m, 12H, H^3, H$^{3''}$), 8.55 (m, 12H, H^4, H$^{4''}$), 8.41 (m, 6H, H$^{3'}$, H$^{5'}$), 8.38 (m, 6H, H^{aryl}), 8.27 (m, 6H, H^{aryl}), 8.09 (m,

3H, H^{olefin}), 7.9 (m, 24H, H^5, H$^{5"}$, H^6, H$^{6"}$), 7.46 (m, 2H, H^{aryl}), 7.41 (m, 4H, H^{olefin}), 7.20 (m, 4H, H^{aryl}), 7.16 (m, 4H, H^{aryl}), 4.73 (m, 6H), 4.14 (m, 6H, H^{alkyl}), 3.96-3.19 (m, 550H, PEG backbone), 1.78 (m, 12H, H^{aryl}), 1.56 (m, 12 H, H^{alkyl}), 1.29 (m, 48H, H^{alkyl}), 0.89 (m, 24 H, H^{alkyl}).

63F$_2$: Yield: 25%. ^{1}H-NMR (400 MHz, CD$_3$CN, 25 ˚C): δ (ppm) = 9.07 (s, 6H, H$^{3'}$, H$^{5'}$), 8.69 (m, 12H, H$^{3,3"}$), 8.52 (m, 12H, H^4, H$^{4"}$), 8.43 (m, 6H, H$^{3'}$, H$^{5'}$), 8.39 (m, 6H, H^{aryl}), 8.28 (m, 6H, H^{aryl}), 8.09 (m, 3H, H^{olefin}), 7.9 (m, 24H, H^5, H$^{5"}$, H^6, H$^{6"}$), 7.46 (m, 2H, H^{aryl}), 7.41 (m, 4H, H^{olefin}), 7.20 (m, 4H, H^{aryl}), 7.16 (m, 4H, H^{aryl}), 4.72 (m, 5H), 4.07 (m, 6H, H^{alkyl}), 3.85-3.44 (m, 550H, PEG backbone), 1.78 (m, 12H, H^{aryl}), 1.55 (m, 12H, H^{alkyl}), 1.29 (m, 48H, H^{alkyl}), 0.88 (m, 24H, H^{alkyl}).

63F$_3$: Yield: 30%. ^{1}H-NMR (400 MHz, CD$_3$CN, 25 ˚C): δ (ppm) = 9.07 (s, 6H, H$^{3'}$, H$^{5'}$), 8.69 (m, 12H, H^3, H$^{3"}$), 8.52 (m, 12H, H^4, H$^{4"}$), 8.43 (m, 6H, H$^{3'}$, H$^{5'}$), 8.39 (m, 6H, H^{aryl}), 8.28 (m, 6H, H^{aryl}), 8.09 (m, 3H, H^{olefin}), 7.9 (m, 24H, H^5, H$^{5"}$, H^6, H$^{6"}$), 7.46 (m, 2H, H^{aryl}), 7.41 (m, 4H, H^{olefin}), 7.20 (m, 4H, H^{aryl}), 7.16 (m, 4H, H^{aryl}), 4.72 (m, 5H), 4.07 (m, 6H, H^{alkyl}), 3.80-3.39 (m, 550H, PEG backbone), 1.79 (m, 12H, H^{aryl}), 1.57 (m, 12H, H^{alkyl}), 1.28 (m, 48H, H^{alkyl}), 0.87 (m, 24H, H^{alkyl}).

Synthesis of Ru(II) AB diblock "tetra-star" (65)

Analog to **56** using the following 4 eq. MeO-PEG$_{44}$-RuCl$_2$(DMSO) **50**, 4 eq. AgSbF$_6$ and 1 eq. *tetra*-terpyridine ligand **64**. Final purification was performed by preparative size exclusion chromatography (BioBeads SX-1, acetone). Yield: 28%. ^{1}H-NMR (400 MHz, CD$_3$CN, 25 ˚C): δ (ppm) = 9.07 (s, 8H, H$^{3'}$, H$^{5'}$), 8.69 (m, 16 H, H^3, H$^{3"}$), 8.52 (m, 16H, H^4, H$^{4"}$), 8.43 (m, 8H, H$^{3'}$, H$^{5'}$), 8.39 (m, 8H, H^{aryl}), 8.28 (m, 8H, H^{aryl}), 8.09 (m, 4H, H^{olefin}), 7.9 (m, 32H, H^5, H$^{5"}$, H^6, H$^{6"}$), 7.46 (m, 2H, H^{aryl}), 7.41 (m, 4H, H^{olefin}), 7.20 (m, 4H, H^{aryl}), 7.16 (m, 4H, H^{aryl}), 4.73 (m, 8H), 4.07 (m, 8H), 4.44-3.57 (m, 730H, PEG backbone), 1.78 (m, 16H, H^{aryl}), 1.56 (m, 16 H, H^{alkyl}), 1.29 (m, 64H, H^{alkyl}), 0.89 (m, 24 H, H^{alkyl}).

Synthesis of the Ru(II) chain extended polymer (66)

A mixture of *bis*-terpyridine PEG$_{180}$ **13** (150 mg, 0.0183 mmol), the metal salt RuCl$_3$ × 3 H$_2$O (3.795 mg, 0.0183 mmol), *n*-butanol (426 µL) and *N*-ethyl-morpholine (115 µL) was stirred under reflux for 24 hours. The crude product was purified and fractionated by preparative size exclusion chromatography (BioBeads SX-1, CH$_2$Cl$_2$). Yield: 73%. ^{1}H-NMR (300MHz, CD$_3$CN, 25 ˚C): δ (ppm) = 8.60 (m, 4H, H^3, H$^{3"}$), 8.48 (s, 4H, H$^{3'}$, H$^{5'}$), 7.93 (m, 4H, H$^{4'}$, H$^{4"}$), 7.40 (m, 4H, H^6, H$^{6"}$), 7.17 (m, 4H, H^5, H$^{5"}$), 4.719 (m, 4H, O-C*H$_2$*), 4.06 (m, 4H, O-CH$_2$-C*H$_2$*-), 3.81-3.46 (m, 1150H, PEG backbone). UV-Vis (CH$_2$Cl$_2$): λ_{max} (ε) = (L mol^{-1} cm^{-1}): 490 (14 900), 305 (50 600), 268 (47 200). SEC (DMF system; PEG calibration): M_n = 30,400 g/mol, M_w = 70,100 g/mol, PDI = 2.30.

4.8 References

1   J.-M. Lehn, *Chem. Soc. Rev.* **2007**, *36*, 151.
2   J.-M. Lehn, Supramolecular Chemistry - Concepts and Chemistry; VCH: Weinheim, Germany, **1995**.
3   G. R. Newkome, E. He, C. N. Moorefield, *Chem. Rev.* **1999**, *99*, 1689.
4   U. S. Schubert, H. Hofmeier, G. R. Newkome, *Modern Terpyridine Chemistry*, Wiley-VCH, Weinheim, **2006**.
5   B. G. G. Lohmeijer, U. S. Schubert, *Macromol. Chem. Phys.* **2003**, *204*, 1072.
6   J.-F. Gohy, B. G. G. Lohmeijer, U. S. Schubert, *Macromol. Rapid Commun.* **2002**, *23*, 555.
7   H. Hofmeier, R. Hoogenboom, M. E. L. Wouters, U. S. Schubert, *J. Am. Chem. Soc.* **2005**, *127*, 2913.
8   C. D. Eisenbach, U. S. Schubert, *Macromolecules* **1993**, *26*, 7372.

9   S. Schmatloch, A. van den Berg, A. S. Alexeev, H. Hofmeier, U. S. Schubert, *Macromolecules* **2003**, *36*, 9943.

10   M. Kimura, M. Sano, T. Muto, K. Hanabusa, H. Shirai, *Macromolecules* **1999**, *32*, 7951.

11   S. Bernhard, K. Takada, D. J. Díaz, H. D. Abruña, H. Mürner, *J. Am. Chem. Soc.* **2001**, *123*, 10265.

12   G. D. Storrier, S. B. Colbran, D. C. Craig, *J. Chem. Soc. Dalton Trans.* **1997**, 3011.

13   W. Y. Ng, X. Gong, W. K. Chan, *Chem. Mater.* **1999**, *11*, 1165.

14   U. S. Schubert, C. Eschbaumer, P. Andres, H. Hofmeier, C. H. Weidl, E. Herdtweck, E. Dulkeith, A. Morteani, N. E. Hecker, J. Feldmann, *Synth. Metals* **2001**, *121*, 1249.

15   M. Heller, U. S. Schubert, *Eur. J. Org. Chem.* **2003**, 947.

16   M. Heller, U. S. Schubert, *J. Org. Chem.* **2002**, *67*, 8269.

17   G. R. Newkome, A. K. Patri, E. Holder, U. S. Schubert, *Eur. J. Org. Chem.* **2004**, 235.

18   B. G. G. Lohmeijer, U. S. Schubert, *Angew. Chem. Int. Ed.* **2002**, *41*, 3825.

19   F. Barigeletti, L. Flamigni, V. Balzani, J.-P. Collin, J.-P. Sauvage, A. Sour, E. C. Constable, A. M. W. Cargill Thompson, *J. Am. Chem. Soc.* **1994**, *116*, 7692.

20   S. Berhard, J. I. Goldsmith, K. Takada, H. D. Abruña, *Inorg. Chem.* **2003**, *42*, 4389.

21   F. Barigeletti, L. Flamigni, G. Calogero, L. Hammarström, J.-P. Sauvage, J.-P. Collin, *Chem. Commun.* **1998**, 2333.

22   A. Winter, D. A. M. Egbe, U. S. Schubert, *Org. Lett.* **2007**, *9,* 2345.

23   T. Joon Cho, C. N. Moorefield, S.-H. Hwang, P. Wang, L. A. Godínez, E. Bustos, G. R. Newkome, *Eur. J. Org. Chem.* **2006**, 4193.

24   I. P. Evans, A. Spencer, G. J. Wikinson, *Chem. Soc., Dalton Trans.* **1973**, 204.

25   M. Brindell, E. Kuliś, S. K. C. Elmroth, K. Urbanska, G. Stochel, *J. Med. Chem.* **2005**, *48,* 7298.

26   E. Alessio, G. Mestroni, G. Nardin, W. M. Attia, M. Calligaris, G. Sava, S. Zorzets *Inorg. Chem.* **1988**, *27*, 4099.

27   E. C. Constable, A. M. W. Cargill Thompson, *Dalton Trans.* **1992**, 3467.

28   G. R. Newkome, E. He, *J. Mater. Chem.* **1997**, *7*, 1237.

29   G. R. Newkome, T. J. Cho, C. N. Moorefield, P. P. Mohapatra, L. A. GodÌnez, *Chem. Eur. J.* **2004**, *10*, 1493.

30   M. Schmittel, H. Ammon, *Chem. Commun.* **1995**, 687.

31   M. T. Indelli, C. A. Bignozzi, F. Scandola, J.-P. Collin, *Inorg. Chem.* **1998**, *37*, 6084.

32   A. Khatyr, R. Ziessel, *Tetrahedron Lett.* **1999**, *40*, 5515.

33   R. Ziessel, *Synthesis* **1999**, *11*, 1839.

34   A. Khatyr, R. Ziessel, *J. Org. Chem.* **2000**, *65,* 3126.

35   S. Schmatloch, U. S. Schubert, *Macromol. Rapid Commun.* **2002**, *23*, 957.

36   M. Heller, U. S. Schubert, *Macromol. Rapid Commun.* **2001**, *22*, 1362.

37   H. Hofmeier, U. S. Schubert, *Macromol. Chem. Phys.* **2003**, *204*, 1391.

38   J.-F. Gohy, B. G. G. Lohmeijer, U. S. Schubert, *Chem. Eur. J.* **2003**, *9*, 3472.

39   E. C. Constable, *Adv. Inorg. Chem. Radiochem.* **1986**, 30, 69.

40   M. Schütte, D. G. Kurth, M. R. Linford, H. Cölfen, H. Möhwald, *Angew. Chem. Int. Ed.* **1998**, *37*, 2891.

41   M. A. R. Meier, D. Wouters, C. Ott, P. Guillet, C.-A. Fustin, J.-F. Gohy, U. S. Schubert, *Macromolecules* **2006**, *39*, 1569.

42   S. Kelch, M. Rehahn, *Macromolecules* **1999**, *32*, 5818.

43   P. Guillet, C.-A. Fustin, B. G. G. Lohmeijer, U. S. Schubert, J.-F. Gohy, *Macromolecules* **2006**, *39,* 5484.

44   J.-F. Gohy, B. G. G. Lohmeijer, U. S. Schubert, *Chem. Eur. J.* **2003**, *9*, 3472.

45   C.-A. Fustin, P. Guillet, U. S. Schubert, J.-F. Gohy, *Adv. Mater.* **2007**, *19*, 1665.

46   C.-A. Fustin, B. G. G. Lohmeijer, A.-S. Duwez, A. M. Jonas, U. S. Schubert, J.-F. Gohy, *Adv. Mater.* **2005**, *17*, 1162.

47   K. Aamer, G. Tew, *Macromolecules* **2007**, *40,* 2737.

48   V. Grosshenny, R. Ziessel, *J. Organomet. Chem.* **1993**, *453*, C19.

49   R. Ziessel, V. Grosshenny, M. Hissler, C. Stroh, *Inorg. Chem.* **2004**, *43*, 4262.

50   V. Duprez, M. Biancardo, H. Spanggaard, F. C. Krebs, *Macromolecules* **2005**, *38*, 10436.

51   J. R. Lakowicz, *Principles of Fluorescence Spectroscopy,* 2nd ed., Kluwer Academic-Plenum Publishers, New York, **2002**.

52   J.-P. Collin, A. Harriman, V. Heitz, F. Odobel, J.-P. Sauvage, *J. Am. Chem. Soc.* **1994**, *116*, 5679.

53   A. Juris, V. Balzani, F. Barigelletti, S. Campagna, P. Belser, A. von Zelewsky, *Coord. Chem. Rev.* **1988**, *84*, 85.

54   J.-F. Gohy, B. G. G. Lohmeijer, U. S. Schubert, *Macromolecules* **2002**, *35,* 4560.

55   L. Zhang, A. Eisenberg, *Science* **1995**, *268*, 1728.

56   O. Regev, J.-F. Gohy, B. G. G. Lohmeijer, S. K. Varshney, D. H. W. Hubert, U. S. Schubert, *Colloid Polym. Sci.* **2004**, *282*, 407.

57   H.-A. Klok, S. Lecommandoux, *Adv. Mater* **2001**, *13*, 1217.

58   C. Demas, G. A. Crosby, *J. Phys. Chem.* **1971**, *75*, 991.

58   D. E. Discher, A. Eisenberg, *Science* **2002**, *297*, 967.

59   D. Yan, Y. Zhou, J. Hou, *Science* **2004**, *303*, 65.

60   A. Winter, C. Friebe, U. S. Schubert, manuscript submitted.

61   R. Hoogenboom, U. S. Schubert, *Chem. Soc. Rev.* **2006**, 35, 622.

62   F. S. Han, M. Higuchi, D. G. Kurth, *Adv. Mater.* **2007**, *19*, 3928.

63   R. Dobrawa, F. Würthner, *J. Polym. Sci., Part A: Polym. Chem.* **2005**, *43*, 4981.

64   J.-F. Gohy, B. G. G. Lohmeijer, A. Alexeev, X.-S. Wang, I. Manners, M. A. Winnik, U. S. Schubert, *Chem. Eur. J.* **2004**, *20*, 4315.

65   G. R. Newkome, P. Wang, C. N. Moorefield, T. J. Cho, P. P. Mohapatra, S. Li, S.-H. Hwang, O. Lukoyanova, L. Echegoyen, J. A. Palagallo, V. Iancu, S.-W. Hla, *Science* **2006**, *312*, 1782.

66   M. A. R. Meier, B. G. G. Lohmeijer, U. S. Schubert, *Macromol. Rapid Commun.* **2003**, *24*, 852.

67   M. Chiper, M. A. R. Meier, J. M. Kranenburg, U. S. Schubert, *Macromol. Chem. Phys.* **2007**, *208*, 679.

68   J. Hjelm, E. C. Constable, E. Figgemeier, A. Hagfeld, R. Handel, C. E. Housecroft, E. Mukhtar, E. Schofield, *Chem. Commun.* **2002**, 284.

69   H. Hofmeier, S. Schmatloch, D. Wouters, U. S. Schubert, *Macromol. Chem. Phys.* **2003**, *204*, 2197.

70   S. Kelch, M. Rehahn, *Macromolecules* **1997**, *30*, 6185.

71   P. R. Andres, U. S. Schubert, *Synthesis* **2004**, *8*, 1229.

72   H. R. Kricheldorf, M. Rabenstein, M. Maskos, M. Schmidt, *Macromolecules* **2001**, *34,* 713.

73   H. R. Kricheldorf, G. Schwarz, *Macromol. Rapid Commun.* **2003**, *24*, 359.

74   M. Chiper, M. A. R. Meier, D. Wouters, S. Hoeppener, C.-A. Fustin, J.-F. Gohy, U. S. Schubert, *Macromolecules* **2008**, *41*, 2771.

75   H.-G. Elias, *An Introduction to Polymer Science*, Wiley-VCH, **1997**.

76   M. Maestri, J. N. Armaroli, V. Balzani, E. C. Constable, A. M. W. Cargill Thompson, *Inorg. Chem. 1995, 34,* 2759.

77   E. C. Constable, P. Harverson, C. E. Housecroft, E. Nordlander, J. Olsson, *Polyhedron* **2006**, *25*, 437.

Chapter V

Supramolecular systems

based on zinc(II) *bis*-terpyridine complexes

Abstract

In this chapter the zinc(II) complexation of a series of 2,2':6',2"-terpyridine ligands bearing different π-conjugated substituents in their 4'-position is described. Characterization of the resulting Zn(II) model complexes is discussed based on various techniques proving the formation, stability and purity of the synthesized structures. The dependence of photophysical and electrochemical properties on the nature of the conjugated spacer of the Zn(II) model complexes is discussed. In order to understand the influence of the conjugated substituents on the photophysical properties of the Zn(II) model complexes, a representative theoretical study is performed on a terpyridine ligand and its corresponding Zn(II) model complex. Furthermore, the telechelic terpyridine ligands bearing conjugated spacers in the 4'-position were polymerized via Zn(II) ions. Characterization of the resulting Zn(II) coordination polymers was performed by various techniques including UV-Vis absorption and emission spectroscopy, photoluminescence quantum yield, cyclic voltammetry, DFT (Density Functional Theory) and Raman spectroscopy. These types of supramolecular assemblies were found to be appealing systems for the construction of photoluminescent and electroluminescent materials.

5.1 Introduction

Metal-ligand coordination has nowadays become an important concept in the field of supramolecular chemistry for designing novel materials having new properties.[1] By choosing metal-ligand combinations, specific supramolecular systems can be realized and their stability is considerably influenced by the main characteristics of the constituent ligand and the utilized metal ion.[2] Thus, properties such as *e.g.* binding strength, stability, specificity, solubility (already discussed in the previous chapters of the present thesis) are important features of such designed metallo-supramolecular materials.

2,2':6',2"-Terpyridines substituted at the 4'-position are intensively used as tridentate supramolecular ligands since the formation of octahedral metallo *bis*-terpyridine complexes with a wide range of transition metal ions in low oxidation states is well-known and synthetically accessible.[3] Generally, by tuning the transition metal ion, the entire range from kinetically labile to inert *bis*-terpyridine complexes can be synthesized. For example, systems such as Ru(II) and Ni(II) *bis*-terpyridine complexes are characterized by high stability and non-luminescent properties (at room temperature) while Zn(II) *bis*-terpyridine systems are characterized by lower stability but enhanced photoluminescent and electroluminescent properties, at room temperature. That is why, besides the heavy transition metal ions, such as *e.g.* Ru(II), Os(II) or Ir(III), Zn(II) ions have recently gained much interest for the construction of photoluminescent (PL) or electroluminescent (EL) metallo-polymers with well-defined structures.[4-10]

Coordination *via* Zn(II) ions of mono and ditopic terpyridines bearing π-conjugated spacers at the 4'-position, enhances the electron delocalization on the polymer backbone, causing a red shift in the emissions as already described in literature.[6] As a result, such designed systems could be suitable for the preparation of electroluminescent devices. Würthner *et al.* focused their scientific work on studying the self-assembly of *bis*-terpyridine functionalized perylene bisimide dyes *via* Zn(II) complexation evidencing the influence of the metal ion on the electroluminescence properties of the synthesized metallo-assemblies.[11] Newkome *et al.* synthesized Zn(II)-hexameric metallocycles[12] and Pang *et al.* reported Zn(II)-based grafted structures[13] with increased electroluminescent properties. It is well-known from literature, that metal-to-ligand charge transfer (MLCT) processes do not occur for metal ions with filled electron shells, such as Zn(II) which has a d^{10} configuration.[14] Hence, only intra-ligand charge transfer (ILCT) is observed between the terpyridine-zinc(II) units and the chromophores, even in metallo-polymers.[15] Thus, the development of Zn(II)-containing metallo-polymers with

well-designed chromophores or π-conjugated spacers can lead towards high-performance emissive host materials for polymer light emitting diode (PLED) applications.

In this chapter the synthesis of a series of Zn(II) *bis*-terpyridine complexes, as model substrates for analog Zn(II)tpy$_2$ coordination polymers, will be discussed. A detailed study of the designed Zn(II)tpy$_2$ systems focusing on tuning the photophysical and electrochemical properties depending on the terminal π-conjugated substituents is investigated as well. The broad choice of the terpyridine ligands bearing various substituents in the 4'-position was done in order to gain first insights on the influence of the type of substituent on the photophysical and electrochemical properties of the synthesized Zn(II) model complexes. For a better understanding of all phenomena, theoretical calculations were performed of a representative terpyridine ligand and its subsequent Zn(II) model complex. Furthermore, coordination *via* Zn(II) ions of similar ditopic terpyridine ligands bearing π-conjugated spacers will be presented and the properties of the novel synthesized metallo-polymeric materials will be discussed in detail.

5.2 Zn(II) *bis*-terpyridine complexes (model systems)

5.2.1 Synthesis and characterization
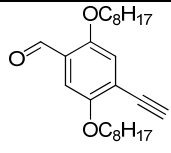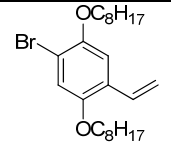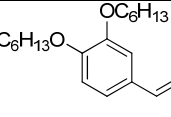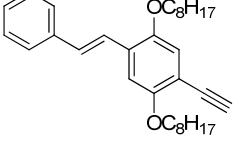
All Zn(II) model complexes discussed here are based on a set of 2,2':6',2''-terpyridine ligands **L** bearing π-conjugated substituents in their 4'-position. The additional alkoxy-groups of **67e-h** are crucial to retain good solubility of the ligands and the corresponding Zn(II) complexes in organic solvents. The preparation and characterization of the chelating ligands **67a-h** was not part of the presently discussed work and was reported elsewhere.[16,29] The corresponding homoleptic Zn(II) *bis*-terpyridine complexes [Zn(L)$_2$](PF$_6$)$_2$ **68a-h** were obtained in high yields (> 81%) by reacting the terpyridine ligands **67a-h** with Zn(II) acetate, at a ratio of 2:1, in methanol at ambient conditions, followed by subsequent anion exchange with ammonium hexafluorophosphate (Scheme 5.1, Table 5.1).
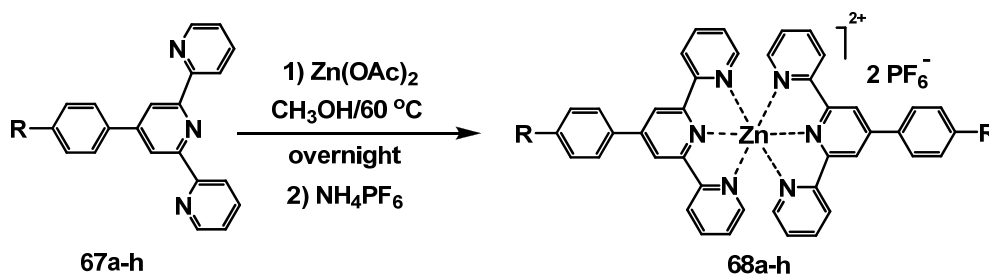
Scheme 5.1: *Schematical representation of the synthesis of the Zn(II) bis-terpyridine model complexes **68a-h** bearing various conjugated spacers (R) in the 4'-position.*

The usage of mild reaction conditions for the preparation of the model complexes based on the Zn(II)tpy$_2$ connectivity reflects the fact that the formation of the desired Zn(II) *bis*-terpyridine complex is mainly kinetically driven.

Table 5.1: *Overview of the synthesized homoleptic Zn(II) bis-terpyridine model complexes [Zn(L)$_2$](PF$_6$)$_2$ 68a-h.*

R	Model complex	R	Model complex
H	[Zn(**L$_a$**)$_2$](PF$_6$)$_2$ **68a**		[Zn(**L$_e$**)$_2$](PF$_6$)$_2$ **68e**
Br	[Zn(**L$_b$**)$_2$](PF$_6$)$_2$ **68b**		[Zn(**L$_f$**)$_2$](PF$_6$)$_2$ **68f**
CH=CH$_2$	[Zn(**L$_c$**)$_2$](PF$_6$)$_2$ **68c**		[Zn(**L$_g$**)$_2$](PF$_6$)$_2$ **68g**
C≡CH	[Zn(**L$_d$**)$_2$](PF$_6$)$_2$ **68d**		[Zn(**L$_h$**)$_2$](PF$_6$)$_2$ **68h**

Characterization of the purified Zn(II) model complexes **68a-h** was performed by means of ^{1}H-NMR, UV-Vis and emission spectroscopy as well as ESI-MS. The ^{1}H-NMR spectra of the synthesized model complexes **68a-h**, recorded in deuterated CD$_3$CN, revealed well-resolved signals in the aromatic region. In comparison to the uncomplexed ligand **L**, the H$^{3',5'}$, H$^{3,3''}$, H$^{4,4''}$ and H$^{5,5''}$-signals of the terpyridine units showed a distinct downfield shift. Due to the octahedral geometry of the *bis*-terpyridine metal complexes, the protons in 6,6''-position were directed towards the shielding region of the central pyridine ring of the orthogonal neighbouring ligand resulting in considerable upfield-shielding of these signals.[17] Representatively, the ^{1}H-NMR spectra of the vinyl-substituted terpyridine ligand **67c** and the corresponding complex [Zn(L$_c$)$_2$](PF$_6$)$_2$ **68c** are depicted in Figure 5.1. The complete assignment of the proton resonances of the Zn(II) model complexes was performed using ^{1}H-^{1}H correlation spectroscopy (^{1}H-^{1}H-COSY). Figure 5.2 shows as an example the ^{1}H-^{1}H-NMR-COSY recorded for the model complex **68h**.
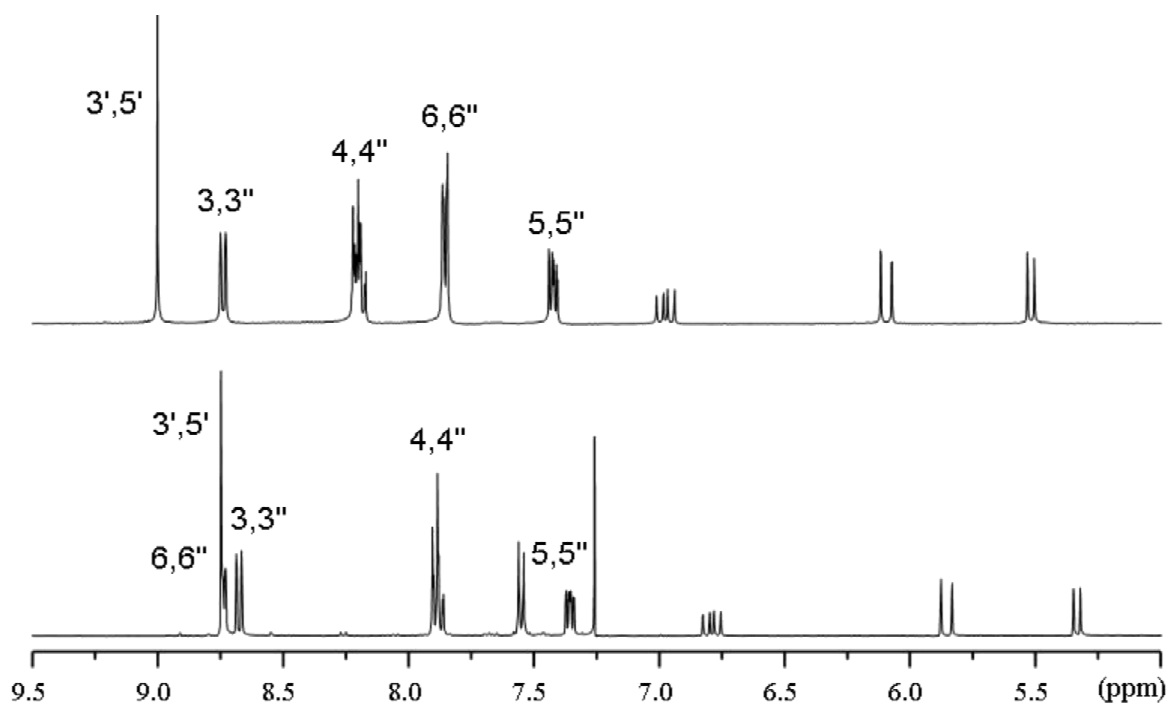
Figure 5.1: *Representative ^{1}H-NMR attributions of the terpyridine protons of **67c** (bottom) in CD$_3$Cl and [Zn(L$_c$)$_2$](PF$_6$)$_2$ **68c** (top) in CD$_3$CN.*
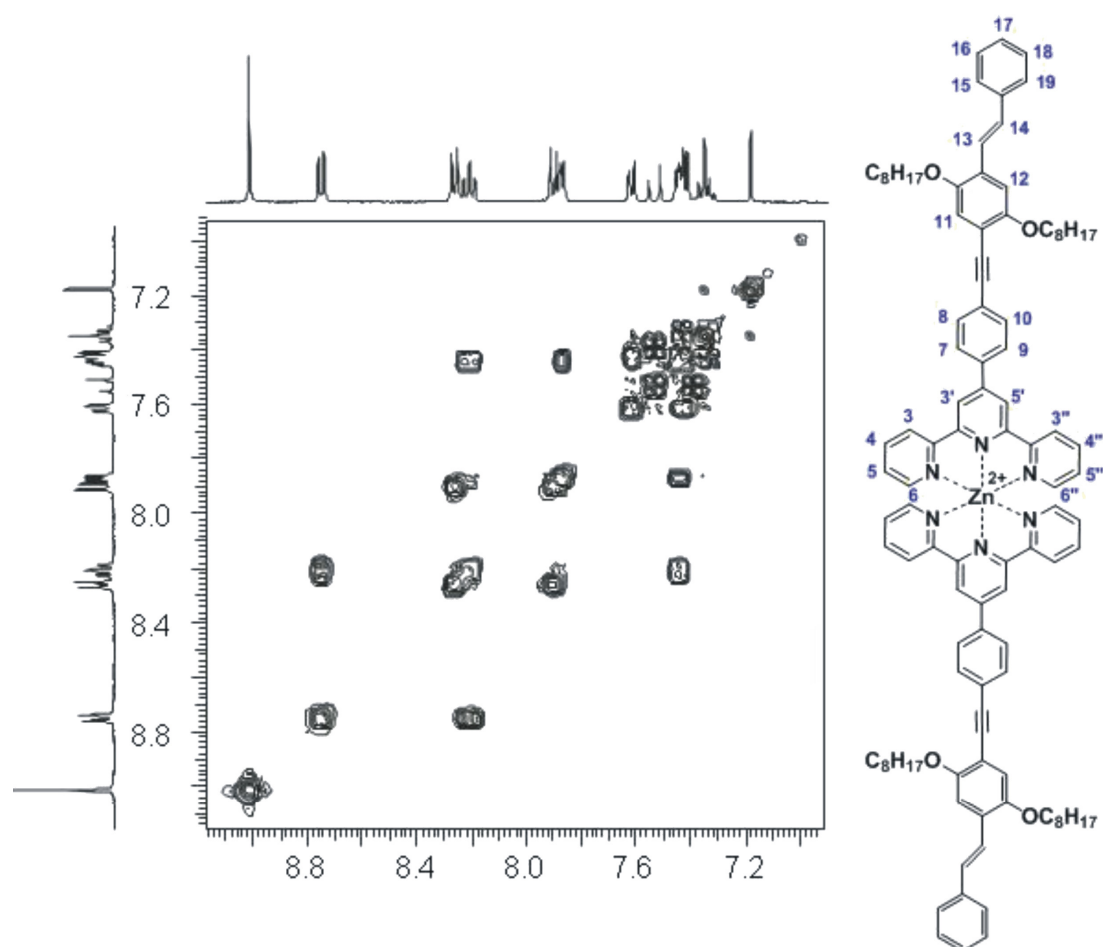
Figure 5.2: *^{1}H-NMR spectra (respective projections) with ^{1}H-^{1}H correlation spectroscopy (^{1}H-^{1}H COSY) of [Zn(L$_h$)$_2$](PF$_6$)$_2$ **68h** (in CD$_3$CN).*

Electrospray-mass spectrometry (ESI-MS) was used for investigating the formation of the metallo-terpyridine structures. Figures 5.3 shows an example of the detected species while measuring $[Zn(L_h)_2](PF_6)_2$ **68h**. Both species, meaning the complex cation with one PF_6^- and without any PF_6^- as counter ions were observed.
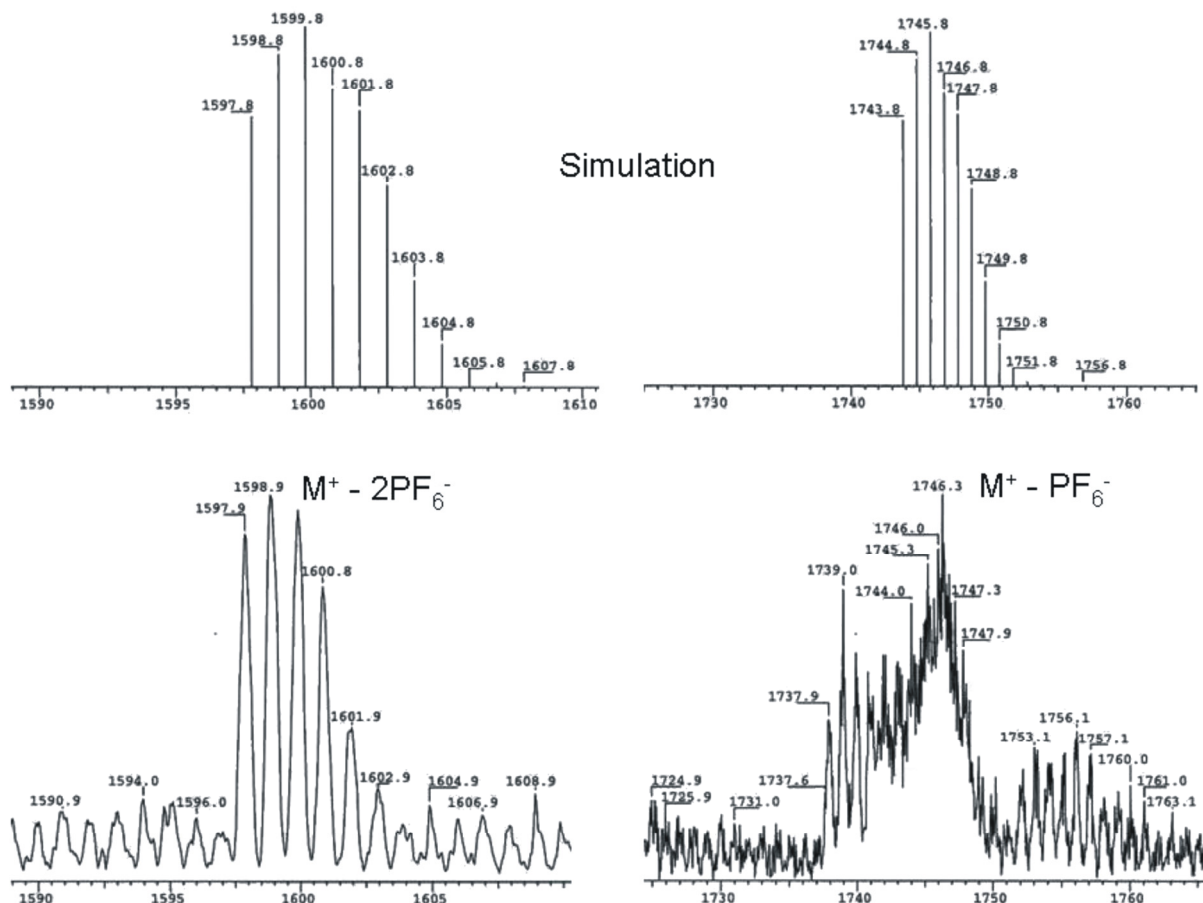
Figure 5.3: *Example of an ESI-MS spectra of the model complex $[Zn(L_h)_2](PF_6)_2$ **68h**.*

5.2.2 Photophysical properties

The photophysical properties of the synthesized Zn(II) *bis*-terpyridine model complexes **68a-h** were investigated by measuring the UV-Vis absorption and photoluminescence spectra in dilute solutions. All photophysical characteristics are summarized in Table 5.2. In order to make a clear comparison between the complexed and its corresponding uncomplexed ligands, the following discussion includes also the properties of the uncomplexed ligands **67a-h** (reported elsewhere[29]).

A representative comparison of the UV-Vis spectra obtained for the free ligands **67d** and **67e** and the corresponding Zn(II) model complexes **68d** and **68e** is depicted in Figure 5.4. In general, three major absorption regions have been observed for the free ligands **L**. The bands

between 280 and 295 nm belong to the terpyridine units, the bands between 310 and 350 nm are assigned to a phenylene localized transition and the broad band between 350 nm and 450 nm is assigned to a transition corresponding to the subsequent extended π-system of the phenylene-R unit in **67e**, **67f**, **67g** and **67h**, respectively.

In contrast to the tpy-assigned absorption band, the phenylene-assigned absorption band of **67d** showed a slight bathochromic shift upon complexation. This shift could be expected due to the increase in the electron density distribution and in the ellipticity in the phenylene-pyridine-bond in $[Zn(L_d)_2]^{2+}$ **68d** due to complexation. Since this enlargement of the π-system occurs along the phenylene-pyridine-bond, it rather lowers the energy of the phenylene-involving CT (charge transfer) than the energy of the tpy-long-axis CT (transition moment perpendicular to the ph-py-bond). The tpy-long-axis CT is expected to be of lower energy and of lower oscillator strength than the transition corresponding to the short tpy-axis. Because the transition dipole moment of the tpy-short-axis CT is parallel to the ph-py-bond it should be influenced more by the higher electron density distribution (ρ) and ellipticity (ε) in the phenylene-pyridine-bond. A significant corresponding bathochromic shift was not observed in the hypsochromic edge of the tpy-assigned absorption band (280-295 nm) of $[Zn(L_4)_2]^{2+}$ **68d** compared to **67d**.
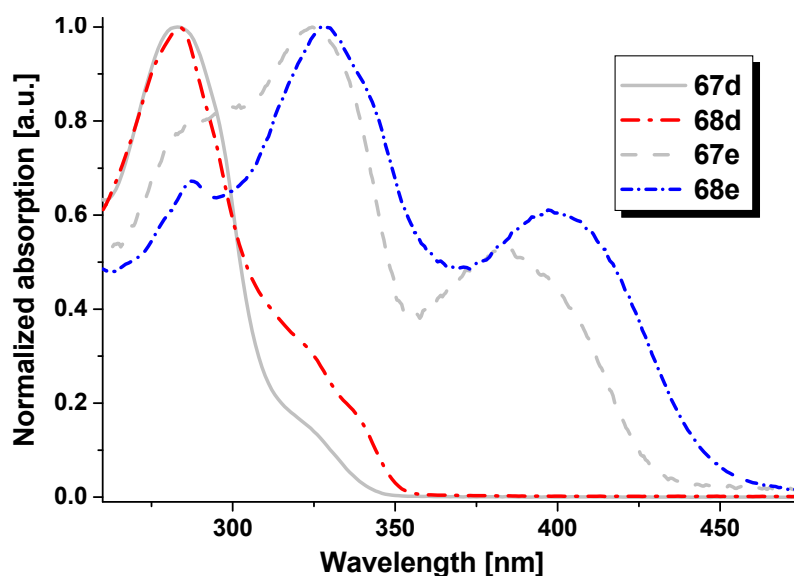
Figure 5.4: *UV-Vis spectra of **67d** (solid line) and **67e** (dotted line) and the corresponding model complexes [Zn(**L**$_d$)$_2$](PF$_6$)$_2$ **68d** (dash dotted line) and [Zn(**L**$_e$)$_2$](PF$_6$)$_2$ **68e** (short dash doted lines).*

The bathochromic shift between the absorption spectrum of **67e** and the derived Zn(II) model complex **68e** is more pronounced compared to **67d** and its Zn(II) model complex **68d**. Here

the phenylene located band is shifted roughly 4 nm (**67d**: 325 nm, $[Zn(L_d)_2]^{2+}$ **68d**: 329 nm) and the band assigned to the extended ph-R π-system about 17 nm (**67e**: 383 nm, $[Zn(L_e)_2]^{2+}$ **68e**: 400 nm) due to complexation. The presence of further substituents expanding the conjugated system has led to a distinct bathochromic shift of these bands and a loss of intensity. Likewise, the broad band around 375 nm, attributed to the CT transition of the conjugated system, has become more pronounced. In addition, the uncomplexed ligands revealed strong photoluminescence (Φ_{PL} up to 0.80) with emission maxima ranging from 350 nm to 450 nm.

To comprehend the influence of the conjugated substituents on the photophysical properties of the Zn(II) model complexes, a representative theoretical study performed on **67d** and its subsequent Zn(II) model complex **68d** will be discussed in detail in section 5.2.3.

The photoluminescence (PL) spectra of the Zn(II) model complexes **68a-h** were measured in acetonitrile solution and the results are summarized in Table 5.2. The effect of incorporating Zn(II) and various conjugated spacers in the 4'-position of the terpyridine moiety revealed spectroscopic properties that are more pronounced in the fluorescence measurements, which can be rationalized by efficient exciton migration along the conjugated groups. Figure 5.5 shows as an example the emission spectra of the analyzed model complexes $[Zn(L_d)_2](PF_6)_2$ **68d** and $[Zn(L_e)_2](PF_6)_2$ **68e** at excitation wavelengths of 330 and 400 nm that revealed strong emissions at 426 and 447 nm for **68d** and **68e**, respectively.
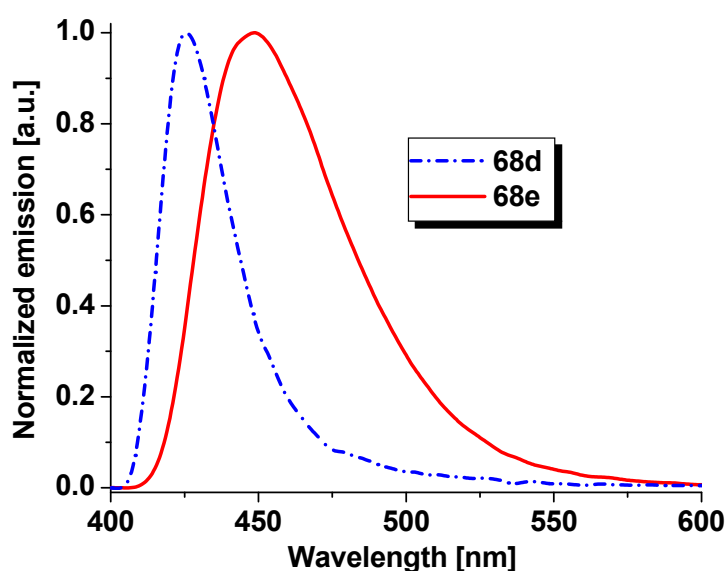
Figure 5.5: *Emission spectra of Zn(II) model complexes $[Zn(L_d)_2](PF_6)_2$ **68d** (short dash doted line) and $[Zn(L_e)_2](PF_6)_2$ **68e** (solid line).*

Table 5. 2. *Overview of the photophysical properties of the terpyridine ligands **67a-h**, their Zn(II) model complexes [Zn(L)₂](PF₆)₂ **68a-h** and [Zn(tpy)₂]²⁺ **69** used as standard comparison.*

Compound	$\lambda_{abs,max}$ [nm] [a]	E_g^{opt} [eV] [b]	$\lambda_{PL,max}$ [nm] [a]	λ_S [nm]	Φ_{PL} [a]
67a	278	3.37	340	62	0.31
67b	278	3.47	355	77	0.19
67c	286	3.30	359	73	0.16
67d	282	3.14	362	80	0.19
67e	348	2.91	440	92	0.28
67f	358	2.99	459	101	0.21
67g	348	3.45	465	117	0.43
67h	381	3.30	495	114	0.48
[Zn(tpy)₂]²⁺ 69	280, 319, 333	3.61	422	89	0.34
[Zn(Lₐ)₂]²⁺ 68a	282, 323, 337	3.59	425	88	0.37
[Zn(L_b)₂]²⁺ 68b	276, 320	3.65	427	107	0.14
[Zn(L_c)₂]²⁺ 68c	284, 320	3.55	437	117	0.59
[Zn(L_d)₂]²⁺ 68d	284, 325	3.59	428	103	0.34
[Zn(L_e)₂]²⁺ 68e	281, 321, 384	2.96	448	64	0.20
[Zn(L_f)₂]²⁺ 68f	285, 327, 392	2.75	454	62	0.06
[Zn(L_g)₂]²⁺ 68g	284, 325, 392	2.71	488	96	0.35
[Zn(L_h)₂]²⁺ 68h	284, 326, 397	2.71	470	73	0.53

[a]*Absorption and photoluminescence spectra as well as absolute quantum efficiencies have been measured in dilute CH₂Cl₂ solutions (10⁻⁶ M for all compounds).* [b]*Optical bands gaps have been estimated from the absorption spectra at 10% absorption on the longer wavelength side.*

The electrochemical behavior of the synthesized Zn(II) model complexes **68a-h** has been studied in dichloromethane solutions by cyclic voltammetry (CV) and is summarized in Table 5.2. Figure 5.6 displays a characteristic voltammetry response observed for the Zn(II) model complexes which generally exhibits two reduction waves correlated to the nature of the substituent in the 4'-position.[18]
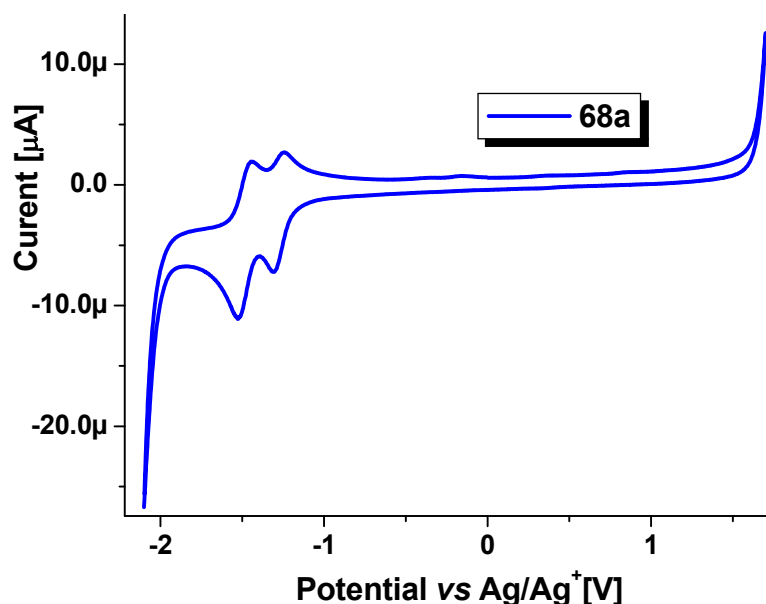
Figure 5.6: *Representative electrochemical behavior for the model complex [Zn(L$_a$)$_2$](PF$_6$)$_2$ **68a**. The measurement was performed in CH$_2$Cl$_2$ containing 0.1 M TBAPF$_6$.*

5.2.3 Structural characterization and examination of the electron density distribution using DFT and Raman spectroscopy for L$_d$ and [Zn(L$_d$)$_2$](PF$_6$)$_2$

The most important possibility to influence the photophysical properties of a given system is to extend the chromophor, usually realized by appending unsaturated substituents, or to create metal complexes. In the following, a representative theoretical study performed on the ligand **67d** and its corresponding model complex [Zn(L$_d$)$_2$](PF$_6$)$_2$ **68d** will be discussed regarding the changes in the geometrical structure, the Raman spectrum and in the electron density distribution of the pyridine-phenylene bond due to complexation. Via the phenylene substituent in the 4'-position of the terpyridine unit the chromophor was extended. Subsequent enlargement of the π-system was realized by ethenyl-phenylen or ethynyl-phenylen groups, whereas the ethenyl/ethynyl groups served as spacers between the aromatic rings to avoid torsion due to sterical effects, which would lower the conjugation of the system.[19] In the case of the chelating terpyridine unit and the neighboring phenylene moiety the two aromatic

subsystems are tilted significantly with respect to each other because of the repulsion of the hydrogen atoms. Such torsions between neighboring aromatic rings lower the π-electron delocalization between the rings and thus, influence the electrical and photophysical properties of the system. Recently, reported results point to the influence of the torsions on the photophysics of conjugated polymers and related model compounds.[20] Hence, with respect to the manipulation of the photophysical as well as the conducting properties, the interest was focused on the question, to which extent the disturbance of the delocalization of the π-system between the terpyridine and the phenylene moiety is influenced by the *para* substituents of the phenylene unit on one hand and by the complex-formation of the zinc ion on the other hand. To address this particular question we studied the changes in the geometry *via* DFT (Density Functional Theory) calculations in combination with Raman spectroscopy. In particular, the geometrical changes of the phenylene-pyridine-bond indicate the change of the π-electron delocalization between the respective aromatic subsystems. For example, a bond shortening suggests an increasing bond-order and a lower dihedral angle between phenylene and pyridine goes along with a higher degree of p-orbital overlapping.

5.2.3.1 Characterizing the ligand L$_d$ *via* DFT optimized geometries and Raman spectra

The ligand **67d** was chosen since it is the structurally simplest ligand with an extended π-system in addition to the phenylene group featuring an ethynyl group in the *para*-position. Thus, the computational effort to perform geometry optimization with subsequent calculation of the Raman spectra of various conformers of the free ligand and of the zinc complex is acceptable and there is no need to assume simplified structural approximations. The geometry optimizations with subsequent calculations of the Raman spectra of various conformers of the free ligand and of the zinc complex were performed using the BP86 functional and the TZVP basis set.[21] This combination has shown to provide accurate molecular structures, frequencies and Raman intensities for medium sized molecules.[22]

When simulating the experimental Raman spectrum of **67d**, the different conformers of **67d** should be accounted. The two most important conformers are the all-*cis* and the all-*trans* structures with respect to the terpyridine moiety. This is because the orientation of the terminal pyridines in the all-*cis*-conformer is somehow comparable to the situation in the complex, while the all-*trans*-conformer is expected to correspond to the global energetic minimum of the free ligand. The electronic energy of the all-*trans*-conformer has been calculated to be −1050.065 h and the Gibbs enthalpy is 670.78 kJ/mol. The electronic energy

of the all-*cis*-conformer is about 0.02 h higher (–1050.045 h) and the corresponding Gibbs enthalpy is about 3 kJ/mol lower (667.94 kJ/mol) than for the all-*trans*-conformer. The errors of these DFT energies have been estimated to be below 0.1 mh/atom.[23] This allows the estimation of the accuracy of the computed energies of the **67d** conformers (83 atoms) to be about 0.008 h. The most obvious differences in the geometry of the two conformers are the dihedral angles between the aromatic rings. The geometry optimization of the all-*trans*-conformer confirmed the expected planar structure in the terpyridine unit while the phenylene group is tilted about 33.2° out off plane. This dihedral angle was calculated to be about 3° larger (36.5°) in the case of the all-*cis*-conformer, while the angle between the pyridine rings is about 41°. The bond length of the ph-py-bond differs negligible between the all-*cis*- and the all-*trans*-conformer, which is shown in Figure 5.8 in section 5.2.3.2 in context with the influence of the complexation. In Figure 5.7 the experimental Raman spectrum of **67d** is compared with the DFT-calculated Raman spectra of the all-*cis*- and the all-*trans*-conformer of **67d**. The most intense bands are at comparable wavenumber positions with an equivalent intensity pattern. In the DFT calculated Raman spectra of **67d** the intense band at 980 cm^{-1} can be assigned to the trigonal ring breathing vibrations located in the terpyridine moiety with quasistationary carbon atoms forming the inter aromatic ring bonds. The band at 1347 cm^{-1} is assigned to a trigonal ring breathing vibration basically located on the central pyridine ring and the phenylene unit. It involves strong movements of the inter-aromatic-ring-bond carbon atoms, which are accompanied by a pronounced stretch vibration of the phenylene and pyridine connecting bond (C-(H) and N in the central py quasistationary). The bands at 1575 and 1600 cm^{-1} are assigned to aromatic in plane vibrations corresponding to Wilson No. 8a, located either in the terpyridine unit (1575 cm^{-1}) or in the phenylene group (1600 cm^{-1}).[24] Finally, the Raman band at 2142 cm^{-1} corresponds to the well-separated stretching vibration of the ethynyl group. These modes can be easily identified in the experimental Raman spectrum (RS) of the free ligand **67d** (Figure 5.7). The DFT calculated modes at 980, 1647, 1575, 1600 and 2142 cm^{-1} correspond to the bands at 999, 1362, 1587, 1610 and 2098 cm^{-1} in the experimental RS. The somewhat modified intensity pattern in the experimental RS compared to the DFT calculated one is due to a lower spectrometer sensitivity at higher wavenumbers applying an 830 nm laser line for excitation. The good agreement between the experimental and the DFT calculated Raman spectra suggests that the structural features obtained from the DFT calculations are reasonable.

Figure 5.7 *Raman spectra: experimental (top) and DFT calculated (middle and bottom); BP86 functional, def2-TZVP basis set, RI-approximation) of the **67d**.*

The differences between the DFT-calculated Raman spectra of all-*cis*- and all-*trans*-**67d** allow to determine which of the conformers, primary differing in the dihedral angles between the pyridine rings, is present in the experiment. Monitoring the differences in the dihedral angles directly by Raman spectroscopy appears rather challenging because the corresponding torsional modes are expected to occur in the low wavenumber region with strongly reduced Raman intensities. However, the differences of the dihedral angles between the aromatic rings influence the aromatic in plane vibrational modes that dominate the Raman spectrum in the region between 900 and 1700 cm^{-1}. In particular the rather intense Raman bands calculated to occur at 1296, 1433 and 1556 cm^{-1} in the spectrum of the all-*trans*-conformer are not clearly identifiable in the corresponding Raman spectrum of the all-*cis*-conformer. Hence, they appear to be appropriate marker bands for the *trans*-conformation. Experimentally, these marker bands are observed at 1444 and 1573 cm^{-1}. Though, the calculated marker band of the trans-L at 1296 cm^{-1} cannot be clearly identified in the experimental data, the strong presence of the other trans-characteristic bands in the experimental spectrum of **67d** suggest, that the latter spectrum is mainly dominated by the *trans*-conformer.

5.2.3.2 Investigation of the changes in the geometry upon complexation and discussion of the Raman spectrum of [Zn(L$_d$)^2]$^{2+}$

According to the DFT calculations the terpyridine moiety in [Zn(L$_d$)$_2$](PF$_6$)$_2$ **68d** is planar in contrast to the free *cis*-**67d**. Consequently, the larger overlap of the free electron pairs of the nitrogen atoms with the d-orbitals of the zinc ion in combination with the higher degree of π-delocalization in the planar terpyridine moiety compensates the steric hindrance of the neighbouring hydrogen atoms on the respective pyridines. Furthermore, the dihedral angle between the phenylene and the pyridine ring is with 30.0° slightly but distinctly lower than in both conformers of the uncomplexed ligand as shown in Table 5.3 (*cis*-**67d**: 36.5°, *trans*-**67d**: 33.2°).

The DFT calculations revealed that most of the carbon-carbon bond lengths differ less than 0.005 Å between the uncomplexed **67d** and [Zn(L$_d$)$_2$](PF$_6$)$_2$ **68d** (Figure 5.8). However, bonds that are shortened due to complexation are the pyridine-carbon-carbon-bonds adjacent to the pyridine connecting bonds. The respective bond lengths differ from 0.006 to 0.01 Å (0.4–0.7%) between [Zn(L$_d$)$_2$](PF$_6$)$_2$ **68d** and any of the conformers of **67d** and are colored pale red in Figure 5.8. The most significant shortened bond (0.013 Å, 0.9%) due to complexation is the ph-py-bond with a length of 1.468 Å in [Zn(L$_d$)$_2$](PF$_6$)$_2$ **68d** compared to 1.481 and 1.482 Å in all-*cis*-**67d** and all-*trans*-**67d**, respectively (Figure 5.8, red labels). Besides the bond shortening, significant bond-elongations of 0.008 Å (0.6%) are observed for the pyridine-carbon-carbon-bonds adjacent to the ph-py-bond (Figure 5.8, green labels). The value of the dihedral angle between phenyl and pyridine is lowered upon complexation. Concertedly, the ph-py-bond is shortened indicating a higher degree of π-delocalization between ph and py in [Zn(L$_d$)$_2$](PF$_6$)$_2$ **68d** compared to the free **67d** ligand. The lower dihedral angle goes along with a larger overlap of the π-orbitals of the carbon atoms of the ph-py-bond. Additionally, the shortening of the ph-py-bond indicates a higher bond order and with it also a higher π-character of the ph-py-bond.

Figure 5.8 *Bond lengths in the ligand L₄ and the corresponding complex [Zn(Ld)₂](PF₆)₂* **68d** *as derived from DFT calculations. Significant changes upon complexation. Pale red: 0.006–0.01 Å shortened bonds; red: >0.01 Å shortened bond; green: >0.006 Å elongated bonds.*

Regarding the Raman spectra of **67d** and [Zn(Ld)₂](PF₆)₂ **68d** the most intense Raman bands appear at comparable wavenumbers and with comparable relative Raman intensities (Figure 5.9). Hence, the vibrational pictures of Zn(Ld)₂](PF₆)₂ **68d** underlying these intense bands, *e.g.* the aromatic in plane vibrations, are comparable to the ones of **67d**, described in the previous section. Identical or energetically closely spaced vibrations on both ligands in [Zn(Ld)₂](PF₆)₂ **68d**, with appropriate orientations of the vibrational transition dipole moments, couple. That leads to a splitting of L-modes giving rise to symmetrical and 180° phase shifted modes in [Zn(Ld)₂](PF₆)₂ **68d**, slightly shifted to higher or lower wavenumbers. Hence, the differences in the Raman spectra, *e.g.* the vibration corresponding to the band at 1362 cm⁻¹ in the Raman spectrum of **67d** (see Figure 5.7), is assigned to the band at 1370 cm⁻¹ in the Raman spectrum of [Zn(Ld)₂](PF₆)₂ **68d** (Figure 5.9, Table 5.3), are due to geometrical changes upon complexation and slight shifts caused by mode-coupling in [Zn(Ld)₂](PF₆)₂ **68d** to some extend. The DFT-calculated Raman spectrum is in good agreement with the experimental Raman spectrum (see Figure 5.9) and is based on the fully optimized geometry of the [Zn(Ld)₂](PF₆)₂ **68d**, which is depicted in Figure 5.10 with the respective atomic labels.
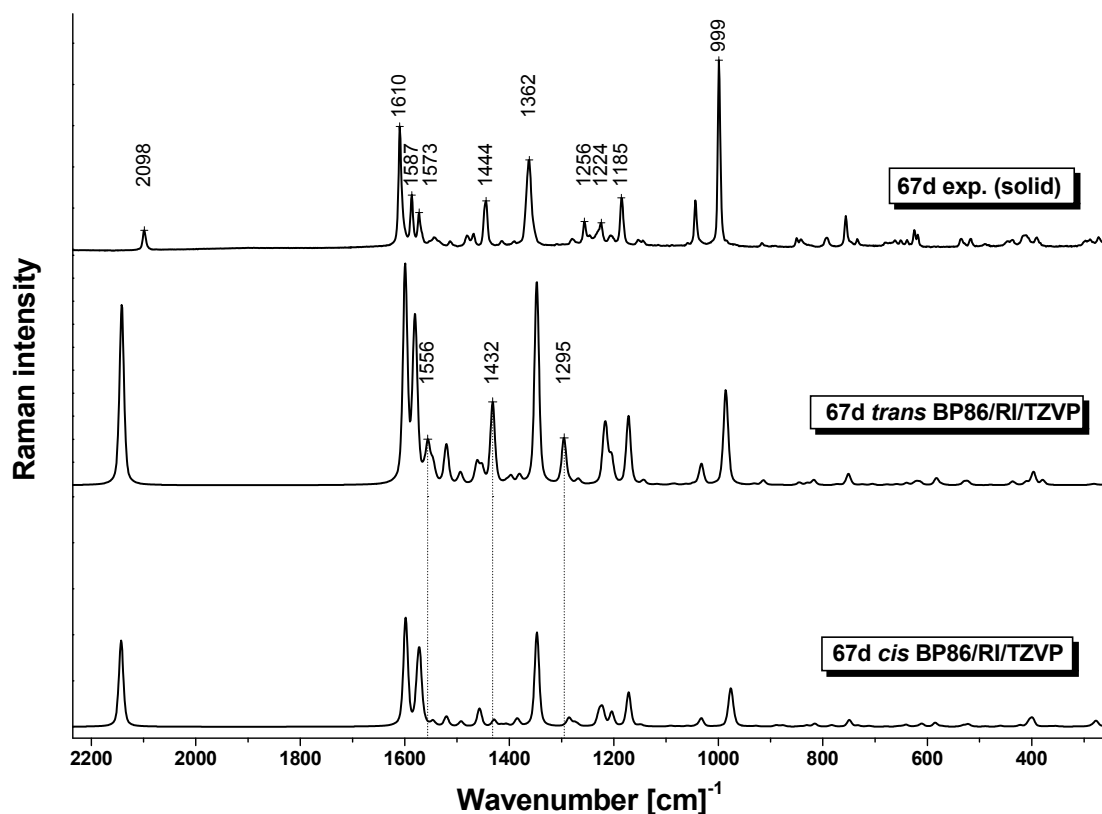
Figure 5.9 *Raman spectra: experimental (top) and DFT calculated (bottom; BP86 functional, def2-TZVP basis set, RI-approximation) of the [Zn(L$_d$)$_2$]$^{2+}$* **68d.**
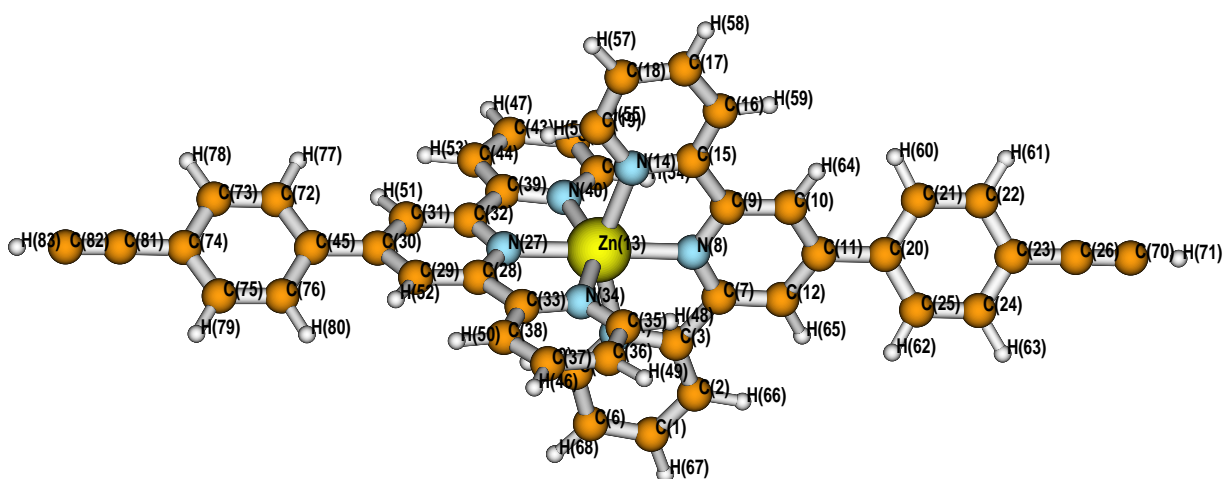
Figure 5.10. *DFT calculated structure of [Zn(L$_d$)$_2$]$^{2+}$* **68d** *with atomic labels.*

5.2.3.3 Tracing the change of the electron density distribution in the ph-py-bond due to complexation by means of Raman spectroscopy

As previously discussed, the changes in the geometry due to complexation, as reflected by the shortening of the ph-py-bond and the lowering of the dihedral angle between ph and py, indicate a higher bond order and with it a higher π-character of the ph-py-bond. It is possible to trace these changes by means of Raman spectroscopy, since a marker band is present, which involves significant ph-py-bond stretchings. This marker band is the trigonal ring breathing mode ρ(ph-py(trig)) involving strong ph-py bond stretchings and appearing around 1365 cm^{-1} in the experimental RS (see Table 5.3). It is basically located on the central pyridine ring with strong movements of the substituted carbon atoms. Thus, strong stretchings of the ph-py bond and the inter-pyridine bonds are involved, as shown in the lower graph of Figure 5.12. An increased bond order due to complexation in the ph-py bond goes along with a higher force constant and is expected to give rise to a shift to higher wavenumbers of (ν(ph-py(trig)). Comparing (ν(ph-py(trig))between **67d** and [Zn(L$_d$)$_2$](PF$_6$)$_2$ **68d** one has to account for the twofold existence of **67d** in the complex and the parallel vibrational transition dipole moments of (ν(ph-py(trig))of the two ligands in [Zn(L$_d$)$_2$](PF$_6$)$_2$ **68d**. The consequential mode-coupling leads to a splitting into a symmetric (ν(ph-py(trig))$_s$) and an asymmetric mode (ν(ph-py(trig)) as 180° phase-shifted **67d**-vibrations). The symmetric vibration is shifted to higher wavenumbers (ν(ph-py(trig))$_s$: 1351 cm^{-1}, Raman activity 6171 Å^4/amu) and the asymmetric vibration is shifted to lower wavenumbers (ν(ph-py(trig))$_{as}$: 1349 cm^{-1}, Raman activity 243 Å^4/amu) following our DFT calculations.

In the experimental Raman spectrum of [Zn(L$_d$)$_2$](PF$_6$)$_2$ **68d** the band at 1370 cm^{-1} has been assigned to (ν(ph-py(trig))$_s$ (ν(ph-py(trig))$_{as}$ not identified), which is correlated with the corresponding vibration in **67d** (ν(ph-py(trig)) at 1362 cm^{-1}. So, we have observed a total shift of the (ν(ph-py(trig)) mode of roughly 8 cm^{-1} when comparing (ν(ph-py(trig)) of **67d** and [Zn(L$_d$)$_2$](PF$_6$)$_2$ **68d**. This difference exceeds the expected wavenumber shift of 1 cm^{-1} due to splitting of this mode in a symmetric and an antisymmetric mode and hence, follows from the higher bond order in the ph-py-bond and with it from the increased π-electron delocalization between phenylene and pyridine upon complexation (see Table 5.3). The correlation between the bond length of the ph-py-bond and the shift of the (ν(ph-py(trig))-vibration to higher wavenumbers is schematically illustrated in Figure 5.11.
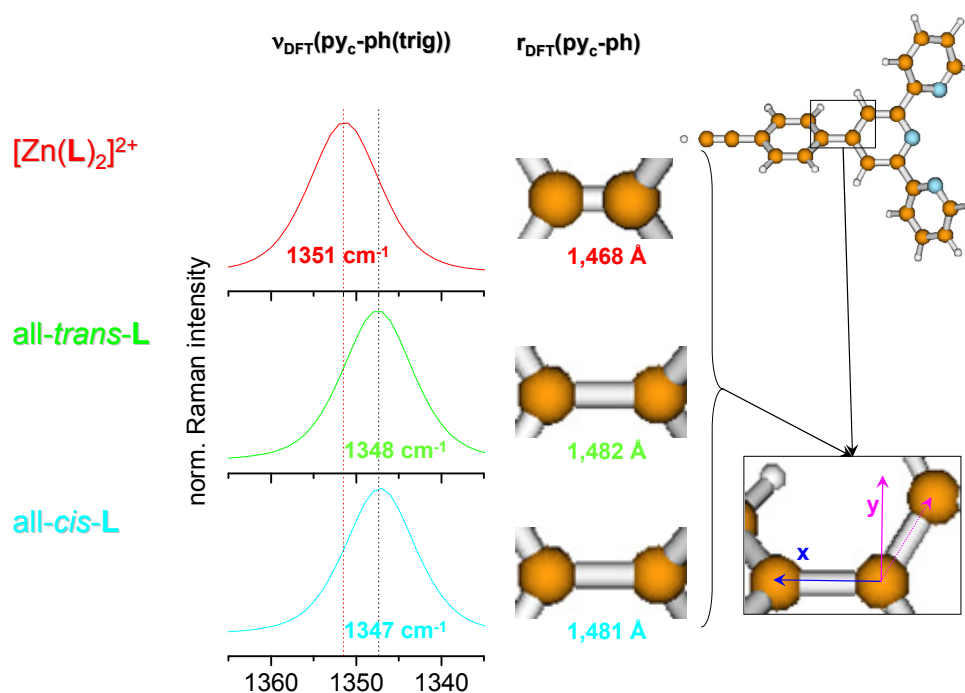
Figure 5.11 *Sketch of the correlation between the Raman shift of ν(ph-py(trig)) and the bond shortening of the ph-py-bond upon complexation. Definition of the central pyridine plane: magenta and blue arrows.*

The higher π-delocalization is further corroborated by the higher calculated Raman activity of $(\nu(\text{ph-py(trig})))_s$ in $[\text{Zn}(L_d)_2](\text{PF}_6)_2$ **68d**. This is due to a higher π-character of the ph-py-bond, which causes a higher electronic polarizability α and, consequently, a higher Raman activity of $(\nu(\text{ph-py(trig)}))$. Together with the Raman activity of $(\nu(\text{ph-py(trig)}))_{as}$ the summed Raman activity is with 6413 Å^4/amu roughly four times higher than in the case of *cis*- and *trans*-**67d** (1400 and 1692 Å^4/amu, respectively). This finding cannot be explained simply by invoking the twofold existence of **67d** in $[\text{Zn}(L_d)_2](\text{PF}_6)_2$ **68d** (2×1692 Å^4/amu = 3384 Å^4/amu) and hence points to an increase of the π-character of the ph-py-bond due to complexation. The calculated increase in the Raman activity of $(\nu(\text{ph-py(trig)}))$ in cause of complex formation is difficult to confirm experimentally, since the two substances exhibit different scattering cross sections. Therefore, the $(\nu(\text{ph-py(trig)}))$ Raman band has been normalized to the band of the trigonal ring breathing mode $(\delta(\text{ip(trig. ring br.)}))$. The vibrational picture of $(\nu(\text{ph-py(trig)}))$ as well as of $\delta(\text{ip(trig. ring br.)})$ is shown in Figure 5.12. The $\delta(\text{ip(trig. ring br.)})$-mode is mainly located at the terpyridine moiety and is assumed to be considerably less dependent on the binding situation in ph-py, since it does not involve $\nu(\text{ph-py})$ vibrations.
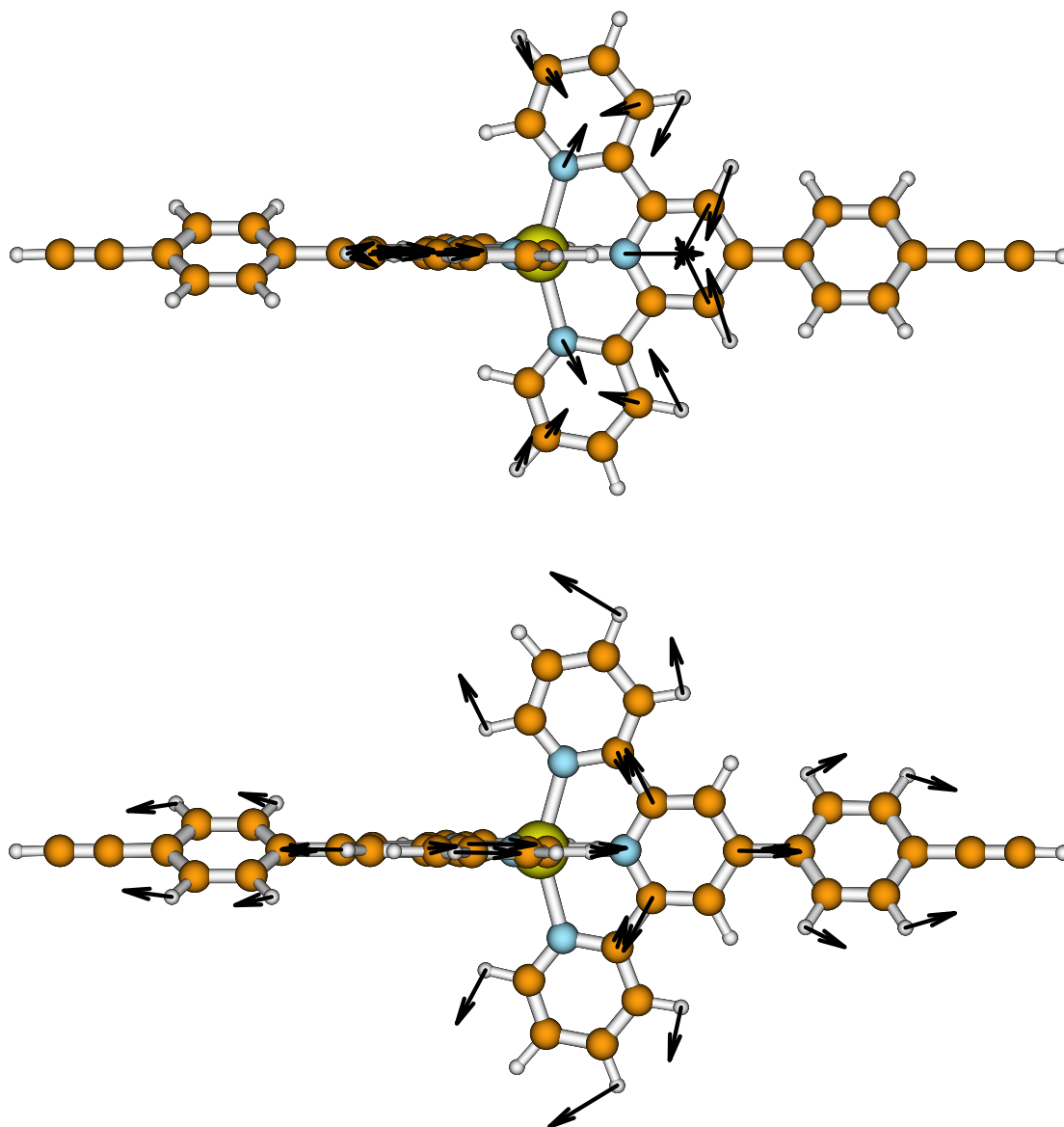
Figure 5.12 *DFT-calculated vibrational pictures of [Zn(L$_d$)$_2$](PF$_6$)$_2$ **68d**. Top: Trigonal ring breathing mode δ$_{ip}$(trig. ring br.) at 1010 cm^{-1}. Bottom: ν(ph-py(trig)) vibration at 1351 cm^{-1}.*

The quotient of the integrated Raman bands corresponding to ν(ph-py(trig)) and to δ$_{ip}$(trig. ring br.) is listed in Table 5.3. As can be seen, the value corresponding to the Raman data of [Zn(L$_d$)$_2$](PF$_6$)$_2$ **68d** (1.35) is roughly twice the value of **67d** (2 × 0.77) confirming the theoretical results (RA{[Zn(L$_4$)$_2$](PF$_6$)$_2$-ν(ph-py(trig))s+as} = 6413 Å^4/amu, 2 × RA{trans-**67d**-ν(ph-py(trig))} = 3384 Å^4/amu). With it, the theoretical predicted increase of the Raman activity of ν(ph-py(trig)) of [Zn(L$_d$)$_2$](PF$_6$)$_2$ **68d** compared to **67d** is confirmed experimentally and further evidences the increase of the π-character of the ph-py-bond in **67d** due to complexation. The changes of geometrical parameters upon complexation as well as the Raman shifts and Raman intensity changes are summarized in Table 5.3.

Table 5.3. *Selected parameters indicating variations in the π-electron delocalization due to complexation.*

Compound	ǫ[°] [a]	r(p$_{yc}$-ph) [Å] [b]	Wavenumber [cm^{-1}] [c]		Raman [c]	
	DFT	DFT	DFT	exp.	Activity [Å^4/amu]	Int. ratio
cis-**L$_d$** 67d	36.5	1.481	1347.2	1362	1400	0.772
trans-**L$_d$** 67d	33.2	1.482	1347.5		1692	
[Zn(L$_d$)$_2$](PF$_6$)$_2$ 68d	30.0	1.468	1351.4	1370	6171	1.345

[a]*Dihedral angle between the central pyridine-ring and the phenyl-substituent (py-ph).* [b]*Bond length between the central pyridine-ring and the phenyl-substituent.* [c]*Raman activity: DFT calculated, Raman intensity ratio: experimentally determined, v(ph-py(trig)).*

5.2.3.4 Conclusion of the theoretical calculations

A general question discussed in context with the photophysical and electrochemical properties is the degree of the disturbance of the π-electron conjugation between adjacent aromatic rings due to the torsion caused by sterical repulsions. Thus, we focused this study on this particular question. As the bathochrome absorption band of the ligand, assigned to phenyl-localized transitions, is red-shifted due to complexation, we supposed a change in the π-character of the ph-py-bond and, thus an increase of the π-delocalization between the phenylene and the terpyridine moiety. The higher π-character of the ph-py-bond in the complex [Zn(L$_d$)$_2$](PF$_6$)$_2$ **68d** compared to the free ligand was verified by DFT calculations as well as experimental Raman studies. Upon complexation, the DFT calculations offered a reduced dihedral angle between ph and py, a shortening of the ph-py-bond and a higher wavenumber of the v(h-py(trig)) vibration, since it involves strong ph-py-bond stretchings, which was be confirmed experimentally. The v(h-py(trig)) vibration revealed a significant higher Raman intensity in [Zn(L$_d$)$_2$](PF$_6$)$_2$ **68d** than in **67d**, which could also be verified experimentally. This correlates well with the higher ellipticity in the bond-critical-point of the ph-py-bond, according to our QTAIM-study, since a higher delocalization corresponds with a higher polarizability. Utilizing various techniques such as *e.g.* Raman-, UV-Vis and photoluminescence spectroscopy studies as well as DFT, it is possible to investigate the influence of different

para-phenylene-substituents on the photophysical properties of the derived zinc(II) complexes. Within this context also the influence of the substituents on the terpyridine-phenylene-π-conjugation will be a focus for further studies in order to design optimized materials for PLED and lighting applications.

5.3 Zn(II) coordination polymers

Coordination polymers are based on reversible interactions that can be manipulated by varying the external factors such as concentration and temperature as already discussed (in Chapters 3 and 4). To construct metallo-chain extended polymers, telechelic monomers with self-assembling end-groups are required. A large variety of telechelic macro-monomers bearing chelating metal-groups are already described in the literature and have been used for metallo-polymerization.[25-27] As previously discussed for Zn(II) model complexes (see 5.2), also in the case of metallo-coordination polymers the importance of the metal ion can not be neglected. Only by varying the metal ion different properties of the metallo-terpyridine assemblies could be achieved such as *e.g.* defined structures and high stability for Ru(II) or Ni(II) ions, switchability but no emissive properties for Fe(II) ions, emissive properties based on MLCT-emission (metal-to-ligand charge transfer) for Ir(III) and Pt(II) ions or ILCT-based emission (*intra*-ligand charge transfer) when Zn(II) ions are utilized. Moreover, π-conjugated polymers are nowadays intensively studied for the possibility of designing systems with applications in display and sensor technologies.[28] By combining the metal binding domains with conjugated systems, new macro-monomers can be made available for further metallo-complexation. Due to their enhanced rigidy, the utilized macro-monomers result in the formation of linear chain extended metallo-assemblies characterized by novel properties and enhanced photophysical qualities compared to the starting materials.[9,11]

5.3.1 Synthesis and characterization

A series of novel Zn(II) coordination polymers containing *bis*-terpyridine ligands bearing various rigid and conjugated spacers were synthesized *via* self-assembling reactions, generally described in Scheme 5.2 and Table 5.4. The synthesis and characterization of the utilized telechelic macro-monomers **70a-d** is discussed elsewhere and it was not part of the present described research.[16,29] The one-step synthesis of Zn(II) chain extended polymers **71a-d** was performed by heating an equimolecular amount (1:1) of one of the telechelic macro-monomers **70a-d** and Zn(OAc)$_2$, in NMP (*N*-methylpyrrolidinone) overnight under reflux

followed by anion exchange with ammonium hexafluorophosphate. The purification of the resulting reaction product was achieved by repetitive precipitations (3 times) of the resulting metallo-polymer from acetonitrile into cold ethylic ether. The purified Zn(II) coordination polymers were further characterized by means of various techniques as will be discussed in the following.
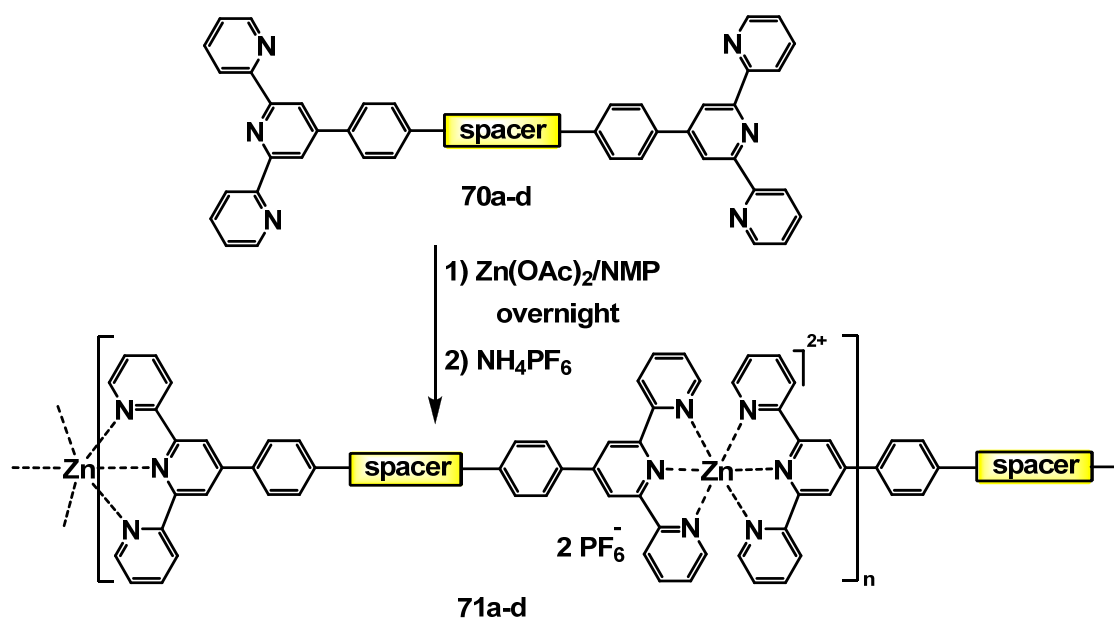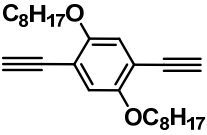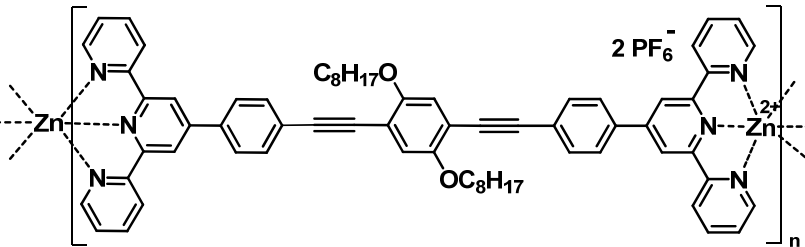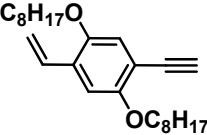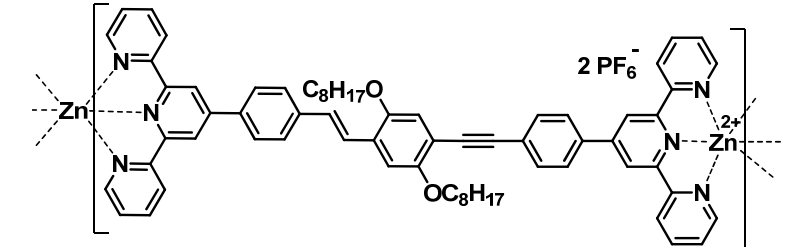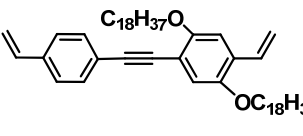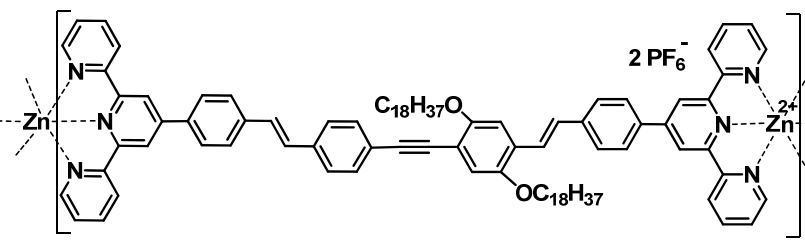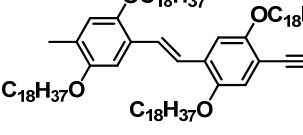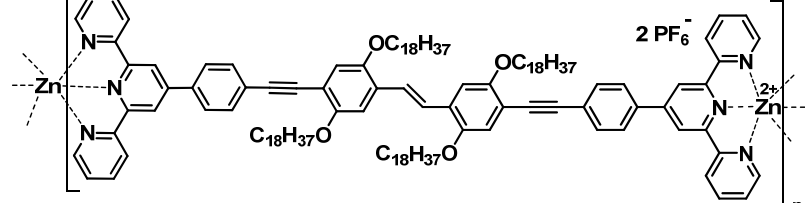
Scheme 5.2: *General representation of the synthesis of Zn(II) bis-terpyridine coordination polymers **71a-d** bearing various conjugated spacers.*

First of all, it was observed that the synthesized Zn(II) coordination polymers exhibited a different solubility behavior compared to the constituent macro-monomers. This behavior could be taken as an indication that the metal ion was attached to the core of the chelating macro-monomer and, subsequently, creates higher molar mass assemblies carrying the rigid spacer of the monomer units. Therefore, the presence of the alkoxy chains as lateral substituents of the phenyl ring from the macro-monomer unit can (partially) solve the frequently met solubility issue for this type of metallo-polymers. Recently improvement of the solubility and processability (spin-coating, inkjet printing, film formation) was performed by incorporation of polymeric side chains.[30] Furthermore, the influence of the counter ion (PF_6^-) should not be neglected, while talking about the solubility, since it is known that by simply changing the counter ion from chloride or acetate to ammonium phosphate, the solubility of such metallo-assemblies could be easily manipulated (see Chapters 3 and 4).

As a result of the characteristic weak binding strength of the Zn(II)tpy$_2$ connectivity compared to the analogous Ru(II) and Ni(II) *bis*-terpyridine complexes, it is not possible to perform

SEC characterizations on Zn(II) coordination polymers.[2,31,32] Thus, the main characterization technique for the synthesized Zn(II) supramolecular polymers is ^{1}H-NMR spectroscopy.

Table 5. 4. *Overview of the synthesized Zn(II) coordination polymers 71a-d based on bis-terpyridine ligands 70a-d.*

Spacer from *bis*-terpyridine ligand L	Zn(II) coordination polymer
70a	71a
70b	71b
70c	71c
70d	71d

The ^{1}H-NMR spectra of **71a-d** recorded in deuterated DMSO revealed a set of broaden signals of the complexed terpyridine protons. The broadening of the signals is a common

observation for polymeric materials. The formation of the Zn(II) coordination polymers is evidently indicated by the appearance of new ^{1}H-NMR signals and the absence of the original uncomplexed ^{1}H-NMR signals from the terpyridine moiety. The clear shifts observed for the complexed terpyridine protons could be taken as a confirmation for the formation of the Zn(II) *bis*-terpyridine connectivity that is characterized by an octahedral conformation which changes the environment of all complexed terpyridine protons. The assignment of ^{1}H-NMR peaks of the complexed terpyridine units in the polymer structures are based on the comparison to the similar Zn(II) model complexes. Figure 5.13 displays the chemical shifts observed for terpyridine protons of polymer **71c** in comparison to the uncomplexed ditopic terpyridine ligand **70c** as a representative example. The unassigned signals are part of the conjugated spacer.
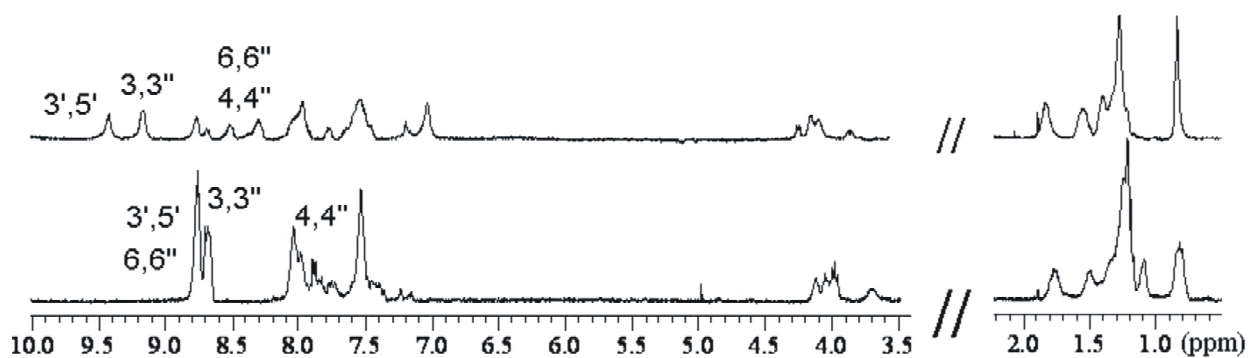
Figure 5.13: *Representative ^{1}H-NMR assigments for the terpyridine protons of 70c (bottom) and the corresponding Zn(II) coordination polymer 71c with PF$_6^-$ as counter ion (top) measured in DMSO-d$_6$ (the solvent is cut off).*

5.3.2 Photophysical properties

The photophysical properties of the synthesized Zn(II) coordination polymers **71a-d** were investigated by measuring the UV-Vis absorption and emission spectra at low concentration in a CHCl$_3$ and DMF (v:v 2:1) solvent mixture at room temperature. The results are summarized in Table 5.5 and compared to the uncomplexed ligands **70a-d**. Thus, the telechelic macro-monomers **70a-d** revealed characteristic absorptions between 250-450 nm, where the shorter absorptions wavelength belong to the terpyridine units and the longer wavelength absorptions are related to the conjugated spacer between the terpyridine moieties. These results are in agreement with the observations for the *mono*-terpyridine ligands **67a-h** and the Zn(II) model complexes already discussed in 5.2. The presence of Zn(II) ions in the molecular structure of the synthesized coordination polymers **71a-d** is clearly indicated by the observed red shifts in the recorded absorption spectra. Apart from the specific ligand absorption bands (including terpyridine moiety and characteristic absorption for the

conjugated spacer), the coordination polymers exhibited ligand-centered (LC) $\pi^* \leftarrow \pi$ or $\pi^* \leftarrow n$ absorption of the Zn(II)tpy$_2$ connectivity. Generally speaking, for this type of metallo-polymeric structures **71a-d** two major effects were observed in UV-Vis absorption spectra: 1) the extinction coefficient decreases compared to the free ligands and 2) the red shifts were about 10 to 30 nm (compared to the uncomplexed ligands), which can be attributed to the inductive effects caused by the presence of the Zn(II) ions. Figure 5.14 illustrates a typical comparison between the absorption spectrum of the telechelic macro-monomer **70d** and the resulting Zn(II) coordination polymer **71d**. The shift observed for **71d** around 415 nm corresponds to a charge transfer (CT) that occured within the macro-monomer unit **70d** between the electron rich central chromophore (phenylene/ethynylene/vinylene etc.) segment and the metal-coordinated (electron-deficient) terpyridine moieties.[33] Table 5.5 displays all absorption data from which it could be concluded that none of the Zn(II) coordination polymers showed major modifications in the absorption transition bands.
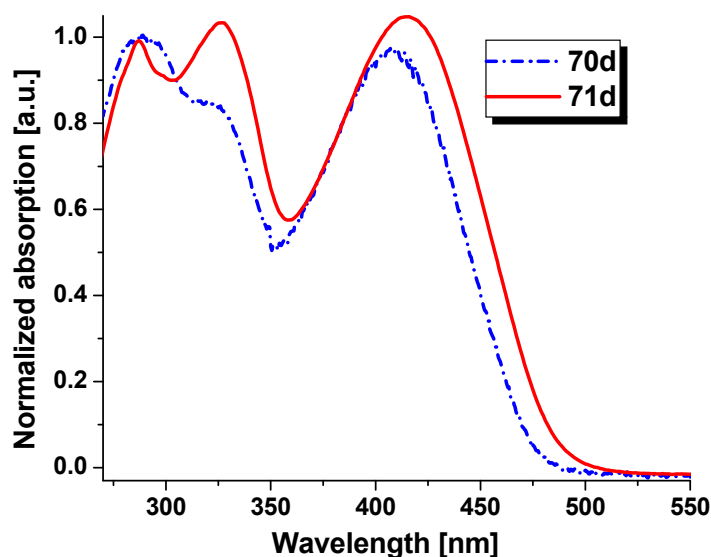
Figure 5.14: *UV-vis spectra of 70d (short dash doted line) and the corresponding Zn(II) coordination polymer 71d (solid line).*

Furthermore, the emission spectra of the discussed systems (**71a-d** compare to **70a-d**) were measured in solution (solvent mixture of CHCl$_3$ and DMF v:v 2:1) at room temperature (Table 5.6). All macro-monomers **70a-d** were emissive and, thus, the resulting Zn(II) coordination polymers **71a-d** were emissive too. Moreover, it was expected that the formed Zn(II)tpy$_2$ connectivity will increase the electron delocalization on the conjugated and rigid spacers, which can be observed in enhanced and red shifted PL emission spectra for **71a-d**. The experimental results obtained from the emission spectra showed that for the analyzed systems **71a-d** smaller Stokes shifts (red shifts) are observed when the samples are measured

in solution. This aspect might be explained by the fact that the synthesized metallo-supramolecular polymers tend to aggregate mainly due to the conjugated and rigid structure of the spacers from the constituent macro-monomers **70a-d**. Figure 5.15 pictures the emission spectra of ligand **70d** in comparison to the Zn(II) coordination polymer **71d** demonstrating the small red shift.
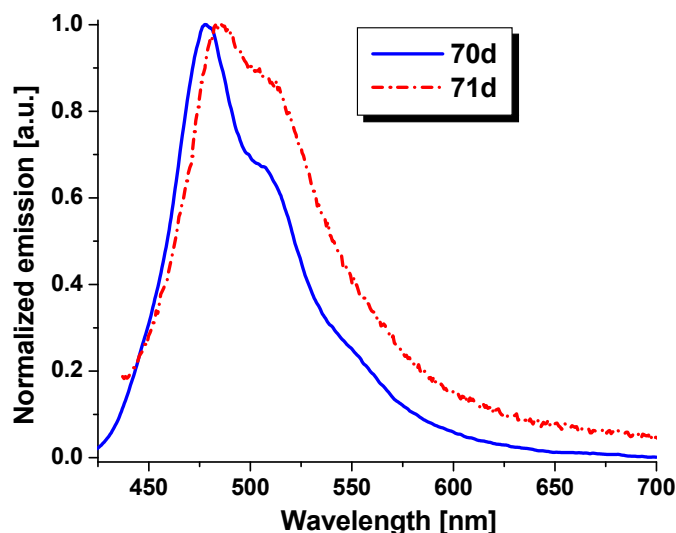
Figure 5.15: *Emission spectra of **70d** (solid line) and the corresponding Zn(II) coordination polymer **71d** (short dash doted line).*

The photoluminescence efficiency of the uncomplexed ligands and their Zn(II) coordination polymers were investigated by the photoluminescence quantum yield, Φ_{PL}. It was observed that upon complexation the emission efficiency decreases considerably. Since the influence of the conjugated spacer is essential in the photophysical properties of the synthesized Zn(II) coordination polymers, increasing the length and conjugation of the rigid spacer could be studied for improving the emissive characteristics of the Zn(II) supramolecular polymers.

5.3.3 Electrochemical properties

To determine the energy band structures of the Zn(II) coordination polymers **71a-d**, cyclic voltammetry (CV) was measured to investigate the reduction behavior of the analyzed structures. The results are summarized in Table 5.5. It was observed that all analyzed structures exhibited a reversible reduction wave around –0.80 V that could be attributed to the terpyridine ligand, as described in literature.[10] Moreover, the influence of various conjugated spacers from the macro-monomer units on the electrochemical behavior of the analyzed Zn(II) coordination polymers could be observed by the presence of other reduction waves.

Figure 5.16 illustrates the differences between the two Zn(II) supramolecular polymers **71b** and **71d** based on two different chelating macro-monomers **70b** respectively **70d**.
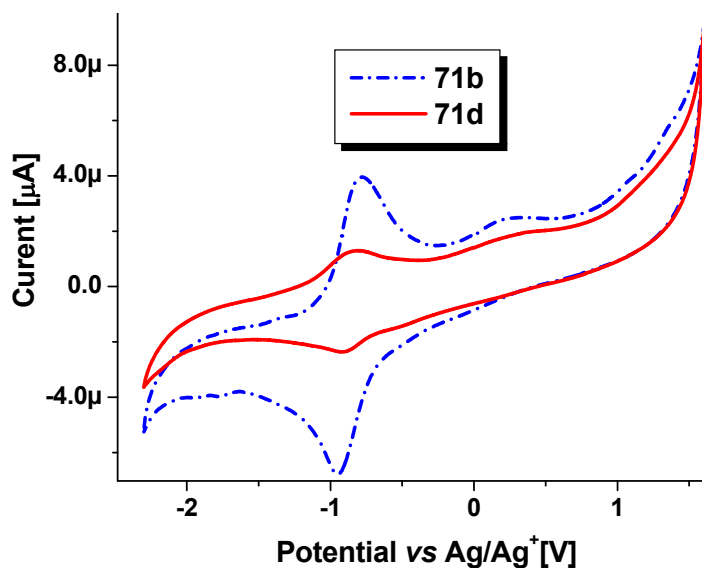
Figure 5.16: *Representative electrochemical properties of the Zn(II) coordination polymers 71b and 71d. The spectra were recorded in DMF containing 0.1 M TBAPF$_6$.*

Table 5.6. *Overview of the photophysical and electrochemical properties of the Zn(II) 71a-d coordination polymers in comparison to the constituent terpyridine ligands 70a-d.*

Compound	$\lambda_{abs,max}$ [nm]^a	$\lambda_{em,max}$ [nm]^a	$\Phi_{PL}{}^a$	$E_{1/2,red}$ [V]^b		
				2+/1+	1+/0	0/-1
70a	292, 321, 465	443	0.34	-	-	-
70b	281, 327, 398	468	0.63	-	-	-
70c	296, 345, 404	470	0.82	-	-	-
70d	295, 323, 409	478	0.90	-	-	-
71a	286, 326, 473	443	0.23	-0.78	-1.30	-1.72
71b	286, 327, 403	468	0.052	-0.80	-1.32	-
71c	286, 331, 403	470	0.36	-0.79	-1.32	-1.71
71d	285, 327, 414	485	0.40	-0.81	-	-

^{a} *Measurements were performed in a mixture of CHCl$_3$ and DMF (v:v 2:1) (10^{-5} M to 10^{-7} M, room temperature). ^{b}Potentials vs. SHE. Measurements were performed in DMF containing 0.1 M TBAPF$_6$.*

5.4 Conclusions

A series of Zn(II) model complexes based on *mono*-terpyridine ligands bearing various conjugated spacers in the 4'-position were synthesized and characterized. The photophysical properties were studied in detail and compared to the constituent chelating *mono*-terpyridine ligands that exhibited good photoluminescence properties. The formation of the Zn(II)tpy$_2$ connectivity was evidenced and discussed by means of various techniques. It was observed that the presence of the Zn(II) ions in the synthesized model complexes revealed interesting spectroscopic properties, in particular, enhanced fluorescence. Such Zn(II) systems are potentially interesting for the construction of PLED or lighting devices. Therefore, theoretical calculation were performed on an ethynyl-phenyl-substituted terpyridine ligand and its corresponding zinc(II) complex in order to model the influence of the substituents on the photophysical properties of the designed structures. The theoretical results will help the selection of further substituents with improved properties required for designing better PL devices. Moreover, *bis*-terpyridine ligands bearing similar conjugated and rigid spacers were used for the preparation of Zn(II) coordination polymers. The properties of the designed Zn(II) supramolecular polymers were investigated and compared to the uncomplexed ligands in order to understand the influence of the Zn(II) ions on the photophysical and electrochemical properties of the designed structures. The synthesized Zn(II) coordination polymers revealed red shifts in the absorption spectra (aprox. 30 nm) and smaller Stokes shifts in the emission spectra compared to the Zn(II) model complexes. Thus, from the experimental results it was concluded that the characteristics of the spacer (length and conjugation) are considerably influencing the photophysical and electrochemical properties of the Zn(II) coordination polymers.

5.5 Experimental section

Materials and general experimental details
Standard chemicals were obtained from Sigma-Aldrich and used as received unless otherwise specified. Compounds **67a-h, 69** and **70a-d** were synthesized by Dr. Andreas Winter.
Instrumentation. Nuclear magnetic resonance spectra were recorded on a Varian Gemini 400 MHz spectrometer at 298 K. Chemical shifts are reported in parts per million (δ) downfield from an internal standard, tetramethylsilane (TMS) in CD$_3$CN or DMSO-*d$_6$*. UV-Vis spectra were recorded on a Perkin Elmer Lamda-45 (1 cm cuvettes, CH$_2$Cl$_2$). Emission spectra were recorded on a Perkin Elmer LS50B luminescence spectrometer (1 cm cuvettes, CH$_3$CN). The photoluminescence quantum yields were determined with a module system of the C9920 series from Hamamatsu Photonics. The included integrated sphere allowed the measurement of absolute quantum yields. All the measurements were carried out at room temperature using non-degassed solvents. Electrochemical experiments were performed using an Autolab PGSTAT30 model potentiostat. A standard three electrode configuration was used, with a platinum-disk working electrode, a platinum-rod auxiliary electrode, and Ag/AgCl

reference electrode. Ferrocene was added at the end of each experiment as an internal standard. The oxidation potentials are quoted *versus* the ferrocene/ferrocenium couple (F_c/F_c^+). The measurements were carried out in different solvents containing 0.1 M TBAPF$_6$. The scan rate was 100 mV/s. The Raman spectra of the solid samples were recorded with a Jobin Yvon Labram HR-spectrometer, equipped with an Olympus BX41 inverse Microscope. The 830 nm output from a diode laser was used as Raman excitation source and the scattered light was detected with a CCD detector. A grating with 300 grooves/mm was applied leading to a spectral resolution of roughly 1 cm^{-1}. DFT calculations were carried out employing the program Turbomole.[34] The pure density functional of Becke and Perdew BP86 and the triple-ξ TZVP basis set (polarization function on all atoms) were used.[35] This Ahlrich-type basis set consists of 5s1p functions contracted to 3s1p for H (according to scheme [311/1]) and 11s6p1d functions contracted to 5s3p according to [62111/411/1] for B to Ne. For all calculations the resolution-of-the-identity (RI) technique was applied.[36]

General procedure for the synthesis of Zn(II) bis-terpyridine complexes [Zn(L)₂](PF₆)₂

To a solution of the *mono*(terpyridine) ligand **L** (1 mmol) in methanol (100 mL) a solution of Zn(OAc)$_2$·2H$_2$O (0.5 mmol) in methanol (30 mL) was added. After stirring at room temperature for 3 h, an excess of NH$_4$PF$_6$ was added. The precipitate was filtered off and washed successively with methanol (3 × 20 mL), water (2 × 20 mL) and diethyl ether (2 × 20 mL). Further purification of the crude product was achieved by recrystallisation from acetonitrile/diethylether. The complexes were finally dried under reduced pressure at 40 °C for 24 h yielding yellow-orange solid.[18]

[Zn(Lₐ)₂](PF₆)₂ (68a)

Yield: 87%. ^{1}H-NMR (400 MHz, CD$_3$CN, 25 ˚C): δ (ppm) = 9.00 (s, 4H, H$^{3'}$, H$^{5'}$), 8.74 (d, ^3J = 8.1 Hz, 4H, H^3, H$^{3''}$), 8.26-8.14 (m, 8H, H^4, H$^{4''}$ & H^{aryl}), 7.85 (d, ^3J = 5.5 Hz, 4H, H^6, H$^{6''}$), 7.78 (m$_c$, 6H, H^{aryl}), 7.42 (m$_c$, 4H, H^5, H$^{5''}$). ^{13}C NMR (CD$_3$CN, 25 ˚C): δ (ppm) = 155.4, 149.6, 147.7, 147.5, 136.5, 135.2, 128.4, 127.8, 127.6, 127.1, 122.8, 121.0. ESI-MS: *m/z* = 827.14 ([M – PF$_6$]$^+$). Anal. calcd. (%) for C$_{42}$H$_{30}$F$_{12}$N$_6$P$_2$Zn: C, 51.79; H, 3.10; N, 8.63. Found: C, 51.66; H, 3.15; N, 8.69.

[Zn(L_b)₂](PF₆)₂ (68b)

Yield: 92%. ^{1}H-NMR (400 MHz, CD$_3$CN, 25 ˚C): δ (ppm) = 8.97 (s, 4H, H$^{3'}$, H$^{5'}$), 8.72 (d, ^3J = 8.1 Hz, 4H, H^3, H$^{3''}$), 8.20 (m, 4H, H^4, H$^{4''}$), 8.12 (d, ^3J = 8.0 Hz, 4H, H^{aryl}), 7.96 (d, ^3J = 8.0 Hz, 4H, H^{aryl}), 7.85 (d, ^3J = 5.3 Hz, 4H, H^6, H$^{6''}$), 7.43 (m, 4H, H^5, H$^{5''}$). ESI-MS: *m/z* = 982.97 ([M – PF$_6$]$^+$). Anal. calcd. (%) for C$_{42}$H$_{28}$Br$_2$F$_{12}$N$_6$P$_2$Zn: C, 44.57; H, 2.49; N, 7.43. Found: C, 44.90; H, 2.31; N, 7.18.

[Zn(L_c)₂](PF₆)₂ (68c)

Yield: 85%. ^{1}H-NMR (400 MHz, CD$_3$CN, 25 ˚C): δ (ppm) = 9.00 (s, 4H, H$^{3'}$, H$^{5'}$), 8.74 (d, ^3J = 8.2 Hz, 4H, H^3, H$^{3''}$), 8.23-8.17 (m, 8H, H^4, H$^{4''}$ & H^{aryl}), 7.86 (m, 8H, H^6, H$^{6''}$ & H^{aryl}), 7.43 (dd, ^3J = 7.1 Hz, ^3J = 5.2 Hz, 4H, H^5, H$^{5''}$), 6.97 (dd, ^3J = 18.3 Hz, ^3J = 11.0 Hz, 2 H, H^{olefin}), 6.09 (d, ^3J = 18.3 Hz, 1H, H^{olefin}), 5.51 (d, ^3J = 11.0 Hz, 1H, H^{olefin}). ESI-MS: *m/z* = 879.18 ([M – PF$_6$]$^+$). Anal. calcd. (%) for C$_{46}$H$_{34}$F$_{12}$N$_6$P$_2$Zn: C, 53.84; H, 3.34; N, 8.19. Found: C, 53.57; H, 3.55; N, 7.87.

[Zn(L_d)₂](PF₆)₂ (68d)

Yield: 81%. ^{1}H-NMR (400 MHz, CD$_3$CN, 25 ˚C): δ (ppm) = 8.9 (s, 4H, H$^{3'}$, H$^{5'}$), 8.73 (d, ^3J = 8.0 Hz, 4H, H^3, H$^{3''}$), 8.26-8.17 (m, 8H, H^4, H$^{4''}$ & H^{aryl}), 7.89 (d, ^3J = 8.5 Hz, 4 H, H^{aryl}), 7.85 (d, ^3J = 4.9 Hz, H^6, H$^{6''}$), 7.43 (m, 4H, H^5, H$^{5''}$), 3.70 (s, 1H, H^{ethynyl}). ESI-MS: *m/z* = 875.15 ([M – PF$_6$]$^+$). Anal. calcd. (%) for C$_{46}$H$_{30}$F$_{12}$N$_6$P$_2$Zn: C, 54.06; H, 2.96; N, 8.22. Found: C, 54.32; H, 3.17; N, 8.05.

[Zn(L_e)₂](PF₆)₂ (68e)

Yield: 81%. ^{1}H-NMR (400 MHz, CD$_3$CN, 25 ˚C): δ (ppm) = 10.41 (s, 2H, H^{CHO}), 9.01 (s, 4H, H$^{3'}$, H$^{5'}$), 8.74 (d, ^3J = 8.1 Hz, 4H, H^3, H$^{3''}$), 8.27 (d, ^3J = 8.8 Hz, 4H, H^{aryl}), 8.21 (m, 4H, H^4, H$^{4''}$), 7.93 (d, ^3J = 8.8 Hz, 4H, H^{aryl}), 7.87 (d, ^3J = 5.0 Hz, H^6, H$^{6''}$), 7.44 (dd, ^3J = 5.0 Hz, ^3J = 7.1 Hz, 4H, H^5, H$^{5''}$), 7.38 (s, 1 H, H^{aryl}), 7.36 (s, 1 H, H^{aryl}), 4.16 (m, 8H, H^{alkyl}), 1.88 (m, 8H, H^{alkyl}), 1.62 (m$_c$, 4H, H^{alkyl}), 1.54 (m, 4H, H^{alkyl}), 1.48-1.30 (m, 32H, H^{alkyl}), 0.91 (m, 12H, H^{alkyl}). ESI-MS: *m/z* = 1595.68

([M − PF$_6$]$^+$). Anal. calcd. (%) for C$_{92}$H$_{102}$F$_{12}$N$_6$O$_6$P$_2$Zn: C, 63.39; H, 5.90; N, 4.82. Found: C, 63.55; H, 6.12; N, 5.07.

[Zn(L$_f$)$_2$](PF$_6$)$_2$ (68f)

Yield: 94%. ^{1}H-NMR (400 MHz, CD$_3$CN, 25 ˚C): δ (ppm) = 9.00 (s, 4H, H$^{3'}$,H$^{5'}$), 8.73 (d, 4H, ^{3}J = 8.1 Hz, H^3,H$^{3''}$), 8.24 (d, 4H, ^{3}J = 7.9 Hz, H^{aryl}), 8.15 (m, 4H, H^4,H$^{4''}$), 7.91-7.85 (m, 8H, H^6,H$^{6''}$ & H^{aryl}), 7.45 (m, 4H, H^5,H$^{5'}$), 7.29 (d, 2H, ^{3}J = 15.7 Hz, H^{olefin}), 7.16-7.09 (m, 4H, H^{aryl} & H^{olefin}), 6.96 (s, 2H, H^{aryl}), 4.05-3.96 (m, 8H, H^{alkyl}), 1.74 (m, 4H, H^{alkyl}), 1.68 (m, 4H, H^{alkyl}), 1.49 (m, 4H, H^{alkyl}), 1.44 (m, 4H, H^{alkyl}), 1.41-1.28 (m, 32H, H^{alkyl}), 0.96 (m, 12H, H^{alkyl}). ESI-MS: m/z = 1699.54 ([M − PF$_6$]$^+$). Anal. calcd. (%) for C$_{90}$H$_{104}$Br$_2$F$_{12}$N$_6$O$_4$P$_2$Zn: C, 58.46; H, 5.67; N, 4.55. Found: C, 58.19; H, 5.34; N, 4.28.

[Zn(L$_g$)$_2$](PF$_6$)$_2$ (68g)

Yield: 88%. ^{1}H-NMR (400 MHz, CD$_3$CN, 25 ˚C): δ (ppm) = 8.98 (s, 4 H, H$^{3'}$, H$^{5'}$), 8.75 (d, ^{3}J = 8.1 Hz, 4H, H^3, H$^{3''}$), 8.26-8.17 (m, 8H, H^4, H$^{4''}$ & H^{aryl}), 7.93-7.87 (m, 8H, H^6, H$^{6''}$ & H^{aryl}), 7.44 (mc, 4H, H^5, H$^{5''}$), 7.36 (d, ^{3}J = 16.9 Hz, 2 H, H^{olefin}), 7.26-7.16 (m, 6H, H^{aryl} & H^{olefin}), 6.97 (d, ^{3}J = 8.3 Hz, 2H, H^{aryl}), 4.07 (t, ^{3}J = 6.5 Hz, 4H, H^{alkyl}), 3.95 (t, ^{3}J = 6.4 Hz, 4H, H^{alkyl}), 1.76 (m$_c$, 4H, H^{alkyl}), 1.67 (m, 4H, H^{alkyl}), 1.50 (m, 4H, H^{alkyl}), 1.44 (m, 4H, H^{alkyl}), 1.40-1.30 (m, 16H, H^{alkyl}), 0.94 (m, 12H, H^{alkyl}). ESI-MS: m/z = 1431.60 ([M − PF$_6$]$^+$). Anal. calcd. (%) for C$_{82}$H$_{90}$F$_{12}$N$_6$O$_4$P$_2$Zn: C, 62.38; H, 5.75; N, 5.32. Found: C, 62.51; 5.63; N, 5.49.

[Zn(L$_h$)$_2$](PF$_6$)$_2$ (68h)

Yield: 83%. ^{1}H-NMR (400 MHz, CD$_3$CN, 25 ˚C): δ (ppm) = 9.02 (s, 4H, H$^{3'}$, H$^{5'}$), 8.75 (d, ^{3}J = 8.1 Hz, 4H, H^3, H$^{3''}$), 8.26 (d, ^{3}J = 9.0 Hz, 4H, H^{aryl}), 8.21 (m, 4H, H^4, H$^{4''}$), 7.90 (d, ^{3}J = 8.7 Hz, 4H, H^{aryl}), 7.87 (d, ^{3}J = 4.2 Hz, 4H, H^6, H$^{6''}$), 7.62 (d, ^{3}J = 7.1 Hz, 4H, H^{aryl}), 7.54 (d, ^{3}J = 16.7 Hz, 2H, H^{olefin}), 7.46-7.40 (m, 10H, H^{aryl}), 7.36 (d, ^{3}J = 15.5 Hz, 2H, H^{olefin}), 7.36 (s, 2H, H^{aryl}), 7.18 (s, 2H, H^{aryl}), 4.20 (t, ^{3}J = 6.8 Hz, 4H, H^{alkyl}), 4.10 (t, ^{3}J = 5.5 Hz, 4H, H^{alkyl}), 1.94-1.85 (m, 8H, H^{alkyl}), 1.68-1.55 (m, 8H, H^{alkyl}), 1.50-1.33 (m, 32H, H^{alkyl}), ESI-MS: m/z = 1743.78 ([M − PF$_6$]$^+$). Anal. calcd. (%) C$_{106}$H$_{114}$F$_{12}$N$_6$O$_4$P$_2$Zn: C, 67.31; H, 6.08; N, 4.44. Found: C, 67.18; H, 5.77; N, 4.56.

General procedure for the synthesis of Zn(II) coordination polymers

A solution of zinc acetate (0.52 mmol) in NMP (10 mL) was added dropwise to a solution of the chelating monomer **70a-d** (0.52 mmol) in 30 mL of *N*-methylpyrrolidinone (NMP). The resulting solution was heated at 105 °C under an argon atmosphere. After overnight heating and stirring, a ten fold excess of NH$_4$PF$_6$ was added to the reaction mixture that was further heated and stirred for an additional hour. Purification of the crude material was performed by repetitive precipitation (3 times) of the obtained metallo-polymer dissolved in acetonitrile into cold diethyl ether. The final polymers were dried under reduced pressure at 40 °C for 24 h and collected as yellow-orange solids.[10]

[Zn(L)$_2$]$_n$(PF$_6$)$_{2n}$ (71a)

Yield: 79%. ^{1}H-NMR (400 MHz, DMSO-d_6, 25 ˚C): δ (ppm) = 9.43 (m, 4H, H$^{3'}$, H$^{5'}$), 9.16 (m, 4H, H^3, H$^{3''}$), 8.77 (m, 4H, H^{aryl}), 8.55 (m, 4H, H^4, H$^{4''}$), 8.35 (m, 4H, H^{aryl}), 7.96 (m, 4H, H^5, H$^{5''}$), 7.68 (m, 4H, H^6, H$^{6''}$), 7.52 (m, 4H, H^{aryl}), 4.11 (m, 8H, H^{alkyl}), 1.83 (m, 8H, H^{alkyl}), 1.54 (m, 4H, H^{alkyl}), 1.53 (m, 4H, H^{alkyl}), 1.48-1.32 (m, 32H, H^{alkyl}), 0.88 (m, 12H, H^{alkyl}).

[Zn(L)$_2$]$_n$(PF$_6$)$_{2n}$ (71b)

Yield: 73%. ^{1}H-NMR (400 MHz, DMSO-d_6, 25 ˚C): δ (ppm) = 9.44 (m, 4H, H$^{3'}$, H$^{5'}$), 9.16 (m, 4H, H^3, H$^{3''}$), 8.76 (m, 4H, H^{aryl}), 8.52 (m, 4H, H^4, H$^{4''}$), 8.35 (m, 4H, H^{aryl}), 7.96 (m, 4H, H^5, H$^{5''}$), 7.68 (m, 4H, H^6, H$^{6''}$), 7.52 (m, 1H, H^{aryl}), 4.10 (m, 8H, H^{alkyl}), 1.85 (m, 8H, H^{alkyl}), 1.55 (m, 4H, H^{alkyl}), 1.54 (m, 4H, H^{alkyl}), 1.48-1.30 (m, 32H, H^{alkyl}), 0.89 (m, 12H, H^{alkyl}).

[Zn(L)$_2$]$_n$(PF$_6$)$_{2n}$ (71c)

Yield: 78%. ^{1}H-NMR (400 MHz, DMSO-d_6, 25 ˚C): δ (ppm) = 9.43 (m, 4H, H$^{3'}$, H$^{5'}$), 9.16 (m, 4H, H^3, H$^{3''}$), 8.76 (m, 4H, H^{aryl}), 8.48 (m, 4H, H^4, H$^{4''}$), 8.29 (m, 4H, H^{aryl}), 7.96 (m, 8H, H^{aryl} & H^6, H$^{6''}$), 7.53

(m, 4H, H^5, H$^{5''}$), 7.18 (m, 2H, H^{aryl}), 7.03 (s, 1H, H^{aryl}), 4.03 (m, 8H, H^{alkyl}), 1.84 (m, 8H, H^{alkyl}), 1.54 (m, 8H, H^{alkyl}), 1.47-1.15 (m, 32H, H^{alkyl}), 0.82 (m, 12H, H^{alkyl}).

[Zn(L)$_2$]$_n$(PF$_6$)$_{2n}$ (71d)
Yield: 66%. ^{1}H-NMR (400 MHz, DMSO-d_6, 25 °C): δ (ppm) = 9.43 (m, 4H, H$^{3'}$, H$^{5'}$), 9.17 (m, 4H, H^3, H$^{3''}$), 8.75 (m, 4H, H^{aryl}), 8.50 (m, 4H, H^4, H$^{4''}$), 8.30 (m, 4H, H^{aryl}), 7.95 (m, 8H, H^{aryl} & H^6, H$^{6''}$), 7.54 (m, 4H, H^5, H$^{5''}$), 7.18 (m, 2H, H^{aryl}), 7.03 (s, 1H, H^{aryl}), 4.03 (m, 16H, H^{alkyl}), 1.84 (m, 16H, H^{alkyl}), 1.55 (m, 16H, H^{alkyl}), 1.47-1.15 (m, 64H, H^{alkyl}), 0.82 (m, 24H, H^{alkyl}).

5.5 References

1   U. S. Schubert, H. Hofmeier, G. R. Newkome, *Modern Terpyridine Chemistry*, Wiley-VCH, Weinheim, **2006**.

2   M. Chiper, M. A. R. Meier, J. M. Kranenburg, U. S. Schubert, *Macromol. Chem. Phys.* **2007**, *208*, 679.

3   U. S. Schubert, C. Eschbaumer, *Angew. Chem. Int. Ed.* **2002**, *41*, 2892.

4   S. C. Yu, C. C. Kwok, W. K. Chan, C. M. Che, *Adv. Mater.* **2003**, *15*, 1634.

5   S. C. Chang, J. Bharathan, Y. Yang, R. Helgeson, J. R. Reynolds, *Appl. Phys. Lett.* **1998**, *72*, 2561.

6   V. N. Bliznyyuk, S. A. Carter, J. C. Scott, G. Klarner, R. D. Miller, D. C. Miller, *Macromolecules* **1999**, *32*, 361.

7   R. Dobrawa, M. Lysetska, P. Ballester, M. Grüne, F. Würthner, *Macromolecules* **2005**, *38*, 1315.

8   C. Xia, R. C. Advincula, *Macromolecules* **2001**, *34*, 5854.

9   Y.-Y. Chen, Y.-T. Tao, H.C. Lin, *Macromolecules* **2006**, *39*, 8559.

10   Y.-Y. Chen, H.-C. Lin, *J. Polym. Sci., Part A: Polym. Chem.* **2007**, 3243.

11   R. Dobrawa, F. Würthner, *Chem. Commun.* **2002**, 319.

12   S.-H. Hwang, C. N. Moorefield, P. Wang, J.-Y. Kim, S.-W. Lee, G. R. Newkome, *Inorg. Chim. Acta* **2007**, *360*, 1780.

13   Q. Chu, Y. Pang, *J. Poly. Sci., Part A: Polym. Chem.* **2006**, 2338.

14   P.-T. Chou, Y. Chi, *Chem. Eur. J.* **2007**, *12*, 380.

15   (a) X. Y. Wang, A. D. Guzreo, R. H. Schmehl, *Chem. Commun.* **2002**, 2344. (b) W. Goodall, J. A. G. Williams, *Chem. Commun.* **2001**, 2514.

16   A. Winter, D. A. M. Egbe, U. S. Schubert, *Org. Lett.* **2007**, *9,* 2345.

17   F. Tessore, D. Roberto, R. Ugo, M. Pizzotti, *Inorg. Chem.* **2005**, *44*, 8967.

18   X. Chen, Q. Zhou, Y. Cheng, Y. Geng, D. Ma, Z. Xie, L. Wang, *J. Luminescence* **2007**, *126*, 81.

19   A. H. Göller, U.-W. Grummt, *Chem. Phys. Lett.* **2002**, *354*, 233.

20   (a) S. Westenhoff, W. J. D. Beenken, R. H. Friend, N. C. Greenham, A. Yartsev, V. Sundström, *Phys. Rev. Lett.* **2006**, *97*, 166804. (b) W. J. D. Beenken, H. Lischka, *J. Chem. Phys.* **2005**, *123*, 144311. (c) S. Westenhoff, W. J. D. Beenken, A. Yartsev, N. C. Greenham, *J. Chem. Phys.* **2006**, *125*, 154903.

21   (a) A. D. Becke, *Phys. Rev. A* **1988**, *38*, 3098. (b) J. P. Perdew, *Phys. Rev. B* **1986**, *33*, 8822. (c) A. Schäfer, C. Huber, R. Ahlrichs, *J. Chem. Phys.* **1994**, *100*, 5829.

22   (a) C. Herrmann, J. Neugebauer, M. Presselt, M. Schmitt, S. Rau, J. Popp, M. Reiher, *J. Phys. Chem. B* **2007**, 111, 6078. (b) M. Reiher, G. Brehm, S. Schneider, *J. Phys. Chem. A* **2004**, *108*, 734.

23   (a) K. Eichkorn, O. Treutler, H. Öhm, M. Häser, R. Ahlrichs, *Chem. Phys. Lett.* **1995**, *240*, 283. (b) K. Eichkorn, F. Weigend, O. Treutler, R. Ahlrichs, *Theor. Chem. Acc.* **1997**, *97*, 119.

24   F. R. Dollish, *Characteristic Raman Frequencies of Organic Compounds*, John Wiley & Sons Inc., **1973**.

25   S. Schmatloch, M. Fernandez Gonzalez, U. S. Schubert, *Macromol. Rapid Commun.* **2002**, *23*, 957.

26   J. B. Beck, J. M. Ineman, S. J. Rowan, *Macromolecules* **2005**, 38, 5060.

27   C. F. Chow, S. Fujii, J.-M. Lehn, *Angew. Chem. Int. Ed*. **2007**, *46*, 5007.

28   D. T. McQuade, A. E. Pullen, T. M. Swager, *Chem. Rev.* **2000**, *100*, 2537.

29   A. Winter, C. Friebe, U. S. Schubert, manuscript in preparation.

30   A. Winter, C. Friebe, U. S. Schubert, *Macromol. Rapid Commun.* **2008**, in press.

31   M. A. R. Meier, B. G. G. Lohmeijer, U. S. Schubert, *Macromol. Rapid Commun.* **2003**, *24*, 852.

32   B. G. G. Lohmeijer, U. S. Schubert, *Macromol. Chem. Phys.* **2003**, *204*, 1072.

33   P. K. Iyer, J. B. Beck, C. Weder, S. J. Rowan, *Chem. Commun.* **2005**, 319.

34   R. Ahlrichs, M. Bär, M. Häser, H. Horn, C. Kölmel, *Chem. Phys. Lett.* **1989**, *162*, 165.

35   (a) A. D. Becke, *Phys. Rev. A* **1988**, *38*, 3098. (b) J. P. Perdew, *Phys. Rev. B* **1986**, *33*, 8822. (c) A. Schäfer, C. Huber, R. Ahlrichs, *J. Chem. Phys.* **1994**, *100*, 5829.

36   (a) K. Eichkorn, O. Treutler, H. Öhm, M. Häser, R. Ahlrichs, *Chem. Phys. Lett.* **1995**, *240*, 283. (b) K. Eichkorn, F. Weigend, O. Treutler, R. Ahlrichs, *Theor. Chem. Acc.* **1997**, *97*, 119.

Chapter VI

Metallo-supramolecular polymers with

lower critical solution temperature (LCST) behavior

Abstract

Metallo-supramolecular polymers offer attractive possibilities to combine the properties of polymers with the characteristics offered by the metal-ligand coordination. In this chapter, we present the combination of metal-bis(terpyridine) complexes and lower critical solution temperature (LCST) polymers that can be switched by addressing either the thermosensitive polymer or the metal complex. The mono-terpyridine-PNIPAM was synthesized via a new synthetic strategy (described in Chapter 2) and was further used for the preparation of Fe(II) and Zn(II) bis-terpyridine-PNIPAM complexes. The comparison of the LCST behavior of the uncomplexed ligands and their metal complexes bearing different counter ions is discussed. Furthermore, the switchability of the synthesized Fe(II) system is demonstrated by a decomplexation reaction followed by the characterization of the uncomplexed ligand.

6.1 Introduction

As we have shown in the previous chapters, the combination of polymer chemistry (based on traditional C-C covalent-bond chemistry) and supramolecular chemistry (based on reversible, non-covalent interactions[1,2] such as, *e.g.*, hydrogen bonds,[3-6] metal-ligand coordination,[7-11] ionic[12,13] or host-guest interactions[14-16]) opens new possibilities for designing functional materials with interesting applications in various fields. For the category of metal-ligand interactions, terpyridine metal-complexes are widely used building blocks in supramolecular chemistry. For this purpose, 2,2':6',2"-terpyridines bearing substituents at the 4′-position can be exploited as tridentate ligands since they form complexes with a wide range of transition metal ions in low oxidation states.[17-22,34] The advantage of having a metal complex linkage is the possibility of reversibly switching this junction point by varying the external parameters (*e.g.* temperature, pH, redox potential, or addition of competitive ligands). This feature is intensively used for the preparation of new "switchable" materials that can be easily tuned by varying the metal ion (also self healing materials are accessible). Moreover, apart from the influence of the transition metal ion, the properties can be significantly altered by exchanging the counterions as described in literature.[23,24]

Another appealing strategy for "smart materials" is the combination of LCST (lower critical solution temperature) polymers with specific and defined supramolecular interactions, such as metal-ligand coordination. Harruna *et al.* described the combination of metallo chelating ligands (bipyridines or terpyridines) and thermosensitive polymers. However, the LCST was not reported for these synthesized metallo-terpyridine compounds.[25,26] From the polymer properties point of view, thermosensitive polymers posses interesting physical behavior by undergoing a transition from soluble to collapsed precipitated chains upon heating in aqueous solution. The precipitation temperature is called the lower critical solution temperature (LCST). In general, thermosensitive polymers exhibit a reversible phase transition upon changing the temperature, which arises from the balance of hydrophilicity and hydrophobicity of the polymers.[27] In addition, LCST transitions have been shown to be sensitive to pH, type and concentration of salts and the utilized solvents.[28,29,31] Such LCST transitions have been extensively studied for, *e.g.*, poly(*N-iso*propylacrylamide) (PNIPAM), poly(*N*-vinylacetamide), poly(dimethylaminomethyl methacrylate) and poly(ethylene glycol methacrylate).[30,31] Therefore, an attractive concept for designing "smart materials" is the combination of supramolecular interactions with LCST polymers allowing the exploitation of the thermoresponsive polymer properties and, at the same time, the characteristics offered by

the supramolecular interactions. Ritter *et al.* have intensively studied the concept of host-guest interactions based on cyclodextrins in combination with LCST polymers.[32] Thus, the combination of more specific and stronger supramolecular interactions, such as metal-coordination and LCST polymers might offer new possibilities for the preparation of materials with new properties.

Here, we describe the metal complexation of PNIPAM end-functionalized with a terpyridine moiety (see Chapter 2 for synthesizes and characterization) with Fe(II) and Zn(II) metal ions in order to obtain metallo-supramolecular dimers. For the prepared Fe(II) and Zn(II) *bis*-terpyridine-PNIPAM, the influence of the counter ions on the LCST behavior was investigated as well. Furthermore, by bringing a competitive ligand into the system, such as HEEDTA (hydroxyethyl ethylenediamine-triacetic acid), the synthesized Fe(II) *bis*-terpyridine-PNIPAM could be opened and re-formed demonstrating the switchability of the designed system.

6.2 Fe(II) and Zn(II) complexation

The *mono*-terpyridine functionalized PNIPAM **30** was complexed with two metal ions: Fe(II) and Zn(II), respectively. It is known that terpyridine ligands are capable to chelate a large variety of transitional metal ions in low oxidation states forming metal-*bis*-terpyridine complexes characterized by different stabilities.[7] We have selected Fe(II) and Zn(II) metal ions as indicative examples with different relative binding strength towards the terpyridine moiety.[33,34] It has been reported that LCST transitions can be influenced by several variables, such as electrolyte concentration, incorporation of co-monomers or molar mass.[27,28,31] To investigate the effect of the metal salt of the terpyridine complex on the LCST, we prepared the corresponding Fe(II) and Zn(II) supramolecular dimers, **72** respectively **73**, in which the counter ions were varied from Cl$^-$ to CH$_3$COO$^-$ to PF$_6^-$, (Scheme 6.1). The metallo-complexation reactions were performed in methanol under reflux for 12 hours using the MCl$_2$ or M(CH$_3$COO)$_2$ metal salts, where M is Fe(II) respectively Zn(II). The resulting Fe(II) and Zn(II) *bis*-terpyridine-PNIPAM **72** and **73** bearing Cl$^-$ or CH$_3$COO$^-$ counter ions were purified by preparative size exclusion chromatography (BioBeads SX-1, THF), followed by precipitation from methanol into cold diethyl ether.

Fe(II) and Zn(II) *bis*-terpyridine-PNIPAM **72** and **73** bearing PF$_6^-$ as counter ions were prepared by an ion exchange reaction between complexes **72** and **73** bearing CH$_3$COO$^-$ as

counter ions with a 10 fold excess of NH_4PF_6. The final purification was performed by double precipitation of the polymeric metal complex from methanol into cold diethyl ether.
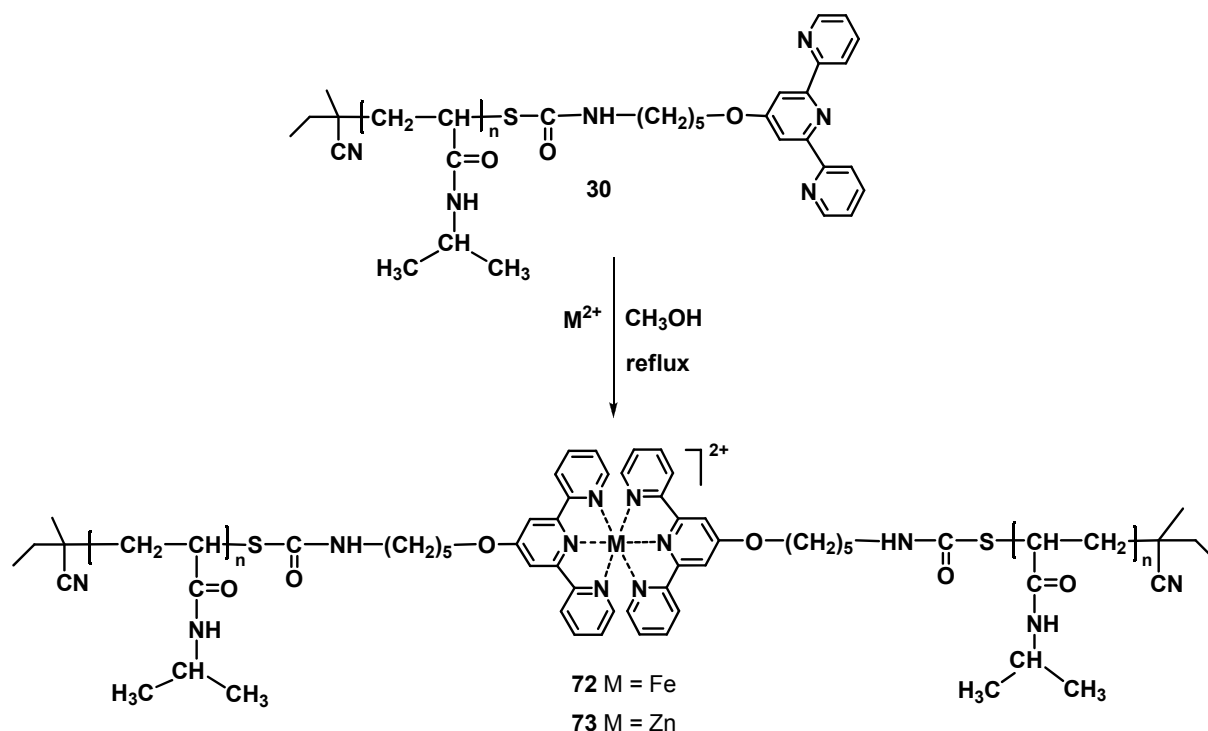
Scheme 6.1: *Schematic representation of the synthesis of Fe(II) bis-terpyridine-PNIPAM 72 respectively Zn(II) bis-terpyridine-PNIPAM 73 (counter ions are omitted for clarity).*

Characterization of the purified Fe(II) polymer **72** and Zn(II) polymer **73** was performed by ^{1}H-NMR and UV-Vis spectroscopy. Taking into account that the utilized metal ions, Fe(II) respectively Zn(II), are characterized by relatively low binding strength towards terpyridine ligands, SEC characterization could not be performed on the synthesized terpyridine metal dimers. For both synthesized metallo-dimers **72** and **73** important shifts were observed in the aromatic region of the ^{1}H-NMR spectra demonstrating that the complexed terpyridine protons were clearly shifted to lower magnetic field due to the influence of the incorporated M(II) ion into the central core of the synthesized metallo-supramolecular dimers. Moreover, the UV-Vis spectra recorded in water also proved the presence of the metal ions in the synthesized structures. Thus, in the case of Fe(II) *bis*-terpyridine-PNIPAM **72** a characteristic metal-to-ligand-charge-transfer (MLCT) was observed at 559 nm, which belongs to the formation of Fe(II)tpy$_2$ connectivity as also indicated by the strong purple color (Figure 6.2 left). For the case of Zn(II) *bis*-terpyridine-PNIPAM **73**, the formation of the Zn(II)tpy$_2$ connectivity was evidenced by the slightly yellowish color and also by the presence of the characteristic LC bands at 308 nm and 319 nm in the recorded spectrum (Figure 6.2 right).
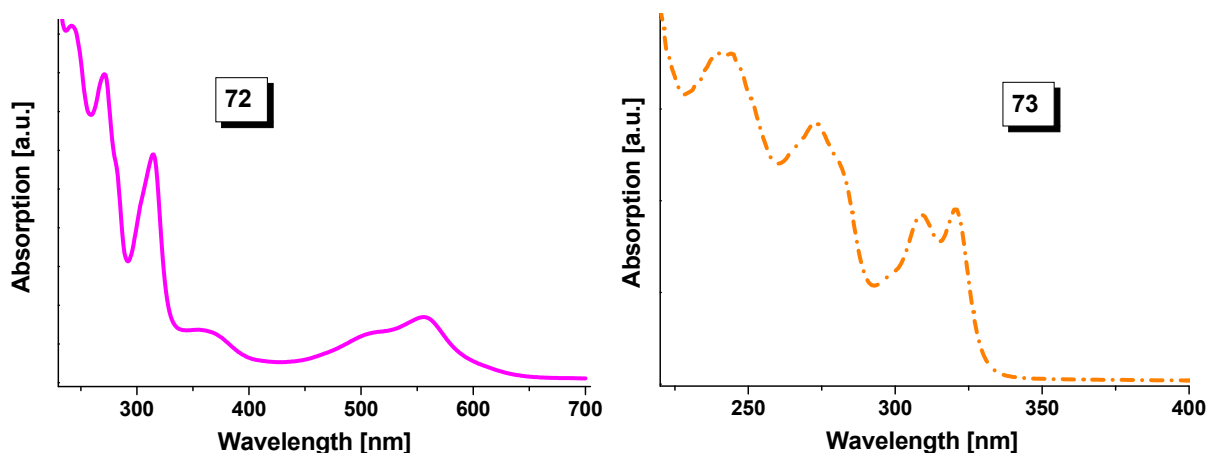
Figure 6.2: *Characteristic UV-Vis absorption of Fe(II) bis-terpyridine-PNIPAM **72** (left) respectively Zn(II) bis-terpyridine-PNIPAM **73** (right) (measured in water).*

6.3 LCST studies

As expected, all synthesized compounds **27**, **30**, as well as **72** and **73** with different counter ions were soluble in water at room temperature. This observation indicates that the solubility properties are mainly governed by the PNIPAM chains since M(II) terpyridine complexes with PF_6^- counter ions are not water soluble. Turbidity measurements (as shown in Figures 6.3-6.5) revealed that aqueous solutions of the synthesized compounds (5 mg/1 mL) exhibited a LCST behavior as indicated by clouding of the solution, *e.g.* a drop in transmittance upon heating.
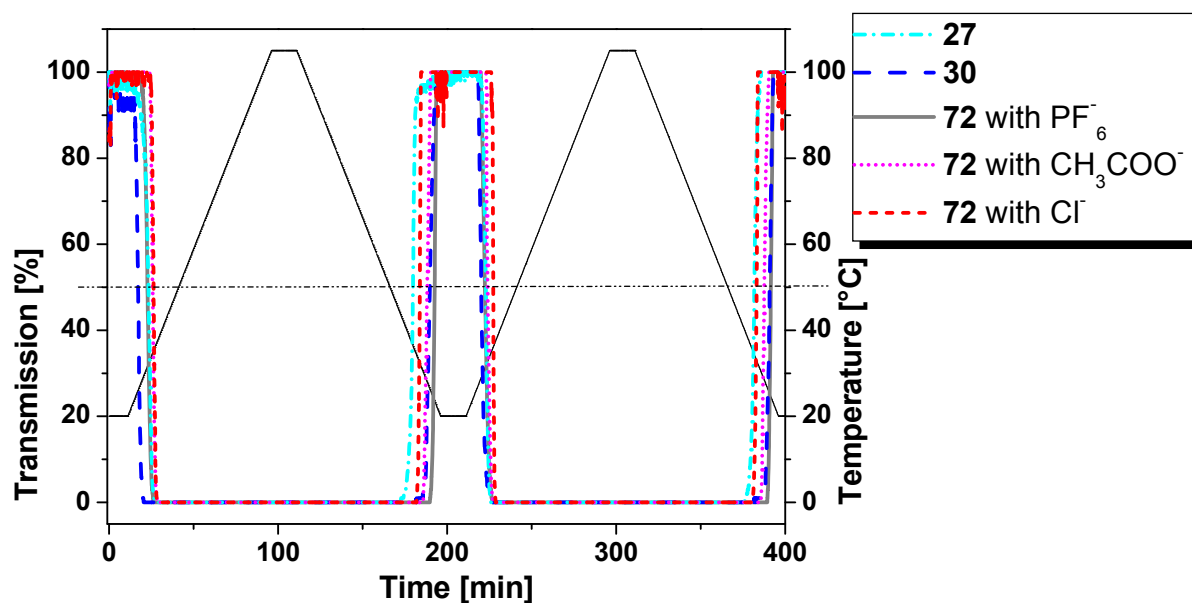
Figure 6.3: *Turbidity measurements during controlled heating-cooling cycles performed on **27**, **30** and **72** with Cl⁻, CH₃COO⁻ and PF₆⁻ counter ions in water (5 mg/1 mL).*

This temperature-responsive aqueous solubility transition of PNIPAM is well-known.[35] Above the LCST of approximately 32 °C, disruption of the hydrogen bonds between the polymer and water causes collapse and aggregation of the macromolecules by dehydratation.[36] It is known from literature that the LCST behavior is strongly influenced by the hydrophilic/hydrophobic balance of the macromolecule/polymer.[37] For the case of PNIPAM the cloud point is only little affected by variation of the molar mass. As expected, the unfunctionalized PNIPAM **27** showed a cloud point at 32.2 °C. In comparison to **27**, the *mono*-terpyridine PNIPAM **30** displayed a lower LCST (26.1 °C) due to the presence of the attached hydrophobic chelating unit at the end of the polymer backbone (Figure 6.4).[38] By complexation of monomer **30** with Fe(II) ions, a higher molar mass metallo-supramolecular dimer has been prepared. Moreover, the addition of a charged metal ion to the core of the mentioned polymer **30**, as well as the corresponding counter ions, influenced the solubility of the newly designed metallo-polymer resulting in different LCST values.
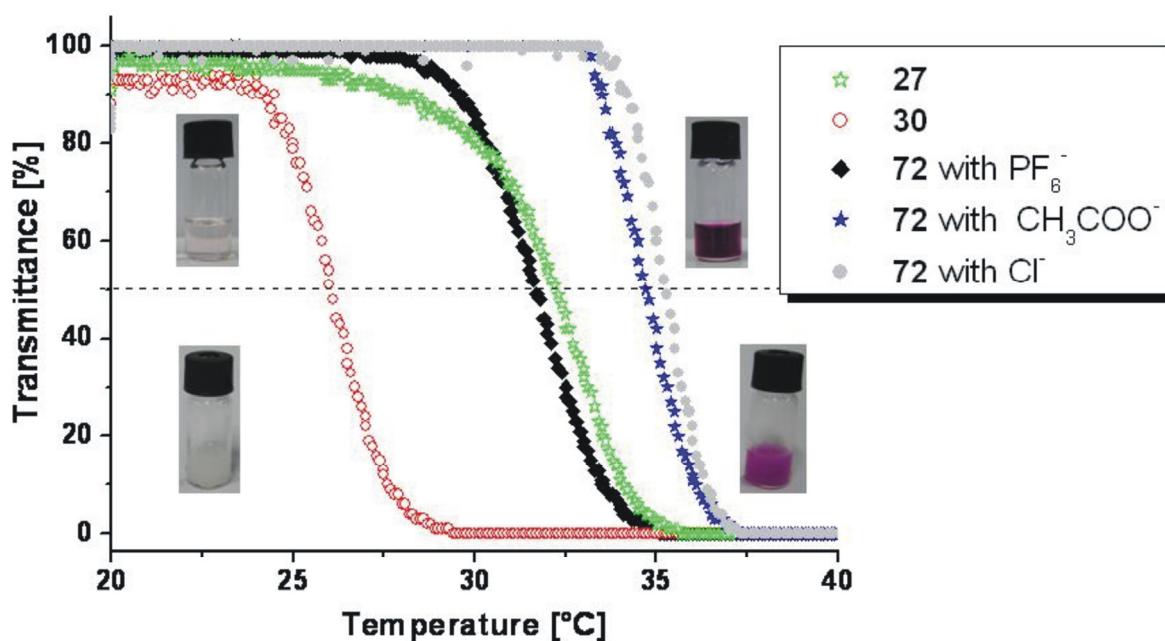
Figure 6.4: *Transmittance versus temperature plot for **27**, **30** and **72** with different counter ions (Cl^-, CH_3COO^- and PF_6^-) in water (5 mg/1 mL). Pictures: vials of **27** below LCST (top left) and above LCST (bottom left); vials of **72** below LCST (top right) and above LCST (bottom right).*

For the case of **72** with PF_6^- as counter ions, the cloud point was found to be 31.6 °C while **72** bearing CH_3COO^- counter ions revealed a cloud point about at 34.7 °C. The last Fe(II) supramolecular dimer with Cl^- counter ions displayed a higher LCST at 35.2 °C. This order in LCST values corresponds with the increased hydrophilicity of the counter ions when going

from PF_6^- to CH_3COO^- to Cl^-. As it is shown in Figures 6.3 and 6.4, the phase transition of compounds **30** and **72** is reversible and the clouding is clearly observed when the samples were heated up above the LCST (see vials in Figure 6.4). In addition, the solution became transparent when cooled below the cloud point.

The second studied metallo-supramolecular dimer, Zn(II) *bis*-terpyridine-PNIPAM **73**, bearing Cl^-, CH_3COO^- and respectively PF_6^- as counter ions, displayed similar behavior as the Fe(II) *bis*-terpyridine-PNIPAM **72**. From the turbidity measurements, Figure 6.5, Zn(II) *bis*-terpyridine-PNIPAM **73** with PF_6^- revealed a LCST at 30.0 ^{o}C and **73** with CH_3COO^- as counter ions showed a cloud point at 33.4 ^{o}C; finally **73** with Cl^- as counter ion revealed a LCST at 39.0 ^{o}C. For the case of Zn(II) *bis*-terpyridine-PNIPAM **73** with PF_6^- as counter ions, the phase transition curve showed an unexpected profile while heating the sample above LCST. Repetition of the experiment revealed a similar solubility response and, in addition, the vial was visually inspected during the turbidity measurement. The visual inspection upon heating the metallo-supramolecular dimer **73** with PF_6^- counter ions showed that above the LCST the precipitated polymer sticks to the stirring bar of the vial causing the unexpected transmission profile.
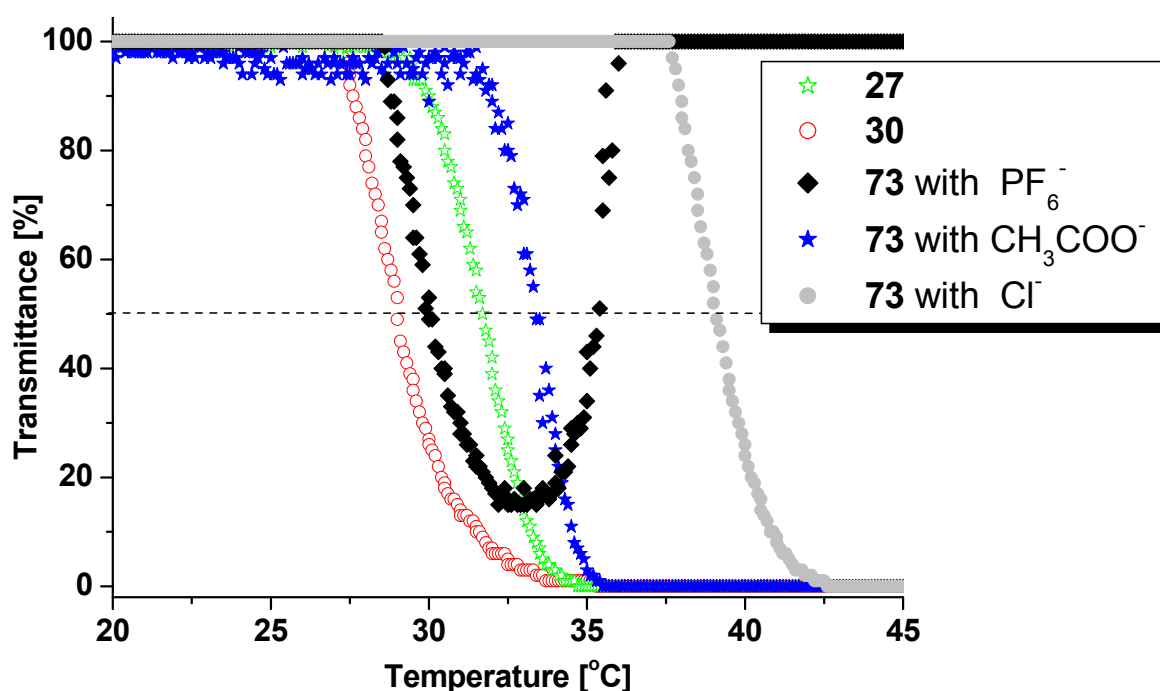
Figure 6.5: *Effect of temperature on the transmittance of 27, 30 and 73 with different counter ions (Cl⁻, CH₃COO⁻ and PF₆⁻) in water (5 mg/1 mL).*

When briefly comparing the uncomplexed ligands **27**, **30** and the metallo-complexes **72** respectively **73**, we observed that the cloud point increased with the increase of the charge content (Table 6.1).[39] The phase behavior of **72** and **73** was further influenced by the nature of the metal ion present in the core of the synthesized metallo-supramolecular dimers and also by the counter ions. These differences demonstrate the importance of the hydrophilic/hydrophobic balance on the LCST behavior. For the analyzed systems **72** and **73** the different influence of the metal ions on the turbidity response might be attributed to the radius of the utilized metal ion (Fe compared to Zn) and to the proximity of the metal and the counter ions.

Table 6.1: *Overview of the observed clouding points for compounds 27, 30, 72 and 73, respectively.*

Compound	LSCT [^{o}C]
27	32.2
30	26.1
72 with PF_6^-	31.6
72 with CH_3COO^-	34.7
72 with Cl^-	35.2
73 with PF_6^-	30.0
73 with CH_3COO^-	33.4
73 with Cl^-	39.0

6.4 Decomplexation studies

Both synthesized Fe(II) and Zn(II) *bis*-terpyridine-PNIPAM complexes, **72** and **73**, are known to exhibit a reversible complexation behavior in the presence of other strong chelating ligands such as HEEDTA.[40] Fe(II) *bis*-terpyridine complexes showed a specific metal-to-ligand charge transfer (MLCT) band at 560 nm and the compounds were characterized by an intensive purple color while Zn(II) *bis*-terpyridine complexes were colorless and did not exhibit any MLCT. In order to clearly demonstrate the reversibility of the synthesized metallo(II)-*bis*-terpyridine systems, we performed a decomplexation experiment on complex **72** (Figure 6.6). By the addition of a strong chelating ligand (HEEDTA) into a chloroform solution with the synthesized Fe(II) *bis*-terpyridine-PNIPAM **72**, the purple color disappeared within a few minutes (Figure 6.6).
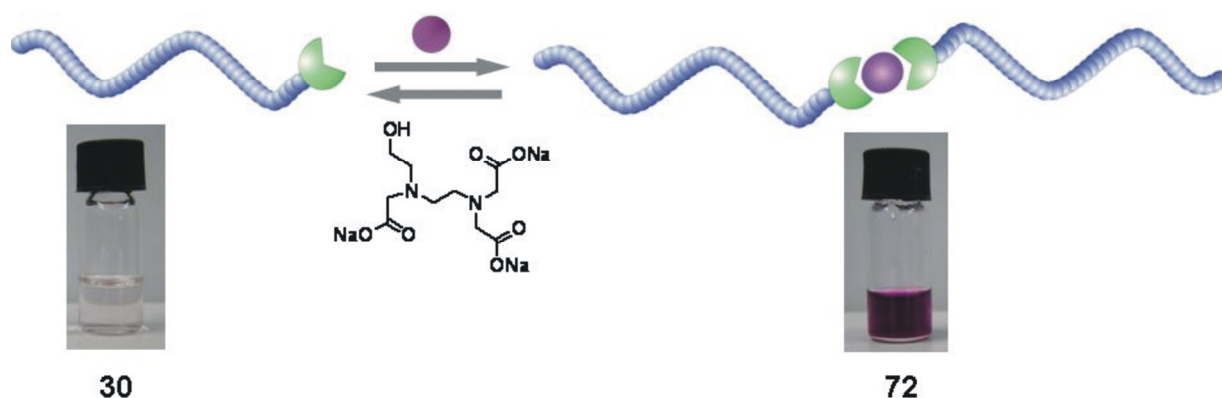
Figure 6.6: *Schematic representation of the complexation of mono-terpyridine PNIPAM 30 with Fe(II) ions and decomplexation of the synthesized Fe(II) bis-terpyridine-PNIPAM 72 with HEEDTA. Photos of the solutions of 30 (left) and 72 (right) in water at room temperature indicate the corresponding color change.*

The decomplexed Fe(II) ligand obtained from the experiment was subsequently extracted with chloroform and then precipitated from chloroform into cold diethyl ether. UV-Vis spectroscopy measurements showed that no complex was present in the isolated fraction and that the LCST of the uncomplexed ligand revealed a similar behavior as the ligand **30** before the complexation (28 °C). The presence of the uncomplexed terpyridine protons in the ^{1}H-NMR spectrum further proved that Fe(II) *bis*-terpyridine-PNIPAM can be used for the preparation of switchable systems that can be opened and closed reversibly by, *e.g.*, the addition of a competitive ligand.
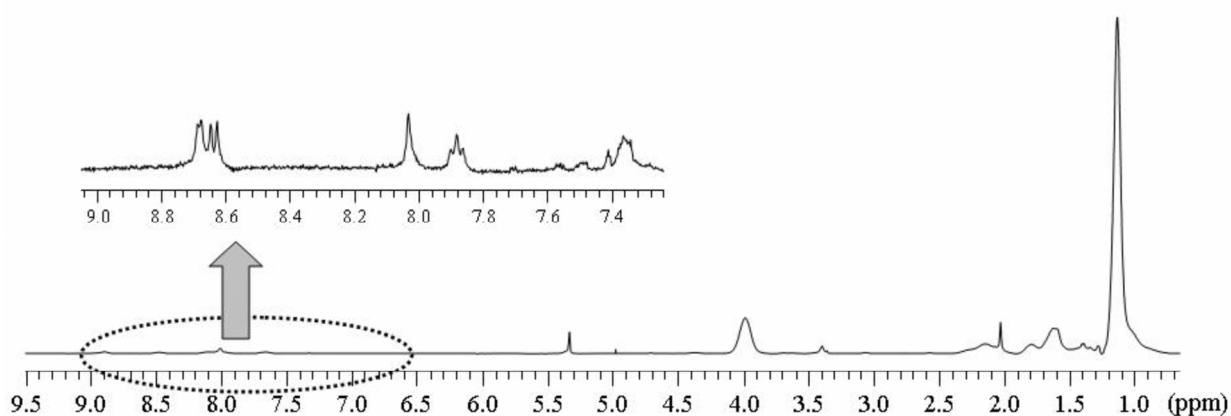
Figure 6.5: *^{1}H-NMR spectrum of the decomplexed ligand mono-terpyridine PNIPAM 30 with detailed zoom of the terpyridine protons (recorded in CD₂Cl₂).*

6.5 Conclusions

The *mono*-terpyridine PNIPAM (synthesis described in Chapter II) was successfully employed as a chelating ligand with LCST features for Fe(II) and Zn(II) complexation. Detailed characterization and LCST investigations of the Fe(II) and Zn(II) *bis*-terpyridine-PNIPAM were performed demonstrating that the cloud point is influenced by the utilized metal and counter ions. Furthermore, the switchability of the designed systems was demonstrated for Fe(II) *bis*-terpyridine-PNIPAM by performing a decomplexation reaction. The decomplexed product presented the same characteristics as the ligands before the complexation. For future work it will be interesting to study the influence of various metallo-(block co)polymers bearing different counter ions on the LCST behavior. In addition, the effect of different solvents, pH and added salts could be an interesting issue to be considered in order to determine structure-property relationships. Finally, the reversibility of the "switching" process addressed specifically to the metal complex from the metallo-supramolecular polymers can reveal interesting behavior.

6.6 Experimental section

Materials and general experimental details
Chemicals were obtained from Sigma-Aldrich and were used as received unless otherwise specified. Compounds **27** and **30** were synthesised as described in Chapter II. Azobis(*iso*butyronitrile) (AIBN) was recrystallized from methanol and NIPAM was recrystallized from hexane. 2-Cyano-2-butyl dithiobenzoate (CBDB) was prepared according to a literature procedure for a related compound.[41] Preparative size-exclusion chromatography was performed on BioBeads S-X1 columns using THF as eluent.
Instrumentation. Nuclear magnetic resonance spectra were recorded on a Varian Gemini 400 MHz spectrometer at 298 K. Chemical shifts are reported in parts per million (δ) downfield from an internal standard, tetramethylsilane (TMS) in CD_3Cl or CD_2Cl_2. UV-Vis spectra were recorded on a Perkin Elmer Lamda-45 (1 cm cuvettes, H_2O). Turbidity measurements were performed by heating the solution of **27**, **30**, **72** and **73** (2.5 mg) in 0.5 mL demineralized water from 20 ^{o}C to 105 ^{o}C with a heating rate of 1.0 ^{o}C per minute followed by cooling to 20 ^{o}C at a cooling rate of 1 ^{o}C per minute after keeping it 15 minutes at 105 ^{o}C. During these controlled heating cycles, the transmission through the solutions was monitored in a Crystal 16 from Avantium Technologies.

Synthesis of Fe(II) bis-terpyridine-PNIPAM (72)
The *mono*-terpyridine PNIPAM **30** (50 mg, 0.0078 mmol) and the metal salt Fe(II) acetate or chloride (0.0039 mmol) were stirred under reflux in 1 mL MeOH overnight. The reaction was monitored by UV-Vis spectroscopy: when no more changes were observed in the UV-Vis spectrum the reflux was stopped. The solvent was removed under reduced pressure and the crude product was further purified by preparative size exclusion chromatography (BioBeads SX-1, THF). The purified fraction was subsequently precipitated from dichloromethane into cold hexane. Yields: 60% (acetate) and 65% chloride respectively.
The Fe(II) *bis*-terpyridine-PNIPAM **72** with PF_6^- counter ions, has been obtained by performing an ion exchange reaction between complex **72** bearing CH_3COO^- as counter ions, with a 10 fold excess of NH_4PF_6. The final purification was performed by double precipitation of the metal complex from

methanol into cold diethyl ether. Yield: 80%. ^{1}H-NMR (400 MHz, CD$_2$Cl$_2$, 25 ˚C): δ (ppm) = 8.55 (bs, 4H, H^3, H$^{3"}$), 7.98 (bs, 4H, H$^{3'}$, H$^{5'}$), 7.87 (bs, 4H, H^4, H$^{4"}$), 7.33 (bs, 4H, H^6, H$^{6"}$), 7.13 (bs, 4H, H^5, H$^{5"}$), 4.65 (bs, 2H, H^a), 4.22-3.84 (bs, 60H), 3.39 (m, 2H, H^e), 2.43-1.93 (m, 120H, -C*H$_2$* backbone), 1.80 (m, 2 H, H^b), 1.52-1.57 (m, 4 H, H^{c,d}), 2.34-2.02 (m, 60H, -C*H* backbone), 1.12 (s, 360H, -C*H$_3$*). UV (H$_2$O): λ_{max} (ε) = (L mol^{-1} cm^{-1}): 556 (1 600), shoulder at 507 (1 468), 362 (1 350), 315 (4 510), 270 (6 500), 242 (7 130).

Synthesis of Zn(II) bis-terpyridine-PNIPAM (73)

The *mono*-terpyridine PNIPAM **30** (60 mg, 0.0093 mmol) and the metal salt Zn(II) acetate or chloride (0.0046 mmol) were stirred under reflux in 0.5 mL MeOH overnight. The solvent was removed in vacuum and the crude product was further purified by preparative size exclusion chromatography (BioBeads SX-1, THF) followed by precipitation from methanol into cold diethyl ether. Yields: 70% (acetate) and 67% (chloride).

The Zn(II) *bis*-terpyridine-PNIPAM **73** with PF$_6^-$ counter ions has been obtained by an ion exchange reaction between complex **73** bearing CH$_3$COO$^-$ as counter ions, with a 10 fold excess of NH$_4$PF$_6$. The final purification was performed by double precipitation of the metal complex from methanol into cold diethyl ether. Yield: 84%. ^{1}H-NMR (400 MHz, CD$_2$Cl$_2$, 25 ˚C): δ (ppm) = 8.89 (bs, 4H, H^3, H$^{3"}$), 8.47 (bs, 4H, H$^{3'}$, H$^{5'}$), 8.01 (bs, 4H, H^4, H$^{4"}$), 7.67 (bs, 4H, H^6, H$^{6"}$), 7.15 (bs, 4H, H^5, H$^{5"}$), 4.38 (bs, 2H, H^a), 4.15-3.98 (bs, 30H), 3.39 (m, 2H, H^e), 2.43-1.93 (m, 120H, -C*H$_2$* backbone), 1.80 (m, 2 H, H^b), 1.52-1.57 (m, 4H, H^{c,d}), 2.35-2.02 (m, 60H, -C*H* backbone), 1.13 (s, 360H, -C*H$_3$*). UV (H$_2$O): λ_{max} (ε) = (L mol^{-1} cm^{-1}): 320 (29 500), 308 (26 800), 272 (47 500), 243 (61 300).

Decomplexation of Fe(II) bis-terpyridine-PNIPAM (72)

HEEDTA (0.5 mL, hydroxyethyl-ethylenediaminetriacetic acid); Trilon D liquid (39.0-41.0 wt.-%) was added to the chloroform solution (2 mL) of **72** (20 mg). While vigorously stirring the reaction mixture, the purple color of the iron complex disappeared within a few minutes. To complete the decomplexation process, the mixture was stirred one hour and it was subsequently extracted with chloroform. The polymer **30** was recovered by precipitation into cold diethyl ether. Yield: 70%. ^{1}H-NMR (400 MHz, CDCl$_3$, 25 ˚C): δ (ppm) = 8.67 (d, 2H, J = 4 Hz; H^6, H$^{6"}$), 8.60 (d , 2H, J = 8 Hz; H^3, H$^{3"}$), 7.99 (s, 2H, H$^{3'}$, H$^{5'}$), 7.86 (t, 2H, J = 7.6 Hz; H^4, H$^{4"}$), 7.35 (t, 2H, J = 6.2 Hz; H^5, H$^{5"}$), 4.23 (m, 2H, H^a), 3.97-3.85 (bs, 30H), 3.40 (m, 2H, H^e), 1.87-1.63 (m, 30H, -C*H$_2$* backbone), 1.80 (m, 2 H, H^b), 1.52-1.57 (m, 4 H, H^{c,d}), 2.34-2.02 (m, 60H, -C*H* backbone), 1.12 (s, 180H, -C*H$_3$*). SEC (DMA system; PS calibration): M$_n$ = 6,450 g/mol, M$_w$ = 7,900 g/mol, PDI = 1.22. UV-Vis (H$_2$O): λ_{max} (ε) = (L mol^{-1} cm^{-1}): 279 (13 150), 234 (16 000).

6.7 References

1   J.-M. Lehn, *Supramolecular Chemistry-Concepts and Chemistry*; VCH: Weinheim, Germany, **1995**.

2   L. Brunsveld, B. J. B. Folmer, E. W. Meijer, R. P. Sijbesma, *Chem. Rev.* **2001**, *101*, 4071.

3   X. Yang, F. Hua, K. Yamato, E. Ruckenstein, B. Gong, W. Kim, C. Y. Ryu, *Angew. Chem. Int. Ed.* **2004**, *43*, 6471.

4   R. P. Sijbesma, F. H. Beijer, L. Brunsveld, B. J. B. Folmer, J. H. K. Ky Hirschberg, R. F. M. Lange, J. K. L. Lowe, E. W. Meijer, *Science* **1997**, *278*, 1601.

5   C. Schmuck, W. Wienand, *Angew. Chem. Int. Ed.* **2001**, *40*, 4363.

6   K. Yamauchi, J. R. Lizotte, T. E. Long, *Macromolecules* **2002**, *35*, 8745.

7   U. S. Schubert, H. Hofmeier, G. R. Newkome, *Modern Terpyridine Chemistry*, Wiley-VCH, Weinheim, **2006**.

8   U. S. Schubert, C. Eschbaumer, *Angew. Chem. Int. Ed.* **2002**, *41*, 2892.

9   J. B. Beck, J. M. Ineman, S. J. Rowan, *Macromolecules* **2005**, *38*, 5060.

10   H. Hofmeier, S. Schmatloch, D. Wouters, U. S. Schubert, *Macromol. Chem. Phys.* **2003**, *204*, 2197.

11   C. D. Eisenbach, U. S. Schubert, *Macromolecules*, **1993**, *26*; 7372.

12   T. P. Russell, R. Jerome, P. Charlier, M. Foucart, *Macromolecules* **1988**, *21*, 1709.

13   Y. Guan, S.-H. Yu, M. Antonietti, C. Böttcher, C. F. Faul, *Chem.-Eur. J.* **2005**, *11*, 1305.

14   H. -J. Schneider, A. K. Yatsimirsky, *Chem. Soc. Rev.* **2008**, *37*, 263.

15   A. Scarso, J. Rebek Jr., *Top. in Curr. Chem.* **2006**, *265*, 1.

16   J. Cram, *Angew. Chem. Int. Ed.* **1988**, *100*, 1041.

17   U. S. Schubert, C. Eschbaumer, O. Hien, P. R. Andres, *Tetrahedron Lett.* **2001**, *42*, 4705.

18   M. Heller, U. S. Schubert, Eur. *J. Org. Chem.* **2003**, *6*, 47.

19   U. S. Schubert, G. Hochwimmer, S. Schmatloch, H. Hofmeier, *Eur. Coating J.* **2003**, *6*, 26.

20   M. Heller, U. S. Schubert, *Macromol. Rapid Commun.* **2002**, *25*, 411.

21   U. S. Schubert, C. Eschbaumer, P. Andres, H. Hofmeier, C. H. Weidl, E. Herdtweck, E. Dulkeith, A. Morteani, N. Hecker, J. Feldmann, *Synth. Metals* **2001**, *121*, 1249.

22   S. Schmatloch, U. S. Schubert, *Macromol. Rapid Commun.* **2002**, *23*, 957.

23   H. Hofmeier, R. Hoogenboom, M. E. L. Wouters, U. S. Schubert, *J. Am. Chem. Soc.* **2005**, *127*, 2913.

24   P. Mi, L.-Y. Chu, X. -J. Ju, C. H. Niu, *Macromol. Rapid Commun.* **2008**, *29*, 27.

25   G. Zhou, I. I. Harruna, C. W. Ingram, *Polymer* **2005**, *46*, 10672.

26   G. Zhou, I. I. Harruna, *Macromolecules* **2005**, *38*, 4114.

27   F. Ganachaud, M. J. Monteiro, R. G. Gilbert, M.-A. Dourges, S. H. Thang, E. Rizzardo, *Macromolecules* **2000**, *33*, 6738.

28   C. de las Heras Alarcón, S. Pennadam, C. Alexander, *Chem. Soc. Rev.* **2005**, *34*, 276.

29   I. Dimitrova, B. Trzebickab, A. H. E. Müller, A. Dworakb, C. B. Tsvetanova, *Prog. Polym. Sci.* **2007**, *32*, 1275.

30   M. Mertoglu, S. Garnier, A. Laschewsky, K. Skrabania, J. Storsberg, *Polymer* **2005**, *46*, 7726.

31   D. Fournier, R. Hoogenboom, H. M. L. Thijs, R. M. Paulus, U. S. Schubert, *Macromolecules* **2007**, *40*, 915.

32   S. Schmitz, H. Ritter, *Angew. Chem. Int. Ed.* **2005**, *44*, 5658.

33   M. Chiper, M. A. R. Meier, J. M. Kranenburg, U. S. Schubert, *Macromol. Chem. Phys.* **2007**, *208*, 679.

34   B. G. G. Lohmeijer, U. S. Schubert, *Macromol. Chem. Phys.* **2003**, *204*, 1072.

35   H. G. Schild, *Prog. Polym. Sci.* **1992**, *17*, 163.

36   X. Qiu, C. M. S. Kwan, C. Wu, *Macromolecules* **1997**, *30*, 6090.

37   S. Aoshima, S. Kanaoka, *Adv. Polym. Sci.* **2008**, *210*, 169.

38   A. P. Vogt, S. R. Gondi, B. S. Sumerlin, *Aust. J. Chem.* **2007**, *60*, 396.

39   F. A. Plamper, A. Schmalz, M. Ballauff, A. H. E. Mueller, *J. Am. Chem. Soc.* **2007**, 129, 14538.

40   H. Hofmeier, U. S. Schubert, *Macromol. Chem. Phys.* **2003**, *204*, 1391.

41   G. Bouhadir, N. Legrand, B. Quiclet-Sire, S. Z. Zard, *Tetrahedron Lett.* **1999**, *40*, 277.

Summary

Advanced supramolecular assemblies based on terpyridine metal complexes: Understanding reaction parameters and designing new materials

Systems based on polymers containing metal-ligand interactions are nowadays used for the synthesis of switchable and self-healing materials that can exploit both sides of the concept: the characteristics of the metal complex (combined properties of the ligand and metal ion) and the classical properties of the polymer. The research described in this thesis was focused on the combination of the 4'-functionalized terpyridine ligands with several transition metal ions. According to the utilized metal ions different stabilities of the synthesized metallo-*bis*-terpyridine complexes could be achieved and therefore various applications of the designed metallo-assemblies could be initiated.

The introduction of the present thesis offers a literature survey that describes recent achievements in the metallo-polymerization of the chelating polypyridyl ligands mainly based on terpyridine structures. The synthesis, characterization and applications of the synthesized supramolecular assemblies containing metallo-*bis*-terpyridine complexes in the polymer backbone were discussed.

The overview of the results starts with the synthesis of the required terpyridine ligands. Thus, nucleophilic substitution of 4'-chloro terpyridine was performed with various polymers and organic molecules bearing hydroxy or thiol functionalities. In this way, a broad range of terpyridine functionalized polymers were made available for subsequent metallo-complexation studies.

The core of this thesis enhanced one of the main characteristics of the metal-ligand coordination interactions: the tuning of the strength of the resulting metallo-*bis*-terpyridine complexes by varying the transition metal ion. The use of different metal ions offered the opportunity of designing new materials with different stabilities, properties and applications. Furthermore, the characterization of the resulting metallo-assemblies had to take in consideration the stability and lability of the synthesized metallo *bis*-terpyridine complexes. For this reason, SEC stability studies were performed on three model systems based on Ni(II), Fe(II) and Co(II) *bis*-terpyridine poly(ethylene glycol). The experimental SEC results revealed that the stability of the $M(II)tpy_2$ connectivity decreases from Ni(II) to Fe(II) and Co(II), respectively. The results showed that only the $Ni(II)tpy_2$ connectivity was suitable for SEC measurements. Further studies were focused on the syntheses of Ni(II) chain extended polymers based on the terpyridine connectivity. For the case of the Ni(II) supramolecular

polymers depth-sensing indentation studies proved an increase in elastic modulus in comparison with the uncomplexed materials due to the presence of the Ni(II) ions. A variety of A-*b*-B-*b*-A triblock copolymers based on a M(II)tpy$_2$ connectivity with the Ni(II), Fe(II) and Co(II) metal ions was synthesized and characterized by various techniques according to their stabilities. The amphiphilic A-*b*-B-*b*-A triblock copolymers self-assembled in solution and the resulting structures were studied by dynamic light scattering (DLS), cryo-transmission electron microscopy (cryo-TEM) and atomic force microscopy (AFM).

Ru(II) ions were used for the synthesis of ABA, AB and A$_n$ supramolecular assemblies based on the terpyridine connectivity. For this case the synthesized supramolecular structures were characterized by high stabilities and, therefore, their characterization could be undertaken using various techniques. The utilized chelating ligands were based on different rigid-rod conjugated ditopic terpyridyl ligands as hydrophobic block B and *mono*-terpyridine poly(ethylene glycol) as hydrophilic block A. The amphiphilicity of the ABA and AB assemblies was studied and discussed by means of DLS, cryo-TEM and AFM. The water soluble supramolecular polymers were prepared *via* Ru(II) polycondensation process performed in an one step synthesis by using as a macro-chelating monomer namely *bis*-terpyridine-poly(ethylene glycol). The optimized reaction conditions and the characterization of the synthesized Ru(II) chain extended polymer were presented.

Zn(II) ions were also used for the syntheses of supramolecular assemblies: model complexes and chain extended polymers where the terpyridine ligands were containing various conjugated spacers. In comparison to the other metal ions, Zn(II) *bis*-terpyridine complexes are characterized by lower stabilities but good photoluminescence properties at room temperature. The synthesized Zn(II)tpy$_2$ assemblies were analyzed by different techniques including ^{1}H-NMR, UV-Vis absorption and emission spectroscopy as well as photoluminescence quantum yield, cyclic voltammetry, density functional theory (DFT) and Raman spectroscopy. Theoretical calculations were performed on an ethynyl-phenyl-substituted terpyridine ligand and its corresponding Zn(II) complex in order to obtain information regarding the influence of the substituents on the photophysical properties of the designed structures. These systems based on the Zn(II)tpy$_2$ connectivity represent promising candidates for the construction of photoluminescent and electroluminescent materials.

The end of the thesis was focused on metallo-supramolecular polymers with thermo-responsible behavior. The combination of the Fe(II) and Zn(II)tpy$_2$ connectivity with thermo-responsible polymers, namely PNIPAM, was studied. The influence of the metal ion and also of the counter ion was analyzed. Due to their outstanding combined properties, these metallo-

supramolecular assemblies could be also suitable for the preparation of switchable systems. Thus, the switchability of the $Fe(II)tpy_2$ connectivity was tested by performing a competitive reaction with HEEDTA. The experimental results proved that indeed it is possible to open and re-close the metallo-terpyridine connectivity by the simple addition of a competitive ligand.

In conclusion, the combination of metal-ligand interactions with polymeric templates provides great potential for designing new materials characterized by a specific behavior compared to their constitutional starting materials. By varying the metal ion different stabilities and properties (*e.g.* photochemical, photophysical) can be achieved. Moreover, the variation of the polymeric spacer attached to the terpyridine moiety offers interesting possibilities for self-assembly applications.

Samenvatting

Geavanceerde supramoleculaire assemblage gebaseerd op terpyridine metaal complexen: begrip van reactie parameters en het ontwerp van nieuwe materialen

Systemen gebaseerd op polymeren die metaal-ligand interacties bevatten worden tegenwoordig gebruikt voor de synthese van schakelbare en zelf-reparerende materialen die de goede kenmerken van beide componenten bevatten: de karakteristieken van het metaal complex (gecombineerde eigenschappen van het ligand en metaal ion) en de klassieke eigenschappen van het polymeer. Het onderzoek dat in dit proefschrift beschreven wordt richt zich op de combinatie van 4'-gefunctionalizeerde terpyridine liganden met verschillende overgangsmetaal ionen. Afhankelijk van het gebruikte metaal ion kunnen verschillen in de stabiliteit van de gesynthetizeerde metaal-*bis*-terpyridine complexen verkregen worden, waardoor verschillende toepassingen van de ontworpen metaal-assemblages geinitieerd kunnen worden.

De introductie van dit proefschrift omvat een literatuuroverzicht dat recente ontwikkelingen in het gebruik van metaal-ligand interacties voor polymerizatie beschrijft gebaseerd op polypyridyl liganden, hoofdzakelijk terpyridine structuren. De synthese, karakterisatie en toepassingen van de gesynthetiseerde supramoleculaire assemblages, die metaal-*bis*-terpyridine complexen in de hoofdketen van het polymeer bevatten, wordt tevens beschreven.

Het overzicht van de resultaten begint met een beschrijving van de synthese van de benodigde liganden. Nucleofiele substitutie van 4'-chloorterpyridine werd toegepast met verschillende polymeren en organische moleculen, welke een hydroxy of thiol functionaliteit hebben. Op deze manier is een brede reeks van terpyridine gefunctionalizeerde polymeren gemaakt welke vervolgens voor metaal-complexatie onderzoeken gebruikt worden.

De kern van dit proefschrift omschrijft de verbetering van één van de hoofdzakelijke karakteristieken van de metaal-ligand coördinatie interacties: het controleren van de sterkte van de resulterende metaal-*bis*-terpyridine complexen door het variëren van het overgangsmetaal ion. Het gebruik van verschillende metaalionen biedt de mogelijkheid om nieuwe materialen te ontwerpen met verschillende stabiliteiten, eigenschappen en toepassingen. De karakterisatie van de resulterende metaalcomplexen moet afgestemd worden op de stabiliteit en labiliteit van de gesynthetiseerde metaal-*bis*-terpyridines. Hiervoor werden stabiliteitstudies gedaan met gel permeatie chromatografie (GPC) aan drie model systemen die gebaseerd waren op Ni(II), Fe(II) en Co(II) *bis*-terpyridine poly(ethyleen glycol). De

experimentele GPC resultaten lieten zien dat de stabiliteit van de M(II)tpy$_2$ verbinding afnam van achtereenvolgend Ni(II) naar Fe(II) en Co(II). De resultaten lieten tevens zien dat alleen Ni(II)tpy$_2$ verbinding stabiel genoeg was voor GPC metingen. Verdere studies waren daarom gericht op de synthese van polymeren met Ni(II) in de hoofdketen door middel van complexatie met terpyridine. In het geval van Ni(II) supramoleculaire polymeren lieten nanoindentatie studies een toename in de elasticiteitsmodulus zien in vergelijking met de ongecomplexeerde materialen door de aanwezigheid van Ni(II) ionen. Een variété van A-*b*-B-*b*-A triblok copolymeren met M(II)tpy$_2$ verbindingen met Ni(II), Fe(II) en Co(II) metaal ionen als B blok en poly(ethyleen glycol) als A blok was gesynthetiseerd en gekarakteriseerd met behulp van verschillende technieken aangepast aan hun stabiliteit. De amfifylische A-*b*-B-*b*-A triblok copolymeren vertonen zelfassemblage in waterige oplossing en de resulterende structuren werden gemeten met dynamische lichtverstrooiing, cryo-transmissie elektronen microscopie en rastersondemicropscopie.

Ru(II) ionen werden gebruikt voor de synthese van ABA, AB en A$_n$ supramoleculaire assemblages gebaseerd op de terpyridine verbinding. In dit geval werden de gesynthetiseerde supramoleculaire structuren gekenmerkt door hun grote stabiliteit en daarom konden ze gekarakteriseerd worden aan de hand van verschillende technieken. De gebruikte metaal coordinerende liganden waren gebaseerd op verschillende rigide geconjugeerde bifunctionele terpyridine liganden als hydrofoob blok B en mono-terpyridine poly(ethyleen glycol) als hydrofiel blok A. De amfifiliciteit van de ABA en AB assemblages is bestudeerd en bediscussieerd aan de hand van dynamische lichtverstrooiing, cryo-transmissie elektronen microscopie en rastersondemicropscopie. De water oplosbare supramoleculaire polymeren welke gemaakt werden via een één-staps Ru(II) polycondensatie proces door gebruik te maken van *bis*-terpyridine-poly(ethyleen glycol). De geoptimaliseerde reactie omstandigheden en de karakterisatie van de gesynthetiseerde polymeren met Ru(II) complexen in de hoofdketen zijn gepresenteerd.

Zn(II) ionen zijn ook gebruikt voor de synthese van supramoleculaire assemblages: model complexen en polymeren met Zn(II) in de hoofdketen gebaseerd op terpyridine liganden met verschillende geconjugeerde verbindingsstukken. In vergelijking met andere metaal ionen worden Zn(II) *bis*-terpyridine weliswaar gekenmerkt door een lagere stabiliteit, maar beschikt over goede fotoluminscerende eigenschappen bij kamer temperatuur. De gesynthetiseerde Zn(II)tpy$_2$ assemblages zijn geanalyseerd middels verschillende technieken, inclusief ^{1}H-NMR spectroscopie, UV-Vis absorptie en emissie spectroscopie, evenals fotoluminescente quantum opbrengst bepalingen, cyclische voltammetrie, "*density functional theory*" (DFT)

189

modellering en Raman spectroscopie. Theoretische berekeningen werden gemaakt op een ethynyl-fenyl-gesubstitueerd terpyridine ligand en zijn corresponderende Zn(II) complex om informatie te verkrijgen over de invloed van de substituenten op de fotofysische eigenschappen van de ontworpen structuren. Deze op Zn(II)tpy$_2$ verbinding gebaseerde systemen lijken veelbelovende kandidaten te zijn de constructie van fotoluminescerende en electroluminescerende materialen.

Het laatste gedeelte van het proefschrift richt zich op metaal-supramoleculaire polymeren met thermoresponsieve eigenschappen. De combinatie van Fe(II) en Zn(II)tpy$_2$ verbindingen met thermoresponsieve polymeren, zoals poly(*N*-isopropylacrylamide), zijn onderzocht. De invloed van het metaal ion en ook het tegenion werden bestudeerd. Vanwege hun buitengewone gecombineerde eigenschappen kunnen deze metaal-supramoleculaire assemblages ook geschikt zijn voor het maken van schakelbare systemen. Om deze reden is de schakelbaarheid van de Fe(II)tpy$_2$ verbinding getest door een competitieve reactie aan te gaan met HEEDTA. De experimenten wezen uit dat het inderdaad mogelijk is om de metaal-terpyridine verbinding te openen en opnieuw te sluiten door een simpele additie van een competitief ligand.

Concluderend kan gezegd worden, dat de combinatie van metaal-ligand interacties met polymere structuren een groot aantal mogelijkheden biedt voor het ontwerpen van nieuwe materialen, welke gekenmerkt worden door een specifiek gedrag in vergelijking met hun constitutionele uitgangsmaterialen. Door het variëren van het metaal ion kunnen verschillende stabiliteiten en eigenschappen (bijvoorbeeld fotochemisch, fotofysisch) verkregen worden. Verder biedt de variatie van de polymere verbindingsstukken die verbonden is aan het terpyridine gedeelte interessante mogelijkheden voor zelfassemblage toepassingen.

Curriculum Vitae

Manuela Chiper was born on 2nd of March 1975 in Panciu (Romania). She graduated in 2000 from the "Politehnica" University of Bucharest, Faculty of Industrial Chemistry-Technology of Organic Chemistry Department. The diploma thesis entitled "Synthons for syntheses of optically active α-amino-acids" was supervised by Prof. Dr. Sorin Rosca (Organic Chemistry Department). One year later she received her MSc. diploma specialized in "Drugs and Cosmetics", from the same university in Bucharest (supervised by Prof. Dr. Sorin Rosca) working on synthesis and characterization of various arene-tricarbonyl-chromium complexes. She was employed as a research assistant at the Organic Chemistry Department from 2001 to 2003. In May 2003 she moved to Università degli studi di Milano, Dipartimento di Chimica Organica e Industriale, Italy, working on the project entitled "Design, discovery and synthesis of functional molecules" under supervision of Prof. Dr. Cesare Gennari. In October 2004 she started her PhD thesis, in the field of metallo-supramolecular chemistry, as part of the Dutch Polymer Institute (DPI) program (project #447) in the group of Prof. Dr. Ulrich S. Schubert, Laboratory of Macromolecular Chemistry and Nanoscience, Eindhoven University of Technology, the Netherlands. The results of her research are presented in this thesis.

Refereed publications:

☐ M. Chiper, A. Winter, R. Hoogenboom, C.-A. Fustin, J.-F. Gohy, U. S. Schubert
   Supramolecular rod-coil AB ruthenium(II)-terpyridine assemblies
   Manuscript in preparation.

☐ M. Chiper, R. Hoogenboom, U. S. Schubert
   New terpyridines macroligands as potential synthons for supramolecular assemblies
   Manuscript in preparation.

☐ A. Winter, C. Friebe, M. Chiper, U. S. Schubert, M. Presselt, B. Dietzek, M. Schmitt,
   J. Popp
   Synthesis, characterization and electrooptical properties of Zn(II) complexes with π-conjugated terpyridines as ligands
   ChemPhysChem submitted.

☐ M. Chiper, R. Hoogenboom, U. S. Schubert
   Towards main chain metallo-terpyridyl supramolecular polymers - "the metal does the trick"
   Macromol. Rapid Commun. submitted.

☐ M. Chiper, R. Hoogenboom, U. S. Schubert
   Linear coordination polymers based on Ru(II)-*bis*-terpyridine-poly(ethylene glycol): synthesis, optimization and characterization
   e-polymers **2008**, in press.

☐ A. Winter, M. Chiper, C. Friebe, U. S. Schubert, M. Presselt, B. Dietzek, M. Schmitt,
   J. Popp
   Zinc(II) *bis*-terpyridine complexes: the influence of the cation on the π-conjugation between terpyridine and the lateral phenyl-substituent
   J. Phys. Chem. C **2008***,* in press.

☐ M. Chiper, A. Winter, R. Hoogenboom, D. A. M. Egbe, D. Wouters, M. A. R. Meier,
   S. Hoeppener, C.-A. Fustin, J.-F. Gohy, U. S. Schubert
   Synthesis and micellization of coil-rod-coil ABA ruthenium(II)-terpyridine triblock-copolymers
   Macromolecules **2008**, in press.

☐ C. Haensch, M. Chiper, C. Ulbricht, A. Winter, S. Hoeppener, U. S. Schubert
   Reversible supramolecular functionalization of surfaces: terpyridine ligands as versatile building-blocks for supramolecular architectures
   Langmuir **2008**, in press.

☐ M. Chiper, D. Fournier, R. Hoogenboom, U. S. Schubert
   Towards thermosensitive and switchable Fe(II) and Zn(II)-bis-terpyridine supramolecular polymers
   Macromol. Rapid Commun. **2008**, *29*, 1640-1647, (front cover).

☐ S. Landsmann, A. Winter, M. Chiper, S. Höppener, D. Wouters, U. S. Schubert
   Poly(dimethylsiloxane)-substituted 2,2′:6′,2″-terpyridines: synthesis and characterization of novel amphiphilic supramolecular diblock-copolymers
   Macromol. Chem. Phys. **2008**, *209*, 1666-1672.

□ <u>M. Chiper</u>, M. A. R. Meier, D. Wouters, S. Hoeppener, C.-A. Fustin, J.-F. Gohy, U. S. Schubert
Supramolecular self-assembled Ni(II), Fe(II) and Co(II) ABA triblock copolymers,
Macromolecules **2008**, *41*, 2771-2777.

□ <u>M. Chiper</u>, M. A. R. Meier, J. M. Kranenburg, U. S. Schubert
New insights into nickel(II), iron(II) and cobalt(II) *bis*-complex based metallo-supramolecular polymers
Macromol. Chem. Phys. **2007**, *208*, 679-689 (front cover).

Non-refereed publications:

□ <u>M. Chiper</u>, A. Winter, D. A. M. Egbe, R. Hoogenboom, D. Wouters, S. Hoeppener, C.-A. Fustin, J.-F. Gohy, U. S. Schubert
Amphiphilic well-defined ABA ruthenium(II)-*bis*-terpyridine block copolymers
Polym. Preprints **2008**, *49*, 406-407.

□ <u>M. Chiper</u>, A. Winter, D. A. M. Egbe, U. S. Schubert
New metallo-supramolecular architectures based on polymers functionalized and rigid π-conjugated terpyridine
Polym. Preprints **2007**, *48*, 716-717.

□ S. Landsmann, <u>M. Chiper</u>, A. Winter, U. S. Schubert
Novel polysiloxane functionalized terpyridines and their transition metal complexes
Polym. Preprints **2007**, *48*, 695-696.

□ <u>M. Chiper</u>, D. Fournier, R. Hoogenboom, U. S. Schubert
Towards thermosensitive metallo-terpyridine supramolecular polymers
Polym. Preprints **2007**, *48*, 691-692.

□ D. Wouters, C. Ott, M. Chiper, M. A. R. Meier, U. S. Schubert
(Metallo-supramolecular)block copolymers in solution: microscopic study of micellization
Polym. Preprints **2007**, *48*, 687-688.

□ A. Winter, M. Chiper, E. Tekin, D. A. M. Egbe, U. S. Schubert
Rigid π-conjugated 2,2':6',2''-terpyridines as building blocks for new supramolecular assemblies
Polym. Preprints **2007**, *48*, 633-634.

□ D. Wouters, C. Ott, J. M. Kranenburg, M. Chiper, B. Lohmeijer, A. V. Kyrylyuk, U. S. Schubert
Thin film characterization of metallo-supramolecular assemblies
Polym. Preprints **2007**, *48*, 601-602.

□ M. Chiper, M. A. R Meier, D. Wouters, U. S. Schubert,
Supramolecular ABA triblocks: understanding reaction parameters and designing new materials
Polym. Preprints **2007**, *48*, 564-565.

On these last pages, my PhD journey will end. For that reason, I would like to thank the people who accompanied and supported me during these years.

First of all, I would like to thank Professor Ulrich S. Schubert for giving me the opportunity to join his group. Uli, thank you for your continuous energy, freedom, financial generosity and great work facilities offered! Spending these years in SMN was a unique and unforgettable experience.

I would like to thank the members of the defence committee, Prof. Dr. Ulrich S. Schubert, Prof. Dr. Jean-Francois Gohy, Dr. Richard Hoogenboom, Prof. Dr. Rint Sijbesma, Prof. Dr. Wolfgang Binder, and Prof. Dr. Jay S. Siegel for making time to read and comment on my thesis, and for taking part in my PhD defense committee.

DPI is acknowledged for the financial support to perform my PhD research.

Very special thanks go to my co-promotor Richard Hoogenboom. Richard, thanks for making time to rigorously proof-reading my thesis. Also, many thanks for the comments on the manuscripts and for the friendly and nice collaboration that we had. Thank you for your high level of professionalism and for being here, always willing to find scientific solutions to the addressed questions.

Special thanks go to Prof. Jean-Francois Gohy for making the corrections of my thesis in a very short time frame. JF thank you for all of the comments you made on this book but also on other manuscripts. I also thank JF and Charles-Andre Fustin for the very good collaboration regarding the micellization part described in my thesis. Charles-Andre, thank you for performing the last experiments while I was writing this book.

I would also like to thank Mike Meier for the very important collaboration, discussions and corrections of manuscripts on the topic we worked together.

Andreas Winter is acknowledged for the kind offer of the conjugated terpyridine ligands and for the very nice collaboration, followed by joined papers. Daniel Egbe is acknowledged for offering the precursors needed for the Ru(II) ABA assemblies. Prof. Jürgen Popp, Martin Presselt, Benjamin Dietzek, and Dr. Michael Schmitt from F.S. Univ. Jena and Inst. Phys. Chem Jena, Germany are acknowledged for performing the Raman spectroscopy and theoretical calculations included in Chapter V.

Special thanks go to David Fournier for the very enjoyable collaboration that we had. Dear David, thank you for bringing the very pleasant "French flavour" to the group, even if only for a very short stay. Thank you for your valuable friendship and support.

Emma, thank you for the important help offered all these years, regarding many organizational issues. Thank you for the many, many coffee-chocó, chatting, optimism, and your multitudes of pink outfits, which always brought a big smile ☺ to my face. Ciao bella!

Hanneke, Rebecca, Antje, Caroline, and Martin, are acknowledged for taking care of the chemical orders, GPC maintenance, elemental analysis measurements, and - more importantly - for taking care of all lab machines. Tina and Nicole thank you for the MALDI-TOFMS measurements. Daan and Stephanie are acknowledged for the AFM and cryo-TEM measurements performed on my "painful micelles". Hans is acknowledged for depth-sensing indentation studies performed on my polymers and for the help in translating many Dutch documents.

I also want to thank the rest of SMN, current and former members, for their contribution to various activities: Martin H. (for the friendly attitude and for taking the risk to be "the good & good messenger☺" of "my last minute corrections"); Jurgen (for the help with my never-ending computer crash stories); Christoph & Stefi & Emma (for providing the wok food in the coffee corner on many Friday evenings); Bas L. (for sharing with me the very busy fumehood at the beginning of my PhD); Jolke, Carlos and Christina (for the nice trip to lovely Ireland and the beer drinking action in the Irish pub); Christina and Hans (for the time spent as office mates); Remzi (for pressing the red button during an unforgettable Franco-Romanian-Turkish combi-experiment, which ended with a lot of smoke but no fire☺, and also for the "live" burning of my new coat while I was giving my presentation to the audience); Daan and Claudia (for the unforgettable "swimming" lesson in Austria); Mathias (in the lab, Holly Ghost still exists!☺…); Meta (for the unforgettable trip back from Lunteren….what a fancy car!☺…); Bobby (for the many funny moments and comments☺); Steve, Claudia and Christian F. (for the collaboration on joined papers); Jolke (for making possible the Dutch translation of the summary of my thesis; also for the always friendly chatting); Frank, Hector….

To my long term office-mates Andreas and Christoph, a special thank you for the enjoyable "working" atmosphere. Thank you for the nice holiday in Boston, after the ACS meeting; Andreas you are the best guide ever! Christoph, thank you for accompanying me in the many lab-working weekends/evenings, for the daily teasing training(!) and "singing", and for your friendly attitude. Definitely, you are the best chair-breaker!☺

I would like to thank Veronica for being a sincere and constant friend along these years. Vero, mulţumesc pentru suportul necondiţionat oferit de tine la inceputul PhD-ului meu si pentru susţinerea morala oferită in toţi aceşti ani. Emine, thank you for your friendship,

moral support and help regarding the preparation of my thesis. Also, Emine and Adem, thank you for solving the last minute technical problems of my PhD cover book. Tamara, thank you for your special kindness, friendship, and enjoyable non-chemical conversations. Oana mulţumesc pentru optimismul degajat si pentru momentele in care am putut "povesti" in româneşte. Ramona mulţumesc pentu "micile taifasuri☺" si pentru informaţiile oferite la finalizarea tezei.

Karina, thank you for your friendship and for many, many chatting hours, which I sincerely appreciated/appreciate! Inma, thanks for welcoming me here in the Netherlands with your warm Spanish friendship, which started many years ago in a wonderful place.

I especially thank the people who inspired me and shared unforgettable moments with me over these years (Christelle, Philipe, Geraldine, JP, Cleo, Loz, Fab). Very special thanks to Christelle, my dear friend, for the help, fun (a lot of fun☺!) and for the many, many talks whenever I needed.

Multe mulţumiri merg catre Cristina si Alin pentru plăcutele vacanţe petrecute impreună. Cristina mulţumesc pentru caldura prieteniei tale pe care o apreciez din tot sufletul!

Deasemeni, aş dori sa mulţumesc familiei Nilă pentru importanta contribuţie adusă la educaţia mea.

Familiei mele ii mulţumesc pentru eforturile făcute de alungul anilor. Mamă, iţi mulţumesc pentru susţinerea morala, nelimitata incredere in mine si mai ales iti mulţumesc pentru puterea de a ma lasa sa imi urmez deciziile uneori destul de dure. Din tot sufletul meu vă dedic această carte, vouă, parinţilor mei.

Manuela